Freie Universität Berlin

MDC MAX DELBRÜCK CENTER FOR MOLECULAR MEDICINE IN THE HELMHOLTZ ASSOCIATION

Establishment of a FRET-based Aggregate Seeding Assay to study the pathogenic role of self-replicating mutant HTT fibrils in Huntington's disease

Inaugural-Dissertation

to obtain the academic degree

Doctor rerum naturalium (Dr. rer. nat.)

Submitted to the Department of Biology, Chemistry and

Pharmacy of Freie Universität Berlin

By

ANNE AST

From Frankfurt (Oder)

January 2019

The work was conducted from February 2014 until January 2019 under supervision of Prof. Dr. Erich E. Wanker at the Max Delbrück Center for Molecular Medicine in the Helmholtz-Association.

I hereby confirm that I have written the thesis independently using solely the aids mentioned and without illicit assistance from third parties.

1. Reviewer: Prof. Dr. Erich E. Wanker
2. Reviewer: Prof. Dr. Oliver Daumke

Disputation: 24.05.2019

Summary

Huntington's disease (HD) is progressive neurodegenerative disorder with an autosomal dominant inheritance, manifesting with a triad of motor, cognitive and behavioral symptoms. HD is an incurable disease caused by a CAG trinucleotide repeat expansion in the *HTT* gene, which translates into an expanded polyglutamine tract in the huntingtin (HTT) protein. This expansion renders the conformation of the HTT protein unstable and promotes the assembly of amyloidogenic protein aggregates, predominantly composed of N-terminal HTT fragments. Amyloidogenic mutant HTT (mHTT) aggregates share common features with prion proteins, being able to self-propagate their corrupted conformation and to spread between adjacent cells. However, the role of mHTT aggregates and their prion-like features in the pathogenesis of HD remains elusive.

To address this question, I developed a FRET-based aggregate HTT seeding assay (FRASE) for the detection of self-replicating mHTT aggregates. I optimized the assay for the sensitive quantification of mHTT seeding activity (HSA) in biological samples from HD patients and disease models. I could show that mHTT seeds are present early in the pathogenesis and increase in abundance with progression of disease, suggesting that HSA quantitatively tracks disease progression. Biochemical investigations of mouse brain homogenates demonstrated that small, rather than large, mHTT structures are responsible for the HSA measured in FRASE assays. Using the FRASE assay, I assessed HSA in an established inducible *Drosophila* model of HD and found a strong correlation between HSA and increased mortality in transgenic HD flies, suggesting that self-replicating mHTT seeds are disease relevant, neurotoxic structures causing severe phenotypic consequences *in vivo*. Next, I used structure-guided mutagenesis to generate protein variants of the N-terminal mHTT exon 1 fragment (mHTTex1), as a tool to explore the relationship between the structural properties of mHTTex1 aggregates and their putative proteotoxicity. Recombinant mHTTex1 protein variants were distinct in their aggregation properties and revealed fibrillar aggregates with different stabilities and morphologies. In order to relate these structural features to mHTTex1-induced proteotoxicity, protein variants were pan-neuronally expressed in a newly developed *Drosophila* model. Behavioral and biochemical analysis of transgenic flies confirmed the concurrence of mHTTex1 aggregates and toxicity and indicated that aggregate stability influences neurotoxicity in transgenic HD flies.

Taken together, my studies emphasize the importance of self-replicating mHTTex1 aggregates in HD pathogenesis and provide novel tools for basic and clinical disease research.

Zusammenfassung

Die Huntington-Krankheit (HK) ist eine progressive, autosomal-dominant vererbte neurodegenerative Erkrankung, die sich mit motorischen, kognitiven und psychiatrischen Symptomen manifestiert. Die HK ist bis heute unheilbar und wird durch die Expansion des CAG-Trinukleotid-Repeats im *HTT*-Gen verursacht. Diese hat eine Verlängerung der Polyglutamin-Sequenz im Huntingtin-Protein (HTT) zur Folge, wodurch die Konformation des Proteins instabil wird und es zur Bildung von amyloidogenen Proteinaggregaten kommt, die hauptsächlich aus N-terminalen HTT Fragmenten bestehen. Amyloidogene Aggregate des mutierten HTT (mHTT) weisen gemeinsame Merkmale mit Prionen auf, da sie in der Lage sind, ihre fehlgefaltete Struktur auf nativ gefaltetes mHTT zu übertragen und sich zwischen benachbarten Zellen auszubreiten. Die Bedeutung von mHTT-Aggregaten und deren prionenähnlichen Eigenschaften für die Pathogenese der HK ist jedoch nur wenig erforscht. Um dieser Frage nachzugehen, habe ich einen FRET-basierten HTT-Seeding-Assay (FRASE) zum Nachweis selbstreplizierender mHTT-Aggregate („seeds“) entwickelt und ihn für den sensitiven Nachweis der Replikationsaktivität (HSA) in biologischen Proben von Patienten mit der HK und Modellsystemen optimiert. mHTT „seeds“ konnten früh im Krankheitsverlauf nachgewiesen werden und nahmen in ihrer Häufigkeit zu, was darauf hindeutet, dass durch die Messung der HSA das Fortschreiten der Krankheit quantitativ verfolgt werden kann. Biochemische Untersuchungen von Maushirnhomogenaten zeigten, dass eher kleine als große mHTT-Aggregatspezies für die gemessene HSA verantwortlich sind. Mit dem FRASE-Assay untersuchte ich HSA in einem etablierten induzierbaren *Drosophila*-HD-Modell und beobachtete eine starke Korrelation zwischen HSA und erhöhter Mortalität in transgenen Fliegen, was nahelegt, dass mHTT „seeds“ krankheitsrelevante neurotoxische Strukturen sind. Mittels strukturgestützter Mutagenese habe ich anschließend Proteinvarianten des mHTTex1 Proteins generiert, um die Auswirkungen der Struktur von mHTTex-Aggregaten auf deren Toxizität zu untersuchen. Die generierten mHTTex1-Proteinvarianten unterschieden sich in ihren Aggregationseigenschaften und bildeten fibrilläre Aggregate mit unterschiedlicher Stabilität und Morphologie. Um die Proteotoxizität von strukturell unterschiedlichen mHTTex1 Aggregaten *in vivo* zu untersuchen, wurden die Proteinvarianten in neu entwickelten Drosophila-Modellen panneuronal exprimiert. Die phänotypische und biochemische Charakterisierung der transgenen Fliegen zeigte, dass die Aggregatbildung mit der Toxizität korreliert und dass diese auch von der Stabilität der Aggregate beeinflusst wird. Zusammengefasst weisen meine Studien darauf hin, dass selbstreplizierenden mHTTex1-Aggregate bei der Pathogenese der HK eine wichtige Rolle spielen. Außerdem entwickelte ich eine Vielzahl neuer Methoden und Werkzeuge, die nun in der Krankheitsforschung angewendet werden können.

Table of contents

1. Introduction

The human nervous system is a fascinatingly complex and highly interconnected network of neuronal and support cells. It comprises ~86,000,000,000 neurons and forms an incredible large number of connection points (~ 5×10^{14} synapsis)[1-3]. It receives and conducts stimuli from the external and internal environment, processes them and commands adequate responses to the ever-changing environment. This is how the nervous system directs our movements, controls our behavior and allows abstract thinking and creativity. Rationally, malfunctioning of this central switchboard implies devastating consequences.

Neurodegenerative diseases cause dysfunction or death of neuronal cells and thereby trigger malfunctioning of the nervous system[4,5]. They manifests with a variety of symptoms ranging from progressive impairment of motor control to mood disorders and cognitive deficits[6,7]. Currently, neurodegenerative diseases, such as Alzheimer's disease, Parkinson's disease and Huntington's disease are incurable and predicted to increase in frequency with continues growth and increasing life expectancy of the world population. These diseases do not only have a strong impact on the life of patients and their families, but will place an enormous financial burden on healthcare systems[8-10]. Investigating the underlying pathological mechanisms of these diseases is of major importance in order to identify molecular targets for specific and effective therapeutic intervention[6,7].

1.1. Huntington's Disease

Huntington's disease (HD) is an autosomal dominant progressive neurodegenerative disorder which manifests with a triad of symptoms affecting motor, psychiatric and cognitive function and ultimately leads to premature death. Historical descriptions of HD cases date back to the 15th century[11,12]. Referring to the jerky involuntary movements of affected individuals, this obscure disease was initially termed "dancing mania", "that disorder" or "San Vitus dance", stigmatizing those who are affected as being possessed by the devil[12]. The first accurate medical description was published in 1872 by the young doctor George Huntington who became eponymous for the condition - today known as Huntington's disease. In his article "On Chorea" he gave a clear and concise description of HD symptoms and highlighted the hereditary nature of the disease as one of its predominant characteristics[13]. Over the following century, this publication not only changed the societal perception of HD sufferers, but also spurred multiple attempts to find communities of persons at risk to develop HD with the ultimate goal to identify the genetic cause underlying the disease. In the 1950's, HD was diagnosed in a large community of people living around Lake Maracaibo in Venezuela. Twenty years later, this location became the center

of interdisciplinary and cooperative research which was initiated and coordinated by Nancy Wexler and laid the foundation for the identification of the HD gene and many future studies of Huntington's disease[11,14,15].

1.1.1. Etiology and Epidemiology

The genetic defect leading to HD was identified in 1993 by The Huntington's Disease Collaborative Research Group[16]. The researchers reported that HD is linked to the *IT15* gene which is located on the short arm of chromosome 4 (4p16.3) and contains a polymorphic trinucleotide repeat in its first exon, consisting of C (cytosine), A (adenine) and G (guanine). Examination of this genetic locus in non-HD control individuals revealed a repeat size of 6 to 35, whereas individuals with HD had 40 or more CAG repeats[16]. This led to the conclusion, that HD is caused by the expansion of the instable CAG repeat in the *IT15* gene. The *IT15* gene was subsequently named huntingtin (*HTT*) gene[16]. Later studies refined the role of the CAG repeat length in disease onset and progression. It was confirmed, that individuals develop HD with full penetrance when exceeding a threshold of 39 CAG repeats, whereas repeat sizes lower than 27 are considered normal. Reduced penetrance of HD has been reported for individuals with a CAG repeat ranging from 36 to 39[17]. CAG repeats of 27 to 35 are considered as the intermediate range and do not lead to the development of HD. However, as the CAG repeat is meiotically instable and tends to expand in successive generations, a CAG repeat of intermediate size bares a greater risk of transmitting the disease to the next generation[18]. This phenomenon, known as genetic anticipation, is predominantly observed when the CAG repeat expansion is inherited from the father, implying repeat instability during spermatogenesis[18-20].

The length of the CAG repeat in the *HTT* gene not only destines an individual to develop HD, but also greatly determines the age of symptomatic onset and the rate of pathogenesis. Individuals with a longer CAG repeat will develop HD earlier in life and show faster disease progression (Figure 1)[21-23]. Disease manifestation as well as progression is dominantly determined by the allele with the longer CAG repeat[24].

Despite the strong inverse correlation, the length of the CAG repeat can only partially explain the variance in age of onset[25-27]. Disease manifestation may differ in patients even though the length of the CAG repeat is the same, indicating that environmental and/or genetic factors influence the course of the disease[28,29]. Supporting this hypothesis, a recent genome-wide association study (GWAS) suggested genes involved in DNA repair, mitochondrial fission and oxidoreductase activity to modify HD pathogenesis[30].

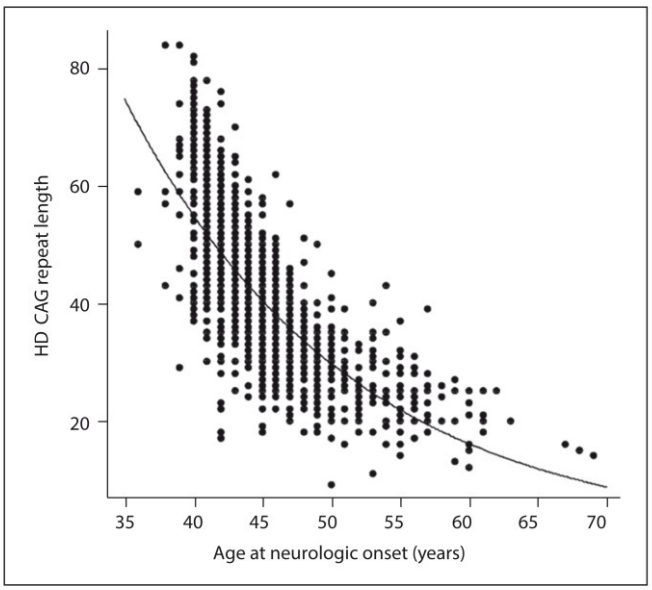

Figure 1: Inverse correlation of age of onset and CAG repeat length

The plot displays the CAG repeat length measured in blood DNA (x-axis) and age at neurologic onset (y-axis) of 1200 HD patients. Best-fit simple logarithmic regression to the data is represented by the black line. The CAG repeat length accounts for approximately 67% of the overall variation in age at onset (Image from Gusella et al., 2009[31]).

Huntington disease is endemic to all populations, but occurs with different frequencies in different ethnic groups. The highest prevalence has been observed in Western populations (Europe and North America) with 10-13.7 affected individuals per 100 000[32]. HD is less frequently diagnosed in African (0.1 per million in black people, 22 per million in white and mixed ancestry subpopulation) and Asian populations (1-7 individuals per million), whereby it has been observed that individuals with European descent exhibit a higher prevalence for HD than the native population[32,33]. Ancestry-specific prevalence rates are thought to be related to genetic differences at the *HTT* locus among different populations. Longer CAG repeats in the general population (18.4-18.7 repeats in European, 17.5–17.7 in East Asian and 16.9–17.4 in African populations) are associated with higher numbers of *de novo* cases and higher prevalence of HD[34]. This may be explained by the genetic instability of the CAG repeat and the increased frequency of CAG repeat expansions with longer CAG repeats[25,34,35].

1.1.2. Clinical Manifestation and Neuropathology

Huntington's disease (HD) generally manifests in adult life at an average age of ~45 years[35]. In the pre-manifest or prodromal phase, subtle changes in cognition, behavior and movement can already be noticed. These can occur up to 15 years before HD is clinically diagnosed through the onset of motor disturbance as evaluated by the Unified HD Rating Scale (UHDRS) total

motor score (TMS)[36-38]. Once started, symptoms will progressively deteriorate and ultimately lead to premature death approximately 15-20 years after motor-onset[25]. The triad of HD symptoms comprises motoric difficulties, cognitive deficits and neuropsychiatric abnormalities[35]. Motor abnormalities usually occur biphasically in adult-onset HD patients. Initially patients show a hyperkinetic behavior which is characterized by involuntary and unpredictable body movements (Chorea). However, when HD progresses most patients enter a hypokinetic phase, which is marked by bradykinesia, dystonia and rigidity and worsens up to the point of complete immobility[39,40]. Cognitive abilities will also deteriorate over time[41]. Patients show deficits in emotion recognition, processing speed, visuospatial and executive function and sometimes suffer from full blown dementia in the end stages of the disease[41,42]. In addition, neuropsychiatric difficulties such as apathy, anxiety, irritability, depression, obsessive compulsive behavior and psychosis may become more prominent[43-45]. However, apathy is the only neuropsychiatric symptom that progresses with disease[46]. Although the most prominent clinical features of HD are CNS-related, patients also suffer from metabolic and immune disturbances, skeletal-muscle wasting, weight loss, cardiac failure, testicular atrophy, and osteoporosis[47-49]. The cumulation of all these symptoms over time will first decrease the patient's life quality, their ability to cope with daily life and will ultimately demand for all around care. Disease symptoms will lead to secondary complications, such as pneumonia and cardiovascular disease, which are the two leading courses of death for HD patients[50-52].

Although, HD has mainly been recognized as an adult-onset disease, juvenile cases have been reported for 5-10 % of all HD cases. They are characterized by a disease onset before the age of 20 years and have a slightly different disease pattern. Hyperkinetic chorea-like symptoms are less prominent and movement difficulties are predominantly hypokinetic[53-55]. Cognitive and neuropsychiatric symptoms are reported to be severe[56,57]. Seizures have been reported for 30-50 % of the patients. Juvenile HD is generally associated with elongation of the CAG repeat beyond 60[56]. It progresses more rapidly and individuals affected, die within 10 – 15 year after onset[58].

Neuropathological research on post mortem brains of HD patients identified brain atrophy in the striatum[59]. The striatum, comprising the caudate nucleus and the putamen, is mainly composed of GABA-ergic medium spiny neurons (MSNs). These neurons receive and integrate multiple excitatory signals from different brain regions and are a major component of the motor and reward system[60]. Similar to the motor abnormalities, neuronal loss in the striatum occurs biphasically. Initially MSNs of the indirect pathway are lost. These neurons are responsible

for the inhibition of motor neurons, thereby preventing the initiation of movement[61]. Their loss results in the hyperkinetic phase, marked by involuntary movement. Second, MSNs of the direct pathway are lost. Under normal conditions these neurons indirectly activate motor neurons and therefore contribute to the initiation of movement. Naturally their loss will result in the hypokinetic symptoms[25,35,62].

Pathological changes leading to HD symptomology were long thought to be confined only to the striatum. Although, striatal brain regions seem to be particularly susceptible, HD is characterized by a wide spread brain atrophy (Figure 2), that results from neuronal loss within different regions of the brain[59,63-65]. Therefore, HD is considered a multisystem degenerative disease of the human brain. Aside from the striatum, degenerative changes have been described for the thalamus, pallidum, brainstem, cerebellum and different regions of the cerebral cortex[62,66].

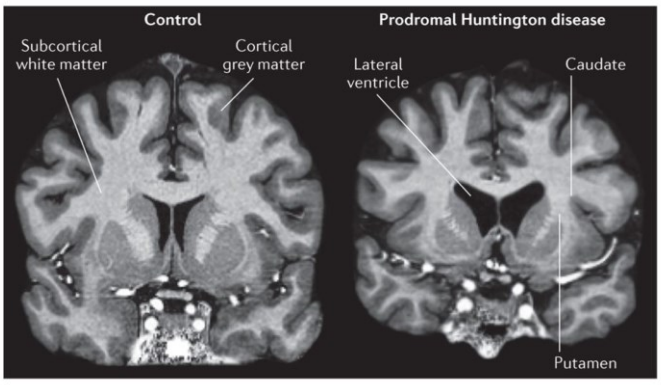

Figure 2: Magnetic resonance image reveals brain atrophy in prodromal HD

Bilateral atrophy of the caudate and putamen and subcortical white matter as well as an increase in size of the fluid-filled lateral ventricle is observed in gene carriers at a prodromal HD stage. (Image from Bates et al., 2015[35])

1.2. The Huntingtin Protein

1.2.1. Structure and Function

The *HTT* gene spans 67 exons and is translated into the huntingtin (HTT) protein. It is ubiquitously expressed in all body tissues with slightly higher levels in the CNS[67]. Within the cell HTT is located in the cytoplasm and to a lesser extend in the nucleus[68]. In addition to the canonical form, the *HTT* gene has a second mRNA transcript containing a 3' UTR (untranslated region) sequence[69]. Additional isoforms are generated by alternative splicing, including a variant that only spans the first CAG repeat containing exon[70-74].

Introduction

The canonical HTT protein is relatively large (3144 amino acids, 350 kDa) and was predicted to contain 36 HEAT and HEAT-like repeats dispersed over the entire length of the protein (Figure 3)[75,76]. HEAT repeats were named after a group of proteins in which they were initially identified (**H**TT, **E**longation factor 3, protein phosphatase 2**A**, and **T**arget of rapamycin 1). They are composed of paired antiparallel amphiphilic alpha helices and are arranged into several clusters. These HEAT repeat clusters feature a flexible, superhelical, solenoid-like structure and facilitate protein-protein interactions. HEAT repeat domains are interspaced by several disordered regions. The large C-terminal part of the HTT protein encoded by exon 2 to 67 is evolutionary conserved, whereas the N-terminal part encoded by the *HTT* exon 1 has evolved more recently[68,77,78]. Although it comprises only ~ 2 % of the HTT protein, the N-terminal HTT exon 1 (HTTex1) protein fragment has been most extensively studied, as it contains the gene product of the disease-causing CAG repeat - an expandable polyglutamine (polyQ) stretch. Within the HTTex1 the polyQ stretch is preceded by 17 amino acids (N17) and followed by a proline rich domain (PRD). The N17 domain forms an amphipathic α-helix and is important for membrane interaction and functions as a nuclear export signal (NES)[79,80]. The polyQ stretch itself is conformationally flexible and can adopt different structures[81,82]. The PRD has also been observed to be flexible, but can adapt a relatively rigid poly-L-proline type II (PPII) helix[81,83,84].

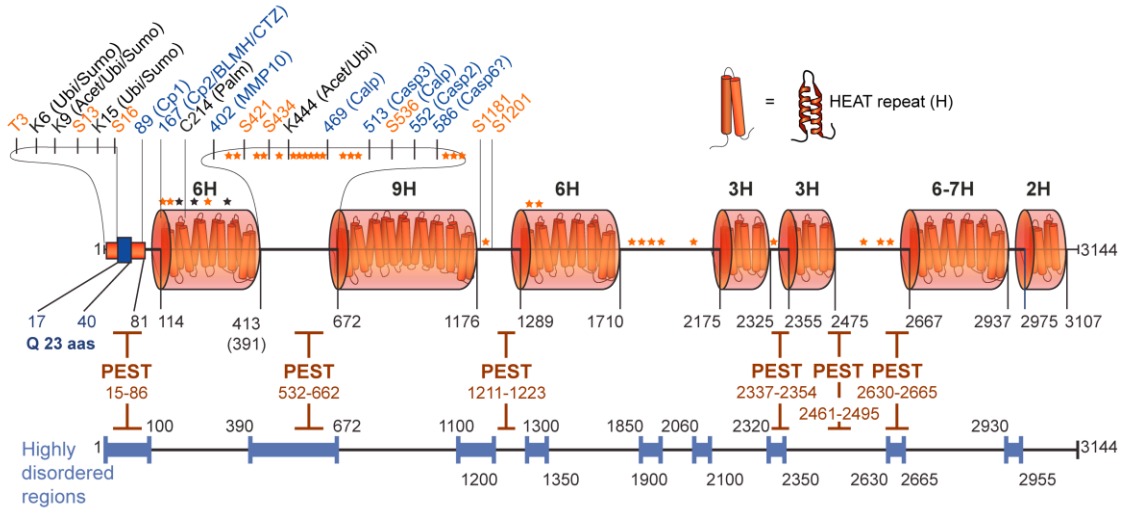

Figure 3: Schematic illustration of the huntingtin protein

This cartoon illustrates confirmed sites of phosphorylation (orange) and other post-translational modifications (black) as well as protease cleavage sites (blue). Orange and black stars indicate phosphorylation and acetylation sites identified by mass spectrometry with no further confirmations. HEAT (orange barrels, H: number of predicted HEAT repeats), PEST, and highly disordered regions are indicated with their respective amino acid range. Ubi, ubiquitin; Sumo, sumoyl; Acet, acetyl; Palm, palmitoyl; MMP10, metalloproteinase 10; Calp, calpain; Casp3/2/6, caspase 3/2/6. (Image adapted from Saudou and Humbert et al., 2016[68])

Due to the flexibility of the HTT protein, attempts to resolve the 3-dimensional structure were hampered in the past[85]. However, using the stabilizing effect of the HTT-HAP40 (HTT associated protein 40) interaction, Gou and colleagues recently determined a high-resolution structure of the full-length HTT protein in complex with HAP40 using cry-electron microscopy[86]. In this complex the HTT protein consists of three distinct domains. The N-HEAT domain (residues 91 - 1684, 21 HEAT repeats) forms an α-solenoid structure and harbors two putative membrane binding domains. The C-HEAT domain (residues 2092 - 3098) consists of 12 HEAT repeats and features a ring-like structure. Both domains are linked by a smaller flexible bridge domain (residues 1685 - 2091). In addition to these major structural features, several disordered regions have been identified, including the N-terminal HTTex1, which could not be resolved in this study. The 3D orientation of the domains to each other is mainly stabilized by the HAP40 interaction. Otherwise the N-HEAT and C-HEAT domains are only weakly connected via loop interactions, indicating high structural flexibility of the HTT protein in the absence of an interaction partner. It also highlights the possibility of alternative HTT conformations in the presence of other inter- and intramolecular interactions[85,86].

HTT is subject to proteolytic cleavage by multiple proteases, including caspases, calpains cathepsins and the metalloproteinase MMP10[87-91]. Cleavage sites are found in so called PEST domains (proline (**P**); aspartic acid (**E**) or glutamic acid (**D**); serine (**S**); threonine (**T**)) which are mainly located in disordered regions of the protein[11,68]. Wild-type HTT is subject of proteolytic cleavage, which may modify its cellular functions[92,93]. In HD, proteolysis is increased which results in the generation of toxic N-terminal fragments containing the expanded polyQ stretch[88,94,95]. In addition, HTT is post-translationally modified (phosphorylation, acetylation, palmitoylation, ubiquitylation, sumoylation). These modifications are critical for its intracellular localization and influence HTT structure and its interactions with other proteins[96,97].

The large size of the HTT protein, its structural flexibility and the high number of interaction partners supports the idea that HTT acts as molecular scaffold that facilitates protein complex formation and coordinates molecular functions. Previous studies indicate the involvement of the HTT protein in multiple cellular processes, such as cellular trafficking, protein turnover, gene expression and cellular stress response[68,77,98].

HTT has been shown to participate in vesicle transport. It complexes with motor proteins (HAP1, dynactin) and controls transport of synaptic precursor vesicles, BDNF containing vesicles, autophagosomes, endosomes and lysosomes along microtubules[99-104]. In addition, HTT interacts with the glycolysis enzyme GAPDH, thereby coupling motor proteins with the required energy

supply and enhancing transport velocity[105]. Furthermore, HTT's phosphorylation status at S241 determines whether retrograde or anterograde transport is facilitated[106].

Apart from vesicle transport, HTT participates in endocytosis and autophagy on a different level. The role of HTT in endocytosis may be explained via its interaction with HIP1 and HIP1R, which are involved in membrane invagination and clathrin coating, the initial steps of clathrin-mediated endocytosis[107-109]. In addition, HTT was found in a complex with endophilin, amphiphysin and dynamin and might therefore be involved in vesicle fission[110,111].

Evidence for HTT's involvement in autophagy comes directly from its secondary structure. Domains of the HTT protein show high similarity to yeast autophagy proteins Atg23, Vac8 and Atg11, suggesting that it is an autophagy-related protein[112]. HTT contains 11 LC3-interacting repeats (LIRs), which are essential motives in autophagy receptor proteins for linking cargos to LC3, thereby mediating selective autophagy. Furthermore, HTT binds to the ULK1 protein and thereby decreases its interaction with the protein mTOR, which in turn promotes phagophore formation[112,113].

Several lines of evidence point to the fact that HTT plays a role in gene expression. HTT has been shown to regulate the polycomb repressive complex 2 (PRC2) and to facilitate histone methylation[114]. In this way HTT influences the chromatin structure and regulates gene expression by transcriptional silencing. In addition, the polyQ domain in HTT enables the direct interaction with multiple transcription factors (cAMP-response element binding protein (CBP), specific protein-1 (SP1), nuclear factor-kB (NF-kB)) and transcriptional regulators (co-activator TAFII130, the repressor element-1 transcription factor/neuron restrictive silencer factor (REST/NRSF))[75,115-117]. HTT might act as a scaffold for transcriptional complexes and thereby either stimulate or repress gene transcription. More recently, HTT has also been shown to regulate gene expression on a post-transcriptional level by influencing P-body formation and RNA transport[118].

Furthermore, HTT was shown to be involved in the cellular stress response[119-124]. In this line the N17 domain was recently found to act as a sensor for reactive oxygen species (ROS), which trigger nuclear translocation of the protein, where it forms a complex with the ataxia-telangiectasia mutated protein (ATM) and participates in base excision repair[119,120]. HTT also regulates the activity of pro- and anti-apoptotic proteins (Bc-L2, Caspase 3/9, HIP-1, HIPPI) and modulates cell death and survival in response to cellular stress[121-124].

HTT function has been shown to be essential for embryogenesis and CNS development[77]. However, although many molecular functions have been assigned to the protein its precise physiological role in the adult brain remains elusive.

1.2.2. Protein Aggregation of Mutant HTTex1

Several N-terminal fragments of HTT, including HTTex1, emerge from proteolytic cleavage and alternative splicing events[73,74,88,125,126]. In case of HD, these fragments contain an expanded polyQ stretch that facilitates misfolding of the HTT protein fragments and triggers the formation of aggregates[127-132]. Intracellular deposition of mutant HTT aggregates into large, SDS-insoluble inclusion bodies counts as a pathological hallmark of HD. It has been shown that these supramolecular structures merely consist of mutant HTT fragments but also contain other cellular proteins such as ubiquitin, autophagy and UPS proteins and transcription factors[115,133,134].

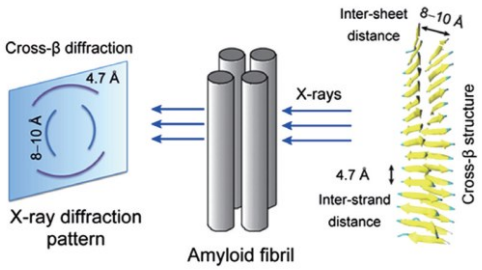

Figure 4: Amyloid fiber organization

Schematic illustration of a typical x-ray diffraction pattern of amyloid fibrils (left). Amyloid fibers have a cross-β-core structure consisting of multiple β-sheets forming along the fibrillar axis (middle, grey columns). β-sheets are composed of multiple molecules that are arrange perpendicular to the fibril axis (right). The acquired x-ray diffraction pattern provides information about the inter-strand and inter-sheet distance within the amyloid fiber. (Image adapted from Wen-Hui et al., 2016[135])

Looking more closely, these inclusions are composed of amyloid fibrils, which are highly organized crystal-like protein structures (Figure 4). Typically, the cross-β sheet core of an amyloid fiber is formed by several interacting β-sheets running in parallel to the axis of the fibril. Within these β-sheets, protein monomers in β-strand conformation are arranged perpendicular to the fibril axis and are stacked atop each other along the fibril axis. However, different types of amyloid fibers have been reported, whereby the precise molecular architecture as well as the forces stabilizing inter- and intramolecular interactions are determined by the protein that forms the amyloid fiber[136-138]. Within the last years significant advances have been made to understand the fibrillar structure of HTTex1 aggregates. Using solid state nuclear magnetic resonance (ssNMR) analysis, the expanded polyQ stretch within the HTTex1 has been shown to form an intramolecular β-hairpin, in which two β-strands of the same molecule are linked by a β-turn structure[139]. Multiple molecules with a β-hairpin conformation are stacked atop each other, stabilized by intra- and intermolecular hydrogen bonds between atoms of the protein backbones, thereby forming a tightly interconnected β-sheet. At the interface of adjacent β-sheets, side chains are believed to

intermesh and form steric zipper structures, that allow hydrogen bonding between stacked side chains and thereby facilitates a tight connection. As described before, within the HTTex1 fragment the polyQ stretch is flanked by N17 and PRD domains. These domains do not participate in the formation of the amyloid core structure[140]. Instead, they are immobilized and tightly clustered around the core structure, but distal parts of the N17 and PRD retain a certain degree of flexibility and solvent interaction (Figure 5). Within the mature fibril the PRD features a poly-L-proline type II helix which extends to the last glutamine residue of the amyloid core structure. The N17 domains form amphipathic α-helices that interact but remain flexible and loosely packed and help to stabilize the fibrils via molten-globule-like assemblies[140].

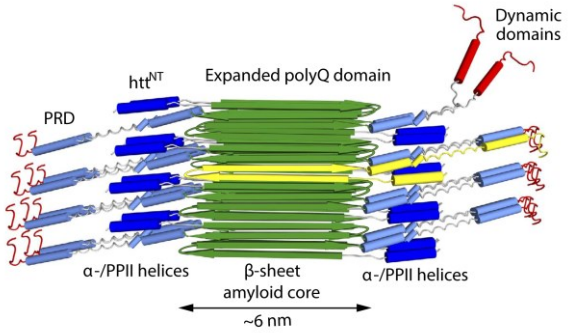

Figure 5: Proposed model of HTTex1 fibrils

The N17 α-helices (dark blue) and PRD poly-L-proline type II (PPII) helices (light blue) are immobilized and tightly clustered around the rigid amyloid core (green β-strands). An individual HTTex1 monomer with its β-hairpin-based polyQ core is shown in yellow. C-terminal tails of the PRD show higher structural flexibility. (Image was adapted from Lin et al., 2017[141])

The formation of amyloid fibers, starting from the HTTex1 monomer, is a complex and extensively debated process. As described before the HTTex1 molecule is highly flexible, [81,142,143]. It is considered as an intrinsically disordered protein (IDP) and switches rapidly between different conformations. At the beginning of the aggregation process occurs a conformational change of the polyQ domain from its flexible state to a β-sheet conformation of higher structural stability. This β-sheet formation is the initial creation of the amyloid architecture. It is also described as a primary nucleation event[98,138,144-146]. The rate of primary nucleation depends on the protein concentration and the length of the polyQ stretch[130,147]. It is more likely to occur with higher protein concentration and with longer glutamine tracts. Furthermore, this process is influenced by both the N17 and the PRD domain which exert opposing effects on the aggregation propensity of the HTTex1 molecule. Whereas the N17 domain has been reported to facilitate aggregation, the PRD was shown to counteract this process[148-150]. The PRD folds into a poly-L-proline type II (PPII) helix. It has been demonstrated that this conformation is propagated into the upstream

polyQ stretch, potentially increasing the energy barrier for the transition of the polyQ domain into the β-sheet conformation[83,84]. In contrast, the N17 domain has been reported to adopt an amphipathic α-helical conformation, possibly facilitating the docking of multiple HTTex1 molecules via coiled-coil interactions[151-153]. In accordance with Wetzel's proximity model this association brings polyQ stretches of different molecules into close proximity, consequently enhancing the polyQ-polyQ interaction and facilitating a coil-to-β-sheet transition (Figure 6)[154-157]. The initial formation of semi-stable oligomers involves conformational changes that are slow and unlikely to occur and therefore manifest in a lag phase when looking at the aggregation process from a kinetic point of view. After the formation of the primary nucleus, new monomers are recruited. They hydrogen-bond to the exposed beta-strands of the fibril ends and adapt the structure pre-specified by the amyloid core[98,138]. Fibril elongation is a rapid process as the conformational change occurring within newly recruited monomers is templated by the existing fibril[158,159].

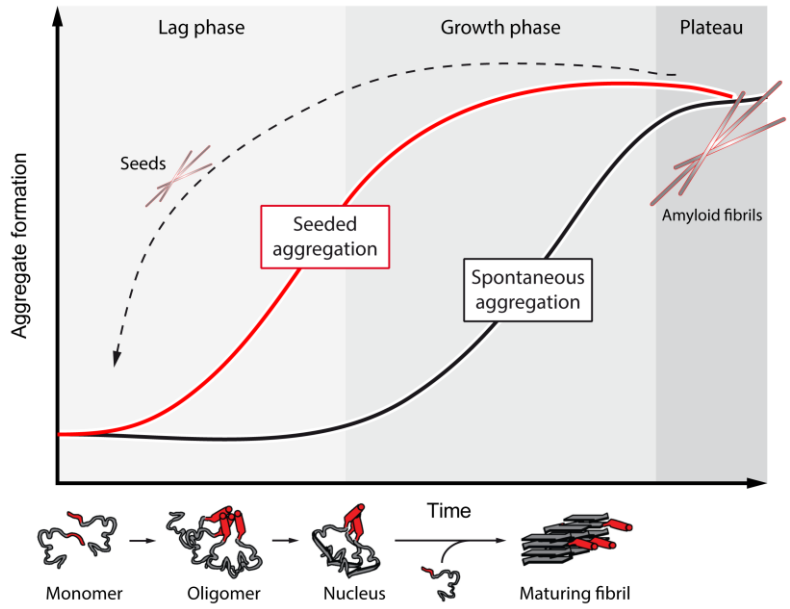

Figure 6: Schematic model of the N17-initiated HTTex1 aggregation process and its kinetic phases

Soluble HTTex1 monomers are considered intrinsically disordered and lack a well-defined structure. Spontaneous aggregation of HTTex1 is believed to be initiated through coiled-coil interactions of N17 domains. The N17 domain (red barrel) can adapt an amphipathic α-helical conformation which enables multiple molecules to interact. This brings polyQ domains (grey structure) of multiple molecules into close proximity and facilitates the transition to a β-sheet conformation within the polyQ domain (primary nucleation). The time-consuming conformational changes occur during the lag phase, when energetically very unstable nuclei are spontaneously formed. Thereafter, the fibrils mature through the template-mediated addition of monomers (growth phase). The N17 domain persist in an α-helical conformation outside the amyloid core. The PRD is not shown in this illustration. Once all monomers are integrated into amyloid fibrils the aggregation process reaches a plateau phase. The addition of preformed aggregates (Seeds) accelerates the aggregation of HTTex1 monomers. (Images in part from Sivanandam et al., 2011[160])

In addition to the elongation of the fibril ends, fibril breakage, branching and secondary nucleation on the surface of the fibrils have been reported to influence the aggregation process of HTTex1 and other amylogenic proteins[144,159]. When looking at the aggregation in a closed system, containing a finite number of HTTex1 monomers, the aggregation process will eventually reach a plateau phase in which all monomers are consumed and integrated into fibrillar assemblies. Therefore, the aggregation kinetics measured *in vitro* comprise a lag phase, a growth phase and a plateau phase and follow a typical sigmoidal curve which is indicative of the nucleation-dependent aggregation mechanism of HTTex1 (Figure 6)[144].

1.2.3. The Prion Hypothesis – Seeding and Spreading of HTTex1 Aggregates

As HTTex1 aggregation follows a nucleation dependent mechanism, it is hardly surprising that soluble HTTex1 monomers aggregate faster in the presence of pre-formed HTTex1 aggregates or oligomeric nuclei. This phenomenon, known as template-mediated aggregation or seeding, is accomplished through self-propagation of the administered seed hence bypassing the initial rate-limiting step of primary nucleation (Figure 6)[137,138,144]. The initiation of protein aggregation by templated conformational changes has been shown to be the cause of transmissible spongiform encephalopathies (TSEs) or prion diseases[161-163]. Originally, prions were defined as 'proteinaceous infectious particles' lacking nucleic acid and causing neurodegenerative diseases in humans and other mammals[163]. Aggregated prion proteins convert their natively folded counterpart into the amylogenic conformation (molecule-to-molecule transmission). They are transmitted from cell-to-cell via multiple mechanisms[164-167]. In addition, prion proteins are infectious in the microbiological sense of the term. Which means they are able to transmit the conformational change and the accompanied biological consequences from one organism to another (host-to-host transmission)[168,169].

Brain pathology in many neurodegenerative disorders follows a stereotypic pattern and is accompanied by the presence of protein aggregates[170-172]. This suggests that protein aggregates could act as the causative agent that spreads from one brain region to another causing pathological changes in a prion-like fashion. Therefore, the resemblance of HTT aggregates and prions gained increasing attention. HTT aggregates have been shown to accelerate the aggregation of purified HTTex1 protein or polyQ peptides in cell-free experiments[130,173]. In addition, HTTex1 and polyQ aggregates are able to penetrate cellular membranes and promote intracellular aggregation of fluorescently labeled HTTex1 molecules with a pathogenic or a non-pathogenic polyQ stretch[174-176]. Similar effects have been observed when HTT aggregates, derived from HD models or patients, were used as seeds[173,177]. This indicates that HTT aggregates, similar to prion aggregates, can transmit there conformations to another soluble HTT molecules

and trigger aggregation. In addition, cell-to-cell spreading has been observed for HTT aggregates[178-181]. Several mechanisms have been suggested to contribute to this process. Neurons, differentiated from human embryonic stem cells or induced pluripotent stem cells, were transplanted into organotypic brain slices of an HD mouse model and showed uptake of mutant HTT into grafted neurons followed by degeneration of the recipient cells. The transneuronal spread could be reduced by the admission of botulinum toxin, implying a transsynaptic mechanism[179]. Other studies proposed that transfer of mutant HTT aggregates might occur through tunneling nanotubes, extracellular vesicles or direct penetration of the plasma membrane[175,178,182,183].

There is increasing evidence that HTTex1 aggregates can initiate the misfolding of soluble HTT proteins and can propagate this conformational change to neighboring and remotely connected cells[175,178,182,183]. However, HTT aggregates differ from classical prion aggregates as they have not been shown to be transmitted between different hosts and are therefore not considered to be infectious. Nevertheless, the potential pathological role of HTT aggregates and their intercellular spread is intensively debated and an ongoing field of research.

1.3. Potential Mechanisms in Huntington's Disease

Huntington's disease is caused by the expansion of the CAG repeat in the coding region of the *HTT* gene. Although the genetic origin of HD has been identified long ago, the underlying pathological mechanisms are not fully understood[16].

As described before, HD is autosomal dominantly inherited, which implies that just one copy of the mutant gene is sufficient to cause the disease[24]. In addition, HD shares a similar disease pattern with the other nine polyglutamine diseases (dentatorubral pallidoluysian atrophy (DRPLA), spinobulbar muscular atrophy (SBMA) and spinocerebellar ataxia (SCA) type 1-3, 6, 7, 12 and 17) and expression of the expanded polyglutamine alone can cause toxicity in different disease models[184,185]. This supports the hypothesis that HD pathology is caused by a gain-of-function mechanism. However, many unique molecular functions have been assigned to the wild-type HTT protein and brain-specific knockout of HTT in adulthood leads to a neurodegenerative phenotype in mice, which argues that a loss-of-function mechanism could contribute to HD pathogenesis[68,103,186].

Understanding the course of events that lead to neurodegeneration would require to pin point the molecular species at the root of cellular dysfunction (Figure 7). In HD several possible culprits need to be taken into consideration: the HTT RNA, the monomeric HTT protein and the protein aggregates consisting of misfolded HTT proteins. Support that RNA-mediated effects might play a role in HD comes from studies on triplet repeat disorders in which neurodegeneration

is caused by elongated CAG repeat motifs in untranslated regions (UTRs)[187]. Hence, the presence of a CAG repeat-containing RNA, without translation into an expanded polyQ stretch, seems to be sufficient to cause toxicity[187,188]. It has been shown that HTT transcripts containing expanded CAG repeats can form hairpin conformations that bind and sequester different proteins into nuclear RNA foci leading to aberrant transcription and splicing[189-191]. The second potential cause of the disease is the monomeric mutant HTT protein. Expansion of the polyQ stretch and the associated alterations in proteolytic cleavage and post-translational modifications might change the protein's conformation, localization and interactions with other proteins[92,97,192]. Hence, HD could originate from the loss, gain or modulation of protein-protein interactions that perturb signaling pathways and lead to cellular dysfunction. The third candidate that could initiate the pathological cascade are misfolded protein assemblies of various size and stability. The hypothesis that mutant HTT aggregates potentially drive disease pathology arises from the correlation of CAG repeat length with aggregation propensity of the resulting polyQ stretch and disease onset[24,130]. This is further supported by studies in which HTT aggregation was enhanced through suppression of the proteostasis network, which leads to increased toxicity[193,194]. HTT aggregates sequester other cellular proteins as reported for several transcription factors, autophagy and UPS related proteins[195,196]. This might deplete aforementioned proteins from the cellular environment and disturb the processes they are essential for[115,197]. In addition, protein aggregation might cause an imbalance of proteostasis, as the quality control system is overwhelmed with constantly occurring misfolding events[198,199]. The formation of large inclusions might block intracellular routes of transportation[11,200]. Previously, large intracellular inclusions have been thought to be the main pathological species among the broad spectrum of misfolded HTT assemblies. However, an increasing number of studies brought the attention to submicroscopic soluble aggregates as potential major players in disease pathology and hypothesized that large inclusion bodies might have a protective role through sequestration of small highly reactive species[201,202]. Yet another layer of complexity was added with the discovery of repeat-associated non-ATG (RAN) translation in HD[203]. Due to the formation of secondary RNA structures, translation can be initiated independently of the start codon and can occur in sense and antisense direction in all three reading frames. In the HTT context, this leads to the expression of four additional repeat-containing proteins (polyAla, polySer, polyLeu, and polyCys) which also have been shown to form aggregates and to cause toxic effects in cells[203].

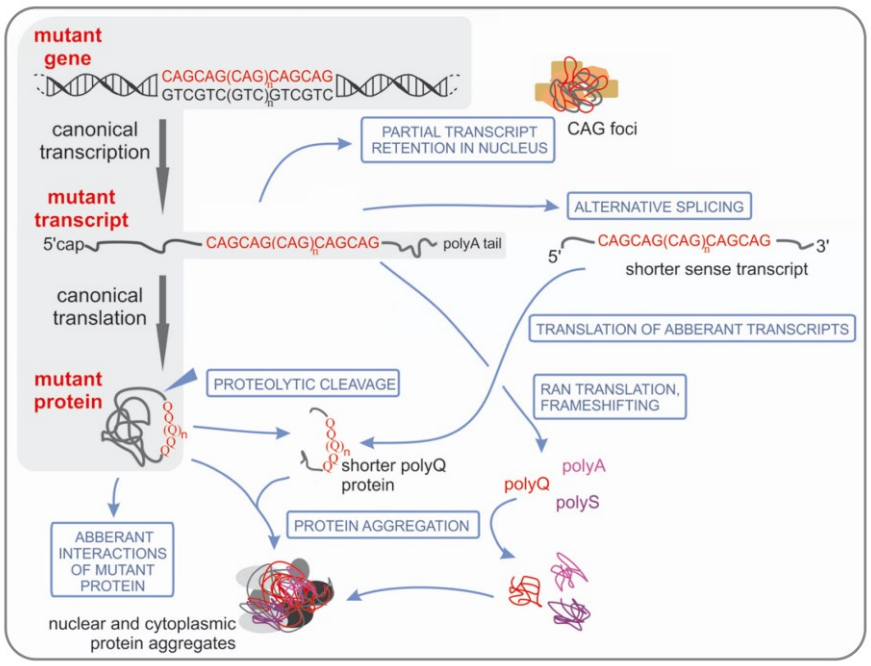

Figure 7: Potential toxic entities in the pathogenesis of Huntington's diseases

HD is caused by the CAG repeat expansion in the HTT gene. The main products of the mutant gene are the mutant transcript containing the expanded CAG repeats and the mutant protein containing the expanded polyQ tract. The mutant transcript shows an aberrant interaction with RNA binding proteins and is partially retained in the nucleus in the form of RNA/CAG foci. Alternative splicing of the mutant transcript and the translation of these splice products leads to the production of shorter N-terminal HTT fragments. Furthermore, the mutant transcript is subject to repeat-associated non-ATG (RAN) translation, leading to the formation of alternative repeat-containing proteins (polyA, polyS, polyL). The expanded polyQ stretch in mutant HTT might disturb protein-protein interactions. Furthermore, proteolytic cleavage of mutant HTT generates shorter polyQ-containing fragments that have the potential to form nuclear and cytoplasmic inclusions. (Image was adapted from Fiszer et al., 2014[204])

Although the pathological mechanism of HD has not been fully elucidated, several disease relevant changes were observed in HD models and patients. These include increased levels of oxidative stress, mitochondrial impairment, transcriptional dysregulation, disruption of protein homeostasis and disturbance of intracellular trafficking[205,206]. Future studies will need to distinguish cause and consequences in order to delineate the pathological mechanisms and to identify a causative treatment.

1.4. Biomarkers and Therapeutic Strategies

Down to the present day, there are no available disease-modifying drugs against Huntington's disease. Instead, treatment is symptomatic and involves a combination of pharmacological and non-pharmacological interventions[25,206-208]. On the non-pharmacological side, HD management involves physicians, nurses, speech therapists, dieticians and physiotherapists. Pharmacologically, the treatment options are limited. Tetrabenazine is the only

licensed drug to treat chorea symptoms[209]. Psychiatric symptoms, such as depression and irritability, are often treated as in non-HD patients[210,211]. With regard to the cognitive symptoms, there is currently no pharmacological treatment available[212,213].

In search of causal treatment options, several different strategies are pursued. This includes reduction of aggregate load[214], inhibition of caspases[215], upregulation of autophagy[216,217], and reduction of oxidative stress[206,208,218]. In each case initial results in mice were promising, but subsequent experiments or clinical trials in HD patients have not been successful[215,216,219-221]. Transplantation of neuronal tissue was considered as an approach to correct deficits once symptoms are manifest. However, a recent study following up on early human graft transplantations showed mutant HTT protein in the transplanted tissue[222]. A promising new strategy aims to lower the levels of mutant HTT by priming its RNA for degradation through the use of antisense oligonucleotides (ASOs), RNA interference (RNAi) or small molecule splicing modifiers[223-225]. Moreover, targeting the *HTT* gene directly has been considered as a treatment option[226]. As HD is a monogenic disorder, it would be a prime candidate for genetic correction using the rapidly developing gene editing approaches (CRISPR/Cas9 or Zinc finger nucleases). All these approaches have been successfully tested in rodent models and ASOs are currently under investigation in phase I clinical trials[224,227].

In order to test the efficacy of newly developed therapeutic candidates, sensitive biomarkers are needed that detect pathological changes early and track them over time. These markers need to be objectively measurable, predict a clinically meaningful endpoint, have an association with known disease mechanisms and respond to therapy[207]. Clinical markers have been established, but the assessment of motor, cognitive and psychiatric parameters shows only little changes in the pre-manifest phase of the disease and their assessment remains subjective[228]. Image based techniques, such as magnetic resonance imaging (MRI), have revealed atrophy of specific brain regions years before symptomatic onset [229]. Several biofluidic parameters are currently evaluated for their use as biomarkers. Levels of neurofilament light chain (NFL) in cerebrospinal fluid (CSF) and blood or the levels of mutant HTT in CSF are promising candidates and correlate with disease progression[230-232]. The development and validation of new biomarkers is an important ongoing endeavor, that might support future clinical trials and empower the search for a cure of Huntington's disease.

2. Aim of the study

Aggregation of the mutant HTT (mHTT) protein is a major hallmark of HD pathology. The deposition of misfolded mHTT proteins has been proposed to be either the cause of disease or a byproduct in the pathogenic cascade *(Chapter 1.3)*. It is essential to better understand the role of prion-like mHTT aggregates in HD in order to develop effective therapeutic strategies. Therefore, one aim of this study was to establish a sensitive assay for the detection of seeding-competent mHTT aggregates in biological samples prepared from HD patients and model organisms. Seeding-competent aggregates should be characterized regarding their size and morphology. Furthermore, it should be analyzed whether the abundance of these structures correlates with disease-associated phenotypes in model systems and whether seeding-competent mHTT aggregates could be used as a biomarker to monitor progression or onset in HD. In the second part of this study the established mHTT seeding assay should be used to address the question whether seeding-competent mHTT aggregates drive HD pathology. For this purpose, structure-guided mutagenesis was utilized in order to change the aggregation properties of mHTTex1 proteins. The effects of targeted amino acid exchanges on aggregation and proteotoxicity should be analyzed *in vitro* and in newly generated *Drosophila* models using a combination of biochemical and behavioral assays. These experiments were intended to assess the relationship between aggregate properties, seeding activity and aggregate-induced toxicity in an HD *in vivo* model.

3. Results

3.1. Mutant HTT seeding activity: a marker of disease progression and neurotoxicity in models of Huntington's disease*

Self-propagating protein aggregates are a pathological hallmark of a large number of neurodegenerative diseases (NDs) including Huntington's disease (HD)[137,171]. To understand the involvement of such structures in disease development and progression, it is critical to monitor the activity of self-propagating protein aggregates in complex biosamples. Until now a few cell-free and cell-based assays have been established that facilitate the quantification of seeding activity of amylogenic aggregates by taking advantage of the phenomenon that ordered protein aggregates accelerate spontaneous aggregation of the monomeric protein[177,233-236]. In cell-free assays seed-mediated amyloid polymerization is indirectly monitored through the reporter dye Thioflavin T (ThT), which changes its fluorescence emission upon binding to ordered amyloid fibrils[173]. Cell-based seeding assays rely on ectopically expressed aggregation-prone reporter proteins with fluorescent tags as biosensors for detecting amyloidogenic aggregates[177,234]. Both strategies exhibit weaknesses when monitoring seed-mediated aggregation. Binding of ThT is decreased when competing proteins are present[237], which demands additional sample preparation else reduces the sensitivity of the assay when biosamples such as brain homogenates are analyzed. Cell-based assays are more laborious and typically measure only a specific endpoint of the seed-mediated aggregation instead of monitoring the kinetic process, thereby loosing relevant information.

To overcome these limitations, in the first part of my studies I focused on the development and optimization of a dye- and cell-free seeding assay that facilitates the detection and quantification of seeding-competent mHTT aggregates based on the physical principle of fluorescence resonance energy transfer (FRET). I further describe the application of this assays with the aim to quantify seeding activity in biological samples and to elucidate the role of seeding-competent mHTT aggregates in HD.

3.1.1. Development of a FRET-based mutant HTT aggregate seeding (FRASE) assay

To monitor mHTT seeding activity, a cell-free aggregation assay with recombinant fluorescent reporter proteins was developed (Figure 8A). An aggregation-prone N-terminal HTT exon 1 protein fragment with 48 glutamines (Ex1Q48) was fused N-terminally to

* *The text and figures in chapter 3.1 have been reused with modifications from the published version: Ast, A. et al. mHTT Seeding Activity: A Marker of Disease Progression and Neurotoxicity in Models of Huntington's Disease. Mol Cell 71, 675-688 e676, doi:10.1016/j.molcel.2018.07.032 (2018) - https://doi.org/10.1016/j.molcel.2018.07.032.*

glutathione S-transferase (GST) and C-terminally to CyPet or YPet (GST-Ex1Q48-CyPet or -YPet). The N-terminal GST tag enables purification of the fusion proteins via glutathione sepharose chromatography and prevents spontaneous aggregation of Ex1Q48.

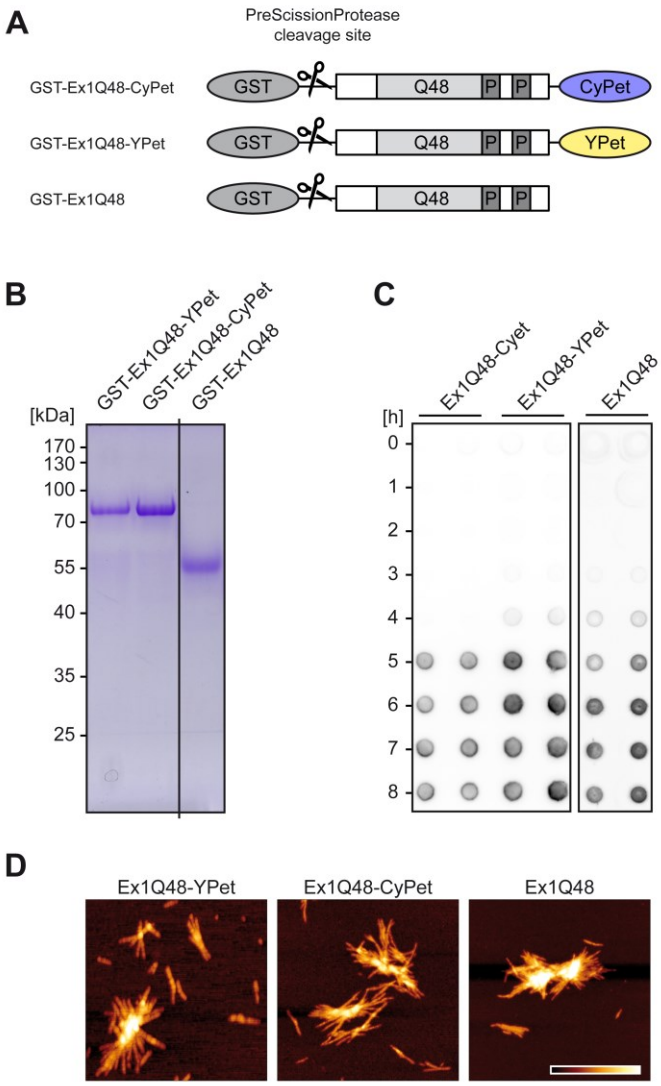

Figure 8: Development and characterization of GST-Ex1Q48-CyPet and -YPet reporter proteins

(A) *Schematic representation of the applied GST-tagged HTTex1 fusion proteins with pathogenic polyQ tracts. P, proline-rich regions.* ***(B)*** *The recombinant GST-Ex1Q48-CyPet and -YPet and GST-Ex1Q48 fusion proteins were affinity purified using glutathione-coated sepharose beads. Purity was assessed by SDS-PAGE and subsequent Coomassie blue staining.* ***(C)*** *Analysis of the aggregation propensity of proteolytically cleaved GST-Ex1Q48-CyPet and -YPet and GST-Ex1Q48 fusion proteins. Proteins (3 µM) were individually incubated at 25 °C with PreScission protease (PSP); time-dependent formation of SDS-resistant aggregates was analyzed by FRA (500 ng protein per dot). Spontaneously formed aggregates of fluorescently tagged and untagged Ex1Q48 proteins were visualized by an anti-GFP (ab290) antibody and an anti-HTT (CAG35b) antibody respectively.* ***(D)*** *Atomic force microscopy (AFM) analysis of spontaneously formed Ex1Q48-CyPet, Ex1Q48-YPet and Ex1Q48 aggregates (3 µM) after 24 h. Scale bar: 1 µm; color gradient represents 0-20 nm height.*

Reporter proteins were produced in E. coli and purified to ~90% homogeneity (Figure 8B). First, I performed aggregation assays with both reporter proteins and untagged GST-Ex1Q48 protein (Figure 8A and B), in order to assess whether the fluorescent tags change the aggregation behavior of the reporter proteins or the morphology of the resulting aggregates. Recombinant proteins were cleaved with PreScission protease (PSP) to release GST and to initiate the spontaneous aggregation of the fusion proteins. The assembly of the tagged and untagged Ex1Q48 proteins into insoluble aggregates over time was monitored using an established filter retardation assay (FRA), which specifically detects large SDS-stable mHTT aggregates[238]. I found that Ex1Q48-CyPet and -YPet proteins rapidly self-assemble into SDS-stable aggregates, similar to untagged Ex1Q48 (Figure 8C). To investigate the morphology of spontaneously formed Ex1Q48-CyPet and -YPet aggregates, aggregation reactions were analyzed with atomic force microscopy (AFM). Tagged Ex1Q48 fusion proteins, similar to the untagged Ex1Q48 protein[159], form large fibrillar protein aggregates (Figure 8D). These results suggest that C-terminal fusion of the fluorescent proteins CyPet or YPet does not significantly change the aggregation behavior of Ex1Q48. Hence, Ex1Q48-CyPet and -YPet fusion proteins can be used to monitor mHTTex1 aggregation *in vitro*.

I hypothesized that co-aggregation of CyPet- and YPet-tagged HTTex1 fragments should lead to a time-dependent increase of FRET as the fluorescent tags are brought in close proximity when fibrillar aggregates are formed (Figure 9A). Mixtures of fusion proteins (1:1 molar ratio; 1 - 3 µM concentrations) were treated with PSP and the spontaneous formation of Ex1Q48-CyPet/-YPet co-aggregates was quantified by repeated FRET measurements. I observed a time- and concentration-dependent increase of FRET efficiency (Figure 9B), indicating that FRET measurements are suitable to quantify HTTex1 co-aggregation. In contrast, no time-dependent increase of FRET efficiency was observed in samples that were not treated with PSP, underlining that the removal of the GST tag from CyPet- and YPet-tagged Ex1Q48 fragments is critical for the self-assembly of co-aggregates. AFM analysis confirmed that the samples indeed contain typical fibrillar HTTex1 aggregates (Figure 9C).

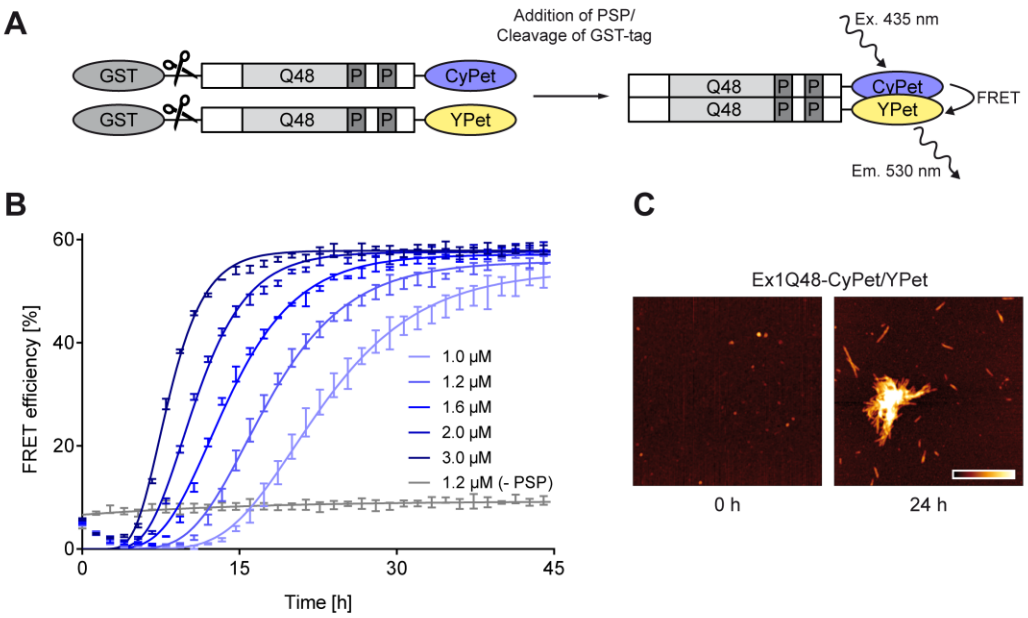

Figure 9: Monitoring spontaneous Ex1Q48-CyPet/-YPet co-aggregation by FRET

(A) *Schematic model of the spontaneous FRET-inducing Ex1Q48-CyPet/-YPet co-aggregation reaction in cell-free assays. Initially, the N-terminal GST-tag keeps the fusion proteins in a soluble state and prevents spontaneous aggregation. After PSP-mediated cleavage of the fusion proteins, Ex1Q48-CyPet and -YPet fragments are released and spontaneously co-aggregate over time. FRET signal is detected when fluorescent tags come into close proximity in ordered protein aggregates.* ***(B)*** *Investigation of spontaneous co-aggregation of sensor proteins by time-dependent quantification of FRET. Indicated concentrations of the GST-tagged sensor proteins Ex1Q48-CyPet and -YPet (1:1 mixture) were incubated at 25 °C in the presence and absence of PSP. The initial FRET signal of ~6% is due to oligomerization of uncleaved GST fusion proteins under non-denaturating conditions. FRET efficiency is displayed as mean ± SD of technical triplicates.* ***(C)*** *AFM analysis of the co-aggregated sensor proteins Ex1Q48-CyPet/-YPet (3 µM). Scale bar: 1 µm; color gradient represents 0-20 nm height.*

In order to assess whether preformed Ex1Q48 fibrils can seed the co-aggregation of Ex1Q48-CyPet/-YPet, a 1:1 mixture of the GST fusion proteins was incubated with PSP and different amounts of preformed Ex1Q48 fibrils as seeds (prepared by site-specific cleavage of the GST tag and spontaneous self-assembly for 24 hours) (Figure 8D). I observed that addition of fibrils shortens the lag phase of Ex1Q48-CyPet/-YPet polymerization in a concentration-dependent manner (Figure 10A), suggesting that they possess seeding activity. Next, I asked whether shortening of the lag phase indeed results from the templating effect of mHTTex1 aggregates or merely from an increase in mHTTex1 protein concentration when untagged Ex1Q48 protein is added. In order to address this question, I prepared Ex1Q48 protein samples from different aggregation states (soluble, partially aggregated and fully aggregated) by treating GST-Ex1Q48 with PSP and collecting samples at different time points (0, 1, 2, 3, 4, 24 h). Equal amounts of these samples were added to Ex1Q48-CyPet/-YPet polymerization reactions and co-aggregation of the reporter proteins was monitored by FRET measurements (Figure 10B). In parallel, these samples

were analyzed for the formation of mHTTex1 aggregates using the FRA (Figure 10C). Protein samples taken directly (0 h) or 1 h after the addition of PSP did not contain fibrillar aggregates, as confirmed by FRA. This indicates that theses samples predominantly contain soluble GST-Ex1Q48 and Ex1Q48 protein fragments. The addition of these samples to Ex1Q48-CyPet/-YPet reporter proteins did not accelerate their co-aggregation. In contrast, the addition of samples with partially aggregated Ex1Q48 protein (taken 2 - 3 hours after PSP addition) shortened the lag phase of reporter protein assembly. This effect was even more pronounced when fully aggregated Ex1Q48 protein samples (taken 4 and 24h after addition of PSP) were analyzed for their propensity to seed the polymerization of Ex1Q48-CyPet/-YPet (Figure 10B-C). This indicates that the observed shortening of the lag phase cannot be ascribed to an increase in mHTTex1 protein concentration, but indeed results from the templating effect of Ex1Q48 aggregates.

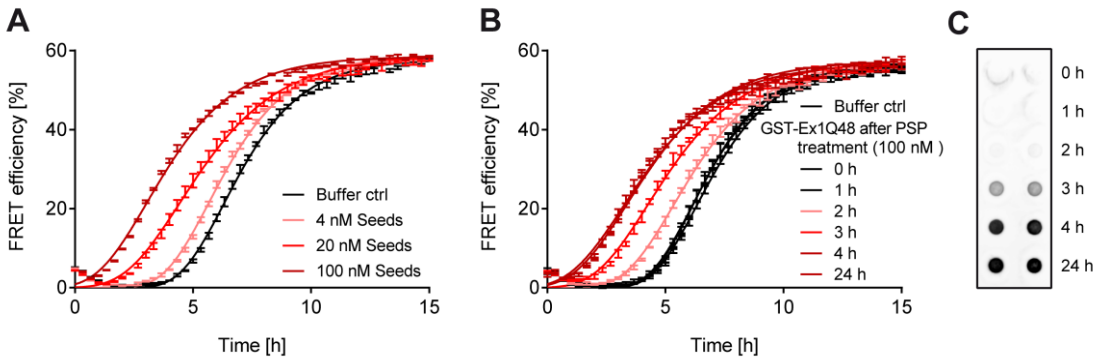

Figure 10: Recombinant Ex1Q48 aggregates are seeding-competent structures

(A) *Preformed, fibrillar Ex1Q48 aggregates (seeds) induce a concentration-dependent acceleration of Ex1Q48-CyPet/-YPet (2 µM) polymerization in cell-free assays. Co-aggregation of the fluorescence sensor proteins was monitored by quantification of FRET. Indicated seed concentrations are equivalent to initially applied monomer concentrations. FRET efficiency is displayed as mean ± SD of technical triplicates.* ***(B)*** *Analysis of reporter protein (2 µM) aggregation in the presence of 100 nM Ex1Q48 protein at different aggregation states. FRET efficiency is displayed as mean ± SD of technical triplicates.* ***(C)*** *Detection of large SDS-stable aggregates by filter retardation assay (FRA) in Ex1Q48 (2.5 µM) protein preparations (500 ng/dot) assessed in* ***B.*** *Aggregates were immuno-detected using the anti-HTT antibody CAG53b.*

In order to substantiate these results, I performed independent control experiments with GST-HTTex1 fusion proteins containing 23, 48 and 75 glutamines (Figure 11A). Fusion proteins were treated with PSP to release Ex1 protein fragments. The formation of large SDS-stable aggregates was assessed by FRA after 24 h. As expected, HTTex1 protein fragments containing a glutamine stretch in the pathogenic range (Ex1Q48 and Ex1Q75) assembled into SDS-stable aggregates as indicated by the presence of immunoreactive dots 24 hours after PSP-mediated cleavage of the GST tag. In comparison, Ex1Q23 contains a glutamine stretch in the non-pathogenic range and does not form SDS-stable aggregates under the conditions applied in

this experiment (Figure 11B). AFM analysis was performed and confirmed that Ex1Q48 as well as Ex1Q75 proteins form fibrillar HTTex1 aggregates after incubation for 24h (Figure 11C). Finally, these protein samples were analyzed for their potential to seed the co-aggregation of Ex1Q48-CyPet/-YPet reporter proteins. I found that Ex1Q48 and Ex1Q75 aggregates were both capable of accelerating the co-aggregation of sensor proteins, whereas the addition of proteolytically cleaved GST-Ex1Q23 did not shorten the lag phase of Ex1Q48-CyPet/-YPet polymerization (Figure 11D).

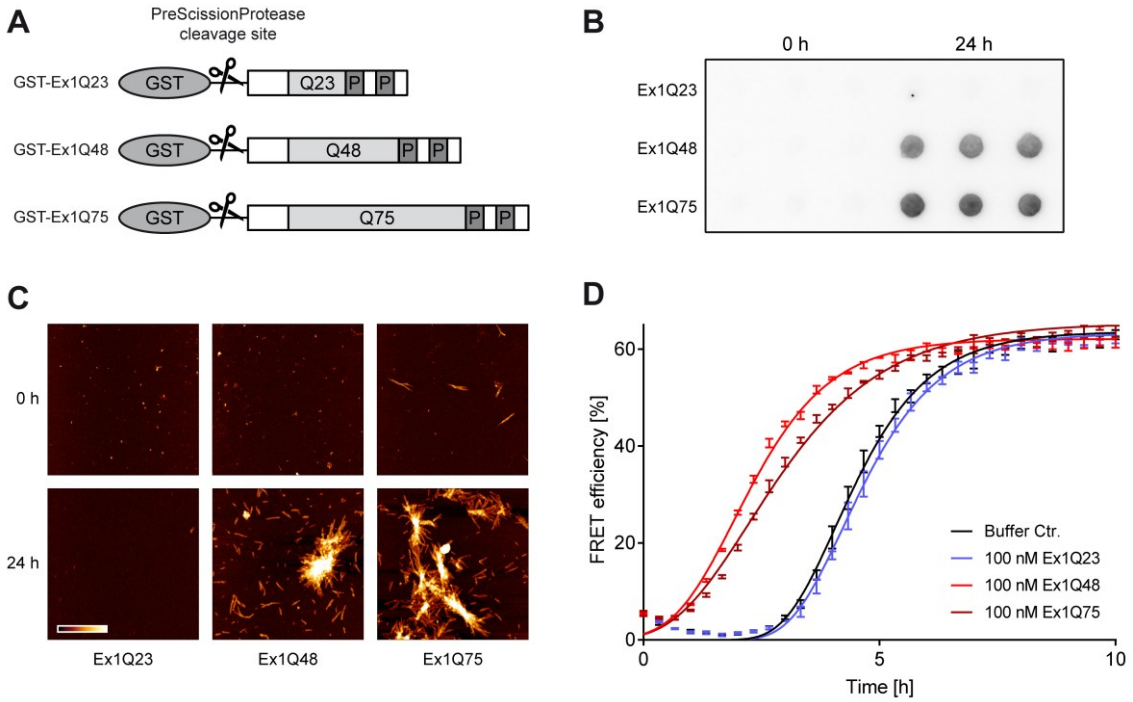

Figure 11: HTTex1 proteins with pathogenic polyQ tracts form seeding-competent aggregates

(A) *Schematic representation of GST-tagged HTTex1 fusion proteins with pathogenic and non-pathogenic polyQ tracts. P, proline-rich regions.* ***(B)*** *Analysis of spontaneously formed aggregates from HTTex1 proteins (2 µM) with pathogenic and non-pathogenic polyQ tracts using FRA. Immunodetection was performed using an anti-HTT (CAG53b) antibody.* ***(C)*** *AFM analysis of samples analyzed in* ***B****. Scale bar: 1 µm; color gradient represents 0-20 nm height.* ***(D)*** *FRET-based assessment of Ex1Q48-CyPet/-YPet (2 µM) co-aggregation in the presence of 100 nM HTTex1 proteins with pathogenic and non-pathogenic polyQ tracts. FRET efficiency is displayed as mean ± SD of technical triplicates.*

In order to compare seeding effects of different samples it is necessary to precisely quantify to which extend reporter protein aggregation was accelerated. For this purpose, FRET efficiencies measured over time (Figure 12A) were curve fitted by Richard's five-parameter dose-response curve using GraphPad Prism to obtain t_{50} values (time at half-maximal FRET efficiency) for each of the analyzed curves (Figure 12B). Subsequently, the temporal shifts (Δt_{50}), resulting from the addition of seeds, were quantified by subtracting the t_{50} values of the respective

sample from t_{50} value of the negative control (Figure 12C). The established method, which permits the detection of mHTT seeding activity (Δt_{50}, HSA) in samples of interest, was termed FRET-based HTT aggregate seeding (FRASE) assay.

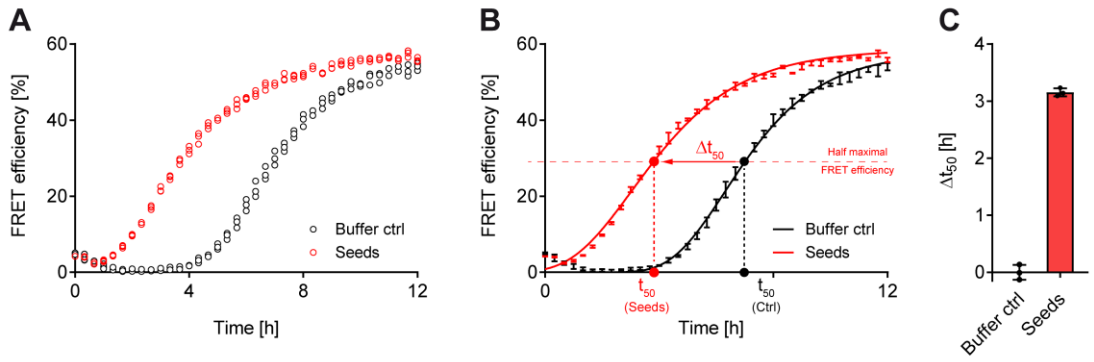

Figure 12: Quantification of mHTT seeding activity (HSA)

(A) Exemplified FRET efficiency measurements over time of seeded (red) and spontaneous (black) reporter protein polymerization. (B) Curve fitted aggregation profile of A as an example to calculate mHTT seeding activity (HSA; Δt_{50}) by subtracting the t_{50} value of the seeded Ex1Q48-CyPet/-YPet aggregation reaction from the t_{50} value of the spontaneous aggregation reaction. (C) Depiction of HSA quantified from B.

3.1.2. Optimization of mHTTex1 seed detection

The FRASE assay is intended to measure seeding activity in biological samples. For this purpose, the assay needs to reliably detect seeding-competent mHTT aggregates with high sensitivity. The following chapter will describe the optimization of the FRASE assay regarding its sensitivity.

Initial experiments indicate that large bundles of Ex1Q48 or Ex1Q75 fibrils (~1-2 µm in length; Figure 11C) possess mHTT seeding activity (HSA)(Figure 10 and Figure 11). I reasoned that fragmentation of these large aggregates will naturally increase the number misfolded mHTT assemblies and consequently enlarges the area of exposed surface, which functions as initiation point of template-mediated mHTTex1 aggregation. Hence, fragmentation of mHTTex1 fibrils prior to FRASE analysis could increase assay sensitivity. In order to test this hypothesis, large preformed Ex1Q48 fibrils were sonicated for different periods of time and subsequently analyzed by FRASE assays (Figure 13A). I observed that the longer preformed Ex1Q48 fibrils were sonicated the higher was the detected seeding activity (Figure 13A and B). To confirm that indeed small fibrils are produced, I analyzed the generated samples by FRA[238]. Large Ex1Q48 aggregates were detected in non-sonicated samples (Figure 13C), while they were not observed in sonicated samples (>30 sec). This indicates that sonication (>30 sec) leads to fibril breakage and the formation of small mHTTex1 structures that are no longer retained on filter membranes (0.2 µm pore size).

Next, the samples were analyzed by dot blot (DB) assays, which allow the identification of protein assemblies on filter membranes independent of their size[239]. These experiments revealed Ex1Q48 immunoreactivity in both sonicated and non-sonicated samples (Figure 13C), confirming the presence of Ex1Q48 protein in all samples. Finally, I analyzed the generated samples with AFM, demonstrating that small fibrillar Ex1Q48 structures are produced by sonication (Figure 13D). These results suggest that sonication of samples prior to FRASE analysis can increase the sensitivity of the measurement and facilitate the detection of low amounts of seeding-competent aggregates. Furthermore, my analysis demonstrates that FRASE assays detect both large and small

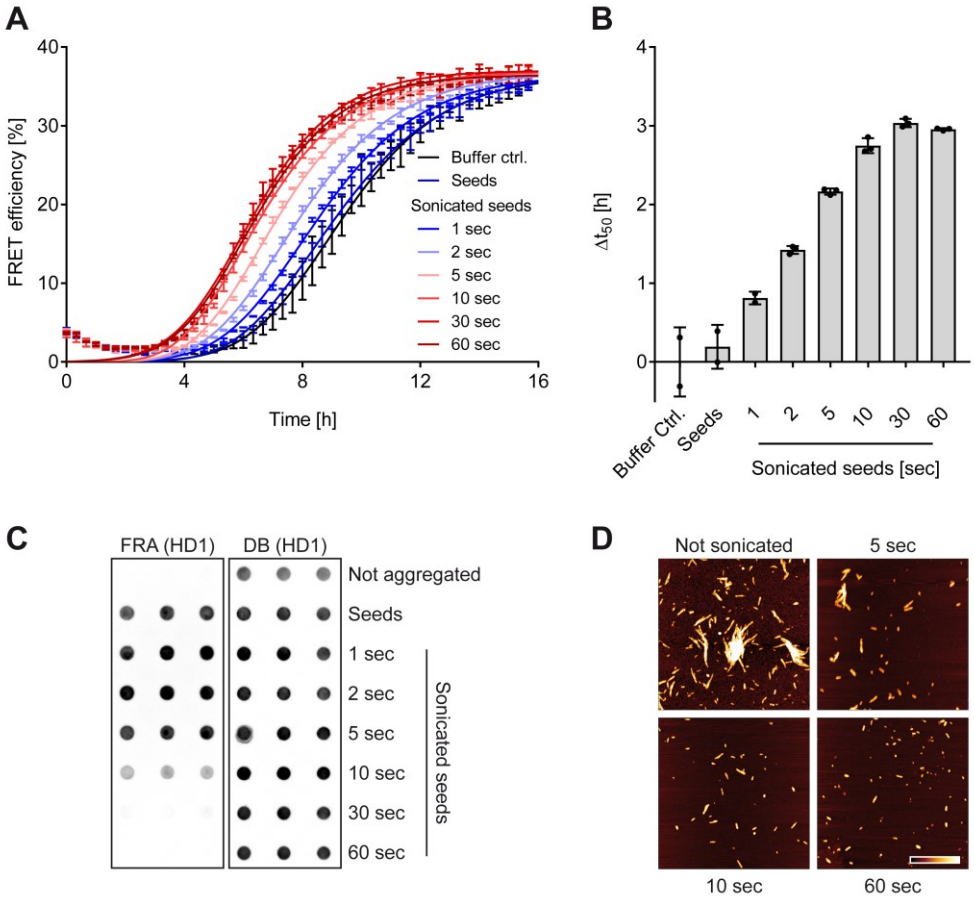

Figure 13: Fragmentation of recombinant Ex1Q48 aggregates enhances seeding activity

(A) *Sonication of preformed, fibrillar Ex1Q48 aggregates enhances HSA detected by FRASE. Fibrillar Ex1Q48 aggregates were produced by incubating GST-Ex1Q48 fusion protein (2 µM) for 24 h at 25 °C. Preformed Ex1Q48 aggregates (1 nM) were added to the Ex1Q48-CyPet/-YPet (2 µM) aggregation reactions. Data are shown as means ± SD of 3 technical replicates.* ***(B)*** *Calculated Δt_{50} values from Ex1Q48-CyPet/-YPet aggregation profiles in* ***A****. Individual Δt_{50} values of each triplicate are displayed as black dots (●) and mean ± SD of technical triplicates.* ***(C)*** *Analysis of sonicated and non-sonicated Ex1Q48 seeds by denaturing filter retardation (FRA, left panel) and dot blot (DB, right panel) assays using an anti-HTT (HD1) antibody. Fragmentation of large fibrillar Ex1Q48 aggregates by sonication prevents their detection in FRAs.* ***(D)*** *Preformed Ex1Q48 fibrils were sonicated for the indicated times and visualized by AFM. Sonication reduces the size of preformed fibrillar Ex1Q48 aggregates. Scale bar: 1 µm; color gradient represents 0-20 nm height.*

mHTTex1 aggregates which is an advancement over state-of the-art aggregate detection methods such as the FRA, which is limited to the detection of large SDS-stable aggregates.

Besides pre-treatment of sample material prior to FRASE analysis, the reporter system itself was optimized. Seeding activity is defined as shortening of the lag phase in comparison to an unseeded aggregation reaction of the reporter proteins. This implies that the length of the lag phase of an unseeded reaction influences the sensitivity of the assay and the resolution that can be reached to distinguish samples of different seed concentrations. Hence, extending the lag phase of Ex1Q48-CyPet/-YPet polymerization, might improve assay sensitivity and resolution.

In accordance with the standard aggregation protocol of the Wanker lab, reporter proteins are ultracentrifuged prior to each FRASE assay in order to remove small preformed protein assemblies that could act as seeds in the aggregation reaction. Under the assumption that active seeds may be protein assemblies with extremely low sizes, it is unlikely that ultracentrifugation will completely remove them from the applied fluorescent GST-tagged reporter proteins. Nevertheless, increasing the speed of ultracentrifugation would clear the protein solution of even smaller assemblies resulting in a reporter protein solution containing less seeding-competent material. Hence, unseeded polymerizations of reporter proteins should have a longer lag phase which offers the opportunity to detect even lower amounts of mHTTex1 seeds. In order to experimentally address these questions, GST-Ex1Q48-CyPet and -Ex1Q48-YPet fusion proteins were ultracentrifuged under standard conditions (163,348 x g, Figure 14A) or at even higher speed (187,972 x g, Figure 14B) prior to their use as seeding sensors in the presence of sonicated Ex1Q48 seeds. As expected, stronger centrifugation increased the duration of the lag phase of spontaneous reporter protein polymerization (represented by t_{50} values in Figure 14C). In addition, low concentrations of sonicated Ex1Q48 seeds, which were undetectable when reporter proteins were centrifuged under standard conditions (0.05 and 0.01 nM), can now be quantified with the FRASE assay (Figure 14D). Together these studies indicate that assay sensitivity was improved by increasing the centrifugation speed in the preparation of sensor proteins for FRASE measurements.

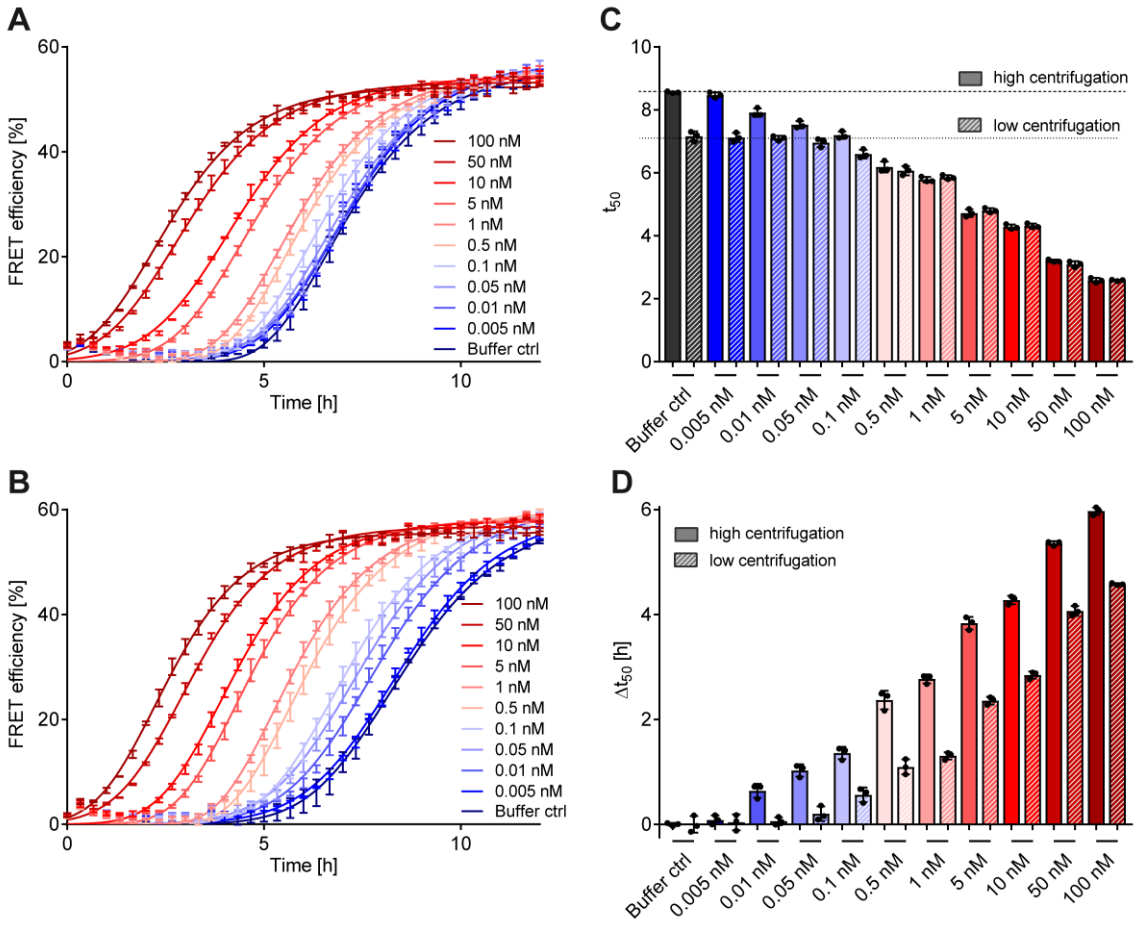

Figure 14: Increasing the centrifugation speed during sensor protein preparation improves seed detection

(A) *FRASE analysis of different concentrations of sonicated Ex1Q48 seeds using Ex1Q48-CyPet/-YPet proteins (2 µM) centrifuged for 40 min at 163,348 x g (low centrifugation) or* ***(B)*** *at 187,972 x g (high centrifugation) prior to their application as reporter proteins.* ***(C)*** *Analysis of* t_{50} *values calculated from* ***A*** *and* ***B*** *indicates a longer lag phase for the spontaneous aggregation of reporter proteins when they were centrifuged at higher speed. Lag phase of seeded reactions are shortened in a concentration dependent manner.* ***(D)*** *Calculation of HSA from* ***A*** *and* ***B*** *illustrates that lower concentrations of preformed Ex1Q48 seeds can be detected when the reporter proteins are centrifuged at a higher speed prior to their use in FRASE assays. Data are mean ± SD of technical triplicates.*

As described previously, mHTTex1 aggregation is a nucleation-dependent process[159]. The rate of primary nucleation, which is the initial conformational conversion of soluble mHTTex1 monomers to a stable β-sheet structure, largely depends on the protein concentration and the length of the polyQ stretch. Therefore, reducing the concentration of sensor proteins or shortening the length of the polyQ stretch in the sensor proteins is expected to decrease the propensity of primary nucleation. This is supposed to extend the lag phase and might therefore improve the sensitivity of the assay.

First, I assessed whether seed detection can be improved by reducing the concentration of sensor proteins. Ex1Q48-CyPet/-YPet polymerization was monitored at different

concentrations in the absence or presence of 1 nM preformed Ex1Q48 seeds (Figure 15A). For spontaneous aggregation reactions I observed a clear extension of the lag phase, when lower concentrations of the reporter proteins (Ex1Q48-CyPet/-YPet) were applied. Upon the addition of Ex1Q48 seeds, HSA was detectable in all cases regardless of the sensor protein concentration. Quantitative analysis revealed the largest temporal shift for the lowest sensor protein concentration, indicating that a reduction of sensor protein concentration can improve the sensitivity of the assay (Figure 15B). In order to validate this finding, the Ex1Q48-CyPet/-YPet reporter proteins, at a concentration of 1.2 µM, were incubated with different amounts of sonicated ExQ48 seeds and HSAs were quantified (Figure 15C and D).

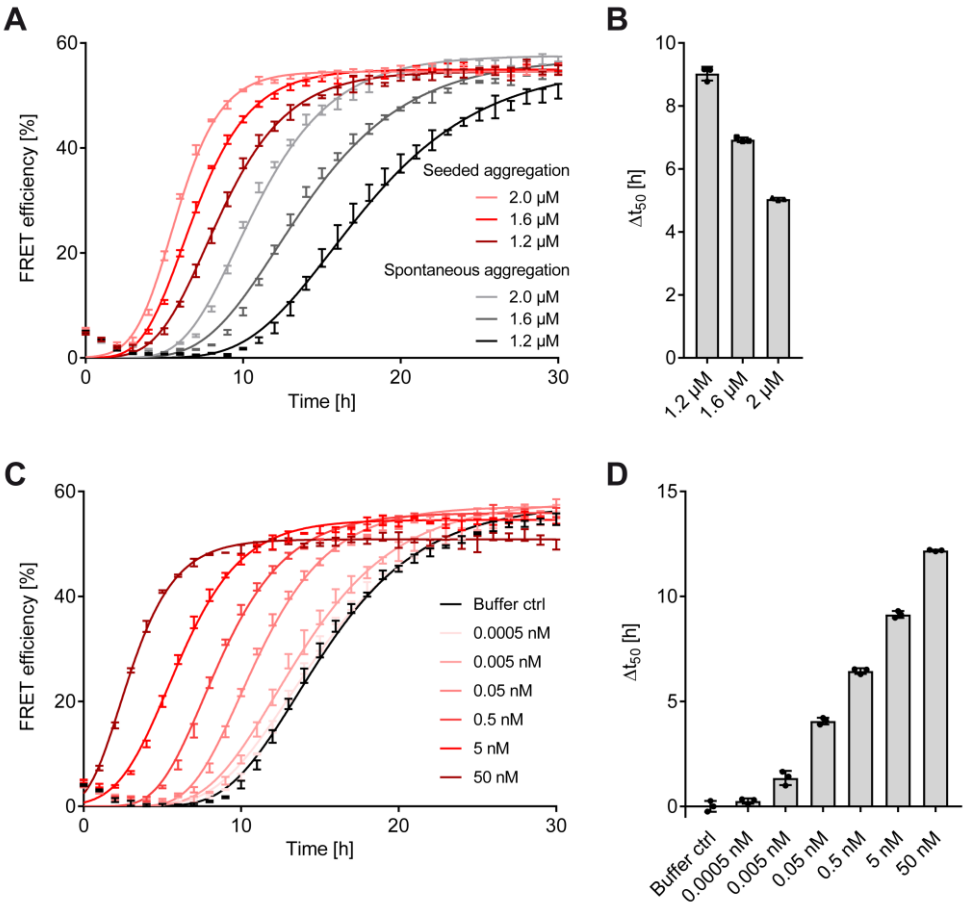

Figure 15: Lowering the sensor protein concentration improves the sensitivity of the FRASE assay

(A) *Monitoring mHTTex1 co-aggregation at indicated concentrations of the reporter proteins Ex1Q48-CyPet/-YPet in the absence or presence of 1 nM sonicated Ex1Q48 seeds.* ***(B)*** *Calculation of HSA from seeded and spontaneous aggregation reactions in* ***A*** *reveals higher* Δt_{50} *values for lower reporter protein concentrations.* ***(C)*** *FRASE analysis of indicated concentrations of preformed sonicated Ex1Q48 seeds (equivalent to monomers) using a low concentration of the reporter proteins Ex1Q48-CyPet/-YPet (1.2 µM).* ***(D)*** *Quantification of HSA from aggregation profiles in* ***C****. Seeds are already detectable at a concentration of 0.005 nM. All data are mean ± SD of technical triplicates.*

Previous experiments revealed that seed concentrations of 0.01 nM are detectable when sensor protein concentrations of 2 µM are applied (Figure 14D). Using a sensor protein concentration of 1.2 µM, however, HSA was already detectable with a seed concentration of 0.005 nM, confirming that lowering the sensor protein concentration improves the detection of mHTTex1 seeds.

Next, I investigated whether a shortening of the polyQ tracts in the reporter proteins influences the sensitivity of seed detection with FRASE assays.

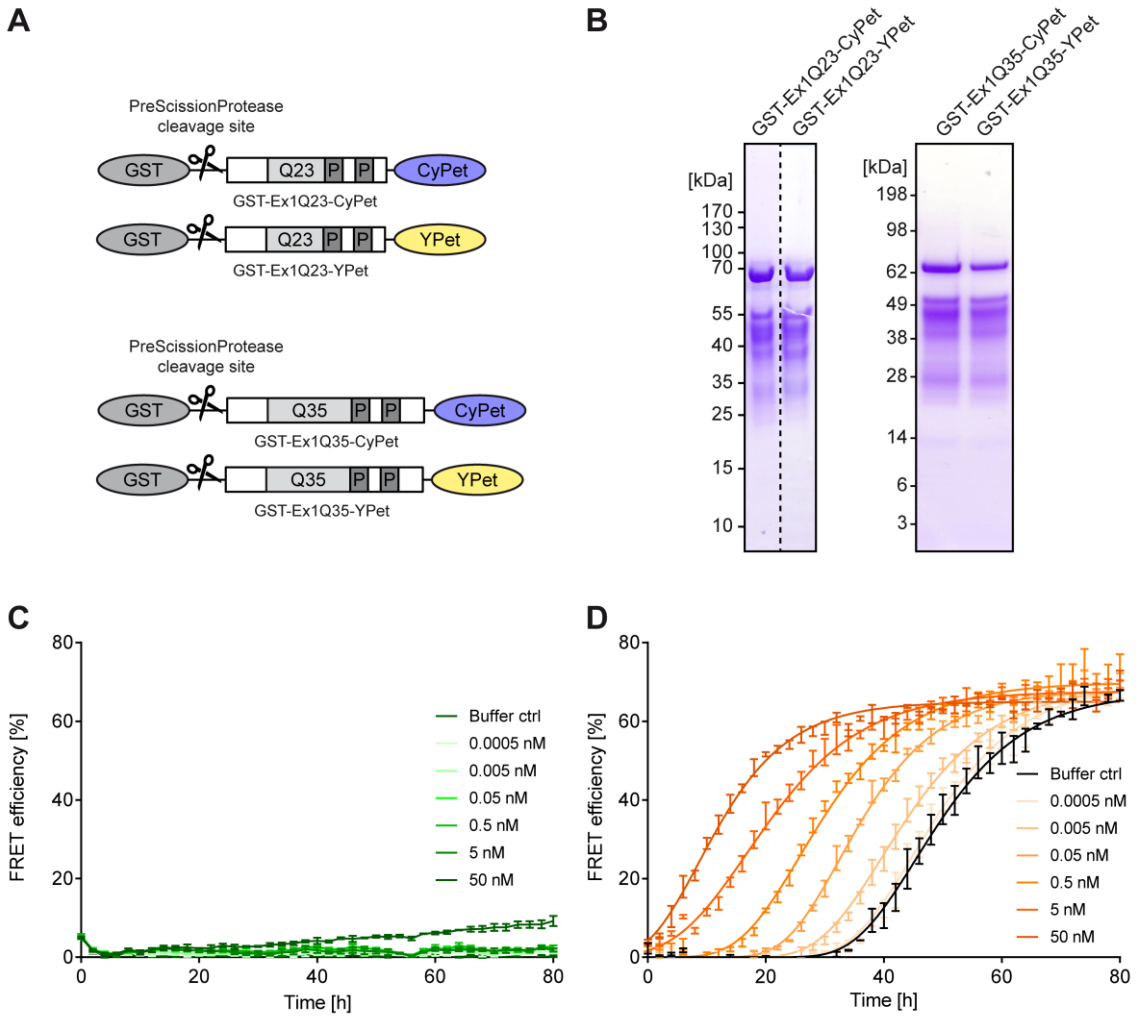

Figure 16: Shorter polyQ tracts in sensor proteins do not improve the sensitivity of FRASE assays

(A) *Schematic representation of GST-tagged HTTex1 fusion proteins containing polyQ tracts of 23 (left) and 35 (right) glutamines. P, proline-rich regions.* ***(B)*** *The recombinant GST-Ex1Q23-CyPet and -YPet and GST-Ex1Q35-CyPet and -YPet fusion proteins were affinity purified using glutathione-coated sepharose beads. Purity was assessed by SDS-PAGE and subsequent Coomassie blue staining.* ***(C)*** *FRET measurements displaying the aggregation behavior of Ex1Q23-CyPet/-YPet reporter proteins (1.2 µM) in the absence or presence of sonicated Ex1Q48 seeds.* ***(D)*** *Aggregation profiles obtained of spontaneous and seeded Ex1Q35-CyPet/-YPet (1.2 µM) co-polymerization reactions monitored by FRET measurements. All data are mean ± SD of technical triplicates.*

For this purpose, I produced and purified two sets of additional fusion proteins, GST-Ex1Q35-CyPet/-YPet and GST-Ex1Q23-CyPet/-YPet (Figure 16A and B). They were incubated with PSP and different amounts of preformed sonicated Ex1Q48 seeds. Aggregation profiles were recorded by FRET measurements. For the protein pair Ex1Q23-CyPet/-YPet no increase in FRET efficiency was observed in the absence of Ex1Q48 seeds, indicating that the HTTEx1 fusion proteins with a polyQ stretch in the non-pathogenic range do not co-polymerize spontaneously into large fibrillar aggregates under the tested conditions (Figure 16C). Similarly, the addition of seeds also did not induce the aggregation of these reporter proteins. Interestingly, I observed a slight time-dependent increase in FRET efficiency when very high amounts of seeds were added to reactions. This indicates that FRET-positive Ex1Q23-CyPet/-YPet assemblies are formed *in vitro*. However, these results strongly differ from the typical sigmoidal shaped aggregation profiles that are observed with mutant HTTex1 reporter proteins, indicating that the assembly process differs in its kinetic properties. In conclusion, the recombinant proteins Ex1Q23-CyPet/-YPet are not well suitable as reporters to detect seeding-competent mHTTex1 aggregates with FRASE assays.
In contrast, the fusion proteins Ex1Q35-CyPet/-YPet did spontaneously aggregate after a lag phase of ~40 hours and addition of sonicated Ex1Q48 seeds accelerated their aggregation in a concentration dependent manner (Figure 16D). Despite the fourfold extension of the lag phase, in comparison to the spontaneous aggregation of Ex1Q48-CyPet/-YPet, the lowest detectable seed concentration was likewise 0.005 nM. As the application of Ex1Q35-CyPet/-YPet as sensor proteins did not result in any significant improvement in sensitivity, the Ex1Q48-CyPet/-YPet reporter proteins were used in all subsequent experiments

3.1.3. FRASE assays detect HSA with high sensitivity and specificity

Following the optimization of the assay conditions, I investigated the sensitivity, robustness and specificity of the FRASE assay for the detection of recombinant seeds. As described before, recombinant Ex1Q48 seeds were generated by sonication (Figure 13). Seeds were analyzed by blue native PAGE and immunoblotting. Sonication for 60 sec led to the formation of Ex1Q48 structures with an average molecular weight of ~1,250 kDa (~90mers) (Figure 17A), whereas aggregates with a much larger size were detected in the gel pocket in non-sonicated samples.

Next, a large range of concentrations of sonicated Ex1Q48 aggregates were analyzed for their seeding activity in FRASE assays. As expected, a dose-dependent shortening of the lag phase was observed when sonicated Ex1Q48 structures were added to polymerization reactions (Figure 17B and C). Considering the molecular weight of the applied seeds, a threshold of ~60 fM for detecting Ex1Q48 seeds was determined. Furthermore, FRASE assays responded quantitatively to

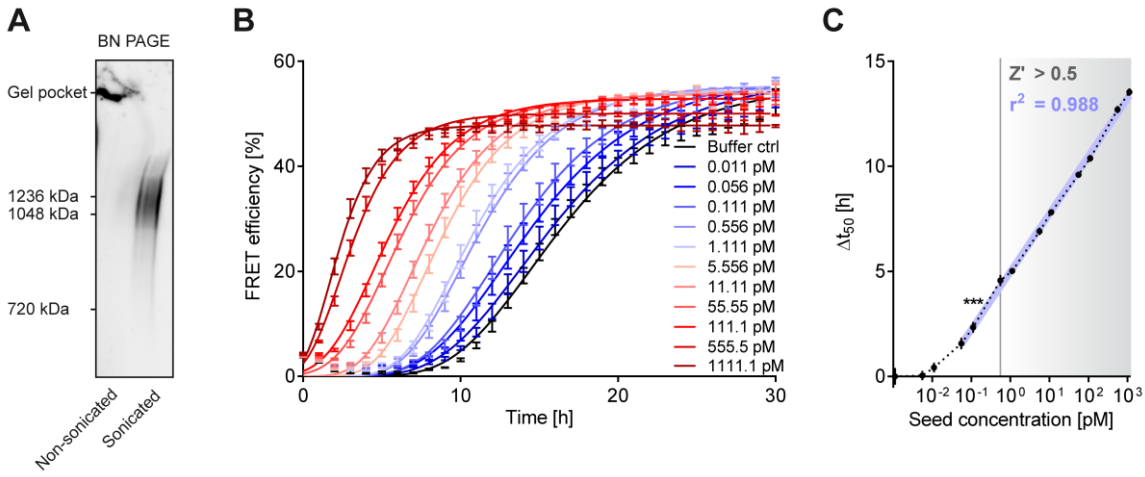

Figure 17: The FRASE assay detects sonicated Ex1Q48 aggregates with high robustness and sensitivity

(A) Analysis of sonicated (1 min) and non-sonicated preformed fibrillar Ex1Q48 aggregates by blue native (BN) PAGE and immunoblotting using the anti-HTT antibody (HD1). (B) Defining the detection limit of FRASE assays. A dilution series of sonicated Ex1Q48 seeds was systematically analyzed; seed concentrations were calculated using an average aggregate size of 1,250 kDa. Ex1Q48-CyPet/-YPet (1.2 µM). Data are mean ± SEM (n = 5). (C) Calculation of Δt_{50} values from aggregation profiles in B results in a detection threshold for sonicated Ex1Q48 seeds of 56 fM. The assay responds quantitatively to added seeds over more than four orders of magnitude (r^2 = 0.988). Above a seed concentration of 556 fM the Z' factor exceeds 0.5. Data are mean ± SEM (n = 5).

seeds over a dynamic range of 4 orders of magnitude (Figure 17C). At a concentration of ~560 fM the Z' factor[240] exceeds 0.5 (Figure 17C), demonstrating the robustness of this assay at very low concentrations and its suitability for high throughput applications.

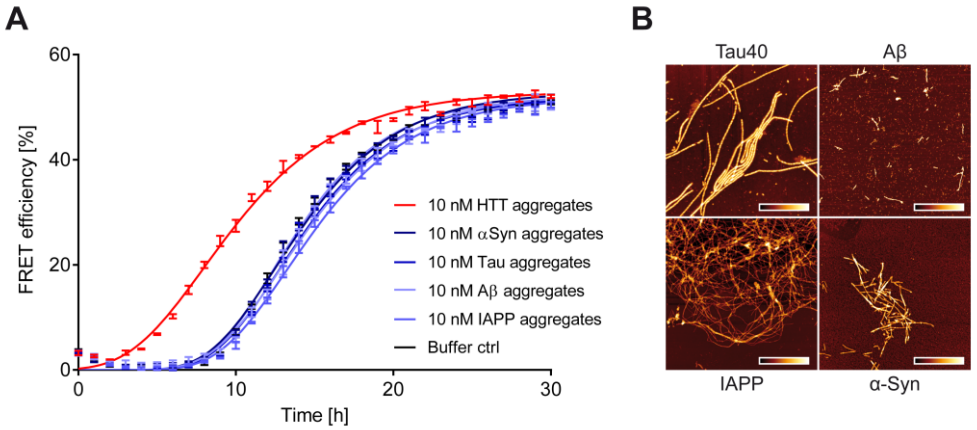

Figure 18: The FRASE assay specifically responds to preformed Ex1Q48 aggregates

(A) Fibrillar aggregates prepared of amyloidogenic non-polyQ polypeptides do not accelerate the co-aggregation of the reporter proteins Ex1Q48-CyPet/-YPet (1.2 µM). Data are mean ± SD of triplicates. (B) Analysis of preformed amyloidogenic α-synuclein (α-Syn), amyloid-ß42 (Aß), islet amyloid polypeptide (IAPP) and Tau (Tau40) protein aggregates by AFM. Scale bars: 1 µm; color gradients represent the following heights: 0-10 nm (α-Syn), 0-5 nm (Aß), 0-30 nm (IAPP) and 0-10 nm (Tau40).

Finally, I investigated the specificity of the FRASE assay for detecting mHTTex1 aggregates. Fibrillar α-synuclein, tau, amyloid-β and IAPP aggregates were produced *in vitro* and subsequently analyzed in FRASE assays. The unrelated fibrillar aggregates did not significantly influence Ex1Q48-CyPet/-YPet polymerization (Figure 18A), indicating that the FRASE assay specifically detects amyloidogenic polyQ aggregates. AFM analysis confirmed that fibrillar α-synuclein, tau, amyloid-β and IAPP aggregates were added to reactions (Figure 18B).

3.1.4. HSA is detectable in brains of HD mice and patients

After the establishment of standardized conditions for the reliable and sensitive detection of recombinantly produced mHTTex1 seeds, I investigated whether FRASE assays can detect HSA in complex biological samples. Figure 19A displays a schematic representation of the FRASE assay

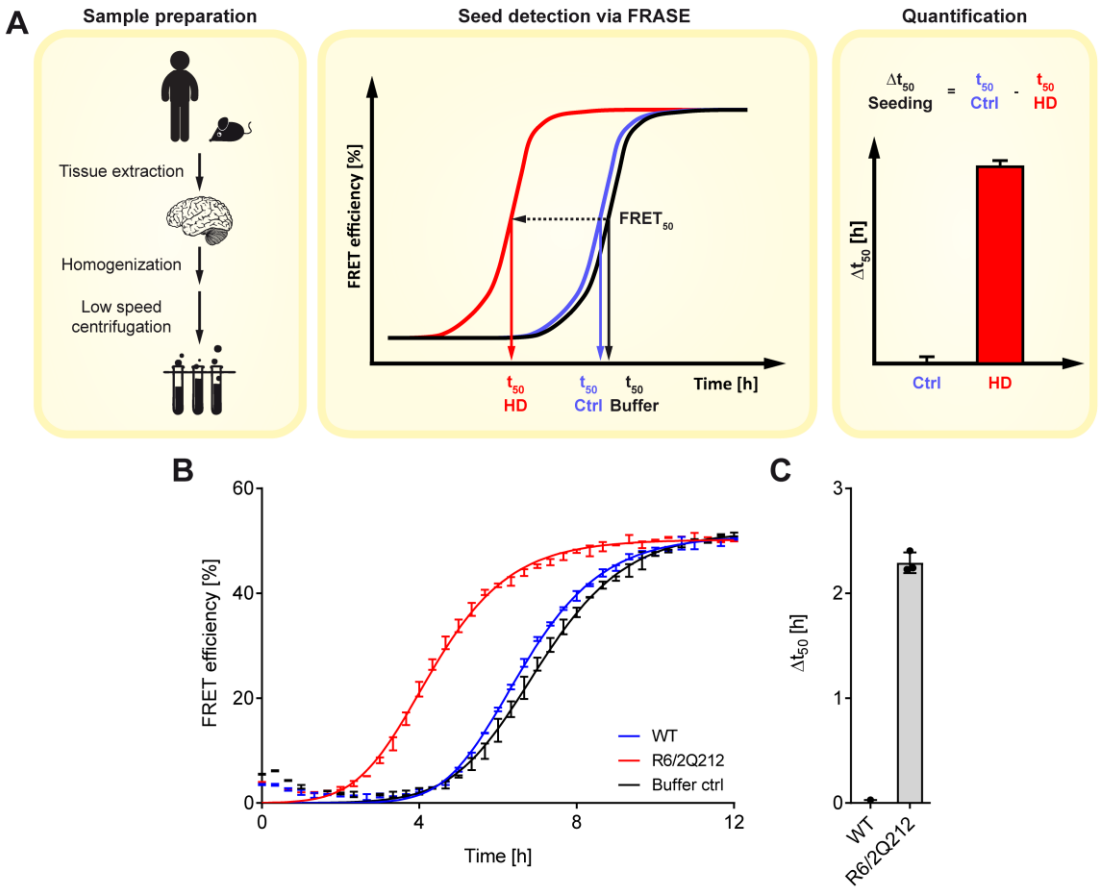

Figure 19: HSA is detectable in brain homogenates of R6/2Q212 mice

***(A)** Schematic representation of the FRASE assay workflow for detecting HSA in tissue homogenates. Icons used in this figure were taken from Freepik (https://de.freepik.com/) **(B)** FRASE analysis of brain homogenates prepared from a HD R6/2Q212 transgenic mouse and a wild-type littermate control. The concentration of the sensor proteins GST-Ex1Q48-CyPet/-YPet was 3 µM. Data is presented as mean ± SD of technical triplicates. **(C)** Calculation of Δt_{50} values from aggregation profiles in **B**. Δt_{50} is displayed as individual values (black ●) and as mean ± SD of technical triplicates. Comparable results were obtained in two independent experiments.*

workflow. Tissues of interest are homogenized in detergent-free buffer and cleared from cell debris by low-speed centrifugation. Ex1Q48-CyPet/-YPet sensor proteins are supplemented with defined amounts of the prepared crude protein extracts. Subsequently, co-aggregation of the sensor proteins is monitored in 384-well plates by quantification of FRET. The presence of mutant HTT seeds in the analyzed biosamples shortens the lag phase of Ex1Q48-CyPet/-YPet co-aggregation. HSA (Δt_{50}) in tissue samples is calculated from Ex1Q48-CyPet/-YPet aggregation profiles of seeded and non-seeded reactions as described before.

Following this strategy, I first assessed brain homogenates prepared from 12-week-old R6/2Q212 transgenic mice (carrying ~212 CAGs) and age-matched controls. R6/2Q212 mice express low levels of the human HTTex1Q212 protein[73], show motor abnormalities from 8 weeks of age[241] and typical mHTTex1 inclusion bodies from 3-4 weeks onwards[242]. Strikingly, I measured high levels of HSA in brain homogenates of R6/2Q212 mice but not in those of age-matched littermate controls (Figure 19B and C).

In order to investigate whether HSA in R6/2Q212 brain homogenates indeed originates from mutant HTT aggregates, immunodepletion experiments were performed. Brain extracts from symptomatic 12-week-old R6/2Q212 mice and littermate controls were prepared and potential seeding-competent mHTTex1 aggregates were immunodepleted using the monoclonal anti-HTT antibody MW8[243]. The parental lysate (input) as well as the post-IP supernatant were analyzed using FRASE assays. I observed a dramatic decrease of HSA in MW8-immunodepleted R6/2Q212 brain homogenates (Figure 20A) but not in homogenates treated with an isotype control antibody (Figure 20B). As expected, HSA was not detected in crude brain extracts of age-matched wild-type control mice. SDS-PAGE and immunoblotting confirmed the depletion of mHTTex1 protein aggregates from brain homogenates by MW8 antibody treatment (Figure 20C), whereas mHTTex1 protein aggregates remained in the supernatant fraction when brain homogenates were treated with the isotype control antibody (Figure 20D). This demonstrates that removal of mHTTex1 aggregates from R6/2Q212 brain lysates decreases the detectable seeding activity which in turn indicates that HSA indeed originates from mutant HTTex1 aggregates.

Thus far, I demonstrated HSA in brain homogenates of R6/2Q212 mice. This model is based on the expression of an aggregation-prone N-terminal fragment of the HTT protein with an extremely long polyQ stretch and is widely used to study mHTTex1 aggregation and HD pathology[244-246]. Since the creation of the R6/2 mouse, several other murine models have been developed, which express longer mHTT fragments or the full length HTT protein. In order to show that HSA is not a unique feature of a particular HD mouse model, but a universal phenomenon

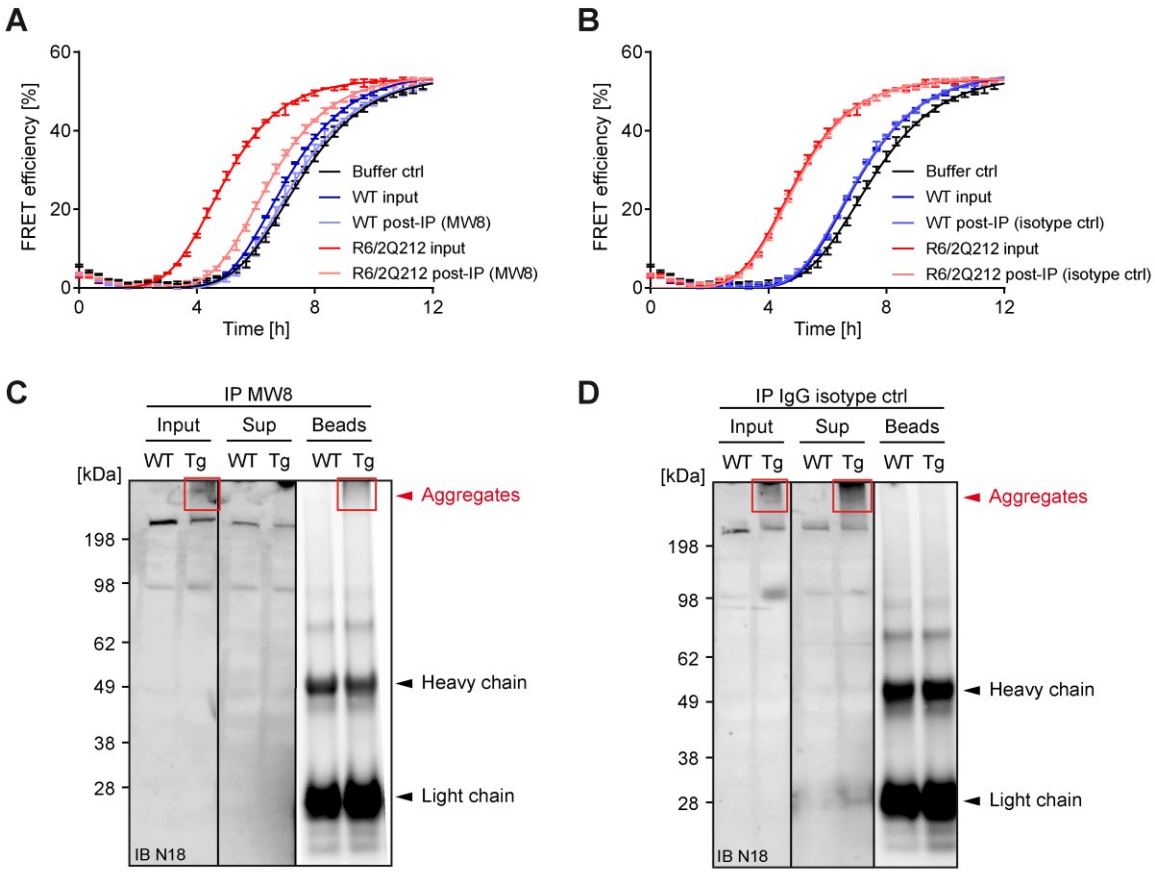

Figure 20: Immunodepletion of HTTex1 aggregates from mouse brain homogenates decreases HSA

(A) *Immunodepletion of mutant HTTex1 aggregates from R6/2Q212 mouse brain homogenates decreases their seeding activity in FRASE assays. Brain homogenates prepared from transgenic mice and littermate controls (12 weeks) were incubated with MW8 antibody-coated protein G beads; supernatant (post-IP) and input samples were applied to FRASE analysis using 3 µM of sensor proteins. FRET efficiency is plotted as mean ± SD of technical triplicates.* ***(B)*** *Same procedure as in* ***A*** *but with an IgG isotype control antibody.* ***(C and D)*** *Immunoblots of samples analyzed in* ***A*** *and* ***B****. HTTex1 aggregates appear as a smear at the upper edge of the blot (red rectangles). Input, brain extract before immunodepletion; Sup, supernatant after immunodepletion; Beads, antibody-coated protein G beads after immunodepletion. HTTex1 aggregates are depleted from mouse brain homogenates with the anti-HTT antibody MW8 but not with an IgG isotype control antibody.*

detectable in various HD models and patients, I also quantified HSA in brain tissues of additional four HD mouse models and HD patients.

First, I assessed whether HSA is detectable in brain extracts of 12-week-old R6/2Q51[247] mice, which express a HTTex1Q51 fragment. In comparison to the R6/2Q212 model, these mice have a much shorter polyQ stretch of 51 glutamines, which corresponds more closely to the average repeat length observed in HD patients (44 glutamines)[248]. At 12 weeks of age these mice do not show a disease-related phenotype, suggesting that HSA should be lower. FRASE analysis revealed that brain homogenates of prodromal 12-week-old R6/2Q51 mice do not possess

significant HSA (Figure 21A), while seeding activity was detectable in extracts of very old mice (104-105 weeks).

Next, brain tissue of N171-82Q HD mice was analyzed. This mouse model expresses a longer N-terminal fragment comprised of the first 171 amino acids of human HTT with 82 CAG repeats. Its expression is controlled by the mouse prion protein promoter and is therefore restricted to neurons[249]. These mice show an overall brain atrophy and the formation of neuronal inclusions[249,250]. Previous studies demonstrated motoric and cognitive deficits with 15 weeks of age. Compared to the R6/2Q212 model, N171-82Q mice display a milder phenotype with the appearance of symptoms at 10 weeks of age and a survival of 10 – 24 weeks[11,249]. I analyzed brain tissue homogenates of symptomatic N171-82Q and corresponding WT littermates using FRASE assays. Significantly higher HSA was observed in N171-82Q mice compared to age-matched control mice (Figure 21B).

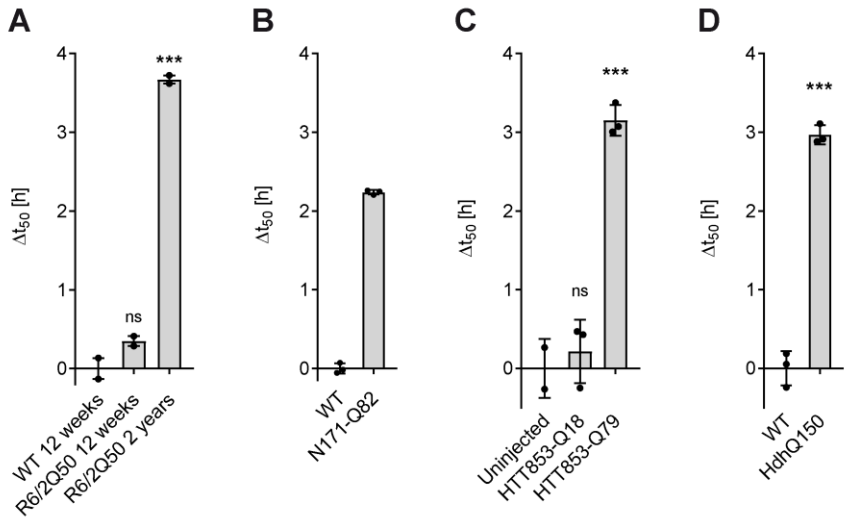

Figure 21: HSA is detectable in various HD mouse models at symptomatic stage

(A) *Analysis of brain extracts prepared from R6/2Q51 transgenic mice and controls using FRASE assays (1.2 µM Ex1Q48-CyPet/-YPet). HSA measured for each mouse is displayed as black dots (●). Bars are mean ± SEM. Statistical significance was assessed by One-Way ANOVA followed by Dunnett's multiple comparisons test (n = 2).* ***(B)*** *Quantification of HSA in brain homogenates of 12 weeks-old N171-82Q mice and corresponding littermates using FRASE analysis (3 µM Ex1Q48-CyPet/-YPet). Data is presented as mean ± SD of technical triplicates (n = 1). Comparable results were obtained in independent experiments.* ***(C)*** *Quantification of HSA in hypothalamic brain homogenates of FVB/N mice expressing the proteins HTT853Q18 or HTT853Q79. The concentration of sensor proteins was 3 µM. Data are mean ± SEM (n = 3). Individual measurements are displayed as black dots (●). Statistical significance was assessed by One-Way ANOVA followed by Dunnett's multiple comparisons test.* ***(D)*** *Investigation of brain extracts prepared from cortex of 8-month-old HdhQ150 heterozygous knock-in and corresponding WT mice (1.2 µM Ex1Q48-CyPet/-YPet). HSA is presented as mean ± SEM (n = 3). Individual Δt_{50} for each mouse are displayed as black dots (●). Statistical significance was assessed by Student's t test.*

I also investigated whether HSA is detectable in the hypothalamus of mouse brains, in which the proteins HTT853-Q79 or HTT853-Q18 were overexpressed for 8 weeks using viral vectors. Previous studies have demonstrated that hypothalamic expression of HTT853-Q79 leads to a gain of body weight and the formation of insoluble mHTT protein aggregates[251]. FRASE analysis revealed HSA in hypothalamic tissue homogenates of HTT853-Q79 compared to HTT853-Q18 and controls mice (Figure 21C).

Subsequently, I analyzed *HdhQ150* knock-in mice that express a full-length mHTT protein with a pathogenic polyQ tract of 150 glutamines[252]. These mice show onset of depressive-like symptoms by 12 months of age[253] and impairment of motor function at ~18 months of age. Widespread deposition of mHTT aggregates throughout the brain is observed by 8 months of age[254]. FRASE analysis of tissue homogenates prepared from cortex of 8 month-old heterozygous *HdhQ150* mice and littermate controls demonstrated high seeding activity in *HdhQ150* mice (Figure 21D).

Finally, HSA was examined in different brain regions of HD patients. Protein extracts prepared from postmortem tissue (cerebral cortex, caudate nucleus and cerebellum) from HD patients and control individuals were systematically analyzed using the FRASE assay. HSA was invariably detected in HD but not in control samples (Figure 22), indicating that the method is suitable to discriminate between patients and healthy individuals. Interestingly, HSA was detectable in the cerebral cortex and the caudate nucleus, which are severely affected in HD patients[11], while it was not observed in the cerebellum, which is less affected in disease.

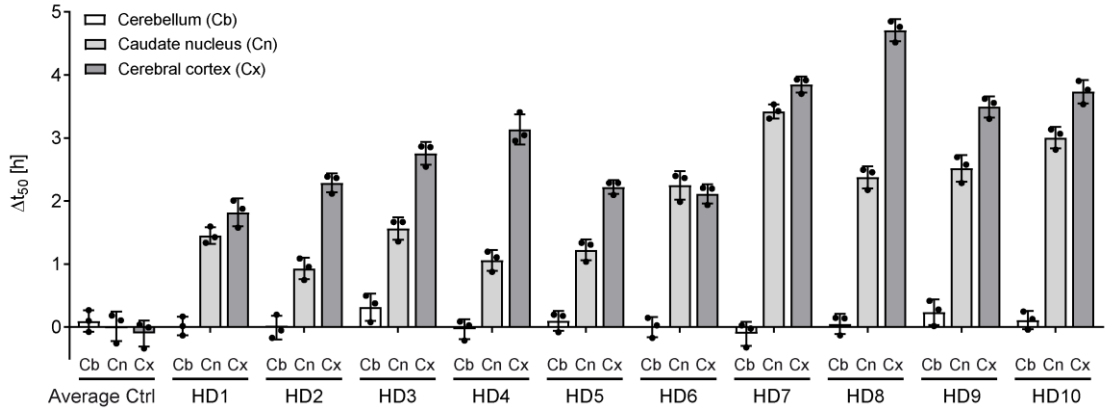

Figure 22: Detection of HSA in post mortem human brain tissue

Quantification of HSA in brain homogenates prepared from cerebellum, caudate nucleus and cerebral cortex of HD patients and controls with FRASE assays. For clarity, the average Δt_{50} values obtained from 3 healthy control samples are depicted (Average Ctrl). Individual values of Δt_{50} (black ●) and mean ± SD of triplicates are displayed.

Equivalently to the *in vitro* studies (Figure 18) I performed control experiments to assess whether the FRASE assay specifically detects seeding activity of mutant HTT aggregates. I previously established that unrelated amylogenic aggregates composed of α-synuclein, tau, amyloid-β and IAPP were unable to accelerate the co-aggregation of Ex1Q48-CyPet/-YPet reporter proteins. In order to substantiate these results, I analyzed cortex samples of APPPS1 mice, a commonly used Alzheimer's disease (AD) mouse model and corresponding littermates at 9 month of age. These mice contain the human transgenes for *APP* and *PSEN1* and harbor two familial mutations known to cause AD (*APP*: Swedish KM670/671NL; *PSEN1*: L166P). The deposition of amyloid-β plaques has been observed at 6 weeks of age in the neocortex and at 3-4 month of age in the hippocampus[255]. Learning and memory deficits were reported at ~7 month of age[255,256]. Brain tissue homogenates were prepared and assessed for their potential seeding activity. As expected, seeding activity was undetectable in both APPPS1 and WT control mice (Figure 23A). Similarly, no HSA was detectable in homogenates of cortex tissue from AD patients (Figure 23B), indicating that unrelated aggregates, such as amyloid-β plaques, do not seed the aggregation of Ex1Q48-CyPet/-YPet reporter proteins.

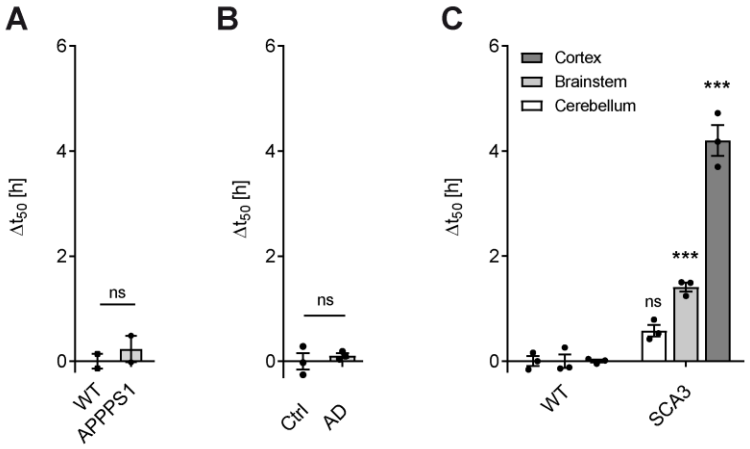

Figure 23: FRASE assays detect mutant ataxin-3 seeding activity in brains of SCA3 transgenic mice

(A) *Detection of HSA in brain homogenates of 9-month-old APPPS1 and age-matched control mice assessed by FRASE assays; 1.2 µM Ex1Q48-CyPet/-YPet; Data are mean ± SEM (n = 2); (●) = Δt_{50} values of individual mice.* ***(B)*** *Brain homogenates prepared from temporal cortex of AD patients were analyzed by FRASE assays and compared to corresponding brain tissue of control individuals. HSA values are plotted individually as black dots (●) and as mean ± SEM (n = 3); cortical tissues from AD patients (Braak 6, Age 73.3 ± 4.6), cortical tissues from controls (Braak 0, Age 66.3 ± 7). Statistical significance was assessed by unpaired t test.* ***(C)*** *FRASE analysis of brain homogenates prepared from cortex, brainstem and cerebellum of 19-month-old SCA3/ataxin-3/CamKII mice in comparison to age-matched littermates reveals HSA of non-HTT polyQ aggregates; 1.2 µM Ex1Q48-CyPet/-YPet; Data are mean ± SEM (n = 3); (●) = Δt_{50} values of individual mice.*

Next, I addressed the question whether a different type of polyQ aggregate could accelerate the aggregation of the reporter proteins. As described before, HD is one of nine diseases resulting from a CAG repeat expansion in the respective disease-associated gene. Although, it is common to all these diseases that a protein with an elongated polyQ stretch is deposited in inclusion bodies, the protein sequences flanking the polyQ stretch are different in each disease protein[184,185]. However, as the expansion of the polyQ stretch leads to protein aggregation in all these diseases a common mechanism of protein aggregation and a similar aggregate architecture can be suspected. Hence, the FRASE assay might also be able to detect the seeding activity of other polyQ-containing protein aggregates. In order to test this hypothesis, I investigated whether I can detect seeding activity in brains of SCA3 (spinocerebellar ataxia type 3) transgenic mice using the FRASE assay . In this model, the full-length human ataxin-3 protein with 77 glutamines is produced under the control of the CamKII promoter, which targets transgene expression primarily to the cortex and only to a lesser extend to other brain regions[257,258]. I analyzed tissue homogenates prepared from cortex, brainstem and cerebellum from 19-month-old SCA3 mice and corresponding littermates. Using the FRASE assay, which was established for HD, I observed seeding activity in all three brain regions, with the highest activity detected in the cortex and lower activities in brainstem and cerebellum (Figure 23C). This indicates that the FRASE assay not only detects mutant HTT aggregates in biosamples but also responds to other pathogenic polyQ aggregates that are formed in related disease models such as SCA3.

3.1.5. HSA is detected early in pathogenesis and increases with disease progression

Using the FRASE assay, HSA was detectable in brain tissues of various HD mice at symptomatic stage, regardless whether an N-terminal fragment of mutant HTT or the full-length protein was expressed. In addition, HSA was detectable in severely affected brain regions of HD patients but not in control individuals. This suggests that the presence of seeding-competent mHTT aggregates is a general phenomenon in HD models and patients and further implies a potential role of these structures in disease development or progression. However, to be regarded as disease relevant and capable of promoting pathogenesis, such structures would need to be present early in disease development or even prior to the appearance of a disease phenotype. Also, their abundance in affected tissues should increase with the severity of disease symptoms.

To address whether HSA is detectable in brains of presymptomatic HD mice, I first analyzed non-sonicated brain homogenates of young R6/2Q212 mice and age-matched controls using the FRASE assay. HSA was detected in brain extracts of 2-week-old R6/2Q212 mice (Figure 24A) and increased progressively over time. A similar result was also obtained with sonicated brain extracts (Figure 24B). With sonication, significant HSA was already detectable in brains of

1-day-old R6/2Q212 transgenic mice, indicating that seeding-competent mHTTex1 structures are present in brains of R6/2Q212 mice long before inclusion bodies can be detected[11,127].

Next, I investigated whether HSA is detectable in presymptomatic *HdhQ150* knock-in mice that express full-length mHTT protein and show a milder and slower progressing disease phenotype in comparison to R6/2Q212 mice[252-254]. I systematically analyzed tissue homogenates prepared from cortex, striatum and hippocampus of 2-, 5- and 8-month-old heterozygous *HdhQ150* mice and littermate controls using the FRASE assay. I observed progressively increasing HSA in protein extracts from all three brain regions of *HdhQ150* but not from control mice (Figure 24C). This confirms that mHTT seeds are detectable in HD mouse brains long before the appearance of inclusion bodies and motor abnormalities and increase in abundance with the development of disease pathology[254].

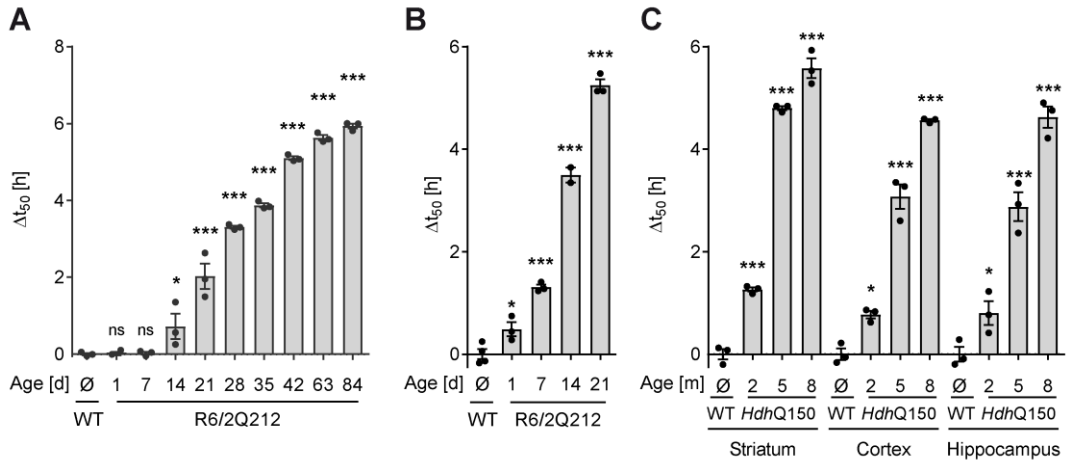

Figure 24: FRASE assay detects HSA in brains of presymptomatic HD mice

(A) *Quantification of mutant HSA in brain extracts prepared from R6/2Q212 transgenic mice. Mice were sacrificed at the indicated age; brain extracts were analyzed using the FRASE assay. Corresponding extracts from wild-type (WT) littermate controls were analyzed for all ages; an average WT Δt_{50} value was depicted for clarity.* ***(B)*** *Analysis of sonicated brain extracts prepared from young R6/2Q212 transgenic mice using the FRASE assay. Results from corresponding littermates are shown as an average Δt_{50} value.* ***(C)*** *Investigation of brain extracts prepared from indicated brain regions of HdhQ150 heterozygous knock-in mice. Corresponding extracts from 2-, 5- and 8-month-old WT mice were also analyzed and average Δt_{50} values are depicted for clarity. All data are mean ± SEM (n = 3). The concentration of the sensor proteins GST-Ex1Q48-CyPet/-YPet was 1.2 µM. HSA measured for each mouse is displayed as black dots (●). Bars are mean ± SEM. Statistical significance was assessed by One-Way ANOVA followed by Dunnett's multiple comparisons test.*

Subsequently, I asked whether similar results can be obtained with brain tissues prepared from HD patients. Based on the temporospatial pattern of degeneration in the striatum, Vonsattel et al. developed a grading system to classify the severity of neuropathological changes into five distinct grades (0 – 5)[259]. Longitudinal examination of HD patients prior to death showed

significant correlation between clinical features and the neuropathological grade assigned postmortem[260]. Here, I analyzed brain homogenates prepared from the putamen of HD patients and control individuals. Neuropathological changes of HD patients had been classified and ranged from grade 2 to grade 4. FRASE analysis demonstrates a significant elevation of HSA in brain tissue with mild neuropathological changes (Figure 25, Grade 2). With the advancement of neuropathological changes, I observed a successive increase of HSA (Figure 25, Grade 3 and 4), indicating that HSA correlates with the severity of neuropathological changes.

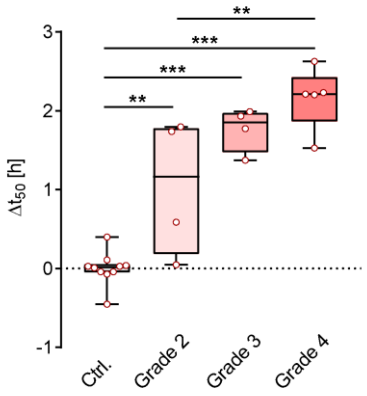

Figure 25: HSA detected in the putamen of HD patients increases with the advancement of neuropathological changes

Assessment of HSA in homogenates prepared from putamen of control individuals and HD patients at different disease stages. Δt_{50} values for each individual are plotted as red circles; Boxes show first and third quartiles, the central band shows the median, and the whiskers show data within 1.5 IQR of the median; putamen tissue from HD patients (Grade 2 (n = 4), CAG repeat length 45.8 ± 0.96, Age 60.25 ± 12.1; Grade 3 (n = 4), CAG repeat length 47.5 ± 1.7, Age 54.5 ± 6.6; Grade 4 (n=5), CAG repeat length 52.0 ± 1.0, Age 44.6 ± 4.9), caudate tissue from controls (n = 10, Age 60.6 ± 9.1), statistical significance was assessed by One-Way ANOVA followed by Dunnett's multiple comparisons test.

3.1.6. Small mHTT structures are predominantly responsible for the measured HSA in mouse brain homogenates

Within the last chapter, I described that HSA is detectable in HD mouse models before the appearance of large mHTT aggregates (Figure 24). However, previous experiments also indicated that indeed small misfolded HTT assemblies could cause the seeding effect measured by FRASE assays (Figure 3B-D). To examine whether large and/or small mHTTex1 aggregates are responsible for the measured HSA in biosamples, I proceeded by investigating the nature of seeding-competent mHTT aggregates. I hypothesize that small mHTT structures, might contribute to the observed HSA, but remain invisible to standard aggregate detection methods such as the FRA or immunohistochemical analysis.

Results

In order to test this hypothesis, I investigated whether HSA is detectable in protein fractions after depletion of large mHTT aggregates by centrifugation. Non-sonicated brain homogenates prepared from symptomatic 12-week-old R6/2Q212 mice were centrifuged for 20 min at 2,700 x g (low speed) or 18,000 x g (medium speed), respectively, and the resulting supernatant and pellet fractions ($S1_{Low}$, $P1_{Low}$ and $S1_{Med}$, $P1_{Med}$; Figure 26A) were analyzed with FRASE assays. Interestingly, HSA was high in the parental crude lysate and in the $S1_{Low}$ fraction, while it was relatively low in the $P1_{Low}$ fraction (Figure 26B), suggesting that it predominantly originates from soluble rather than insoluble mHTTex1 aggregates. A similar result was obtained when the fractions $S1_{Med}$ and $P1_{Med}$ were analyzed (Figure 26B). However, after medium speed centrifugation HSA in the $P1_{Med}$ fraction was higher than in the $P1_{Low}$ fraction, indicating that HTT seeds can be removed from supernatant fractions using a higher centrifugation speed. This trend was even more pronounced when the generated $S1_{Med}$ fraction was subjected to a high-speed centrifugation (190,000 x g), resulting in the supernatant and pellet fractions S2 and P2 (Figure 26A). FRASE analysis revealed a significantly higher HSA in the P2 than in the S2 fraction, indicating that small seeding-competent mHTTex1 aggregates can be removed from the soluble $S1_{Med}$ fraction by high-speed centrifugation.

To obtain a first hint about the size of the seeding-competent mHTTex1 aggregates in the brains of R6/2Q212 mice, the supernatant and pellet fractions were analyzed by FRA^{238}. I found HTT immunoreactivity predominantly in the $P1_{Low}$ and $P1_{Med}$ fractions. In comparison, weak or no immunoreactivity was detected in the fractions $S1_{Low}$, $S1_{Med}$, P2 and S2 (Figure 26C), suggesting that HSA in R6/2Q212 mouse brain extracts predominately originates from small rather than large mHTTex1 protein assemblies.

Finally, transmission immunoelectron microscopy was used to assess the size and morphology of mHTT seeds present in P2 fractions. This fraction exhibits high HSA but does not contain large mHTTex1 aggregates. I detected small, immunoreactive HTT fibrils with diameters of 10.2 ± 3.6 nm and lengths of 157.8 ± 64.1 nm exclusively in P2 fractions of R6/2Q212 but not of WT mice (Figure 26D). This suggests that HSA primarily originates from small rather than large mHTTex1 structures. Additionally, these results indicate that the FRASE assay is capable to detect these small assemblies which is a major advantage over previously applied aggregate detection methods.

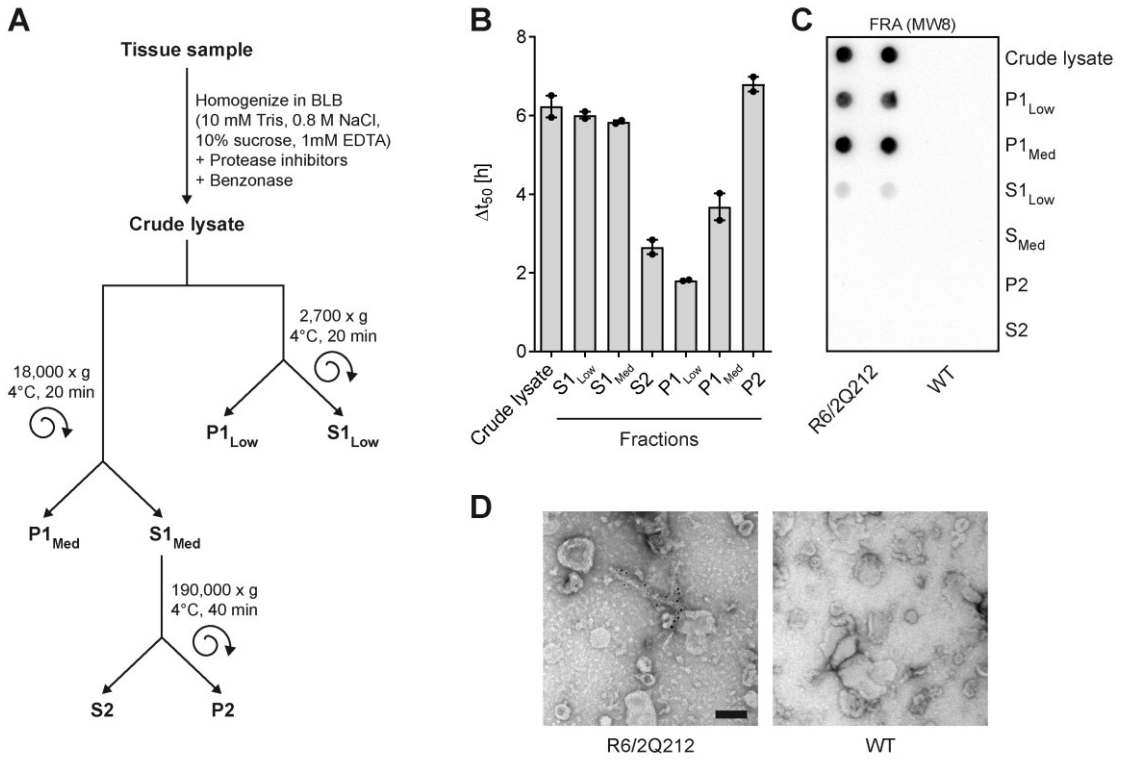

Figure 26: Detection of small seeding-competent mHTTex1 fibrils in soluble brain fractions

(A) Scheme of the different centrifugation steps applied to prepare soluble and insoluble fractions from brain homogenates of 12-weeks-old R6/2Q212 transgenic mice. (B) Quantification of HSA in soluble and insoluble fractions using FRASE assays. In all cases, data obtained for transgenic mice were normalized to age-matched wild-type control mice. Bars are mean ± SEM (n = 2). HSA measured for each mouse is displayed as black dots (●). (C) Analysis of soluble and insoluble fractions prepared by centrifugation from mouse brain homogenates using a denaturing FRA. (D) Analysis of the P2 fraction after high-speed centrifugation by immunoelectron microscopy. The P2 fraction was prepared from 9-week-old R6/2Q212 transgenic mice and age-matched wild-type (WT) controls. Fibrillar HTT aggregates were visualized with the anti-Agg53 HTT-antibody and a gold-labeled secondary antibody. Scale bar corresponds to 100 nm.

3.1.7. Seeding-competent aggregates as potential disease drivers

Hitherto, I could demonstrate elevated HSA in brain tissue of HD patients and mouse models. Seeding activity, which seems to primarily originate from small fibrillar mHTT structures, was detectable very early in disease development and increased with disease progression. This suggests that seeding-competent aggregates might not just be a byproduct in HD pathogenesis, but might potentially drive or promote disease development in a prion-like fashion. If this hypothesis is true the following prerequisites should be fulfilled. First, mHTT aggregates would need to be able to seed aggregation in a cellular context, not just in the test tube as demonstrated before. Second, their presence should disturb cellular functions and lead to a disease-like phenotype.

Results

I first assessed whether preformed mHTTex1 seeds are able to promote the intracellular aggregation of initially soluble reporter proteins. For this purpose I used an inducible stable Chinese Hamster Ovary (CHO) cell line expressing Ex1Q68-CFP and Ex1Q68-YFP under the control of a tetracycline response element[261]. In this model system the expression of the fluorescently labeled HTTex1 proteins is induced through the removal of doxycycline from the cell culture medium. The expressed HTTex1 fragment contains a polyQ stretch in the pathogenic range and was previously reported to spontaneously assemble into intracellular inclusions[261]. However, the addition of mHTTex1 seeds to the media should accelerate this process, if these structures were able to enter the cells and promote intracellular aggregation (Figure 27A). In order to discriminate seeds from seeded intracellular aggregates, I used unlabeled non-fluorescent Ex1Q48 aggregates as seeds and specifically quantified the amount of newly formed fluorescently labeled aggregates in cells. Cells expressing Ex1Q68-CFP/YFP were cultured for 72 h in the absence or presence of different concentrations of preformed recombinant Ex1Q48 seeds or Ex1Q23 protein as a control. Fluorescently labeled aggregates were assessed using high content fluorescence microscopy. I observed a few large spots of high fluorescence intensity in cells that were exposed to Ex1Q23 protein or buffer. These spots represent spontaneously formed Ex1Q68-CFP/YFP aggregates in CHO cells (Figure 27B, lower panel). In comparison, many additional small CFP-positive spots were observed in cells, which were treated with preformed Ex1Q48 seeds (Figure 27B, upper panel). Quantification revealed a concentration-dependent increase in the number of fluorescent spots per cell with increasing seed concentration (Figure 27C). This indicates that preformed Ex1Q48 aggregates are taken up into cells and can seed the intracellular aggregation of the reporter proteins Ex1Q68-CFP/YFP. In order to confirm this result and to validate that in fact SDS-stable mHTTex1 aggregates are formed upon seed addition, I performed additional experiments. Cells were treated as described above, lysed and analyzed by filter retardation assays (FRA) using an anti-GFP antibody for the detection of seed-induced aggregates (Figure 27D). Similar to the microscopic analysis low amounts of spontaneously formed aggregates were observed in cells treated with Ex1Q23 control protein or buffer. Strikingly, the aggregate load was significantly increased in a concentration-dependent manner upon the addition of preformed Ex1Q48 seeds (Figure 27E), confirming that recombinant Ex1Q48 seeds are in fact able to promote the intracellular aggregation of Ex1Q68-CFP/YFP.

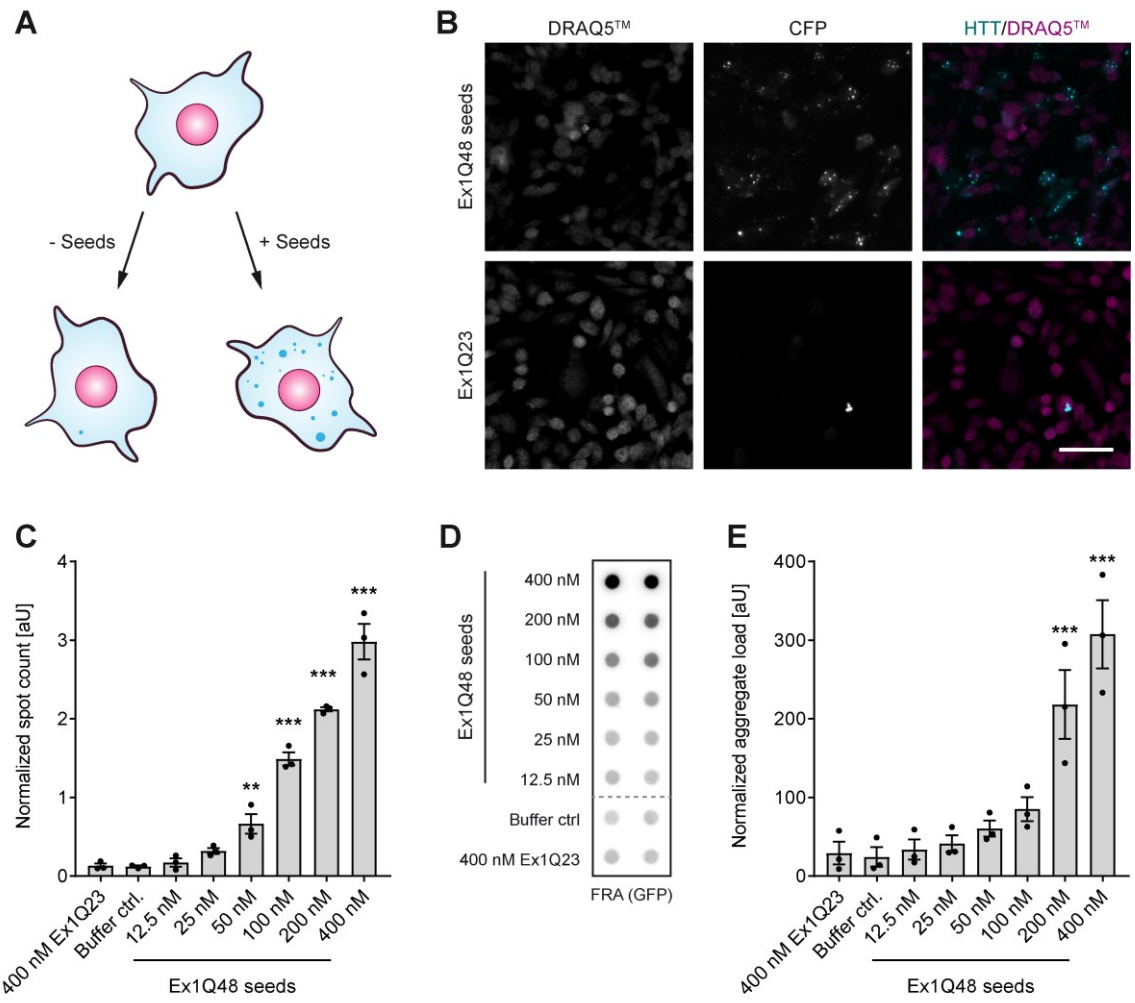

Figure 27: Recombinant Ex1Q48 seeds promote intracellular Ex1Q68-CFP/YFP aggregation

(A) *Schematic illustration of the established cell-based seeding assay. CHO cell expressing the proteins Ex1Q68-CFP/YFP were incubated for 72 h in doxycycline free media containing the indicated concentrations of Ex1Q48 seeds, Ex1Q23 control protein or aggregation buffer.* ***(B)*** *Exemplary fluorescence microscopy pictures of fixed and DRAQ5™-stained CHO cells exposed to 400 nM of Ex1Q48 seeds (top) or Ex1Q23 control protein (bottom). CFP positive puncta represent Ex1Q68-CFP aggregates. Scale bar: 100 µm* ***(C)*** *Quantification of CFP fluorescent puncta (spot count) by high content fluorescent microscopy. Individual measurements are normalized to the average spot count of all conditions and displayed as black dots (●). Bars are mean ± SEM (n = 3).* ***(D)*** *FRA analysis of lysates from CHO cells treated as described above. Ex1Q68-CFP/YFP aggregates were detected using the anti-GFP antibody ab290.* ***(E)*** *Quantification of SDS-stable Ex1Q68-CFP/YFP aggregates detected by FRAs. Individual measurements are normalized to the average dot intensity of all conditions and displayed as black dots (●). Bars are mean ± SEM (n = 3). Statistical significance in* ***C*** *and* ***E*** *was assessed by One-Way ANOVA followed by Dunnett's multiple comparisons test.*

To further elucidate the biological relevance of small seeding-competent HTTex1 aggregates, it is necessary to investigate their phenotypic consequences *in vivo* in the absence of large insoluble aggregates and without continuous overproduction of mutant HTT protein. I hypothesized that expression of mHTTex1 for a short time should lead to the formation of small

amounts of mHTTex1 seeds. These structures might be sufficient to cause proteotoxicity and induce phenotypic changes even though expression of the disease protein is not continued.

To address this question an inducible transgenic HD fly model was used. This fly model was generated and phenotypically characterized in the Wanker Lab by Franziska Schindler as part of her PhD thesis[262]. In brief, cDNAs encoding HTTex1 proteins with normal and pathogenic polyQ tracts (HTTex1Q17 and HTTex1Q97) were integrated into a predetermined intergenic locus using the bacteriophage ΦC31 integration system[263]. HTTex1 protein expression in adult neurons was induced pan-neuronally using the Elav-GeneSwitch (elavGS) system[264] which was applied previously to create adult-onset Drosophila models for spinocerebellar ataxia 7[265] and Alzheimer's disease[266]. Transgene expression in neurons of transgenic elavGS flies is induced when they are supplied with food containing the hormonal inducer RU486. Transgene expression can be switched off again, when flies are transferred back to food lacking the inducer[267,268]. Survival of transgenic elavGS;HTTex1Q17 and GS;HTTex1Q97 flies was analyzed when flies were treated either continuously or only for a short time of 3 or 6 days with the expression activating hormone RU486 (Suppl. Figure 1A and B). Lifespan of chronically RU486 treated elavGS;HTTex1Q97 flies was strongly reduced in comparison to untreated flies and elavGS;HTTex1Q17 control flies, indicating that the neuronal expression of HTTex1Q97 but not of HTTex1Q17 promotes mortality. Strikingly, short-time RU486 treatment also dramatically shortened the lifespan of elavGS;HTTex1Q97 flies, suggesting that both short and long-time expression of HTTex1Q97 in adult neurons induces dysfunction and neurotoxicity with similar phenotypic consequences[262,268].

To investigate whether reduced survival of long- and short-time RU486-treated elavGS;HTTex1Q97 flies is associated with increased deposition of large, SDS-stable HTTex1 aggregates, head lysates were analyzed by FRAs[238]. The abundance of HTTex1Q97 aggregates was much higher in heads of chronically RU486-treated elavGS;HTTex1Q97 flies than in heads of short-time treated flies (Suppl. Figure 1C). This indicates that the formation of high amounts of large, SDS-stable HTTex1Q97 aggregates in neurons cannot explain the observed mortality of HD transgenic flies, which is similar for short- and long-time RU486-treated flies (Suppl. Figure 1B)[262,268].

In addition, aggregate structures in fly brains were quantified using an immunohistochemical (IHC) approach, detecting large HTTex1 aggregates regardless of their stability. As expected, high amounts of HTTex1 aggregates were detected in long-time and lower amounts in short-time (3 and 6 days) hormone-treated HD flies (Suppl. Figure 1D), confirming the results obtained with FRAs. Interestingly, IHC analysis revealed very low amounts of HTTex1Q97 aggregates in brains of 27-day-old non-induced elavGS;HTTex1Q97 flies, indicating that low levels

of mutant HTTex1 protein are expressed despite the absence of RU486-treated. However, this low expression of HTTex1Q97 was not sufficient to significantly shorten the lifespan of HD transgenic flies (Suppl. Figure 1B)[262,268].

Using the FRASE assay I quantified HSA in head lysates prepared from long- and short-time RU486-treated elavGS;HTTex1Q97 flies to determine whether seeding activity better predicts the survival phenotype than the detection of large aggregates by FRA and IHC. Strikingly, I measured high HSA in head lysates of both short- and long-time RU486-treated flies (Figure 28A and B). In comparison, HSA was undetectable in head lysates of elav;HTTex1Q17 control flies. As seeding activity in neurons of short-time treated elavGS;HTTex1Q97 flies cannot result from large fibrillar aggregates, it must originate from smaller structures that are not retained by the filter membrane. This demonstrates that the FRASE assay provides information that is fundamentally different from that obtained with standard aggregate detection techniques (FRA and IHC).

In contrast to the FRA and IHC results (Suppl. Figure 1C and D), HSA levels measured with the FRASE assay (Figure 28A and B) correlate significantly better with the increased mortality of RU486-treated elavGS;HTTex1Q97 flies (Figure 28C). Together, these experiments suggest that the formation of small seeding-competent HTTex1Q97 structures might trigger neuronal dysfunction and lead to reduced survival of elavGS;HTTex1Q97 flies.

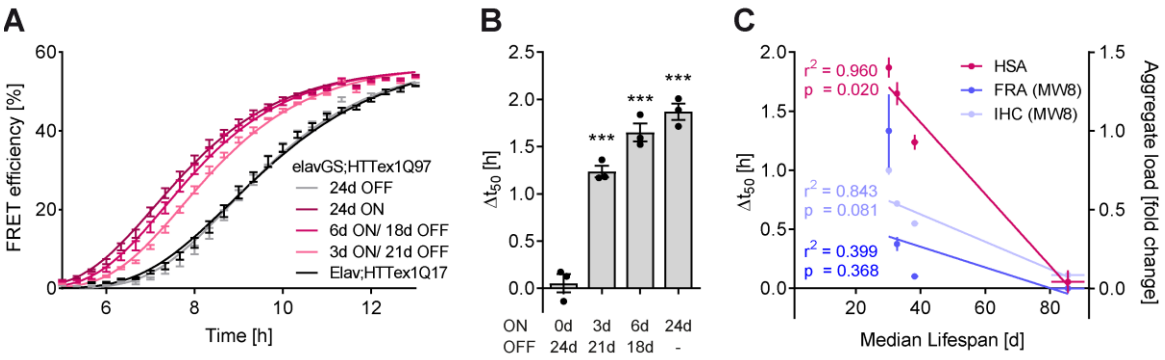

Figure 28: Formation of small seeding-competent HTTex1 aggregates in fly neurons is associated with reduced survival

(A) *FRASE analysis of head lysates from flies expressing HTTex1Q97 either continuously or only for a short time of 3 or 6 days; see treatment scheme Suppl. Figure 1A. Values are plotted as means ± SEM of three biological replicates each performed in triplicates.* ***(B)*** *HSA calculated from aggregation kinetics in* ***A****. Results are displayed as mean ± SEM; Individual measurements are presented as black dots (●); One-way ANOVA Dunnett's post hoc test compared to GS;HTTex1Q97^{OFF} flies.* ***(C)*** *Pearson correlation analysis shows a significant linear relationship between Drosophila lifespan and HSA assessed by FRASE assays (p = 0.020), whereas Drosophila lifespan does not correlate with the aggregate load detected by FRAs or IHC analysis [p = 0.368 (FRA, MW8), p = 0.081 (IHC, MAB5492)]. All data are presented as mean ± SEM of the three individual experiments.*

3.1.8. mHTT seeding activity as potential prognostic marker in HD

I established the FRASE assay as a sensitive tool to quantify HSA in biological samples. Using this tool, I was able to detect HSA at early disease stages and showed its increase with disease progression in model systems as well as HD patients. In addition, I demonstrated that the FRASE assay detects the activity of large HTTex1 aggregates in insoluble inclusions as well as of small seeding-competent aggregates, whereby especially the detection of small HTT fibrils in biosamples constitutes a major advantage over state-of-the-art aggregate detection methods. I found that HSA strongly correlates with mHTT-induced live span reduction in a *Drosophila* model, which indicates that HTT seeds might play an important role in HD pathogenesis. However, this also suggests that HSA measured by FRASE assays might serve as a valuable prognostic marker for HD-induced toxicity and HD-related phenotypes.

I speculated that influencing the disease phenotype in model systems through genetic manipulation or chemical compounds should also alter HSA levels measured by FRASE assays. To address this question, RNAi knockdown experiments were performed in transgenic worms that overproduce the aggregation-prone protein Q35-YFP in body wall muscle cells. Previous studies have demonstrated that Q35-YFP aggregation in these cells leads to motor impairment. This phenotype gets even more severe when the expression of the *hsp-1* gene (encoding the molecular chaperone Hsc70) is knocked down by RNAi[194,269]. Worms expressing Q35-YFP were treated with *hsp-1* RNAi and their motility was assessed at day five. I observed a significant reduction of motility in RNAi-treated in comparison to untreated worms (Figure 29A), confirming previously published results[194]. This phenotypic change was associated with a significant increase in Q35-YFP seeding

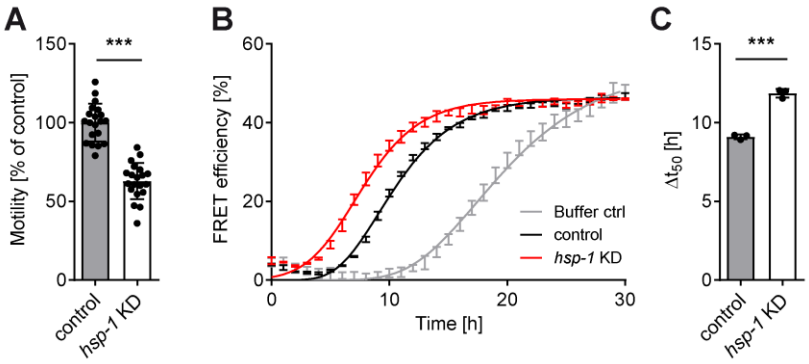

Figure 29: Depletion of Hsc70 increases both toxicity and Q35-YFP seeding activity in a C. elegans model

(A) *Motility phenotype (% motility) of RNAi-treated and untreated Q35-YFP expressing transgenic worms at day 5. Data were normalized to age-matched control worms. Data are mean ± SEM (n = 20). Significance assessment with unpaired t test.* ***(B)*** *FRASE analysis of Q35-YFP seeding activity in RNAi-treated and untreated worms after 5 days. FRET efficiency is displayed as mean ± SD.* ***(C)*** *Quantification of results shown in* ***B****. HSA values are plotted individually as dots (●) and as mean ± SD.*

activity measured by FRASE assays (Figure 29B and C), supporting the hypothesis that HSA could be used as marker of dysfunction and toxicity in model systems.

To further substantiate this finding, I used the afore mentioned *Drosophila* model. Within her PhD Thesis F. Schindler performed a concise screen to identify compounds that reduce mHTTex1 aggregation in *Drosophila*. In brief, elavGS;HTTex1Q97 flies were treated with the respective compounds starting 3 days after hatching (Figure 30A). In addition, flies were treated with the mHTTex1 expression-inducing hormone RU486 for 6 days starting 7 days after hatching. Thereby flies were exposed to the aggregation-inhibiting compounds already 4 days prior to HTTex1Q97 expression, which was intended for compounds to act efficiently even in the very early steps of the aggregation process. Head lysates were analyzed for the amount of mHTT aggregates by FRA and DB assays. It was found that the FDA approved drug Quinidine (Figure 30B) is a potent aggregate reducing agent (Suppl. Figure 2A). However, unexpectedly the survival of Quinidine treated elavGS;HTTex1Q97 flies was shorter than of untreated flies (Suppl. Figure 2B), suggesting that the compound promotes the formation of small mHTTex1 aggregates with high seeding activity.

Assuming that HSA is associated with reduced survival of HD transgenic flies and can in fact be used as a predictive marker, levels of HSA are expected to be higher in Quinidine treated flies, despite the fact that the amount of large SDS-stable aggregates detected by FRA is greatly reduced (Suppl. Figure 2). In order to test this hypothesis, I quantified the HSA in neurons of Quinidine-treated and untreated elavGS;HTTex1Q17 and elavGS;HTTex1Q97 flies. In both cases the expression of the recombinant HTTex1 proteins was induced in adult flies with RU486 for 6 days (see Figure 30A). First, I performed a small-scale survival experiment. ElavGS;HTTex1Q97 flies expressing the transgene for 6 days in the absence of Quinidine showed high mortality in comparison to HTTex1Q17 expressing control flies (Figure 30C). However, mortality further increased when the elavGS;HTTex1Q97 flies were exposed to Quinidine, whereas Quinidine treatment of ElavGS;HTTex1Q17 flies did not change their survival, confirming previous observations[262]. Next, head lysates prepared from elavGS;HTTex1Q17 and elavGS;HTTex1Q97 flies, treated as described above (Figure 30A) were analyzed by FRASE assays. Strikingly, Quinidine treatment significantly increased HSA in brains of elavGS;HTTex1Q97 flies, whereas HSA was not detectable in elavGS;HTTex1Q17 control flies irrespectively whether they were treated with the compound or not (Figure 30D and E).

These results support the initial hypothesis that HSA can be used to monitor genetically or chemically induced phenotypic changes in HD model systems and suggest that it might be a valuable marker for mHTT- induced toxicity.

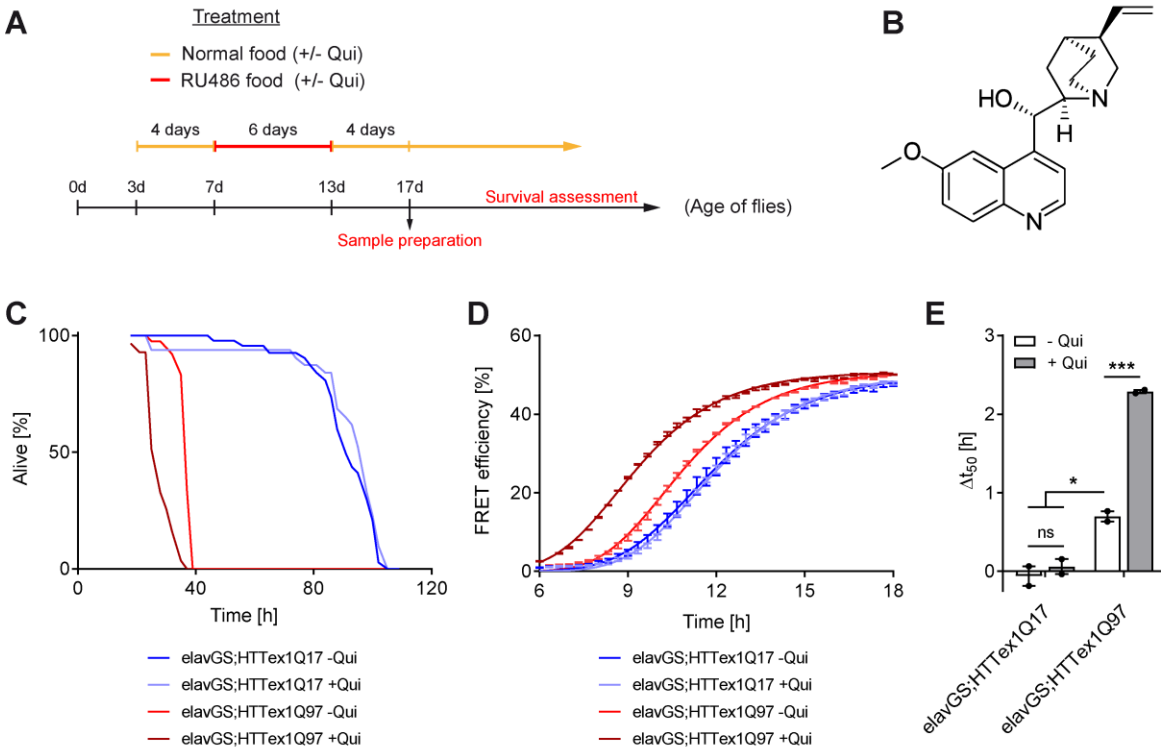

Figure 30: Quinidine-induced exacerbation of mortality correlates with increased HSA in transgenic flies

(A) *Schematic illustration of the RU486 and Quinidine treatment protocol.* ***(B)*** *Chemical structure of Quinidine.* ***(C)*** *Life span analysis of elavGS;HTTex1Q97 and elavGS;HTTex1Q17 flies expressing the respective transgene for 6d in the absence or presence of 1 mM Quinidine (+/- Qui). Life span was plotted as the percentage of surviving flies (~40 flies were analyzed per condition).* ***(D)*** *FRASE analysis of head lysates from elavGS;HTTex1Q97 and elavGS;HTTex1Q17 flies that were treated with and without 1 mM Quinidine. Values are plotted as means ± SEM of two biological replicates each performed in triplicates.* ***(E)*** *HSA calculated from aggregation kinetics in* ***D****. Results are displayed as mean ± SEM; Individual measurements are presented as black dots (●); Two-way ANOVA Bonferroni's multiple comparison test.*

In the long run, HSA measurements might be of high value to monitor disease onset and progression in HD patients. Through the quantification of HSA as part of longitudinal studies, the optimal time point for the initiation of clinical trials could be determined and the efficacy of therapeutic interventions could be monitored. In order to be applied for this purpose, the FRASE assay needs to be optimized for the detection of HSA in biological samples whose collection is technically and ethically possible, like cerebrospinal fluid, blood or muscle tissue.

As a first step, I asked whether seeding competent aggregates are present in non-CSF tissue. Previous studies have demonstrated that inclusion bodies with mHTTex1 aggregates are

found in a wide-range of non-CNS tissues in R6/2 mice[270,271], suggesting that such tissues might also possess HSA. I assessed homogenates of skeletal muscle prepared from R6/2Q212 mice. FRASE analysis revealed seeding-component mHTTex1 aggregates in the quadriceps and the tibialis anterior of 4-, 8- and 12-week-old R6/2Q212 mice but not in respective control tissues (Figure 31A), indicating that mHTT seeds are also present in non-CNS tissues. Similar as in brain tissue, HSA in muscle tissue was detected prior to the appearance of symptoms. In addition, it increased with disease progression, indicating that the measured HSA in muscle tissue might reflect the changes seen in brain tissue.

Muscle tissues can be obtained from HD patients via muscle biopsies[49,272]. They could therefore be analyzed in longitudinal studies. In order to investigate whether HSA can also be detected in HD patients, FRASE assays were performed with muscle tissue homogenates prepared from two HD patients at an early disease stage and two control individuals. Quantitative data analysis did not reveal a significantly higher HSA in HD patients in comparison to control individuals (Figure 31B). However, additional studies with samples from patients with a more severe disease manifestation need to performed to validate this preliminary result.

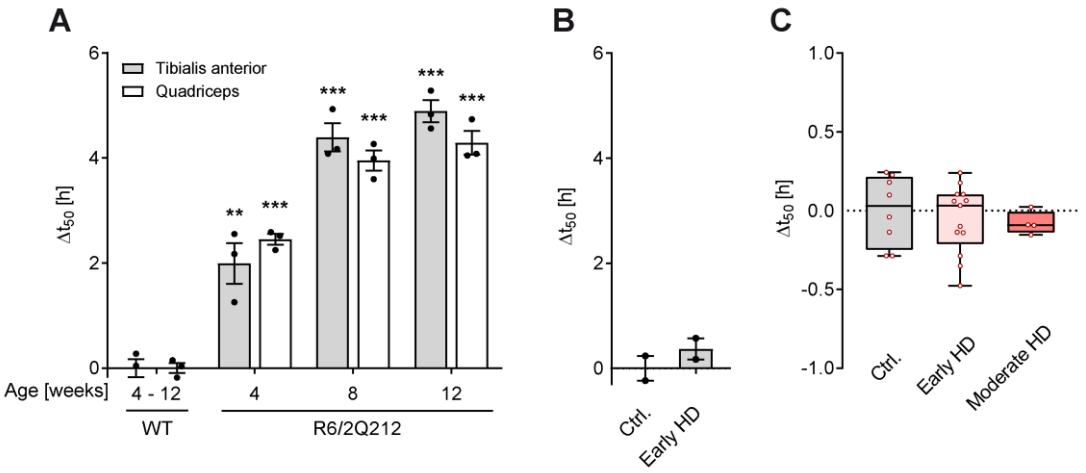

Figure 31: Analysis of HSA in peripheral tissues and biofluids

(A) *Investigation of protein extracts prepared from skeletal muscle tissues of R6/2Q212 mice using FRASE assays shows significant elevation of HSA compared to controls. Extracts from corresponding WT mice were also analyzed and displayed as average Δt_{50} values for clarity. Tissues were collected at the indicated age. Data are mean ± SEM (n = 3), HSA measured for each mouse is displayed as black dots (●), One-Way ANOVA followed by Dunnett's multiple comparisons test.* ***(B)*** *FRASE analysis of skeletal muscle tissue form two HD patients (early disease stage) and two control individuals. Data are mean ± SEM (n = 3), Individual measurements are presented as black dots (●).* ***(C)*** *Assessment of HSA in human CSF samples from patients with early and moderate HD and control individuals. Δt_{50} values for each individual are plotted as red circles; Boxes show first and third quartiles, the central band shows the median, and the whiskers show data within 1.5 IQR of the median.*

Results

Due to their accessibility via minimal invasive procedures, biofluids such as saliva, blood and cerebrospinal fluid (CSF) are the ideal sample types to monitor specific biomarkers in chronic diseases over time[230,231,273,274]. In the case of neurodegenerative diseases, CSF carries the additional advantage of being in direct contact and in continues molecule exchange with the cerebral tissue. For this reason, it seems reasonable to speculate that seeding-competent mHTT aggregates could be detected in the CSF of HD patients. Previous studies indicate that CSF derived from BACHD transgenic rats and human HD subjects can seed the aggregation of a GFP-tagged mutant HTT fragment in a cell-based assay[177]. Therefore, I also investigate whether the FRASE assay is suitable to detect HSA in CSF samples obtained from HD patients and healthy controls. I found that under standard conditions, which were optimized for the detection of mHTT seeds in mouse and human brains, HSA could not be detected in the CSF of HD patients (Figure 31C). However, additional optimization of the assay, regarding sample preparation and sensitivity, may pave the way for the detection of HSA in biofluids in the future.

In summary, in the first part of my thesis I have developed and optimized a FRET-based HTT aggregate seeding (FRASE) assay that enables the quantification of mutant HTT seeding activity (HSA) in biological samples from HD patients and various disease models. Application of the FRASE assay revealed HSA in brain homogenates of presymptomatic HD transgenic and knock-in mice and its progressive increase with phenotypic changes in mouse models as well as HD patients, suggesting that HSA quantitatively tracks disease progression. Biochemical investigations of mouse brain homogenates demonstrated that HSA is high in fractions that contain small HTT fibrils but is low in fractions with large, insoluble mHTT aggregates. This indicates that small rather than large mutant HTT structures are responsible for the HSA measured in FRASE assays. Furthermore, my investigations show that FRASE assays detect misfolded mHTT assemblies that are invisible to standard detection methods and thereby expands the range of mHTT structures that can be detected with biochemical methods. In order to elucidate their biological relevance, the neurotoxicity of mutant HTT seeds was assessed in an inducible *Drosophila* model transgenic for HTTex1. I found a strong correlation between HSA measured in adult neurons and the increased mortality of transgenic HD flies, indicating that FRASE assays detect disease-relevant, neurotoxic, mutant HTT structures with severe phenotypic consequences. In addition, I found that HSA responds to phenotypic changes in HD models when they are manipulated genetically or treated with chemical compounds, suggesting that HSA could be used as a biomarker in the future. The detection of HSA in peripheral tissues or biofluids of HD patients needs further research and optimization.

3.2. Modulation of aggregate formation and HSA by targeted amino acid exchange

My previous results show a strong correlation between seeding activity and disease-related phenotypic changes and suggest that seeding-competent mHTTex1 aggregates are stable, potentially proteotoxic structures. To explore how structural properties of mHTTex1 aggregates are related to their seeding activity and putative proteotoxicity, I generated protein variants of HTTex1 by introducing specific amino acid (AA) exchanges in the N17 and the polyQ domains. Sequence alterations in these domains influence the formation of coiled coil and β-sheet structures and have the potential to change the structure, stability and polymerization rate of HTTex1 aggregates[275]. Furthermore, they might affect seeding activity as well as proteotoxicity of HTTex1 aggregates.

Within this chapter I will describe the generation of six structural variants of HTTex1 and the biochemical characterization of their aggregation properties *in vitro*. In order to study the relationship between aggregate properties, seeding activity and aggregate-induced toxicity, I generated transgenic *Drosophila* strains and performed a comprehensive phenotypic characterization of these strains. Finally, I assessed the formation of mHTTex1 aggregates *in vivo*.

3.2.1. Design of HTTex1 protein variants

The current knowledge of the HTTex1 aggregation mechanism supports the idea that HTTex1 monomers oligomerize via coiled-coil mediated interactions between N17 domains in order to undergo primary nucleation. Coiled coils (CCs) are α-helical supersecondary structures in which two or more α-helices are wound around each other[276].

CCs are formed by proteins that contain a repetitive pattern (heptad repeat: a-b-c-d-e-f-g) of hydrophobic (a and d), charged (e and g) and polar (b, c and f) amino acids that facilitate the formation of an amphipathic α-helix. In some cases hydrophobic residues in positions a/d can be replaced with certain nonhydrophobic amino acids, such as glutamine, which are considered as ambivalent hydrophobes[277]. Within the hydrophilic environment of the cytoplasm, hydrophobic surfaces of multiple helices interact via Van der Waals forces and form a tight-fitting hydrophobic core. Charged amino acids adjacent to the core can stabilize the interaction via ionic bonds. Polar residues are exposed on the surface of the intertwined assembly. This type of interaction is thought to bring the polyQ domains of several mHTTex1 molecules in close proximity and thereby facilitates a coil-to-β-sheet transition. Once the primary nucleus is formed, surrounding monomers are added to the emerging fibrillar structure undergoing a template-mediated conformational change. Within the amylogenic fibril, the polyQ domain exists a β-hairpin

conformation[139]. Intra- and intermolecular hydrogen bond form tight connections of molecules within one β-sheets and between adjacent β-sheets.

In order to elucidate the potential connection between mHTTex1 aggregates and proteotoxicity, I attempted to alter the aggregation properties of mHTTex1 and to investigate the biological consequences. On the basis of a previously published study[275], I designed six protein variants of mutant Ex1Q48 by targeted amino acid (AA) exchange in the N17 and the polyQ domains (Figure 32A). The AA exchanges should either facilitate or hinder the formation of CCs or β-sheets. Structural-guided mutagenesis was assisted by *in silico* prediction of CC (Figure 32B) and amyloid formation (Figure 32C) using the algorithms Coils[278] and Waltz[279,280], respectively.

Figure 32A displays the primary AA sequence of Ex1Q48 and the six protein variants. In the first protein variant, Ex1Q48M1, the amino acids leucine (L) and phenylalanine (F) in the N17 domain are replaced by tryptophan (W). Leucine and phenylalanine are hydrophobic amino acids in a/d position of the coiled-coil heptad repeat. Their substitution with the bulky, however hydrophobic amino acid tryptophan mildly destabilizes the formation of coiled-coils[281] (Figure 32B), but slightly enhances β-sheet propensity[282] (Figure 32C). Thus, one would expect coiled-coil-mediated nucleus formation to be slightly hindered but β-sheet-mediated aggregation and the stable amyloid architecture to be preserved.

In the second protein variant, Ex1Q48M2, leucine and phenylalanine in the N17 domain are substituted with proline residues. Proline is unique among the 21 proteinogenic amino acid as its side chain cyclizes with the amino group of the backbone, forming a ring structure. Proline is considered as hydrophobic amino acid and might therefore be suitable to replace leucine and phenylalanine in a/d position. However, due to the cyclic structure of proline's side chain, it contributes to various bends and kinks in the shape of the protein and is therefore known to disturb the formation of α-helices and β-strands. *In silico* predictions for Ex1Q48M2 support the thought that this protein variant is less likely to form CCs and very unlikely to form amyloid structures (Figure 32B and C). Hence, insertion of proline residues in the N17 domain is assumed to hinder the aggregation process.

To further disrupt the formation of aggregation prone secondary structures, prolines were used to substitute amino acids in the N17 and the polyQ domain in Ex1Q48M3. As discussed before, proline residues introduce kinks into the polypeptide chain which leads to impaired formation of α-helix and β-strand conformation by changing the orientation of AA to each other. The addition of prolines in the polyQ domain might hinder the formation of amyloid structures through a different mechanism. The amyloid core structure is believed to be stabilized by multiple hydrogen bonds between amino acid side chains and the protein backbone. Whereas the polar

amino acid glutamine can act as hydrogen donor as well as hydrogen acceptor and thereby facilitates the formation of hydrogen bonds, proline with its hydrophobic side chain is unable to form hydrogen bonds, which would destabilize the β-sheet core structure. *In silico* predictions indicate that CC and well as amyloid formation are strongly reduced (Figure 32B and C), suggesting that aggregation of Ex1Q48M3 is severely impaired or not possible at all.

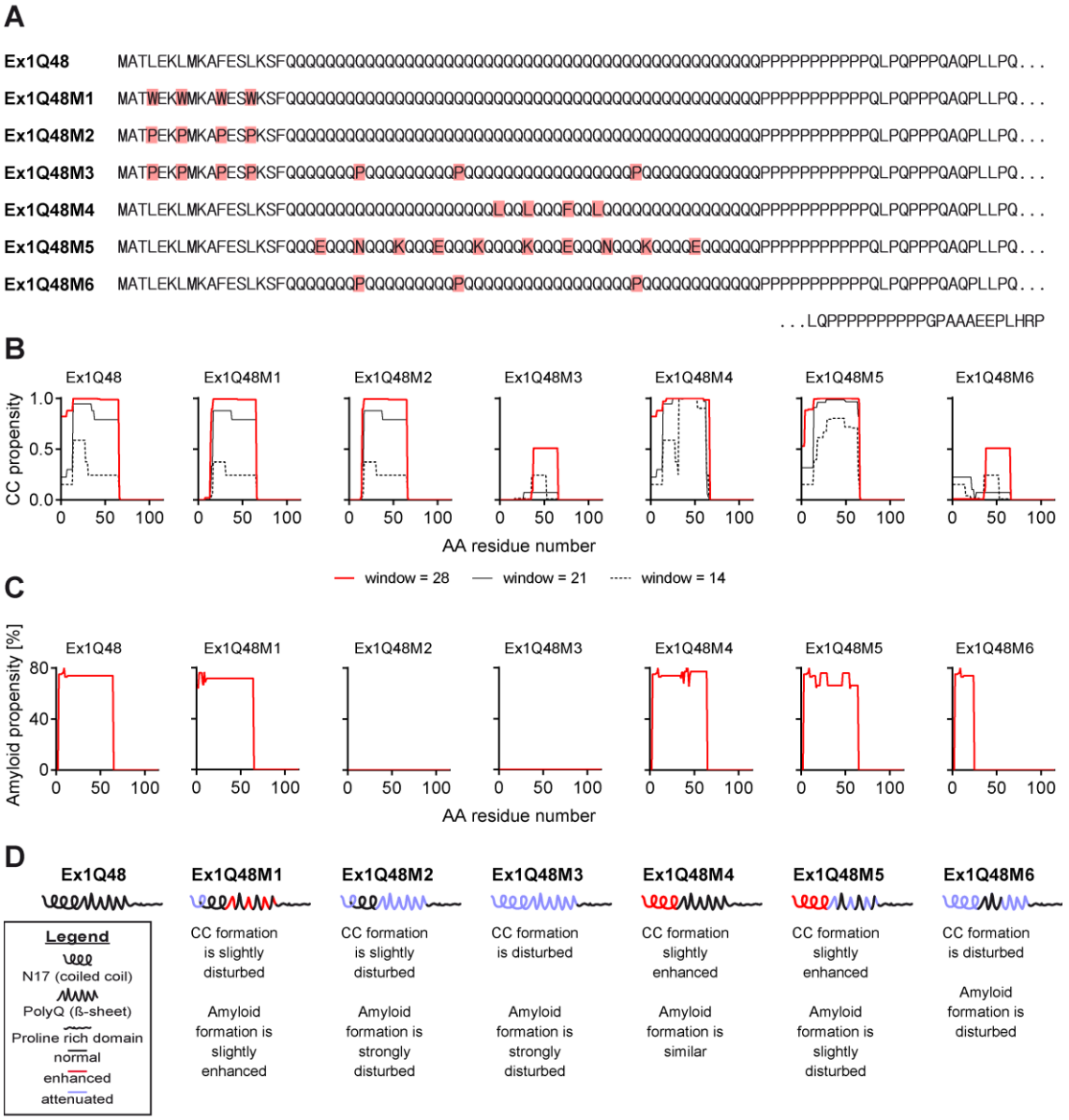

Figure 32: Protein variants of mutant Ex1Q48

(A) *Amino acid (AA) sequence of Ex1Q48 (top) and its protein variants. AA exchanges introduced in the sequence are highlighted in red.* ***(B)*** *In silico analysis of protein variants using the COILS algorithm[278] predicted differences in coiled-coil domain formation. CC probability is displayed as 1 minus the P-score assigned to each amino acid using a window size of 14 (dashed black line), 21 (black line) and 28 (red line) residues.* ***(C)*** *Protein variants were predicted to have different propensities to form amyloid structures using the Waltz algorithm[279,280] (low specificity threshold of 63 and neutral pH 7).* ***(D)*** *Model of Ex1Q48 and its protein variants illustrating predicted structural changes in amyloid and coiled-coil domain formation.*

In the fourth protein variant, Ex1Q48M4, glutamine residues were replaced with the hydrophobic amino acids leucine and phenylalanine in a/d position of the CC heptad repeat. These AA substitutions are intended to improve CC formation and to promote coiled-coil mediated nucleus formation. The formation of CC is predicted to be enhanced (Figure 32B), whereas the propensity for the formation amyloid structures is predicted remain unchanged (Figure 32C).

Next, I replaced several glutamine residues in the polyQ tract by glutamic acid, lysine and asparagine to generate protein variant Ex1Q48M5. Charged amino acids (glutamic acid and lysine) are believed to break β-sheets[283,284]. In contrast to glutamine residues which are polar and can function both as hydrogen donor and acceptor glutamic acid and lysine can only act as hydrogen acceptor or hydrogen donor respectively, which potentially decreases the formation of hydrogen bond-mediated interactions in the amyloid core. Asparagine is a polar amino acid and can, similar to glutamine, act as a hydrogen donor and acceptor. However, in contrast to glutamine, asparagine misses one methyl group in its side chain. In the amyloid core glutamine residues are believed to be arranged as a steric zipper with glutamine side chains arranged directly atop each other as a glutamine ladder. This architecture facilitates the formation of multiple hydrogen bonds and a high degree of stability in the amyloid core. Due to the missing methyl group in its side chain, asparagine cannot align in this structure to the same extend as glutamine, which might also weaken the interacting forces in the amyloid core. The computational predictions revealed a slight increase of CC propensity and a mild decrease of the amyloid forming propensity for Ex1Q48M5 (Figure 32B and C).

In the last protein variant, Ex1Q48M6, several glutamine residues in the polyQ domain were substituted by the AA proline, whereas the N17 domain remains completely unchanged. As described before, proline is a hydrophobic residue imposing a kinked structure onto the polypeptide chain. It is therefore an unfavorable amino acid in the context of β-sheet structures. Formation of CCs and amyloid structures is predicted to be disturbed (Figure 32B and C).

A graphical overview of the Ex1Q48 fragment and its six protein variants is given in Figure 32D and summarizes the predicted structural changes in each molecule.

3.2.2. Biochemical and biophysical characterization of recombinant HTTex1 protein variants and their aggregates

In order to study the aggregation properties of Ex1Q48 and its protein variants *in vitro*, I first generated recombinant proteins. cDNAs encoding for the six variants of Ex1Q48 were generated via gene synthesis (GeneArt® Gene Synthesis). Protein fragments of Ex1Q23, Ex1Q48 and of the protein variants were fused N-terminally to glutathione S-transferase (GST) in order to

increase solubility of the proteins and enable purification of the fusion proteins. The exchange of amino acids in the Ex1Q48 sequence might influence the reactivity of anti-HTT antibodies towards the protein variants and might therefore impede immunodetection which is essential for several biochemical assays. Hence, proteins were C-terminally fused to a V5 tag. This small epitope tag was chosen to guaranty minimal interference with the protein's secondary structure and the aggregation process and simultaneously enable proper protein detection.

Fusion proteins were produced in *E.coli* BL21-RP by IPTG-induced expression and purified via glutathione sepharose chromatography. Purity and integrity of the generated proteins were analyzed by SDS-PAGE followed by Coomassie staining (Figure 33A). GST-Ex1Q23 and GST-Ex1Q48 fusion proteins were purified to ~ 90 % homogeneity. In contrast, GST fusion proteins of Ex1Q48 variants showed a main band (marked with *) and a minor secondary band, which might be a product of protein degradation or incomplete protein synthesis. Interestingly, all proteins show a reduced electrophoretic mobility and therefore run at higher molecular weights than calculated. In addition, GST-Ex1Q48M3, GST-Ex1Q48M4 and GST-Ex1Q48M5 show different migration patterns in comparison to GST-Ex1Q48, although they are expected to have the same molecular weight. Previous studies have shown that polyQ proteins have a decreased electrophoretic mobility in SDS gels, supposedly due to an atypical intrinsic structure[285]. Amino acid exchanges in Ex1Q48 might alter its structure and therefore influence the migration behavior.

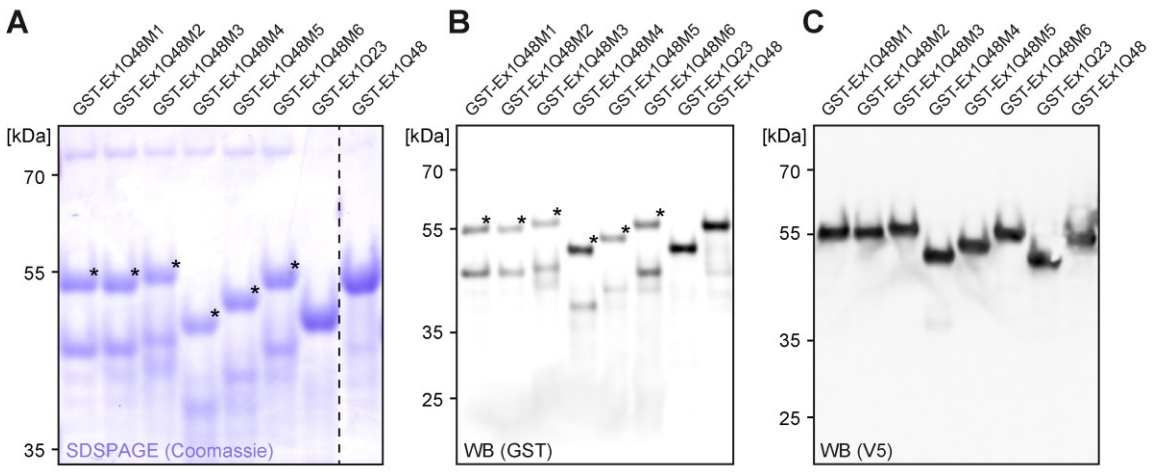

Figure 33: Generation of recombinant Ex1Q48 and its structural variants

(A) *The recombinant GST-tagged HTTex1 fusion proteins were affinity purified using glutathione-coated sepharose beads. Purity was assessed by SDS-PAGE and subsequent Coomassie blue staining. Structural variants showed minor degradation bands. Analysis of recombinant HTTex1 fusion proteins by SDS-PAGE and immunoblotting using the* ***(B)*** *anti-GST or* ***(C)*** *anti-V5 antibody. (* represents full length protein.)*

Next, fusion proteins were immunoblotted to evaluate whether they are detectable by anti-GST (Figure 33B) and anti-V5 antibodies (Figure 33C). The anti-GST antibody recognizes the major band (marked with *), as well the minor band, which migrates faster. The anti-V5 antibody exclusively recognizes the main protein band. This suggests that the minor bands, observed by SDS-PAGE and immunoblotting correspond to N-terminal fragments that no longer contain the V5 tag. Detection of the main band by both the anti-GST and the anti-V5 antibody confirmed that in all cases the expected full-length fusion proteins were successfully purified.

Next, I assessed whether targeted amino acid exchanges in protein variants of Ex1Q48 (Figure 34A) influence the aggregation behavior.

Recombinant proteins at a concentration of 4 µM were cleaved with PreScission protease (PSP) to release GST and to initiate the spontaneous aggregation of V5-tagged proteins. Their assembly was monitored over 168 hours. First, I analyzed the formation of large SDS- and heat-stable aggregates over time using the established filter retardation assay (FRA)(Figure 34B). As expected, Ex1Q48 quickly assembled into SDS-stable aggregates, indicating that the V5 tag does not significantly change the aggregation properties of the protein. Likewise, the protein variants Ex1Q48M1, Ex1Q48M2, Ex1Q48M4 and Ex1Q48M6 formed SDS-stable aggregates, even though their assembly proceeded at very different rates. Ex1Q48M1 assembles quickly and shows high amounts of aggregates already 6 h after the addition of PSP. In contrast, SDS-stable Ex1Q48M6 aggregates are detectable after 48 h and further increased in their abundance over time. For the protein variants Ex1Q48M2 and Ex1Q48M4, I detected faint immunoreactive dots after 168 h, suggesting that aggregation proceeds much slower in comparison to Ex1Q48. FRA analysis revealed that Ex1Q23, Ex1Q48M3 and Ex1Q48M5 do not form SDS-stable aggregates under the applied conditions.

The substitution of amino acids in the Ex1Q48 sequence might not only change the rate of aggregate formation, but might also influence the stability of the resulting aggregate structures. If protein variants formed aggregate structures of lower stability, the traditional FRA would not be able to detect them, as SDS-instable assemblies would be denatured and could therefore not be retained on the filter membrane. Using the dot blot assay, protein assemblies, independent of their size and stability, are immobilized on filter membranes and immunodetected by specific antibodies[239]. Previous studies have demonstrated that epitope specific antibodies preferentially detect monomeric or aggregated HTTex1 proteins as certain epitopes are either exposed or buried depending on the protein's conformation during the aggregation process[159]. The MW8 antibody, which binds to the C-terminus of the HTTex1 protein fragment, was shown to preferentially detect

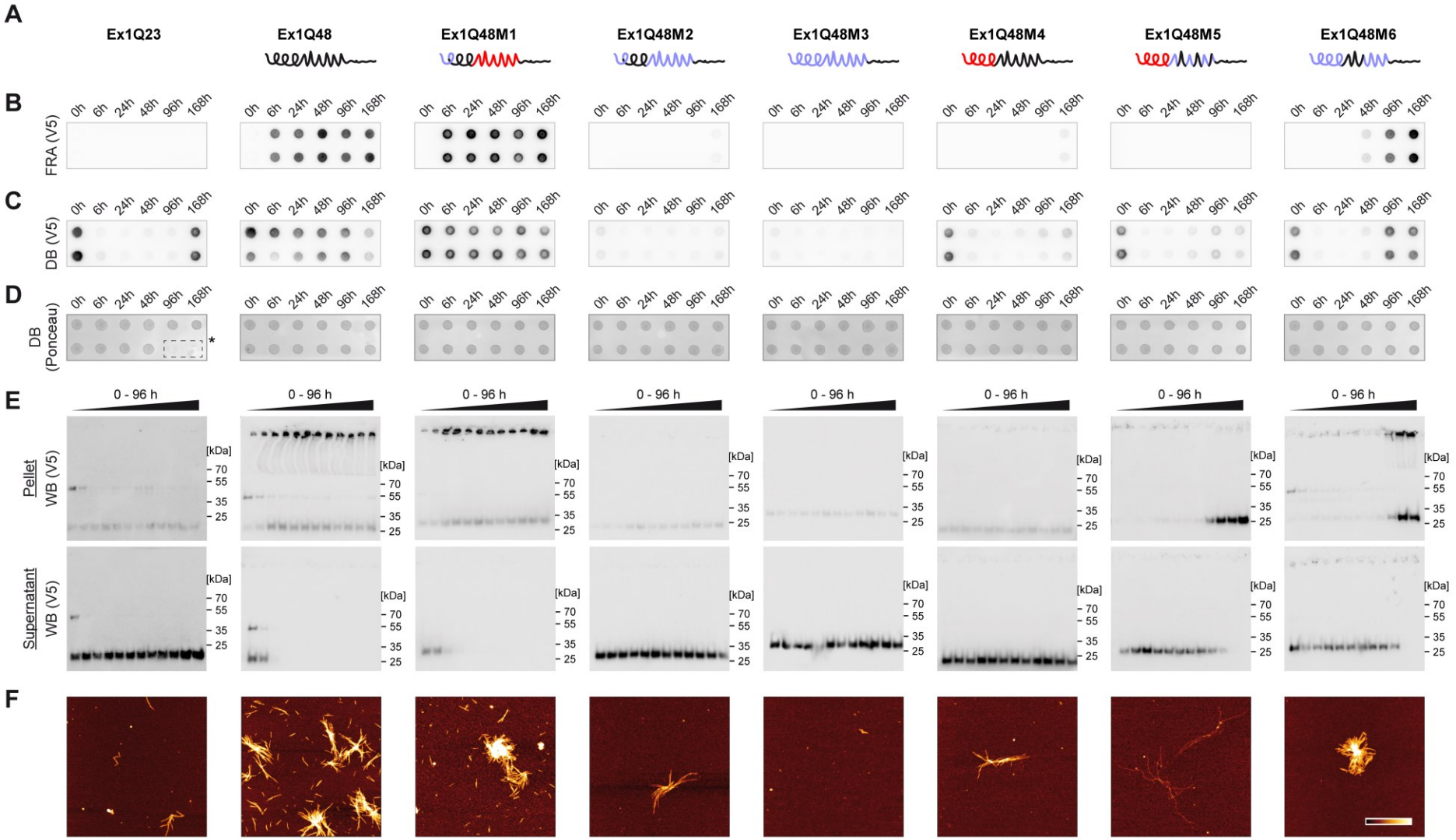

Figure 34: Protein variants of Ex1Q48 show differential aggregation properties (see figure ledgend on the next page)

Figure 34: Protein variants of Ex1Q48 show differential aggregation properties

(A) *Schematic illustration of HTTex1 protein variants.* ***(B)*** *GST fusion proteins of HTTex1 protein variants (4 µM) were individually incubated at 25°C with PreScission protease (PSP). Time-dependent formation of SDS-stable aggregates was analyzed by FRA (500 ng protein per dot). Spontaneously formed aggregates of V5-tagged proteins were visualized by an anti-V5 antibody.* ***(C)*** *Investigation of protein aggregation under non-denaturing conditions using DB assays (250 ng protein per dot). Samples from* ***B*** *were spotted onto a nitrocellulose membrane. Immobilized protein was detected using the anti-V5 antibody.* ***(D)*** *Analysis of samples from* ***B*** *by DB assays followed by Ponceau S staining confirmed that similar amounts of proteins were loaded. *marks empty slots as negative control.* ***(E)*** *Time resolved analysis of spontaneously formed aggregates after 0, 1, 2, 3, 4, 5, 6, 7, 24, 48 and 96 h of incubation with PSP. High and low molecular weight species were fractionated by centrifugation (186,000 x g). Pellet (top) and supernatant (bottom) fractions were analyzed individually by SDS-PAGE and immunoblotting using the anti-V5 antibody.* ***(F)*** *Atomic force microscopy (AFM) analysis of spontaneously formed aggregates of HTTex1 protein variants (4 µM) after 168 h. Scale bars: 1 µm; color gradient represents 0-20 nm height.*

HTTex1 aggregates. As the V5 tag is likewise located at the C-terminal end of the fusion proteins, the anti-V5 antibody might as well identify HTTex1 aggregates. In order to investigate whether Ex1Q48 protein variants form aggregates of lower stability, I performed dot blot assays (DB) followed by immunodetection with an anti-V5 antibody (Figure 34C). For all proteins elevated antibody signal was observed at time point 0 h, indicating that the anti-V5 antibody detects uncleaved fusion proteins in BD assays. Comparable to the analysis by FRA, Ex1Q48 and Ex1Q48M1 showed immunoreactive dots for all other time points analyzed. The protein variants Ex1Q48M6, Ex1Q48M2 and Ex1Q48M4 first showed a decrease of antibody signal, corresponding with the cleavage of GST from the fusion proteins. Starting with the formation of SDS-stable aggregates after 48 h respectively 168 h (Figure 34B) an increase in immunoreactivity was also detected in DB assays (Figure 34C), suggesting that the anti-V5 antibody detects HTTex1 protein and its protein variants in an aggregated conformation. Interestingly, V5 positive dots were detectable for the protein variant Ex1Q48M5 and for Ex1Q23 after 168 h of incubation. As FRA analysis of these proteins demonstrated the absence of SDS-stable aggregates, this observation indicates, that Ex1Q48M5 as well as Ex1Q23 form aggregate structures of lower stability. In contrast, Ex1Q48M3 does not form aggregates under the tested conditions. As a control experiment, I performed DB assays followed by Ponceau S staining. Dots of similar intensities were detectable for all proteins at each time point, demonstrating that equal amounts of proteins were loaded to the DB membranes (Figure 34D). This confirms that the changes in signal intensities, observed when proteins were detected with the anti-V5 antibody, result from a conformational change in the protein and do not result from different amounts of proteins that were loaded onto the membrane.

In order to confirm that protein variants assemble into high molecular weight structures of different stability, I next studied the aggregation process using an experimental approach that

combines ultracentrifugation, SDS-PAGE and Western blot (WB) analysis. After incubation with PSP for 0 – 96 h, protein samples were subjected to ultracentrifugation (186,000 x g) in order to separate high molecular weight aggregates from small soluble protein species. Large protein assemblies regardless of their stability, are expected to concentrate in the pellet, whereas low molecular weight species should remain in the supernatant. Subsequently, pellet and supernatant fractions were examined by SDS-PAGE and WB using the anti-V5 antibody for immunodetection (Figure 34E). Small soluble protein species are expected to appear as a monomer band after immunoblotting of the supernatant fraction. When analyzing the pellet fraction, large SDS-stable aggregates are assumed to remain in the gel pockets as their size and stability permits them to enter the acrylamide gel. In contrast, large SDS-sensitive assemblies, contained in the pellet fraction, will be denatured and are expected to appear as a discrete band at the size of the monomeric protein. When analyzing Ex1Q48 and Ex1Q48M1, I detected that all proteins were cleared from the supernatant fraction already after 3 h of incubation (Figure 34E, bottom). When the corresponding pellet fractions were analyzed, proteins were found in the gel pockets (Figure 34E, top), confirming that Ex1Q48 as well as Ex1Q48M1 quickly assemble into large SDS-stable aggregates. Next, I examined the protein variant Ex1Q48M6. I found that proteins disappeared from the supernatant fraction and appeared in the pellet fraction after 48 h of incubation. Interestingly, proteins in the pellet fractions were partially detectable in the gel pockets but also appeared as a distinct band at the size of the monomeric protein. This indicates that Ex1Q48M6 assembles into aggregates which are less SDS-stable and partially disassemble upon SDS treatment. Similarly, Ex1Q48M5 protein is reduced in the supernatant fraction after 48 h and accumulates in the pellet fraction. Strikingly, all protein detected in the pellet fraction migrates in the gel with the size of the monomer, confirming the initial hypothesis that protein variant Ex1Q48M5 forms large, but SDS instable aggregates. The proteins Ex1Q48M2, Ex1Q48M3, Ex1Q48M4 and Ex1Q23 were detected exclusively in the supernatant fractions, confirming that these proteins do not form SDS stable aggregates within 96 h under these experimental conditions.

Next, I characterized the aggregate morphologies of the HTTex1 protein assemblies. Proteins were incubated with PSP for 168 h and analyzed by atomic force microscopy (AFM)(Figure 34F). Multiple large bundles of fibrillar structures were formed by the proteins Ex1Q48, Ex1Q48M1 and Ex1Q48M6. AFM analysis of Ex1Q23, Ex1Q48M2 and Ex1Q48M4 revealed a few small fibrillar structures, which appear morphologically similar to the structures observed for Ex1Q48 but less mature as they were smaller and less branched. Interestingly, Ex1Q48M5 forms morphologically distinct fibrillar structures. Fibrils were thinner and less branched, but seemed to

be longer and more curvated in comparison to the rather rigid Ex1Q48 fibrils. As expected, no aggregates were observed for the protein Ex1Q48M3.

Finally, I performed FRASE assays to analyze whether preformed aggregates of the different protein variants are able to seed the co-aggregation of Ex1Q48-CyPet/-YPet reporter proteins. Protein variants were incubated with PSP for 168 h and used as seeds at a concentration of 100 nM. Seeding activity was detectable for Ex1Q48 and for the protein variants Ex1Q48M1, Ex1Q48M4, Ex1Q48M5 and Ex1Q48M6 (Figure 35A and B).

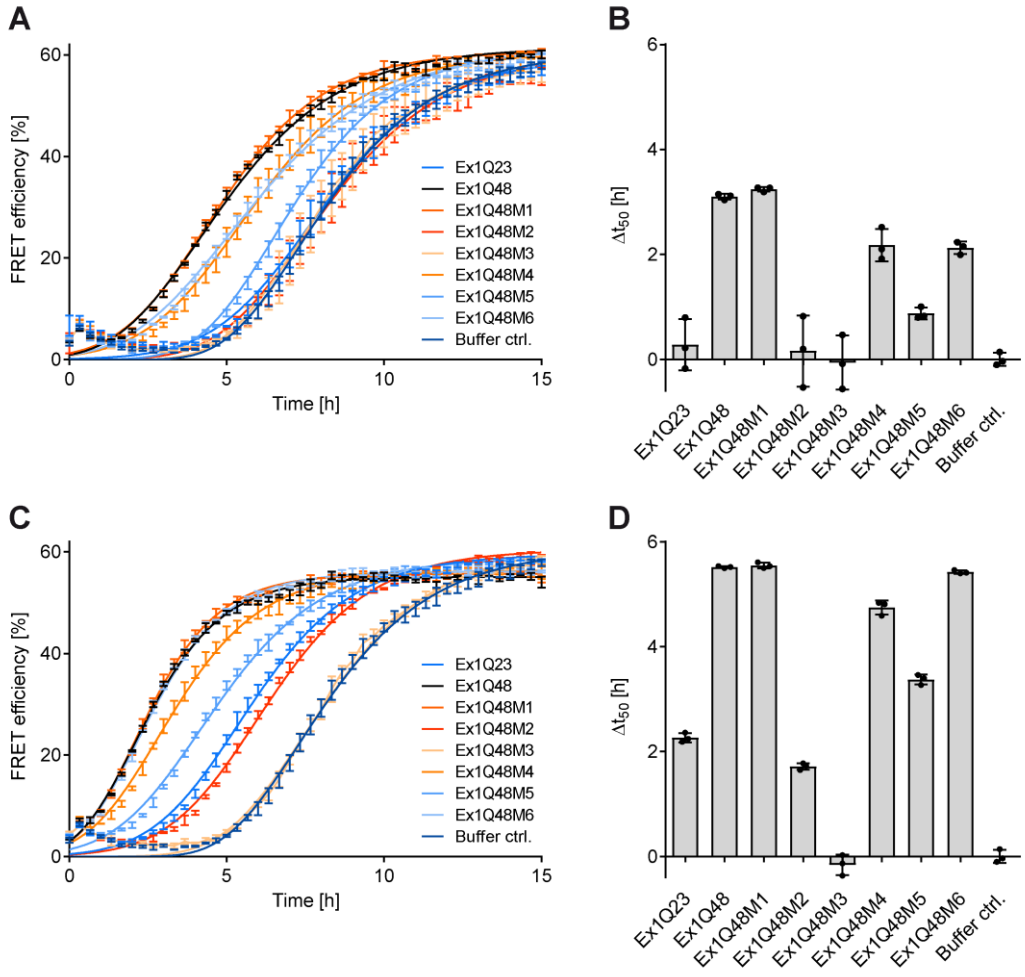

Figure 35: Protein variants of Ex1Q48 form seeding-competent aggregates

(A) *FRET-based assessment of Ex1Q48-CyPet/-YPet (1.2 µM) co-aggregation in the presence of 100 nM HTTex1 protein variants as seeds. The GST-tagged HTTex1 protein variants (4 µM) were incubated with PSP for 168 h prior to FRASE analysis. FRET efficiency is displayed as mean ± SD of technical triplicates.* ***(B)*** *Calculated Δt_{50} values from Ex1Q48-CyPet/-YPet co-aggregation profiles in* ***A****. Individual Δt_{50} values of each triplicate are displayed as black dots (●) and mean ± SD of technical triplicates.* ***(C)*** *FRASE analysis of HTTex1 protein variants as described in* ***A*** *after sonication.* ***(D)*** *Calculated seeding activity from aggregation profiles in* ***C****. Individual Δt_{50} values of each triplicate are displayed as black dots (●) and mean ± SD of technical triplicates.*

In order to detect seeding competent HTTex1 aggregates with the highest possible sensitivity, preformed aggregates were sonicated prior to FRASE analysis. Seeding activity was detectable for all investigated HTTex1 proteins under these conditions, except for the structural variant Ex1Q48M3, which does not form detectable fibrillar aggregates *in vitro* (Figure 34F) and therefore cannot accelerate the co-aggregation of Ex1Q48-CyPet/-YPet reporter proteins.

In summary, biochemical and biophysical analysis of Ex1Q48 variants revealed remarkable differences in their aggregation behavior. In comparison to the aggregation-prone Ex1Q48 protein, all variants, except Ex1Q48M1, aggregate with lower efficiency or did not form aggregates at all (Ex1Q48M3) (Figure 34B-E). Strikingly, all aggregation-prone Ex1Q48 variants self-assemble into structures with a fibrillar morphology, although with very different size and complexity (Figure 34F). A exceptional change in aggregate morphology was observed for Ex1Q48M5, indicating that the substitution of AA in the polyQ tract alters the structure of spontaneously formed HTTex1 protein aggregates. Fractionation experiments revealed that AA exchanges in the polyQ domain do not prevent aggregation, but strongly change the stability of HTTex1 protein aggregates. Certain Ex1Q48 variants assemble into aggregates which lack SDS-stability either partially (Ex1Q48M6) or completely (Ex1Q48M5) (Figure 34E). In addition, I observed that all protein variants that form fibrillar aggregates possess seeding activity (Figure 35).

3.2.3. Creating *Drosophila* models of mutant HTTex1 protein variants

The protein variants of Ex1Q48 showed strong differences in their aggregation behavior which makes them a valuable tool to study the relationship between aggregate formation, seeding activity and proteotoxicity. For this purpose, I aimed to generate *Drosophila* models expressing mutant HTTex1 protein variants and the respective pathogenic and wild type HTTex1 control proteins. Previous experiments indicate that pan-neuronal expression of Ex1Q48 in *Drosophila* causes a very mild disease-related phenotype, whereas expression of Ex1Q97 was shown to cause very severe behavioral changes[262]. AA exchanges might either increase or decrease mHTTex1 induced toxicity. To be able to detect exacerbation as well as amelioration of disease-related phenotypes with sufficient resolution, it was desirable to create the new fly models on the basis of a transgenic HD strain, which shows behavioral changes of intermediate strength. Therefore, I adjusted the length of the polyQ domain to 75 residues and adapted the AA exchanges accordingly (Suppl. Figure 3A). *In silico* analysis demonstrated that the protein variants' individual propensities to form coiled-coil and amyloid structures were preserved after expansion of the polyQ stretch (Suppl. Figure 3B-D and Figure 32). All HTTex1 proteins were equipped with a C-terminal V5 tag to facilitate the detection of the transgenic proteins *in vivo*.

Results

In order to generate the described fly models, cDNAs encoding Ex1Q17, Ex1Q75 and six variants of Ex1Q75 were generated via gene synthesis (GeneArt® Gene Synthesis) and cloned into the pUAST-attB-rfA vector[263]. Plasmid DNA containing the gene of interest and an eye-specific marker gene (*mini-white*) was injected into the posterior end of *white- Drosophila* embryos by Rainbow Transgenic Flies, Inc. (Figure 36A). The *Drosophila* strain (genotype: y1 M[vas-int.Dm]ZH-2A w*; M[3xP3-RFP.attP']ZH-68E) contains a phage attachment site (attP) on the third chromosome (2A3, 68E), which is complementary to the bacteriophage attachment site (attB) of the pUAST-attB-rfA vector. At the time of injection, the *Drosophila* embryo exists as one multinucleated cell (syncytium). During the cellularization process, plasmid DNA is taken up by germ cell precursors (pole cells) and is integrated at the attP site on the third chromosome via ΦC31 integrase mediated recombination.

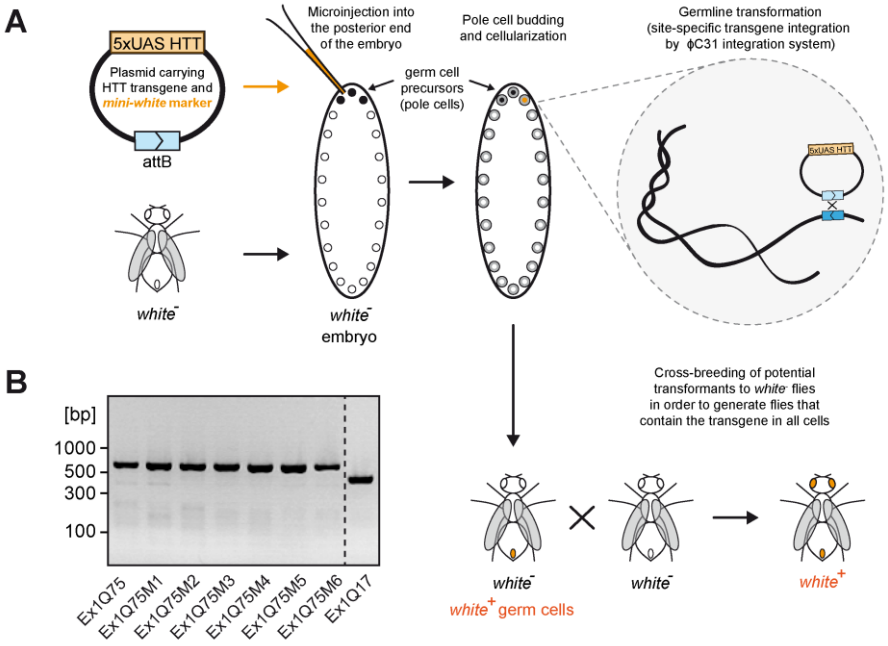

Figure 36: Generation of transgenic Drosophila models of HTTex1 protein variants

(A) *Schematic illustration of Drosophila transgenesis using the ΦC31 integrase system. Transgene DNA containing a mini-white marker (orange) is micro-injected into white- Drosophila embryos. During early developmental stages Drosophila embryos undergo rapid nuclear divisions that occur without accompanying cell divisions, creating a syncytium. Prior to cellularization, germ cell precursors (pole cells, black) bud off at the posterior end. These cells need to take up the transgenic DNA for germ line transmission to occur. Within the pole cells the transgene is integrated into the pre-determined genetic locus through ΦC31 integrase-mediated recombination of the bacteriophage attachment site (attB, light blue) in the transgene DNA and the phage attachment site (attP, dark blue) in the Drosophila genome. If the transgene is integrated into germ cells, it can be passed on to the next generation. Successful integration can be identified by the orange eye color as a result of the mini-white marker.* ***(B)*** *PCR analysis of genomic DNA from newly generated Drosophila models followed by Sanger sequencing confirmed the integration of the correct transgene. PCR products of 621 bp (Ex1Q48, Ex1Q48M1-6) and 502 bp (Ex1Q17) were as expected.*

Though site-specific integration of transgenic DNA at the pre-selected locus, chromosomal position effects are avoided and fly strains expressing different transgenes can be directly compared. Embryos that have successfully integrated transgenic cDNA develop into mature flies containing the new genetic information in their germline. Cross-breeding of the transformant to the *white*- background strain produces offspring that contains the transgenic cDNA in all cells. Transgene integration can be easily identified as the presence of the *mini-white* marker gene results in an orange eye color in an otherwise white-eyed fly strain. Transformants were selected and crossed with the balancer stain $\frac{CyO}{Sp}; \frac{TM6}{MKRS}$ [262] in order to generate a stable fly strain $\frac{CyO}{Sp}; \frac{TM6}{\boldsymbol{HTT\ transgene}}$.

To confirm the genetic identity of the newly generated fly strains, genomic DNA was isolated and used as template for PCR amplification of the HTTex1 sequence. PCR products of the expected size were identified by agarose gel electrophoresis (Figure 36B). Sanger sequencing of PCR products confirmed the correct genetic identity of the novel fly models.

3.2.4. *Drosophila* models expressing protein variants show distinct behavioral phenotypes

Within the following chapter, I will describe the phenotypic consequences that result from the expression of HTTex1 protein variants in *Drosophila melanogaster*. These experiments might provide valuable insights into the relationship between aggregate formation and proteotoxicity.

In order to express the protein variants of HTTex1, I made use of the GAL4/UAS system[264,286,287] (Figure 37A). The GAL4 protein, originally derived from yeast, is a transcriptional activator that specifically binds to the upstream activation sequence (UAS) and activates transcription. To control gene expression in *Drosophila*, the GAL4/UAS system is used as a bipartite approach. A driver strain expresses the GAL4 protein under the control of a tissue-specific promotor. A responder strain contains the gene of interest downstream of the UAS. However, transgene expression is inactive due to the absence of GAL4 protein in the responder strain. Cross-breeding of driver and responder strains results in progenies which combine both elements of the GAL4/UAS system. In the final HD strains (progeny) the GAL4 protein will bind to the UAS and activate transgene expression in a tissue-specific manner (Figure 37A).

Responder strains, containing the genetic information of the HTTex1 protein variants downstream of the UAS, were cross-bred with the Elav-GAL4 driver strain. Elav-GAL4 induces pan-neuronal expression of the transgenes at all developmental stages[288]. To analyze protein expression, head lysates were prepared from 10 day-old flies and examined by SDS-PAGE and

Western blotting using the anti-V5 antibody for immunodetection. Protein expression was detected in all *Drosophila* strains (Figure 37B). To validate antibody specificity I analyzed flies that expressed the GAL4 protein, but do not contain transgene cDNA (Elav;Bkg). Except for a very faint unspecific signal in the upper part of the immunoblot, no protein band was detectable, indicating that the anti-V5 antibody specifically recognizes V5-tagged transgenic proteins. Comparing the two control proteins Ex1Q75 and Ex1Q17, I observed a clear difference in size (~42 kDa and ~20 KDa), resulting from the longer polyQ domain in the pathogenic HTTex1 fragment. As already observed for the recombinant proteins, all proteins show reduced electrophoretic mobility and appear to have a higher molecular weight than calculated in SDS gels (calculated molecular weight of Ex1Q75 and its protein variants: ~18 kDa, calculated molecular weight of Ex1Q17 10 kDa; see Figure 37B). Likewise, similar to the purified recombinant proteins Ex1Q48M4 and Ex1Q48M5 (Figure 33),the proteins Ex1Q75M4 and Ex1Q75M5 migrate faster than Ex1Q75. Surprisingly, Ex1Q75M2 and Ex1Q75M3, both carrying proline substitutions in their N17 domains, show two bands that migrate slower than Ex1Q75. This is potentially due to an altered post-translational modification of the protein variants. In addition, high molecular weight protein aggregates were

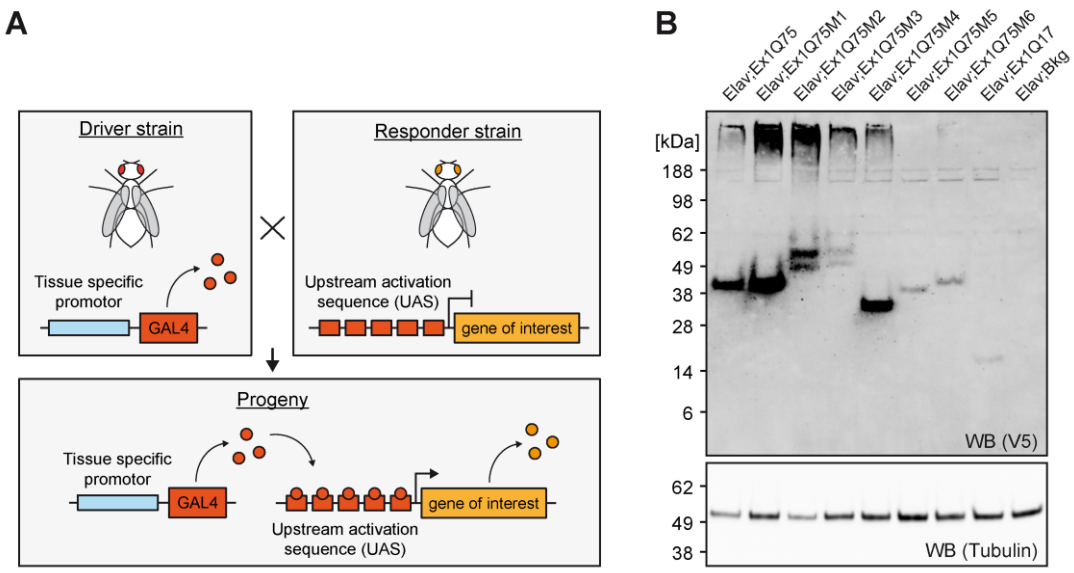

Figure 37: Pan-neuronal expression of Ex1Q75 protein variants in transgenic Drosophila models

(A) *Graphical illustration of the GAL4/UAS expression system[264,286,287]. It is a bipartite system which is used to control transgene expression in a tissue-specific manner. A driver strain expresses the GAL4 protein, a yeast-derived transcriptional activator, under the control of a tissue-specific promotor. A responder strain contains the gene of interest downstream of the upstream activation sequence (UAS). Cross-breeding of both strains combines both elements of the GAL4/UAS system in the progeny. The GAL4 protein will bind to the UAS promoter and activate transgene expression in a tissue-specific manner.* ***(B)*** *Western blot analysis of the HTTex1 protein variants expressed in neurons of HD transgenic flies using anti-V5 antibody. Immunodetection using an anti-Tubulin antibody confirmed that similar amounts of protein lysate were loaded.*

detectable in the gel pockets for Ex1Q75, Ex1Q75M1, Ex1Q75M2, Ex1Q75M3, Ex1Q75M4 and Ex1Q75M6. It needs to be noted that the steady state protein levels differ from strain to strain, suggesting that the proteins are produced or degraded at different rates in fly neurons. In general, protein levels seem to be higher for HTTex1 proteins that form SDS-stable aggregates *in vivo*.

Elav-GAL4 driven pan-neuronal transgene expression occurs in all developmental stages of the *Drosophila* life cycle[288]. In order to investigate whether the expression of HTTex1 protein variants influences fly development, I analyzed the hatching behavior.

Expression of HTTex1 protein variants was induced through cross-breeding of HD responder strains with Elav-GAL4 flies. First, I observed the development of the generated flies. All strains passed from oviposition through the first, second and third instar larval stages. Likewise, flies of all strains pupated and developed from white prepupae to mature pupae (Figure 38A, 9-11 days post oviposition). Eye pigmentation and the development of black wings gives mature pupae a dark appearance which indicatives the imminent eclosion of the adult fly. Flies started to hatch ~13 days post oviposition leaving behind the transparent pupal skin. For the majority of fly strains, hatching was completed within 16-18 days after oviposition, as indicated by the predominant presence of transparent, empty pupae (Figure 38A, 16 – 18 days post oviposition). In contrast, I observed multiple dark pupae for the Elav;Ex1Q75M2 strain, indicating that the majority of flies did not emerge from the pupae.

In order to confirm this finding, hatching flies were counted. The average number of flies that hatched per day are displayed in Figure 38B. On average ~ 80 flies/day emerged from the pupae when no transgene (Elav;Bkg) or a non-pathogenic Ex1Q17 protein was expressed. Eclosion behavior was similar to controls when flies expressed the proteins Ex1Q75, Ex1Q75M3, Ex1Q75M4, Ex1Q75M5 or Ex1Q75M6. In contrast, expression of the proteins Ex1Q75M1 and Ex1Q75M2 drastically reduced the number of hatching flies.

In addition, I assessed the sex ratio of the progeny by counting the number of male and female flies. For the control strains, expressing no transgene or non-pathogenic Ex1Q17, the sex ratio was close to 50 %, indicating that similar numbers of male and female flies emerged (Figure 38C). Likewise, the sex ratio remained close to 50 % when the protein variants Ex1Q75M3, Ex1Q75M5 or Ex1Q75M6 were pan-neuronally expressed. However, a lower proportion of male progeny was observed for Elav;Ex1Q75 and Elav;Ex1Q75M4 flies, indicating a developmental bias towards female flies. This maldistribution became even more obvious for Elav;Ex1Q75M1 and Elav;Ex1Q75M2 flies, for which the percentage of male flies was reduced to 25 % and 10 %, respectively.

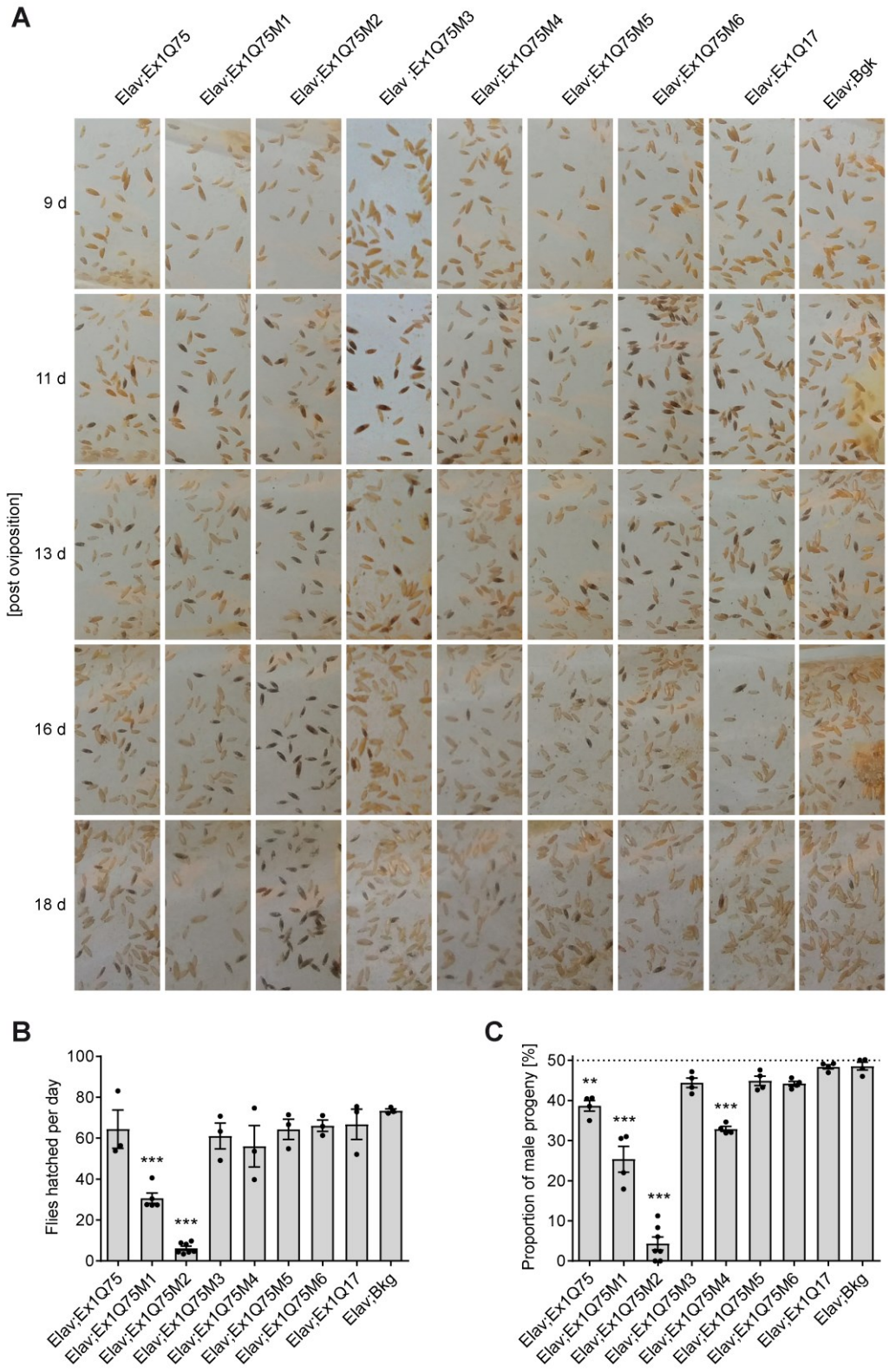

Figure 38: Drosophila models expressing mHTTex1 protein variants show a perturbed eclosion behavior

(A) *Representative photographs documenting the pupal development (9 – 18 days post oviposition) of flies expressing HTTex1 protein variants.* ***(B)*** *Average number of hatching flies per day and crossing vial.* ***(C)*** *Average percentage of male progeny. Fly count/percentage of male flies for an individual experiment (●). Bars are mean ± SEM. Statistical significance was assessed by One-Way ANOVA followed by Dunnett's multiple comparisons test; data were compared to Elav;Ex1Q75 transgenic flies.*

Taken together these results suggest that pan-neuronal expression of Ex1Q75, Ex1Q75M1, Ex1Q75M2 and Ex1Q75M4 causes adverse effects *in vivo* that are manifested already early during fly development.

Following the assessment of fly development, I investigated whether pan-neuronal expression of HTTex1 protein variants influences behavioral phenotypes of adult flies.

At first, I analyzed the survival of HD transgenic flies. Flies were raised from cross-breeding of Elav/GAL4 and the newly generated HTTex1 responder strains. As an additional control ZH-68E flies, which have the same genetic background as the responder strains, but do not contain a transgene to express, were cross-bred with Elav/GAL4 flies (Elav;Bkg). Survival was measured over time by counting dead flies (Figure 39A). Based on the survival curves, I calculated the median life span, representing the age at which half of the analyzed fly population died (Figure 39B). Flies that express non-pathogenic Ex1Q17 have a median lifespan of ~90 days and show no adverse survival effects compared to control flies that do not express a transgene (Elav;Bkg). In comparison, pan-neuronal expression of Ex1Q75 causes a strong reduction in survival (median lifespan of ~26 days), indicating that *Drosophila* is a suitable system to model HTTex1 induced toxicity. The median lifespans of Elav;Ex1Q75M3 (~24 days) and Elav;Ex1Q75M4 (~23 days) flies were very similar to Elav;Ex1Q75 flies. In contrast, fly survival was even further reduced in Elav;Ex1Q75M1 (~18 days) and Elav;Ex1Q75M2 (~14 days) flies, which both already showed strong impairments in their eclosion behavior. In contrast, I observed extended survival in Elav;Ex1Q75M5 (~80 days) and Elav;Ex1Q75M6 (~37 days) flies in comparison to Elav;Ex1Q75 flies (~26 days).

As an additional control, I investigated whether the newly generated fly strains are comparable regarding their survival in the absence of transgene expression. Through cross-breeding of the responder strains with w1118 flies, I generated flies that carry the UAS-transgenes but lack the GAL4 protein and therefore should not produce the HTTex1 protein variants. Measuring the survival over time (Figure 39C), I found that all fly strains behave similarly (median life span ~85 days, Figure 39D), indicating that the integration of transgenes does not significantly influence fly survival. Hence, differences in survival described above result from the expression of Ex1Q75 protein and its variants.

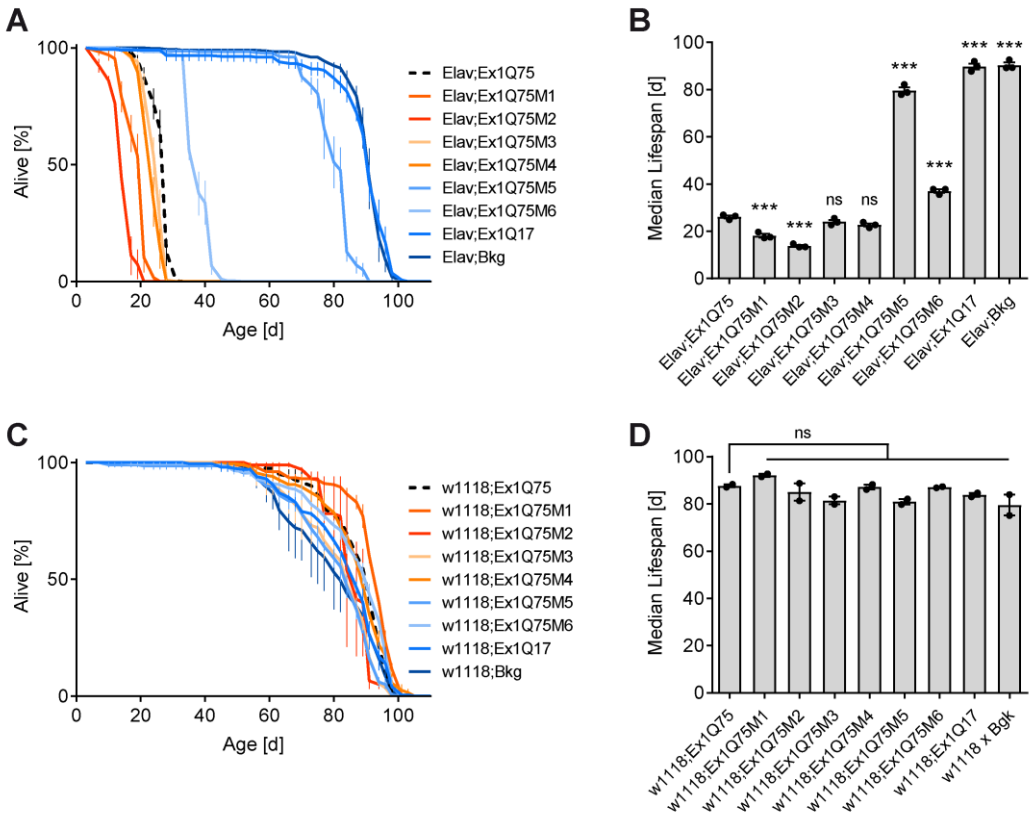

Figure 39: Amino acid exchanges modify the pathological effect of Ex1Q75 on Drosophila survival

(A) *Lifespan analysis of flies expressing HTTex1 protein variants in neurons. Life span is plotted as the percentage of surviving flies of 3 biological replicates ($n^{Elav;Ex1Q75}$ = 86, 94, 88; $n^{Elav;Ex1Q75M1}$ = 81, 94, 62; $n^{Elav;Ex1Q75M2}$ = 50, 48, 8; $n^{Elav;Ex1Q75M3}$ = 94, 98, 100; $n^{Elav;Ex1Q75M4}$ = 101, 98, 94; $n^{Elav;Ex1Q75M5}$ = 88, 83, 86; $n^{Elav;Ex1Q75M6}$ = 98, 95, 85; $n^{Elav;Ex1Q17}$ = 93, 86, 90; $n^{Elav;Bkg}$ = 100, 87, 89).* ***(B)*** *Median life span calculated from survival curves in* ***A****. Average survival of each experiment (n = ~100 flies) is presented as black dots (●). Bars are mean ± SEM from 3 independent replicates; statistical significance was assessed by One-way ANOVA Dunnett's post-hoc test; data were compared to Elav;Ex1Q75 transgenic flies.* ***(C)*** *Lifespan analysis of generated Drosophila models in the absence of transgene expression. Life span is plotted as the percentage of surviving flies of 2 biological replicates ($n^{w1118;Ex1Q75}$ = 97, 92; $n^{w1118;Ex1Q75M1}$ = 85, 93; $n^{w1118;Ex1Q75M2}$ = 97, 88; $n^{w1118;Ex1Q75M3}$ = 89, 86; $n^{w1118;Ex1Q75M4}$ = 96, 93; $n^{w1118;Ex1Q75M5}$ = 96, 92; $n^{w1118;Ex1Q75M6}$ = 89, 84; $n^{w1118;Ex1Q17}$ = 89, 92; $n^{w1118;Bkg}$ = 94, 85).* ***(D)*** *Median life span calculated from survival curves in* ***C****. Average survival of each experiment (n = ~100 flies) is presented as black dots (●). Bars are mean ± SEM from 2 independent replicates; statistical significance was assessed by One-way ANOVA Dunnett's post-hoc test; data were compared to w1118;Ex1Q75 transgenic flies.*

As a behavioral measure of neuronal dysfunction, locomotor activity was assessed using a negative geotaxis (climbing) assay[289] which has been extensively applied to characterize fly models of neurodegenerative diseases[265,266]. With this assay, the proportion of flies that is able to climb a height of 8 cm within 15 seconds is recorded. Flies of the control group (Elav;Bkg) show a progressive decline in locomotor activity over time (Figure 40A). Previous studies demonstrated that decline in locomotor activity is a normal age-related behavior of wild-type flies[290]. As expected, flies expressing Ex1Q17 performed comparable to control flies. In contrast,

pan-neuronal expression of Ex1Q75 and its protein variants reduces locomotor activity. In order to compare the locomotor activity of different strains, I used the recorded climbing curves and calculated the area under the curves as an average measure of motor performance for each strain (Figure 40B). In comparison to Elav;Ex1Q75 flies, Elav;Ex1Q75M5 show a significantly better motor performance. The expression of the other protein variants did not significantly change the overall motor performance compared to Elav;Ex1Q75 flies. However, in depth analysis showed that locomotor activity is significantly different compared to Elav;Ex1Q75 flies during a certain period in the flies' lifespan. I observed significantly reduced locomotor activity in Elav;Ex1Q75M1 (10 - 17 days), Elav;Ex1Q75M2 (7 - 14 days) and Elav;Ex1Q75M4 (14 - 17 days) flies, whereas Elav;Ex1Q75M6 flies (21 - 28 days) showed improved locomotor activity (Figure 40A).

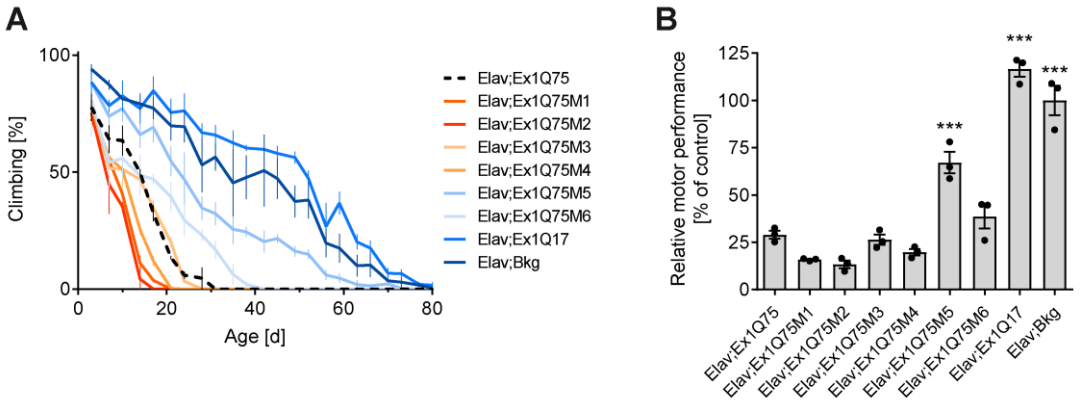

Figure 40: Pathological effects of Ex1Q75 on motor performance are influenced by amino acid exchanges

(A) *Analysis of motor performance of flies expressing HTTex1 protein variants in neurons. Motor performance was assessed over time as the percentage of flies able to climb a height of 8 cm within 15 sec. Results are presented as mean of 3 independent replicates starting with* $n^{Elav;Ex1Q75}$ *= 100, 98, 98;* $n^{Elav;Ex1Q75M1}$ *= 98, 95, 99;* $n^{Elav;Ex1Q75M2}$ *= 5, 63, 19;* $n^{Elav;Ex1Q75M3}$ *= 100, 101, 100;* $n^{Elav;Ex1Q75M4}$ *= 99, 98, 99;* $n^{Elav;Ex1Q75M5}$ *= 99, 98, 101;* $n^{Elav;Ex1Q75M6}$ *= 95, 100, 98;* $n^{Elav;Ex1Q17}$ *= 100, 100, 92;* $n^{Elav;Bkg}$ *= 100, 100, 100 flies.* ***(B)*** *Relative motor performance was analyzed by calculating the area under the curve from climbing curves in* ***A****. Results are expressed as percentage of control (Elav;Bkg). Average motor performance of each experiment (n = ~100 flies) is presented as black dots (●). Bars are mean ± SEM from 3 independent replicates; statistical significance was assessed by One-way ANOVA Dunnett's post-hoc test; data were compared to Elav;Ex1Q75 transgenic flies.*

Next, I investigated whether expression of Ex1Q75 protein and its variants changes circadian locomotor behavior. Male flies raised from cross-breeding of Elav/GAL4 and HTTex1 responder strains, were analyzed using the *Drosophila* Activity Monitor (DAM) system[291]. Flies are maintained individually in sealed glass tubes which are placed into the activity monitor. Three infrared beams are directed at each glass tube. Beam breaks resulting from flies crossing the beam, are interpreted as activity events. Events detected within a 5 min sampling interval are

summed and recorded over 30 days. All fly strains show crepuscular behavior with activity peaks in the dawn and dusk periods (Figure 41A). However, peak activities were remarkably different among different strains. In order to depict the changes in peak activities over time for each fly strain, beam breaks detected in the period between 7.00 – 7.30 am were summed and displayed as dawn locomotor activity for each consecutive day (Figure 41B). Similar as for the climbing assays, control flies (Elav;Bgk) showed an age-dependent decrease in locomotor activity[290].

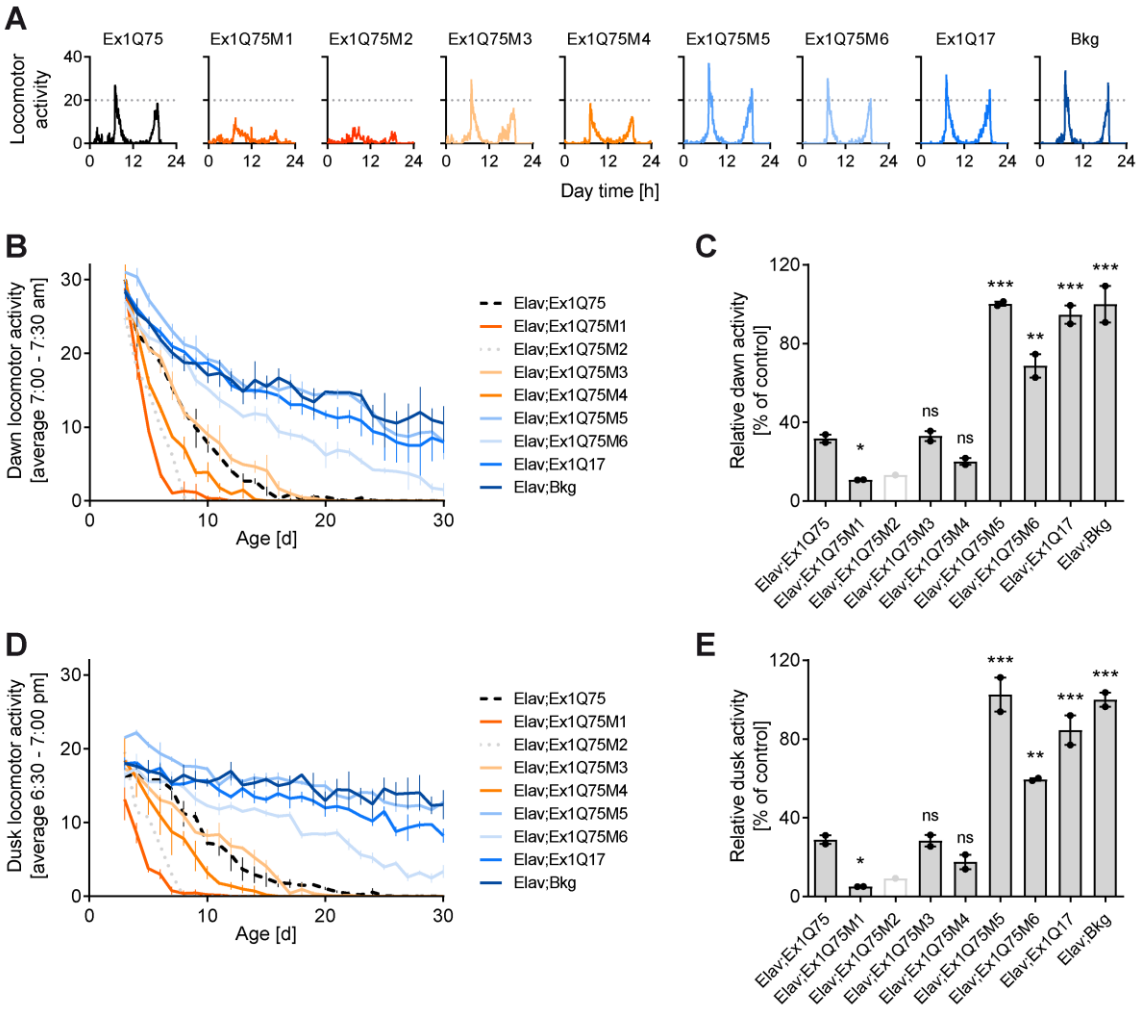

Figure 41: Expression of HTTex1 protein variants influence circadian locomotor behavior of transgenic flies

(A) *Circadian locomotor activity of five days old male flies under 12:12 light-dark cycle with lights on at 7:00 am. Transgenes were expressed pan-neuronally using the Elav-GAL4 gene driver. Due to the low number of male Elav;Ex1Q75M2 progeny (n_{total} = 3), results were exclude from statistical analysis and depicted in grey color.* ***(B)*** *Dawn locomotor activity over time was quantified as sum of beam breaks between 7:00 and 7:30 am for each day.* ***(C)*** *Relative dawn activity was analyzed by calculating the area under the curve from locomotor activity curves in* ***B****. Results are expressed as percentage of control (Elav;Bkg). Relative dawn activity of each experiment (n = ~14 flies) is presented as black dots (●). Bars are mean ± SEM from 2 independent replicates; statistical significance was assessed by One-way ANOVA Dunnett's post-hoc test; data were compared to Elav;Ex1Q75 transgenic flies.* ***(D)*** *Dusk locomotor activity (between 6:30 and 7:00 pm) and* ***(E)*** *relative dusk activity were quantified accordingly.*

Flies expressing Ex1Q17 and Ex1Q75M5 performed comparable to control flies, whereas the expression of Ex1Q75 and of the remaining protein variants caused a rapid decline of the locomotor activity. I quantified the area under the activity curves in order to assess and compare the overall dawn activity of different strains (Figure 41C). Expression of Ex1Q75 reduced dawn activity to ~30 % relative to control flies. In comparison to Elav;Ex1Q75 flies, dawn activity was significantly higher for Elav;Ex1Q75M5 and Elav;Ex1Q75M6 flies and significantly lower in Elav;Ex1Q75M1 flies. Expression of Ex1Q75M3 and Ex1Q75M4 did not significantly change the overall dawn activity in comparison to Elav;Ex1Q75 flies. However, a more detailed analysis revealed that flies expressing Ex1Q75M4 show a decrease in locomotor activity in 5 to 9-day-old flies. Expression of Ex1Q75M2 also seems to cause a reduction of dawn activity in comparison to Elav;Ex1Q75 flies. However, statistical analysis of Elav;Ex1Q75M2 flies could not be performed due to the extremely low number of male flies that were available for this assay (Figure 38). Quantification of dusk activity (6.30 – 7.00 pm) confirmed the observation described above (Figure 41D and E).

In summary, behavioral analysis of flies expressing HTTex1 protein variants revealed remarkable differences in fly development, survival and locomotor activity. Whereas the expression of wild-type Ex1Q17 did not change fly behavior, the expression of pathogenic Ex1Q75 clearly reduced *Drosophila* survival and locomotor activity, suggesting that Ex1Q75 induces dysfunction and neurotoxicity with severe phenotypic consequences. In addition, the phenotypic characterization of flies expressing Ex1Q75 protein variants suggests that amino acid exchanges in the HTTex1 sequence influence HTT induced toxicity. Whereas amino acid exchanges in Ex1Q75M1, Ex1Q75M2 and Ex1Q75M4 exacerbated the pathogenic effects of the Ex1Q75 protein, the amino acid exchanges in Ex1Q75M5 and Ex1Q75M6 had the opposite effect.

3.2.5. Biochemical assessment of aggregates of HTTex1 protein variants formed *in vivo*

In order to investigate whether there is a correlation between mHTTex1 aggregation and proteotoxicity, I quantified aggregate amounts and seeding activity in fly head lysates using FRAs and FRASE assays.

First, I assessed the formation of large SDS-stable HTTex1 aggregates in a time-resolved manner. Flies were raised through cross-breeding of HTTex1 responder strains with Elav/GAL4 flies, triggering pan-neuronal expression of Ex1Q75 and its protein variants. Similarly, I generated control flies, expressing no transgene or wild-type Ex1Q17 protein. Head lysates were prepared at an age of 5, 10, 15 and 20 days and analyzed by FRA)(Figure 42A). I detected large SDS-stable

aggregates in Elav;Ex1Q75 flies which increased in their abundance over time. As expected, no aggregates were detected in control flies (Elav;Bkg) and Ex1Q17 expressing flies. In head lysates of Elav;Ex1Q75M3 and Elav;Ex1Q75M4 flies the abundance of SDS-stable HTTex1 aggregates was similar to Elav;Ex1Q75 flies. Strikingly, higher amounts of SDS-stable aggregates were detected in Elav;Ex1Q75M1 and Elav;Ex1Q75M2 flies, which showed the most severe behavioral changes (Figure 38 - Figure 41), suggesting that aggregation drives the pathogenic process in flies. In contrast, lower amounts of SDS-stable aggregates were found in head lysates of Elav;Ex1Q75M5 and Elav;Ex1Q75M6 flies, substantiating the hypothesis that mHTTex1 aggregates play a critical role in disease.

Finally, I applied the FRASE assay to investigate whether the mHTTex1 aggregates formed in HD flies are seeding-competent structures. Head lysates of flies were analyzed at an age of 5 days. Whereas no seeding activity was detectable in head lysates of Elav;Ex1Q17 flies, it was significantly increased in protein lysates prepared of transgenic flies expressing Ex1Q75, Ex1Q75M1, Ex1Q75M2, Ex1Q75M3 or Ex1Q75M4 (Figure 42B). In comparison to Elav;Ex1Q17 flies, Elav;Ex1Q75M5 and Elav;Ex1Q75M6 flies showed a slight, but not significant increase in HSA.

Together these results illustrate the concurrence of aggregate formation and neurotoxicity in HD transgenic flies, supporting the hypothesis that misfolded protein assemblies play a major role in HD pathology.

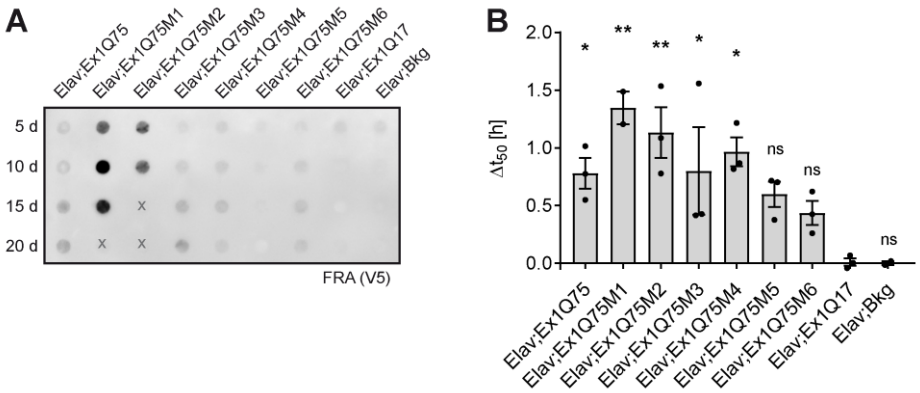

Figure 42: Analysis of aggregate formation in flies expressing HTTex1 protein variants

(A) Detection of large SDS-stable HTTex1 aggregates in fly heads by FRAs immunodetected with the anti-V5 antibody. (B) Quantification of mHTTex1 seeding activity in heads of 5-day-old flies by FRASE assays. Values are plotted as means ± SEM of three biological replicates each performed in triplicates. Individual measurements are presented as black dots (●); One-way ANOVA Dunnett's post hoc test compared to Elav;Ex1Q17 flies.

In summary, in the second part of this thesis I designed six protein variants of mutant HTTex1 through targeted amino acid exchanges and studied their aggregation properties *in vitro*. The generated recombinant mHTTex1 protein variants were distinct in their aggregation properties and revealed fibrillar aggregate species with different stabilities and morphologies. Thus, they are a valuable tool to study the relationship between HTTex1 aggregate formation and toxicity *in vivo*. For this purpose, I generated various new *Drosophila* strains expressing the HTTex1 protein variants pan-neuronally. Behavioral analysis of these flies revealed remarkable differences in fly development, survival and locomotor activity. Finally, I investigated the formation of HTTex1 aggregates in HD transgenic flies Although HTTex1 protein variants show a different aggregation behavior *in vitro* and *in vivo*, the initial biochemical analysis of fly head lysates revealed a correlation between aggregate formation and the observed behavioral phenotypes. This supports the hypothesis that mHTTex1 aggregation may drive pathogenesis in flies.

4. Discussion

In his article "On Chorea", George Huntington described that HD patients are aware of their terrible fate. He wrote: "it is spoken of by those in whose veins the seeds of the disease are known to exist, with a kind of horror […] when it is mentioned as "that disorder""[13]. In the way he phrased this statement he might have possibly captured a fact that modern research is just about to discover.

Huntington's disease (HD) is a devastating neurodegenerative disorder severely affecting the life quality of patients and care givers. Since the discovery of the disease-causing mutation in the *HTT* gene in 1993[16], biomedical research made substantial progress in understanding the molecular basis of the disease. Yet, the precise pathogenic mechanism of HD remains elusive and disease-modifying treatments are unavailable. One of the earliest discoveries in modern HD research was the formation of mutant huntingtin (mHTT) aggregates[127,128]. However, their role in HD pathogenesis has been discussed controversially – being either friends or foes. Within recent years, there is increasing experimental evidence that self-propagating mHTT aggregates, or seeds, play an important role in the development of disease in HD model organisms[170,179,180]. Whether they are indeed critical or even responsible for the appearance and progression of disease, however, is still unclear.

To address this question, I developed a FRET-based biosensor (FRASE) assay that enables the sensitive quantification of mHTT seeding activity (HSA) in complex biosamples. With this assay in hand, I assessed the potential correlation between HSA in affected tissues and the appearance of disease phenotypes in HD patients and transgenic mice. I detected robust HSA in crude brain extracts of mice weeks before manifestation of disease. Furthermore, I observed an increase of mutant HSA in HD patient and mouse brain extracts concomitantly with the appearance of symptoms, suggesting that it quantitatively tracks disease progression. Finally, quantification of HSA in an established inducible *Drosophila* HD model[262] indicates that the formation of small, seeding-competent HTTex1Q97 structures in adult neurons are necessary and sufficient to significantly shorten the lifespan of HD flies, supporting our hypothesis that mHTT seeding is a disease-relevant process causing dysfunction and neurotoxicity. Taken together, these studies indicate that HSA is a valuable early disease marker that can predict severe downstream phenotypic changes in various HD models (*Chapter 3.1)*. In the second part of my thesis, I utilized structure-guided mutagenesis to design protein variants of mHTTex1. Protein variants showed striking differences in their aggregation kinetic, stability and morphology when analyzed *in vitro*, suggesting that they are a valuable tool to analyze the relationship between aggregate formation and toxicity in greater detail. For this purpose, I generated *Drosophila* models expressing mHTTex1

protein variants pan-neuronally. The combination of biochemical and behavioral analysis of the newly developed fly models showed that the highest amounts of mHTTex1 aggregates are detectable in fly strains with the strongest adverse behavioral effects and *vice versa*, further strengthening the hypothesis that neurotoxicity is tightly connected to the formation of mHTTex1 aggregates. In addition, these results allow first speculations about how aggregate properties influence seeding activity and aggregate-induced toxicity (*Chapter 3.2*).

In the following chapter, I will discuss the benefits and limitation of the FRASE assay and its potential future applications. Quantification of HSA as a potential biomarker to monitor progression or onset in HD shall be examined. I will elaborate on the potential toxicity of small seeding-competent mHTT aggregates and resulting implications for the development of therapeutic strategies for HD. Finally, I will discuss the impact of amino acids exchanges on the aggregation behavior of mHTTex1 and their putative effects on the proteotoxicity of mHTTex1 protein variants.

4.1. The FRASE assay is a versatile tool with many applications[†]

The fluorescent dye Thioflavin T (ThT) is a reporter molecule, which is currently utilized in a large number of cell-free assays to monitor the seeding activity of amyloidogenic protein aggregates[173,292]. ThT exhibits enhanced fluorescence when it is bound to β-sheet-rich amyloid structures[293]. However, its binding to such structures is significantly decreased, when competing proteins are present in complex amyloid polymerization reactions[237,293]. Therefore, previously established ThT-based seeding assays are relatively insensitive when complex biosamples such as brain homogenates are analyzed.

To overcome these limitations, I have established a FRET-based biosensor assay, which does not require ThT reporter molecules for the quantification of HSA in biosamples. Two fluorescently tagged aggregation-prone HTT exon-1 fusion proteins with 48 glutamines (Ex1Q48-CyPet/-YPet, Figure 9A) are used as reporter molecules to monitor seeding activity (Figure 10A). In contrast to the frequently used synthetic polyQ-peptides $K_2Q_{44}K_2$[173], HTTex1 is a naturally occurring N-terminal fragment of mHTT that is produced by alternative splicing in HD brains[74,126]. C-terminal fusion of the fluorescent proteins CyPet or YPet does not significantly change the aggregation behavior of Ex1Q48 (Figure 8). Hence, Ex1Q48-CyPet and -YPet fusion proteins can be used to monitor mHTTex1 aggregation *in vitro*. They have been shown to self-assemble into stable fibrillar co-aggregates under both seeded and non-seeded conditions

[†] *The discussion about the FRASE assay and its applications in chapter 4.1 has been reused with modifications from the published version: Ast, A. et al. mHTT Seeding Activity: A Marker of Disease Progression and Neurotoxicity in Models of Huntington's Disease. Mol Cell 71, 675-688 e676, doi:10.1016/j.molcel.2018.07.032 (2018) - https://doi.org/10.1016/j.molcel.2018.07.032.*

and yield FRET-based aggregation profiles from which HSA in biosamples is quantified (Figure 12). This process is highly robust and affected by contaminating proteins in complex biosamples only to a very small extent. Therefore, the FRASE assay can be employed without the need for upstream purification of mHTT seeds, which would complicate the protocol and decrease accuracy of quantification. In comparison to other seeding assays, which were recently developed in the context of HD and other neurodegenerative disorders[173,177,234,292], the FRASE assay has several advantages. It is a one-step assay which is robust and easy to perform. Furthermore, it is highly sensitive and specific (Figure 17 and Figure 18), indicating that it is a suitable tool for high-throughput application in research and development. Considering the molecular weight of sonicated recombinant HTTex1Q48 aggregates the detection limit of the FRASE assays was determined to be 56 fM (1.7 amol per reaction) (Figure 17), which is equivalent to a monomer concentration of 5 pM. In comparison, a seeding assay described by Gupta et al. was tested for its sensitivity using preformed aggregates of the synthetic $K_2Q_{44}K_2$ protein[173]. This assay detects recombinant polyQ seeds in a similar concentration range (detection limit: 3.25 pM)[173]. However, the FRASE assay displayed superior sensitivity for the detection of mHTT aggregates in biosamples. I found that it detects seeding-competent mHTT aggregates in ≤ 2.5 µg crude protein extract of 12-week-old symptomatic R6/2 HD transgenic mice (Figure 20) without upstream purification steps, whereas ~40 µg of repeatedly purified brain extract was needed to detect mHTT seeds using the ThT-based seeding assay described by Gupta et al. [173]. The FRASE assay may be more sensitive because it measures mHTT seeding directly (via fluorescent reporter proteins) rather than indirectly through the binding of ThT molecules to mHTT aggregates. As described above, it is very likely that other proteins in complex biosamples interfere with the interaction between ThT and mHTT fibrils, which decreases the detection limit. In a more recent publication, Tan et al. applied preformed $K_2Q_{40}K_2$ aggregates to lysates derived from HTTex1Q103-EGFP expressing Htt14A2.6 PC12 cells and detected the seeding effect by quantifying GFP positive aggregates using FRA analysis[177]. In comparison to the FRASE assay a much higher seed concentration was needed to show a significant seeding effect (detection limit: 1 nM), demonstrating the superior sensitivity of the FRASE assay. Also, in comparison to a cell-based tau-seeding assay, established by Holmes et al., which detects seeds at a concentrations of 300 fM (56 fM in FRASE assays)[234] and a seeding-assay by Salvadores et al. that detects 3 fmol of Aβ oligomers/reaction (the FRASE assay detects 1.7 amol/reaction)[292], the FRASE assay provides higher sensitivity. Furthermore, the FRASE assay allows time-resolved assessment of seeded and unseeded HTTex1 aggregation, whereas the seeding assays developed by Tan and Holmes solely provide end-point measurements[177,234].

Discussion

Despite the advantages of the FRASE assay discussed above, there are also limitations that need to be considered. As the FRASE assay relies on fluorescence measurements to track mHTTex1 aggregation, fluorescent molecules can interfere with the assay. For example, the addition of blood plasma from 12 week-old R6/2 and aged matched wild-type mice disturbed the FRET measurement (*data not shown*). Due to several endogenous fluorophores (riboflavoproteins, vitamins and precursors, bilirubin and lipoproteins), blood plasma shows an intrinsic fluorescence[294], which overlaps with the emission spectrum of the YPet fluorophore and therefore perturbs the detected fluorescence signal. Hence, for the detection of seeding-competent mHTT aggregates in blood, upstream purification steps are required. Moreover, pilot tests to optimize the homogenization conditions revealed that detergents, even at low concentrations, influence the aggregation kinetics of the Ex1Q48-CyPet/-YPet reporter proteins[295]. In order to gain reliable results, detergents should not be used in the lysis buffer, or otherwise removed from the lysate prior to FRASE analysis. Hence, although the detection of seeding-competent mHTT aggregates in brain tissue of mice and patients was demonstrated to be highly robust and sensitive even without additional purification steps, the detection of seeds in biosamples such a blood, which likely contain very low amounts of mHTT seeds as well as other fluorescent components, might benefit from upstream purification steps or specific seed enrichment procedures.

Upstream sample processing therefore is likely a necessary optimization step to enable the detection of mHTT seeds in human biofluids or peripheral tissue with FRASE assays (Figure 31). Recently, Tan and colleagues detected mHTT seeding activity in cerebrospinal fluid (CSF) prepared from HD transgenic rats and patients. While the FRASE assay readily detects mHTT seeds in disease-relevant brain regions of HD patients (Figure 21 and Figure 22), HSA was undetectable in HD patient CSF (Figure 31C). This was surprising, as the detection limit of the FRASE method (5 pM, based on the monomer concentration) is ~200-fold below that of the seeding assay developed by Tan and colleagues (1 nM $K_2Q_{40}K_2$ aggregates)[177]. Additional upstream processing steps such as proteinase K treatment may be required to unmask the surface of mHTT seeds for their detection in CSF[235]. Otherwise, seed enrichment by ultracentrifugation or immunoprecipitation might be conceivable steps to further improve the detection of mHTT seeds. Alternatively, the FRASE assay could be further optimized regarding its sensitivity. I showed that an extension of the lag phase of reporter protein aggregation increases the sensitivity of the FRASE assay (Figure 14 and Figure 15). Hence, impeding primary nucleation and thereby delaying spontaneous self-assembly of the reporter proteins might further improve the detection limit. As described before, primary nucleation of mHTTex1 depends on the concentration of the protein and the length of the polyQ tract[130,147]. In addition, primary nucleation is greatly influenced by the

amino acid sequences flanking the polyQ domain (N17 and PRD domain). Whereas the N17 domain has been reported to facilitate aggregation, the PRD was shown to counteract this process[148-150]. Therefore, the deletion of the N17 region on the one hand or the expansion of the PRD on the other hand, might be strategies to generate sensor proteins of even higher sensitivity.

The FRASE assay was successfully used to detect seeding-competent mHTT aggregates in affected brain regions in HD patients (Figure 22 and Figure 25), supporting the correlation between mHTT seeding and pathology[179,182,296]. Whether the FRASE method can be translated to more accessible biosamples (such as blood and CSF) remains to be demonstrated. Nevertheless, this assay has considerable potential to be developed into an aggregate-specific prognostic tool. In addition, the assay could also be applied to screen for novel small molecules or proteins that interfere with seeded mHTT aggregation. As the assay can monitor mutant HSA in protein extracts prepared from postmortem patient brain and transgenic animals, it is also feasible to examine the effects of aggregate-targeting therapeutic candidate molecules in the presence of disease-relevant seeds. Finally, it is important to note that the general approach can be adapted to develop similar seeding assays for many other aggregation-prone proteins relevant to protein misfolding diseases.

4.2. Small seeding-competent fibrillar aggregates potentially drive Huntington's disease progression[‡]

Using the FRASE assay, I obtained comprehensive evidence that mHTT seeds are present in brain tissues of multiple HD mouse models and patients. I observed robust mHTT seeding activity (HSA) in HD transgenic mice long before the onset of symptoms (Figure 24). Furthermore, significant HSA was detectable in post mortem brain tissue of HD patients with grade 2 neuropathological changes[259] (Figure 25), supporting the hypothesis that mHTT seeding is an early event in pathogenesis[170,182]. With disease progression, the presence of seeding-competent aggregates increased in brain tissue from HD patients and mice. This is consistent with the assumption that seeding is a causal process and drives disease progression[170,182].

I observed high HSA in soluble fractions of transgenic HD mouse brain extracts (Figure 26), suggesting that greater seeding activity is associated with smaller particles. However, inclusions with insoluble fibrillar HTTex1 aggregates also possess seeding activity. On the one hand, high seeding activity in the soluble fraction might simply be attributed to the high surface to mass ratio of small fibrillar assemblies. I could show that sonication of large bundles of HTTex1Q48 fibrils

[‡] *The discussion about the role of mHTT seeds as potential disease driver in chapter 4.2 has been reused with modifications from the published version: Ast, A. et al. mHTT Seeding Activity: A Marker of Disease Progression and Neurotoxicity in Models of Huntington's Disease. Mol Cell 71, 675-688 e676, doi:10.1016/j.molcel.2018.07.032 (2018) - https://doi.org/10.1016/j.molcel.2018.07.032.*

leads to an increase in HSA (Figure 13), indicating that fragmentation greatly enlarges the overall surface area of mHTTex1 seeds, where templated aggregation of soluble mHTTex1 molecules can take place. On the other hand, small mHTTex1 assemblies might possess a higher seeding activity due to potential differences in their aggregate structure. It has been shown that protein aggregates can have distinct structural conformations, known as strains[297-299]. For human prion diseases it has been demonstrated that the conformation of pathogenic prion aggregates influences the rate of propagation as well as the resulting disease phenotypes[299]. With the appearance of the "prion hypothesis" and the advancement in biophysical tools, researchers focused on the structural characterization of protein aggregates related to other neurodegenerative diseases. Distinct aggregate strains were identified for the polypeptides tau and amyloid-β (both related to Alzheimer's disease[297,298]). Moreover, it was demonstrated that these strains have different propagation rates as well as different abilities to spread from cell-to-cell, suggesting that protein aggregates involved in neurodegenerative diseases might behave as distinct prion-like strains, potentially encoding diverse disease phenotypes[297,298]. More recently, structural polymorphisms have also been shown for HTTex1 aggregates that are formed *in vitro*. Using biochemical methods distinct mHTTex1 aggregates were generated, which showed differences in aggregate morphology, epitope exposure, stability and toxicity[141,300]. Whether mHTT aggregates form distinct strains *in vivo* remains to be investigated. Further studies will be necessary to purify fibrillar mHTT structures from mouse and patient brains in order to study their structural properties and to assess whether they possess specific seeding activities (i.e., seeding activity per unit of protein). I assume that there is a continuum of mutant HTT species in disease brains that all have some seeding activity. However, similar to previously published results for infectious prion species[301], my experiments provide initial evidence that the specific activity may be higher for smaller mutant HTTex1 structures than for larger aggregates.

My results are in agreement with previous investigations indicating that small, fibrillar polyQ-containing mHTT assemblies are detectable in the cytoplasm of cells besides large inclusions with fibrillar aggregates[116,133,201]. They are also consistent with experimental studies demonstrating that proteotoxicity in mammalian cells is associated with small, diffusible mHTT oligomers rather than large inclusions[133,302,303]. However, the present study advances beyond the state-of-the-art, providing experimental evidence that small HTTex1Q97 seeds are associated with dysfunction and neurotoxicity in neurons of HD transgenic flies in the absence of detectable large, insoluble mHTT aggregates (Figure 28 and Suppl. Figure 1).

It remains an open question how fibrillar mHTT aggregates cause cellular dysfunction and toxicity. Several mechanisms are worth considering and involve either a direct or an indirect action

of mHTT seeds. The presence of mHTT protein aggregates might indirectly cause cellular dysfunction, by over taxing the protein quality control systems[198,199]. mHTT aggregates might exhaust the protein folding capacity of the proteostasis network, causing newly synthesized proteins to fold less efficiently and metastable proteins to lose their functional conformation[304]. Consequently, the presence of mHTT aggregates might indirectly induce misfolding and functional loss of diverse cellular proteins[198,304-306]. On the other hand, mHTT seeds might directly cause cellular dysfunction by interacting with cellular membranes or proteins. It has been shown that fibrillar mHTT aggregates are able to interact and even penetrate cellular membranes[175,176]. In this context, fibrils present in polyQ inclusions were found to interact with the endoplasmic reticulum and to perturb membrane organization and dynamics[307]. As several important biological processes take place at the membranes of cellular organelles (e.g. oxidative phosphorylation in mitochondria membranes or protein translation at the membrane of the rough endoplasmic reticulum), aberrant interactions with membranes of different cellular organelles might perturb physiological functions, such as protein synthesis or energy production. In addition seeding-competent structures might directly interact with essential cellular proteins potentially corrupting their native conformation. In this context I would like to discriminate between two hypothetical processes: cross-polymerization and cross-seeding. I define cross-polymerization as the incorporation of cellular proteins into the growing mHTT fibril. A prerequisite for this process is an ongoing aggregation process, which enables the alternating integration of soluble mHTT molecules and other cellular proteins into the emerging fibrillar aggregate. On the other hand, I would like to define cross-seeding as the process in which preformed mHTT fibrils initiate the structural conversion of cellular proteins and their assembly into self-sustained aggregates. Cross-seeding of cellular proteins could therefore occur in the absence of soluble mHTT molecules. Cellular proteins including wild-type HTT have been shown to be sequestered into mHTT fibrils [195,308]. In most studies which mechanistically analyzed protein sequestration, mHTT was continuously produced feeding an ongoing aggregation process[308]. These studies show that cellular proteins cross-polymerize with mHTT. However, they do not provide evidence that mHTT aggregates, independent from an ongoing aggregation process, are capable of inducing protein misfolding. In this study I have shown that the addition of fibrillar Ex1Q48 aggregates to recombinant ExQ23-CyPet/-YPet sensor proteins induces a week increase in FRET efficiency (Figure 16), suggesting that Ex1Q48 seeds induce conformational changes and polymerization of wild-type HTTex1 independently of continuous mHTTex1 aggregation. This finding is in line with studies showing that fibrillar polyQ or HTTex1 aggregates promote intracellular nucleation of wild-type HTTex1 even in the absence of mutant HTT expression[174,175,309]. It further indicates that fibrillar

mHTTex1 structures are able to cross-seed the assembly of cellular proteins with a low intrinsic propensity to self-assemble spontaneously. In contrast to previous studies[174,175,309], I could follow the seeded polymerization of wild-type HTTex1 in a time-resolved manner. In comparison to sigmoidal aggregation profiles obtained with seeded ExQ48-CyPet/-YPet polymerization (Figure 17), the increase in FRET efficiency resulting from the seed-induced assembly ExQ23-CyPet/-YPet reporter proteins was comparably low, had a linear slope and was only observable when very high concentrations of Ex1Q48 seeds were added to reactions (Figure 16). This suggests that the assembly of ExQ23-CyPet/-YPet reporter proteins is rather inefficiently templated by preformed Ex1Q48 aggregates. It remains to be demonstrated, whether mHTTex1 aggregates can also cross-seed other cellular proteins with short polyQ tracts or high glutamine content. Besides the disruption of membranes and proteostasis mechanisms, both processes, cross-seeding and cross-polymerization, could contribute to neurotoxicity in HD transgenic flies. Although transgene expression was switched off, minimal background expression of HTTex1Q97 was observed in the absence of the expression inducing hormone (Suppl. Figure 1), which is why the proteotoxic effects could still be assigned to an ongoing mHTTex1 aggregation process.

The precise mechanism by which mHTT aggregates interfere with cellular function remains elusive. However, this study provides comprehensive evidence that seeding-competent mHTTex1 aggregates might contribute to HD pathogenesis and therefore makes it necessary to reconsider currently pursued therapeutic strategies. A promising new strategy aims to lower the levels of HTT protein[25,226,310,311]. However, the results of this thesis indicate that lowering the expression of mutant HTTex1 once seeding-competent aggregates are formed only insufficiently reduces neurotoxicity. In addition, I would expect that small molecule compounds targeting primary nucleation will only exert their full effects on the disease process before seeding-competent mHTT aggregates are formed, as the presence of seeds would circumvent primary nucleation and thereby subvert the efficiency of these molecules. Considering that mHTT seeds might spread between adjacent cells[178-181], aggregate transfer might be a conceivable therapeutic target.

4.3. Mutant HTT seeding activity is a potential biomarker in HD[§]

In order to monitor disease onset and progression or to test the efficacy of newly developed therapeutic candidates, sensitive biomarkers are needed. As described before, biomarkers should fulfil certain criteria[207]. They should be objectively measurable. They should

[§] *The discussion about HSA as potential biomarker in chapter 4.3 has been reused with modifications from the published version: Ast, A. et al. mHTT Seeding Activity: A Marker of Disease Progression and Neurotoxicity in Models of Huntington's Disease. Mol Cell 71, 675-688 e676, doi:10.1016/j.molcel.2018.07.032 (2018) - https://doi.org/10.1016/j.molcel.2018.07.032.*

have an association with known disease mechanisms or pathology and they should respond to therapy[207]. In this chapter, I will discuss the suitability of mHTT seeding activity (HSA) as a biomarker in HD patients and models.

Mutant HTT seeds in brains of HD transgenic mice as well as in HD patients are an early manifestation of disease and increase in their abundance with the development of disease phenotypes, suggesting an association with disease pathology (see also *Chapter 4.2*). Previous studies argue that the abundance of mHTT aggregates in brains of HD mice and patients is not predictive for the development of symptoms[312,313]. However, these studies used immunohistological methods, which detect large neuronal inclusions with insoluble aggregates, but fail to identify small, seeding-competent mHTT assemblies in disease brains. The application of the FRASE assay overcomes this important limitation (Figure 26) associated with standard histological analysis and enables objective quantification of HSA. Furthermore, HSA correlates with genetically or chemically induced modulation of disease-associated phenotypes (Figure 29 and Figure 30), indicating that it might also responds to therapeutic interventions. Together, this suggests that HSA measured by FRASE assays fulfills the outlined criteria and has therefore great potential to be used as a biomarker. However, independent validation experiments and further improvement of the FRASE assay will be needed.

I propose that in future drug trials with transgenic HD mice HSA could be utilized as an outcome marker to monitor the efficacy of therapeutic molecules *in vivo*, before and independent of changes in phenotypic manifestation. I detected robust HSA in the striatum of 2-month-old HdhQ150 knock-in mice (Figure 24C). Drug treatment could start before that point in time and animals could be assessed for HSA at any age after two months. In addition, the FRASE assay might also be of high value for monitoring disease onset and progression in HD patients if HSA could be quantified in biosamples whose collection is technically and ethically possible, like cerebrospinal fluid, blood or muscle tissue. Through the quantification of HSA in patient samples, the optimal time point for the initiation of clinical trials could be determined and the efficacy of therapeutic interventions could be monitored. In this way, my findings may help to develop novel disease-modifying therapeutic strategies for HD and other polyQ diseases.

4.4. Amino acid substitution changes the aggregation of HTTex1 *in vitro*

Research on human prion proteins has revealed that the structural characteristics of aggregates influence their proteotoxicity[299]. With the intension to alter the aggregation properties of HTTex1 and finally the structure of the resulting aggregates, I generated six protein variants of mutant HTTex1 through amino acid (AA) exchange in the N17 and the polyQ domain (Figure 32 and Suppl. Figure 3). Studying the aggregation behavior of purified protein variants *in vitro*,

revealed strong differences in stability, morphology and the rate of aggregate formation. In the following paragraphs, these differences shall be discussed in the context of the predicted structural changes (Figure 32) and in the light of the prevailing view on the HTTex1 aggregation mechanism (*Chapter 1.2.2*).

I designed a group of protein variants by AA substitution with proline residues (Ex1Q48M2, Ex1Q48M3, Ex1Q48M6, Figure 25). Due to the covalent bond of the side chain to the amino group of the backbone, proline residues introduce kinks into amino acid sequences. They are therefore known as structural breaker of α-helices and β-sheet conformations[283,314]. Hence, it would be expected that proline substitution would hamper the N17 domain to form an amphipathic α-helical structure, which is believed to stimulate the initial interaction of mHTTex1 monomers[151-153]. These associations subsequently trigger the conformational transition of the polyQ domain from a flexible random coil to a stable β-sheet conformation[154-157]. In addition, the introduction of proline residues into the polyQ domain would be expected to perturb β-sheet formation. On the one hand the, the introduction of hydrophobic proline residues in the polyQ domain reduces the number of possible hydrogen bonds that can form between interacting polypeptide chains. On the other hand, they introduce kinks into the AA sequence, which perturb the pleated conformation of polypeptide and hamper the ordered alignment of multiple amino acid side chains in a β-sheet[139]. In both cases the introduction of prolines into the polyQ tract should reduce the propensity of mHTTex1 fragments to form amylogenic β-sheets[137,138]. The introduction of proline residues in both the N17 and the polyQ domain was suggested to have the strongest effect on the HTTex1 structure and was predicted to almost completely abolish the ability of mHTTex1 molecules to form of coiled-coil (CC) and amyloid structures (Figure 32, Ex1Q48M3). As expected, I found that the aggregation process was strongly disturbed by the introduction of proline residues in the N17 and the polyQ domains (Figure 34, Ex1Q48M3). In none of the performed experiments (FRA, DB, SDS-PAGE, AFM, Figure 34) I detected Ex1Q48M3 aggregates. In comparison, the protein variant Ex1Q48M6 was generated by the introduction of proline residues only in the polyQ domain. *In silico* analysis predicted the disturbance of CC formation to be similar to Ex1Q48M3, but the propensity for amyloid formation to be less severe (Figure 32). The *in vitro* experiments with recombinant proteins revealed that Ex1Q48M6 protein assembles into aggregates rather slowly, but with higher efficiency than Ex1Q48 M3 protein (Figure 34). As the CC propensity was predicted to be similar in both Ex1Q48M3 and Ex1Q48M6 these results suggest that mHTTex1 aggregation is predominantly determined by the propensity to form amylogenic β-sheets.

A similar conclusion can be drawn when comparing Ex1Q48M2 and Ex1Q48M1 (Figure 32). Introduction of proline residues in the a/d positions of the N17 domain, as in the protein variant Ex1Q48M2, was expected to reduce the propensity to form CCs. *In silico* analysis confirmed a slight reduction of CC propensity within the N17 region, but also indicated a drastically decreased propensity to form amyloid structures. The investigations with recombinant proteins revealed that Ex1Q48M2 aggregates are formed after an extremely long lag phase (Figure 34). The strong delay in aggregation supports the role of flanking regions in HTTex1 aggregation[148-150]. However, whether this delay in protein aggregation can be assigned to the disturbance of CC formation or rather originates from the disturbance of amyloid formation needs further clarification. In order to evaluate to which extend CC and β-sheet disturbances affect the formation of HTTex1 aggregates, I next want to draw the attention to protein variant Ex1Q48M1 (Figure 32). The introduction of tryptophan residues in the N17 domain, was, similarly to Ex1Q48M2, predicted to slightly reduce the propensity of CC formation. However, the propensity to from amyloid structures was maintained or slightly increased. In contrast to Ex1Q48M2, the introduction of tryptophan residues into the N17 domain did not change the aggregation kinetics of protein variant Ex1Q48M1 to a detectable degree (Figure 34). This result suggests that the slight perturbation of CC formation in Ex1Q48M2 and Ex1Q48M1 is insufficient to drastically delay the aggregation of the HTTex1 protein variants. This in turn indicates that the strong delay in aggregation observed with the protein variant Ex1Q48M2 results from the reduced propensity to form amylogenic β-sheets. Both protein variants are predicted to have a high propensity to from CCs within the polyQ domain. This might still be sufficient to mediate initial contacts between different HTTex1 molecules and could explain why the aggregation behavior of Ex1Q48M1 was not changed. The initial contacts between HTTex1 molecules might occur, however, as the introduction of proline residues in the N17 domain strongly decreases the propensity to form amyloid structures, the conversion of the polyQ domain from a random coil into a β-sheet conformation might be very inefficient, which would in turn prevent or delay the aggregation process[138]. Again, this suggests that β-sheet formation is the main driver of HTTex1 aggregation. This hypothesis is also supported by the observed aggregation behavior of the protein variant Ex1Q48M5. The introduction of charged and polar amino acids in the polyQ domain was predicted to increase the propensity to form CCs, but to slightly decrease the propensity to form amyloid structures (Figure 32). In comparison to Ex1Q48, aggregation of recombinant Ex1Q48M5 protein was delayed (Figure 34), indicating that the slight decrease in amyloid formation propensity has a stronger influence on HTTex1 aggregation than the increase in CC formation propensity.

Finally, I would like to compare the structural variants Ex1Q48M2 and Ex1Q48M3. For both proteins variants the propensity to form amyloids was predicted to be drastically reduced (Figure 32C). However, the protein variant Ex1Q48M2 showed a much higher likelihood to form CC structures (Figure 25B). Monitoring the aggregation behavior of both proteins *in vitro* reveals that the aggregation process is strongly disturbed in both cases. However, the protein variant Ex1Q48M2 did assemble into SDS-stable, fibrillar aggregates within the given timeframe, whereas Ex1Q48M3 proteins were not observed to form aggregates (Figure 34B and F). These results further confirm that the propensity to form amylogenic β-sheets has a strong influence on spontaneous HTTex1 aggregation. They also illustrate that CC structures promote the aggregation process to a minor degree[151-153]. Together these results lead to the hypothesis that both CC and β-sheet formation influence the HTTex1 aggregation process. My theoretical and experimental investigations suggest that the propensity to adapt an amylogenic β-sheet conformation predominantly determines the aggregation propensity of HTTex1 molecules, regardless of whether β-sheet destabilization originates from modifications of the N17 or the polyQ domain. CC formation has a weaker aggregation modulating effect. Admittedly, I observed that Ex1Q48M4, which was predicted to have a high propensity to form amyloids and CCs, aggregated very inefficiently *in vitro* (Figure 34B). This unexpected result does not support the proposed hypothesis, which is why, it requires further investigation to draw a definitive conclusion on the degree to which CC-mediated interactions and amylogenicity influence the aggregation of mHTTex1. In addition, CD spectroscopy analysis is required in order to confirm the predicted secondary structures of the investigated recombinant proteins.

Apart from a change in the rate of aggregation, the resulting aggregates obtained with the HTTex1 protein variants displayed differences in their stability. I found that amino acid exchanges in the polyQ tract that decrease the amyloid formation propensity also lead to the formation of mHTTex1 aggregates with reduced stability (Figure 34E, Ex1Q48M5 and Ex1Q48M6). The stability of the Ex1Q48M5 and Ex1Q48M6 aggregates does not correlate with the predicted propensity to form amyloids or the rate of aggregate formation, but with the number of amino acid substitutions in the polyQ domain. Within the amyloid core structure, the amino acid side chains contribute to the formation of hydrogen bonds between adjacent β-strands within a single β-sheet[137-139]. In addition, they are predominantly responsible to mediate the interactions between adjacent β-sheets within the amyloid fibril[137-139]. Intriguingly, the protein variant Ex1Q48M5 which has completely lost its SDS-stability, displays a very different morphology (Figure 34E and F). Ex1Q48M5 fibrils in comparison to Ex1Q48 fibrils are much thinner, indicating that lateral fibril growth through interconnection of β-sheets might be disturbed[315,316]. However, a reduction in

fibril width was not observed with the proteins Ex1Q48M6 or Ex1Q23 which both show a significantly decreased SDS stability. In order to relate the stability of a HTTex1 aggregate to its molecular structure and morphology further experiments are needed. Electron microscopy analysis of preformed fibrillar aggregates from Ex1Q48 and its protein variants could provide images of higher magnification and might potentially reveal additional morphological variations. Furthermore, solid state nuclear magnetic resonance (NMR) imaging of fibrils form Ex1Q48 and its protein variants could be performed in order to elucidate the molecular architecture of these aggregates. Thereby, structural and morphological characteristics of HTTex1 aggregates could potentially be related to their stability.

Independent of their aggregation behavior and stability, all HTTex1 aggregates detected by AFM display a fibrillar morphology (Figure 34F), indicating that in all cases ordered molecular structures have formed[317,318]. Whereas the formation of amorphous mHTTex1 aggregates has been demonstrated in the presence of chaperones or through AA substitution in the HTTex1 sequence[319,320], my results suggest that regular fibrillar structures are a dominant feature of HTTex1 aggregates. Aggregates with a fibrillar morphology were also observed for the protein Ex1Q23 (Figure 34F), containing a non-pathogenic polyQ tract. This is in line with other *in vitro* studies showing that HTTex1 proteins with non-pathogenic polyQ lengths can form fibrillar aggregates[321]. Similar to my results, aggregate formation of HTTex1 fragments with short polyQ tracts were much slower compared to the mutant HTTex1 protein[321]. Interestingly, all aggregates formed by the HTTex1 protein variants and Ex1Q23 showed seeding activity when they were analyzed by FRASE assays (Figure 35), suggesting that the ordered fibrillar structure qualifies an aggregate to be seeding-competent irrespective of its stability. Interestingly, I observed differences in HSA when preformed aggregates of HTTex1 protein variants were analyzed by FRASE assays (Figure 35). However, as HSA strongly depends on the amount of seeding-competent aggregates, a more detailed analysis will be needed in the future in order to assess whether AA exchanges indeed induce structural differences that influence the specific seeding activity (HSA/protein amount).

4.5. Aggregate formation correlates with HTTex1 induced toxicity in protein variant *Drosophila* models

In order to investigate the relationship between the structural properties of HTTex1 aggregates and their toxicity, I generated different *Drosophila* strains expressing HTTex1 protein variants in neurons (Figure 36). Fly strains were phenotypically and biochemically characterized. I observed remarkable differences in fly development (Figure 38), survival (Figure 39) and

locomotor activity (Figure 40 and Figure 41), whose severity coincided with the formation HTTex1 aggregates (Figure 42), supporting the hypothesis that mHTTex1 aggregates might play a causal role in HD pathogenesis.

However, I found that the HTTex1 protein variants show a different aggregation behavior *in vitro* and *in vivo*. For example, recombinant Ex1Q48M2 proteins aggregated very inefficiently *in vitro* (Figure 34), whereas Ex1Q75M2 proteins rapidly assembled in to SDS-stable aggregates *in vivo* (Figure 42A). In order to understand these results several considerations have to be made. On the one hand the deviant aggregation behavior might result from the longer polyQ tract in the protein variants expressed in *Drosophila* models (compare Figure 32 and Suppl. Figure 3). Although the AA exchanges were adapted in order to generate Ex1Q75 protein variants with similar structural changes, the different length of the polyQ stretch needs to be considered as a possible source of deviations, especially for the structural variants containing AA substitutions in the N17 domain. The N17 domain likely exerts a smaller influence on the aggregation process, when HTTex1 proteins with very long polyQ tracts are expressed in fly neurons. In addition, in the cellular environment, the N17 domain strongly influences the fate of HTTex1 in other ways. It has been shown to act as a nuclear export signal[322], to interact with membranes[153,156] and is an active site of post-translational modifications (PTM)[68]. As a consequence, AA substitutions in the N17 domain might change the subcellular localization[322] or the strength of binding to membranes or cellular proteins[153,156,323] and ultimately might influence the aggregation behavior in a way that cannot recapitulate the *in vitro* situation. This might be an explanation for the strong differences in the aggregation behavior of the proteins Ex1Q75M1, Ex1Q75M2 and Ex1Q75M3, which was seen *in vitro* and *in vivo* (Figure 34 and Figure 42).

In contrast, the protein variants Ex1Q75M5 and Ex1Q75M6 show a reduced aggregation propensity in *Drosophila* neurons (Figure 42) similar to the recombinant protein variants Ex1Q48M5 and Ex1Q48M6 studied *in vitro* (Figure 34). This suggests that the change in aggregation behavior through AA exchanges in the polyQ tract is conserved and not significantly altered by the cellular environment. The introduction of proline residues into the polyQ tract (Suppl. Figure 3, Ex1Q75M6), slightly reduces the aggregate load in *Drosophila* neurons and alleviates mHTTex1 induced toxicity (Figure 39 and Figure 42). Comparable to the recombinant Ex1Q48M5 protein, no SDS-stable aggregates were detectable in transgenic flies expressing Ex1Q75 (Figure 42). However, a slight, yet not significant, increase in HSA might indicate the presence of low amounts of seeding-competent HTTex1 aggregates. The introduction of charged and polar residues in the polyQ tract (Suppl. Figure 3, Ex1Q75M5) resulted in a strong rescue of the Ex1Q75-induced phenotype in HD flies (Figure 39). Considering that both of these protein

variants showed a decreased aggregate stability *in vitro* (Figure 34E), these results might suggest that this biochemical property is critical for the observed proteotoxicity in HD flies. The manipulation of aggregate stability might be of potential therapeutic relevance as small molecule compounds or peptides could be engineered to destabilizes or dissociate mHTT aggregates, potentially giving the proteostasis system an advantage for aggregate clearance. However, as the biochemical analysis of transgenic flies is still preliminary, follow-up analyses are required to confirm this hypothesis.

Within the framework of this study, a definitive conclusion on how structural properties might influence mHTTex1 aggregate-induced toxicity cannot be drawn, yet. However the generation of recombinant protein variants and the corresponding transgenic fly models might help future research to address this question.

5. Material

5.1. Chemicals and consumables

0.5, 1.5, 2 ml tubes	Eppendorf
15 ml, 50 ml tubes	BD Falcon
15 ml, 50 ml tubes	BD Falcon
384 Well Nunc™ Polystyrene Black Microplates	Thermo Scientific
96 Well Cell Culture Microplate, PS, F-Bottom, advanced, black	Greiner Bio-One
Acetic Acid 99-100 %	Roth
Agar-Agar	Gewürzmühle Brecht
Agarose	Biozym
Ampicillin sodium salt	Sigma-Aldrich
Axygen™ 8-Strip PCR Tubes	Corning
Bacto™ Tryptone	BD Biosciences
Beer yeast	Gewürzmühle Brecht
Bromophenol blue	Merck Eurolab GmbH
Cell culture dishes	BD Falcon
Cellulose acetate membrane 0.2 µm	Schleicher and Schuell
Chloramphenicol	Sigma-Aldrich
Chloroform	Merck
Complete™ protease inhibitor cocktail	Roche Applied Science
Coomassie brilliant blue G-250	Merck
Corn flour	Bauck GmbH
Desoxyribonucleotides (dNTPs)	Fermentas
Dialysis membrane, MWCO 10 kDa	SpectraPor® Dialysis
Dimethylsulfoxide (DMSO)	Sigma-Aldrich
Dithiothreitol (DTT)	Serva
DNA Gel Loading Dye (6X)	Life Technologies
Doxycycline monohydrate	Sigma
DRAQ5™ Fluorescent Probe (5 mM)	Thermo Scientific
Ethanol (pure)	Roth
Ethidium bromide (10 mg/ml)	Sigma-Aldrich
Ethylenediaminetetraacetic acid (EDTA)	Merck Eurolab GmbH
Fetal Bovine Serum (FBS)	Life Technologies

Material

Filter paper GB002	Schleicher and Schuell
Fluoronunc 96-well plates	Nunc
Fly vials (plastic) 26, 49 mm diameter	K-TK
G418, Geneticin® (50 mg/ml)	Life Technologies
Glutathione Sepharose 4B	GE Healthcare
Glutathione, reduced	Sigma-Aldrich
Glycerol	Merck Eurolab GmbH
HEPES	Carl Roth
Hygromycin B (50 mg/ml)	Life Technologies
Isopropyl alcohol	Roth
Isopropyl β-D-1-thiogalactopyranoside (IPTG)	AppliChem
Kanamycin A monosulfate	Sigma-Aldrich
L-Glutathione, reduced	Sigma-Aldrich
Malzin	Ulmer Spatz
Methanol	Merck
Methyl 4-Hydroxybenzonate (Nipagin)	AppliChem
Mica: G250-2 Glimmer "v3"	Plano
Mifepristone (ru-486)	Biomol
Nonidet™ Ethylphenyl polyethylen glycol (NP40)	Sigma-Aldrich
NuPAGE® LDS Sample Buffer (4X)	Life Technologies
Paraformaldehyde	Sigma-Aldrich
Penicillin Streptomycin (Pen Strep), 10,000 U/ml	Life Technologies
Polyoxyethylensorbitan-Monolaureat (Tween 20)	Sigma Aldrich
Polypropylene columns 5 ml	Qiagen
Ponceau-S solution	Sigma-Aldrich
Protein LoBind tubes 0.5, 1.5, 2.0 ml	Eppendorf
p-t-Octylphenyl-polyoxyethylen (Triton X-100)	Sigma-Aldrich
Quinidine	Sigma Aldrich
RNase-free water	Ambion
Skim milk powder	Sigma Aldrich
Sodium deoxycholate	Sigma
Sodium hydroxide	Merck
Soy flour	Bauck GmbH
Sucrose	Fluka

Sugar beet sirup	Grafschafter Krautfabrik
TRIS Base, Tris(hydroxymethyl)aminomethane	Merck
Triton™ X-100	Sigma
Trypsin-EDTA (0.05%)	Life Technologies
Tube 13ml, 100x16mm (overnight cultures)	Sarstedt
Ultracentrifuge Tubes (1.5 ml)	Beckman Coulter
Whatman chromatography paper GB004	Whatman

The remaining chemicals necessary for the preparation of buffers (salts, acids, etc.) were purchased from Roth.

5.2. Enzymes, proteins and markers

Antarctic Phosphatase	New England Biolabs
Benzonase® Nuclease, 100,000 U	Merck Millipore
Gateway®BP Clonase™ Enzyme Mix	Thermo Scientific
GeneRuler 1 kb DNA Ladder	Life Technologies
GeneRuler 100 bp DNA Ladder	Life Technologies
Gateway™ LR Clonase™ Enzyme mix	Thermo Scientific
Lysozyme	Sigma-Aldrich
PageRuler™ Prestained Protein Ladder	Life Technologies
PreScission Protease, 500 U	GE Healthcare
Pwo SuperYield DNA polymerase	Roche
Restriction enzymes	New England Biolabs
T4 DNA Ligase	Thermo Scientific

5.3. Kits

BCA Protein assay reagent	Pierce
DNeasy blood and tissue kit	QIAGEN
MSB Spin PCRapace	Stratec Biomedical
NativePAGE™ Novex® Bis-Tris gel system	Invitrogen
NuPAGE MES SDS running buffer	Invitrogen
NuPAGE MES SDS transfer buffer	Invitrogen
NuPAGE™ Novex® Bis-Tris gel system	Invitrogen
QIAprep Spin Miniprep	QIAGEN
WesternBright™ Quantum™ Chemiluminescent HRP substrate	Advansta

5.4. Buffers, solutions and media

4 % PFA	4 g PFA dissolved in 100 ml, pH 7.4
4x SDS loading buffer	200 mM Tris pH 6.8, 400 mM DTT, 8% SDS, 40% glycerol, bromophenol blue
Aggregation buffer, 10x	0.5 M Tris-HCl, 1.5 M NaCl, 10 mM EDTA, pH7.4
Blocking buffer	3 % milk powder in PBS-T
Brain lysis buffer	10 mM Tris-HCl pH 7.4, 0.8 M NaCl, 1 mM EDTA, 10 % Sucrose (fresh), 1x protease inhibitor
Buffer 1	50 mM NaH_2PO_4, 5 mM Tris, 150 mM NaCl, 1 mM EDTA, pH 8.0
Cell lysis buffer	50 mM HEPES pH 7.4, 150 mM NaCl, 1.5 mM $MgCl_2$, 0.1% NP-40, 1 mM EDTA, 1x Complete™ protease inhibitors, 2u/ml benzonase
Coomassie staining solution	30 % ethanol, 10 % acetic acid, 0.05 % Coomassie brilliant blue R250
Denaturation buffer, 2x	4 % SDS, 100 mM DTT
Dialysis buffer	50 mM Tris, 150 mM NaCl, 1 mM EDTA, 5 % Glycerol, pH 7.4
Elution buffer	50 mM NaH_2PO_4, 5 mM Tris, 150 mM NaCl, 1 mM EDTA, 20 mM red. glutathione, pH 8.6
HEPES lysis buffer	50 mM HEPES, 150 mM NaCl, 10 % Glycerin, 1 % NP-40, 20 mM NaF, 1.5 mM $MgCl_2$, 1 mM EDTA, 1 mM DTT, 0.5 % Desoxycholat, 1:10.000 Benzonase, 1x Protease inhibitor
LB-(Luria Bertani) agar	1 % Bacto Peptone, 0.5 % yeast-extract, 1 % NaCl, 2 % Agar

LB-(Luria Bertani) medium	1 % Bacto Peptone, 0.5 % yeast-extract, 1 % NaCl
PBS, 10x	1.37 mM NaCl, 27 mM KCl, 100 mM Na_2HPO_4, 17.6 mM KH_2PO_4, pH 7.4
PBS-T	1x PBS, 0.05 % Tween-20
SOC medium	2 % Tryptone, 0.5 % yeast-extract, 10 mM NaCl, 2.5 mM KCl, 10 mM $MgCl_2$, 10 mM $MgSO_4$, 20 mM Glucose
Special fly medium (6 l)	48 g Agar-Agar, 480 g beer yeast, 120 g Bacto-peptone, 120 g Bacto-yeast, 420 ml sugar beet syrup, 3 g $MgSO_4$, 3 g $CaCl_3$, 6 g Nipagin, 60 ml EtOH, 36 ml propionic acid
Standard fly medium (6 l)	25 g Agar-Agar, 45 g beer yeast, 50 g soy flour, 400 g corn flour, 75 ml sugar beet syrup, 300 ml Malzin, 8 g Nipagin, 25 ml EtOH, 32 ml propionic acid
TBE buffer	89 mM Tris, 89 mM boric acid, 2 mM EDTA, pH 8.0
TBS (10x)	100 mM Tris, 1.5 M NaCl
TBS-T	1x TBS, 0.1 % (v/v) TWEEN® 20
TE buffer	1 mM EDTA, 10 mM Tris, pH 8.0

5.5. Oligonucleotides

Table 1: Oligonucleotides

Name	5' - 3' Sequence
HTTex1 $_{CyPet/YPet}$ - fw	GACGACGAATTCATGGCGACCCTG
HTTex1Q48 $_{CyPet/YPet}$ - rev	GACGACCTCGAGTGGTCGGTGCAGCGG
CyPet - fw	ACGACCTCGAGGGTGGCGGTGGCGGTATGTCTAAAGGTGAAGAATTATTCGG
CyPet - rev	GACGACGCGGCCGCTTATTTGTACAATTCATCCATACCATG
YPet - fw	GACGACCTCGAGGGTGGCGGTGGCGGTATGTCTAAAGGTGAAGAATTATTCACTGG
YPet - rev	GACGACGCGGCCGCTTATTTGTACAATTCATTCATACCCTCG
HTTex1Q23/Q35$_{CyPet/YPet}$ - fw	GACGACGAATTCATGGCGACCCTG
HTTex1Q23/Q35$_{CyPet/YPet}$ - rev	GACGACGCGGCCGCCTCGAGTGGTCGGTGCAGCGG
HTTex1Q23/Q75 - fw	GACGACGAATTCATGGCGACCCTG
HTTex1Q23/Q75 - rev	GACGACGCGGCCGCCTCGAGTTATGGTCGGTGCAGCGG
Phospo-V5 - fw	Phos- TCGAGGGCAGCGGTAAGCCTATCCCTAACCCTCTCCTCGGTCTCGATTCTACGGGCTA AGGTACCGC
Phospo-V5 - rev	Phos- GGCCGCGGTACCTTAGCCCGTAGAATCGAGACCGAGGAGAGGGTTAGGGATAGGCT TACCGCTGCCC
HTTex1$_{Structural\ variant}$ - fw	AGGCCGCATGAATTCATGGCGACCCTGGAA
HTTex1$_{Structural\ variant}$ - rev	CACGATGCGGCCGCGGTACCTTAGCCCGTAGAATCGAGACCGAGGAGAGGGTTAGG GATAGGCTTACCGCTGCCCTCGAGCGGACGATGCAGCGGTTCTTCTGC
pGEX5'	GGGCTGGCAAGCCACGTTTGGTG
pGEX3'	CCGGGAGCTGCATGTGTCAGAGG
HTTex1 $_{attB}$ - fw	GGGGACAAGTTTGTACAAAAAAGCAGGCTAGGCCGCATATGGCGACC
HTTex1 $_{attB}$ - rev	GGGGACCACTTTGTACAAGAAAGCTGGGTTTAGCCCGTAGAATCGAGACCGAGGAG AGGGTTAGGGATAGGCTTACCGCTTGGTCGGTGCAGCGGCTCCTC
pUAST - fw	AACCAAGTAAATCAACTGC
pUAST- rev	ATCTCTGTAGGTAGTTTGTC
HTT $_{genotyping}$ - fw	CGTTAACAGATCTGCGGCC
HTT $_{genotyping}$ - rev	GGTTCCTTCACAAAGATCCTC

Oligonucleotides with HPLC purification grade and were synthesized by BioTeZ Berlin-Buch GmbH in a quantity of 10 nM. Oligonucleotides were dissolved in TE-Buffer.

5.6. Expression Vectors and plasmids

pDONR™221	A Gateway® vector containing attP sites. This vector is used for cloning PCR products and genes of interest flanked by attB sites (expression clones) to generate entry clones. It contains the ccdB gene for negative selection and the kanamycin resistance gene for selection in *E.coli* (Invitrogen).
pGEX-6P1	Expression vector with the synthetic tac-promoter for the IPTG inducible expression of glutathione S-transferase (GST)-fusion proteins. The vector contains an internal lacI q repressor gene for the repression of expression in every strain of *E. coli*. Fusion proteins contain a restriction site for PreScission™ protease directly after the GST-protein sequence, which allows the cleavage of the GST-tag (Amersham Biotech Europe GmbH).
pUAST-attB-rfA	Expression vector for expression in transgenic flies under the GAL4 inducible UAS promoter; contains attB site for site-specific integration in the fly genome by _C31 integrase (provided by Prof. Sigrist, FU Berlin).

5.7. Antibodies

Table 2: Primary antibodies

Name	Species	Supplier
CAG53b	rabbit	Own production[127]
HD1	rabbit	Own production[129]
anti-AGG	rabbit	Own production
MW8	mouse	DSHB (University of Iowa)
anti-GST	goat	GE Healthcare
anti-GFP (ab290)	rabbit	Abcam
anti-HTT (MAB5492)	mouse	Millipore
anti-Tubulin (ab6046)	rabbit	Abcam
anti-V5 (ab9116)	rabbit	Abcam
N-18	goat	Santa Cruz

Table 3: Secondary antibodies

Name	Species	Supplier
anti-rabbit-POD	goat	Sigma
anti-mouse-POD	goat	Sigma
anti-goat-POD	mouse	Sigma

5.8. Biological material and experimental models

Table 4: Biological material and experimental models

Species	Name	Source
Human	Post mortem cerebellum, caudate nucleus and cerebral cortex tissues from HD patients and control individuals	Newcastle Brain Tissue Resource
Human	Post mortem putamen tissues from HD patients and control individuals	Brain tissue provided by the lab of F. Cicchetti (Laval University, Québec, Canada)
Human	Post mortem cortex tissues from AD patients and control individuals	Newcastle Brain Tissue Resource
Human	Muscle tissue from HD patients and control individuals	Muscle tissue provided by the lab of M. Orth (Ulm University, Ulm, Germany)
Human	Cerebrospinal fluid (CSF) from HD patients and control individuals	CSF was provided by E. Wild (UCL Institute of Neurology, London, UK)
Mouse	R6/2Q210[324]	Brain and muscle tissue provided by the lab of G. Bates (UCL Institute of Neurology, London, UK)
Mouse	R6/2Q51[247]	Brain tissue provided by the lab of A.J. Morton (University of Cambridge, Cambridge, UK)
Mouse	N171-82Q[249]	Brain tissue was prepared by B. Tachu (Max Delbrueck Center for Molecular Medicine, Berlin, Germany)
Mouse	FVB/N with AAV-HTT853-Q79/Q18[325]	Brain tissue provided by the lab of Å. Petersén (Lund University, Lund, Sweden)
Mouse	*Hdh*Q150[252]	Brain tissue provided by the lab of G. Bates (UCL Institute of Neurology, London, UK)
Mouse	CamKII/SCA3[257,258]	Brain tissue provided by the lab of Thorsten Schmidt (Universitätsklinikum Tübingen, Tübingen, Germany)
Fly	Elavc[115]-GAL4[326]	Wanker Lab fly stock

Species	Name	Source
Fly	GSelav-GAL4[264]	Wanker Lab fly stock
Fly	w[1118 327]	Wanker Lab fly stock
Fly	Balancer strain (CyO/Sp;MKRS,Sb/TM6,Tb)	Generated by F. Schindler (Max Delbrueck Center for Molecular Medicine, Berlin, Germany)
Fly	HTTex1Q17[268]	Generated by F. Schindler (Max Delbrueck Center for Molecular Medicine, Berlin, Germany)
Fly	HTTex1Q97[268]	Generated by F. Schindler (Max Delbrueck Center for Molecular Medicine, Berlin, Germany)
Fly	HTTex1Q75-V5	Own production
Fly	HTTex1Q75M1-V5	Own production
Fly	HTTex1Q75M2-V5	Own production
Fly	HTTex1Q75M3-V5	Own production
Fly	HTTex1Q75M4-V5	Own production
Fly	HTTex1Q75M5-V5	Own production
Fly	HTTex1Q75M6-V5	Own production
Fly	HTTex1Q17-V5	Own production
C.elegans	Q35 AM140[194] (rmIs132 (unc-54p::Q35::YFP))	Provided by J. Kirstein (Leibniz-Institute for Molecular Pharmacology, Berlin, Germany)
Cell line	CHO AA8 cells expressing HttEx1Q68-CFP and –YFP in a Tet-Off system[261]	Provided by A. Holloschi (University Mannheim, Mannheim, Germany)
E.coli	Mach1™ T1	Invitrogen
E.coli	BL21-CodonPlus(DE3)-RP	Integrated Science (Cat#: 230255)

5.9. Laboratory Equipment

Biophotometer	Eppendorf
C1000TM Thermal Cycler	Biorad
CanoScan8400F	Canon
Cellomics ArrayScan® VTI HCS Reader	Thermo Scientific
Centrifuge Evolution RC	Sorvall
DAM System	TriKinetics
DNA electrophoresis chamber	BioRad
Gene Genius UV imager	Bio Imaging Systems

GeneGenius Bio Imaging System	Syngene
HybriDot Manifold vacuum filtration unit	Whatman
Infinite M200 microplate reader	TECAN
LAS-3000 photo imager	Fujifilm
Magnetic stirrer MR3001	Heidolph
Micro 22R centrifuge	Hettich
Micro scales	Sartorius
Multichannel pipettes	Eppendorf
Nanodrop 8000	Thermo Scientific
Nanowizard AFM with Zeiss Axiovert 200	JPK
Optima™ MAX Ultracentrifuge	Beckman Coulter
Power Pac 1000	BioRad
Shaking Incubator	Infors Unitron
Sonifier 450	Branson
Fisherbrand™ Q500 Sonicator	Fisher Scientific
Tissue Homogenizer VDI12	VWR
Tissue Homogenizer (Pestle)	FischerScientific
Trans-blot semi-dry transfer cell	BioRad
Vacuum pump 2522C-02	Welch-Imvac
ViiA7 Real-time PCR system	Thermo Scientific
Vortex-Genie 2	Scientific industries
Water bath TW8	Julabo

5.10. Software

Adobe® Illustrator	Adobe Systems
Adobe® Photoshop	Adobe Systems
AIDA Image Analyzer v.3.21A	AIDA, Deutschland
ArrayScan VTI software	Thermo Scientific
BioEdit	Ibis Bioscience
CanoScan Toolbox 4.8	Canon
GraphPad Prism	GraphPad software
i-Control 11	Tecan
JPK Data Processing	JPK Instruments
JPK SPM Desktop	JPK Instruments
Serial Cloner 2.5	Serial Basics

6. Methods**

6.1. Molecular biology

6.1.1. Cloning of expression vectors

For the construction of plasmids encoding CyPet- and YPet-tagged HTTEx1Q48 fusion proteins, the coding sequence of HTTEx1Q48 was PCR-amplified from pGEX-6P1-HTTEx1Q48 using the primers 5'-GACGACGAATTCATGGCGACCCTG-3' and 5'- GACGACCTCGAGTGGTCGGTGCAGCGG-3'. The resulting PCR product was digested with the restriction enzymes EcoRI and NotI. Additionally, CyPet cDNA was PCR amplified from pBAD33-CyPet-His (Addgene plasmid #14030)[328] with the primers 5'-ACGACCTCGAGGGTGGCGGTGGCGGTATGTCTAAAGGTGAAGAATTATTCGG-3' and 5'-GACGACGCGGCCGCTTATTTGTACAATTCATCCATACCATG-3'. YPet cDNA was amplified from pBAD33-YPet-His (Addgene plasmid #14031)[328] with the primers 5'-GACGACCTCGAGGGTGGCGGTGGCGGTATGTCTAAAGGTGAAGAATTATTCACTGG-3' and 5'-GACGACGCGGCCGCTTATTTGTACAATTCATTCATACCCTCG-3'. The resulting PCR fragments were cloned into the plasmids pGEX-6P1 using the EcoRI/XhoI/NotI restriction sites to obtain plasmids pGEX-6P1-HTTEx1Q48-CyPet and -YPet, respectively.

To generate the plasmids encoding GST-Ex1Q23-CyPet and –Ypet and GST-Ex1Q35-CyPet and -YPet the coding sequences of HTTEx1Q23 or HTTEx1Q35 were PCR-amplified using the primers 5'-GACGACGAATTCATGGCGACCCTG-3' and 5'-GACGACGCGGCCGCCTCGAGTGGTCGGTGCAGCGG-3'. The resulting PCR product was digested using EcoRI and XhoI endonucleases and cloned into the plasmids pGEX-6P1-HTTEx1Q48-CyPet or -YPet after excision of HTTEx1Q48 fragments by EcoRI/XhoI endonucleases.

To generate the plasmids encoding GST-Ex1Q23 and GST-Ex1Q75 the coding sequences of HTTEx1Q23 and HTTEx1Q75 were PCR-amplified using the primers 5'-GACGACGAATTCATGGCGACCCTG -3' and 5'-GACGACGCGGCCGCCTCGAGTTATGGTCGGTGCAGCGG-3'. The resulting PCR products were digested using EcoRI and XhoI endonucleases and cloned into the plasmid pGEX-6P1-HTTEx1Q48 after excision of HTTEx1Q48 fragments by EcoRI/XhoI endonucleases.

To generate the plasmids encoding GST-Ex1Q23-V5 and GST-Ex1Q48-V5 phosphorylated oligonucleotides (5'-Phos-TCGAGGGCAGCGGTAAGCCTATCCCTAACCCTCTCCTCGGTCTCGATTCTACGGGCTAAGGTACCGC-3',

** *Methods have partially been reused with modifications from the published version: Ast, A. et al. mHTT Seeding Activity: A Marker of Disease Progression and Neurotoxicity in Models of Huntington's Disease. Mol Cell 71, 675-688 e676, doi:10.1016/j.molcel.2018.07.032 (2018) - https://doi.org/10.1016/j.molcel.2018.07.032.*

5’-Phos-GGCCGCGGTACCTTAGCCCGTAGAATCGAGACCGAGGAGAGGGTTAGGGATAGGCTTACCGCTGCCC-3’) were annealed to each other in order to generate the coding sequence of the V5-tag with single stranded 5’ and 3’ overhang imitating XhoI and NotI cleavage sites. Linearization of the plasmids pGEX-6P1-HTTEx1Q23 and pGEX-6P1-HTTEx1Q48 using XhoI and NotI and ligation of linearized plasmid DNA to the annealed oligonucleotides generated the plasmid pGEX-6P1-HTTEx1Q23-V5 and pGEX-6P1-HTTEx1Q48-V5.

In order to generate structural variants of mutant HTT, cDNA encoding HTTex1Q48 with the respective amino acid exchanges were produced by gene synthesis (GeneArt® Gene Synthesis service, Thermo Fisher). cDNAs were PCR-amplified with the primers 5’-AGGCCGCATGAATTCATGGCGACCCTGGAA-3’ and 5’-CACGATGCGGCCGCGGTACCTTAGCCCGTAGAATCGAGACCGAGGAGAGGGTTAGGGATAGGCTTACC GCTGCCCTCGAGCGGACGATGCAGCGGTTCTTCTGC-3’. The primer pair was designed to introduce a cDNA sequence encoding a C-terminal V5-tag and additional endonuclease cleavage sites upstream (EcoRI) and downstream (NotI) of the coding sequence. The resulting PCR products were digested using EcoRI and NotI endonucleases and cloned into the plasmid pGEX-6P1-HTTEx1Q48 after excision of HTTEx1Q48 fragments by EcoRI/NotI endonucleases.

The correct identity of all plasmids was confirmed by Sanger sequencing using the sequencing primers pGEX5’ (5’-GGGCTGGCAAGCCACGTTTGGTG-3’) and pGEX3’ (5’-CCGGGAGCTGCATGTGTCAGAGG-3’).

6.1.2. Cloning of fly vectors

In order to generate structural variants of mutant HTT, cDNA encoding HTTex1Q75 with the respective amino acid exchanges were produced by gene synthesis (GeneArt® Gene Synthesis service, Thermo Fisher). cDNAs were PCR-amplified with the primers 5’-GGGGACAAGTTTGTACAAAAAAGCAGGCTAGGCCGCATATGGCGACC-3’ and 5’-GGGGACCACTTTGTACAAGAAAGCTGGGTTTAGCCCGTAGAATCGAGACCGAGGAGAGGGTTAGGGAT AGGCTTACCGCTTGGTCGGTGCAGCGGCTCCTC-3’. The primer pair was designed to introduce a cDNA sequence encoding a C-terminal V5-tag and attB recombination sites upstream (attB1) and downstream (attB2) of the coding sequence. To generate an entry clone the resulting PCR products were integrated into pDONR221 (Thermo Fisher) through BP recombination reaction. LR recombination reactions were performed to shuttled cDNAs into the destination vector pUAST-attB-rfA (provided by Prof. S. Sigrist, Freie Universität, Berlin).

The correct identity of all plasmids was confirmed by Sanger sequencing using the sequencing primers pUAST - fw (5'-AACCAAGTAAATCAACTGC-3') and pUAST - rev (5'-ATCTCTGTAGGTAGTTTGTC-3').

6.2. Protein biochemistry

6.2.1. Recombinant protein expression

The proteins GST-Ex1Q23, -Ex1Q48, -Ex1Q75, -Ex1Q23-CyPet, -Ex1Q23-YPet, -Ex1Q35-CyPet, -Ex1Q35-YPet, -Ex1Q48-CyPet and -Ex1Q48-YPet were produced in *E. coli* BL21-CodonPlus-RP and affinity-purified on glutathione-sepharose beads. Purified proteins were dialyzed over night at 4 °C against 50 mM Tris-HCl pH 7.4, 150 mM NaCl, 1 mM EDTA and 5% glycerol, snap-frozen in liquid N2 and stored at -80 °C. Protein concentrations were determined with a NanoDrop spectrophotometer. Prior to use, protein solutions were ultra-centrifuged at 187,972 x g for 40 min to remove aggregated material. α -Synuclein (α-Syn) was produced in E. coli BL21 (DE3) and monomeric α-Syn was purified as described elsewhere[329]. Expression of Tau40 protein was performed in E. coli BL21 using a 50 l bioreactor. After cell disruption using a French press, Tau40 protein was purified via cation exchange chromatography and gel filtration. Expression and purification of Tau were performed by InVivo BioTech Services (Hennigsdorf, Germany) using proprietary company protocols.

6.2.2. *In vitro* aggregation and seed preparation

Spontaneous aggregation of HTTex1 proteins and all structural variants were initiated by addition of 14 U PreScission protease (GE Healthcare) per nmol purified GST-Ex1Q48 fusion protein at the protein concentration indicated for the specific experiment. The aggregation reaction was performed in 50 mM Tris-HCl pH 7.4, 150 mM NaCl, 1 mM EDTA and 1 mM DTT at 25 °C and constant agitation (450 rpm) for up to 168 h. Ex1Q23 protein for seeding experiments was prepared from GST-Ex1Q23 fusion protein using the same protocol. Synthetic human IAPP was aggregated as described previously[330]. Lyophilized α-Syn was dissolved in PBS at 500 µM and centrifuged (4 °C, 265.000 x g) after a 5 min sonication step to remove aggregated material. The supernatant was incubated for 7 d at 37 °C under constant shaking in the presence of a single glass bead. Tau40 was aggregated for 6 d at 37 °C under constant shaking in 100 mM sodium acetate, pH 7.4, and 1 mM DTT in the presence of heparin. Synthetic human Aβ1-42 was dissolved in 100 mM NaOH and diluted to 200 µM in low salt buffer (10 mM K3PO4, pH 7.4, 10 mM NaCl). Aggregation was performed for 6 h at 37 °C under constant agitation.

6.2.3. Filter retardation assays (FRAs)

FRAs were essentially performed as described previously[238]. Briefly, equal volumes of 500 ng of protein aggregates and 4 % SDS solution with 100 mM DTT were mixed and boiled at 95 °C for 5 min. By applying vacuum, samples were filtered through a cellulose acetate membrane with 0.2 µm pores (Schleicher and Schuell, Germany) and washed twice with 100 µl 0.1 % SDS. For analysis of tissue homogenates, 60 µg of total protein for mouse brain and 75 µg of total protein for *Drosophila* heads were filtered per dot. Membranes were blocked with 5% skim milk in PBS/0.05 % Tween20 (PBS-T) for at least 30 min. Aggregates retained on the membrane were detected using V5, GFP, N18, MW8, Mab5492 or HD1 antibody followed by an appropriate peroxidase-coupled secondary antibody. Signals were quantified using the AIDA image analysis software (Raytest, Germany).

6.2.4. Dot blot assays

To estimate total HTT protein, native dot blot (DB) assays were performed as described previously[239]. Briefly, 250 ng protein were filtered onto a nitrocellulose membrane and blocked with 5% skim milk in PBS-T. For detection, the membrane was incubated with HD1 antibody followed by an appropriate peroxidase-coupled secondary antibody. Signals were quantified using the AIDA image analysis software (Raytest, Germany). As a loading control for the detection of Ex1 structural variants, 1 µg of protein was filtered onto a nitrocellulose membrane and subsequently detected using Ponceau Red staining.

6.2.5. Blue native PAGE analysis

Protein solutions were mixed with sample buffer and loaded onto a Novex NativePAGE 3-12% Bis-Tris gradient gel (Life Technologies). NativePAGE and immunoblotting were performed according to manufacturer recommendations. Ex1Q48 aggregates were visualized as for SDS-PAGE.

6.2.6. SDS-PAGE and Western blotting

Samples of aggregation reactions were mixed with loading buffer (50 mM Tris-HCl pH 6.8, 2% SDS, 10% glycerol and 0.1% bromophenol blue) and boiled at 95 °C for 5 min. Samples were loaded onto Novex NuPAGE 4-12% Bis-Tris gradient gels (Life Technologies). SDS-PAGE and immunoblotting were performed according to manufacturer recommendations. Immuno-detection was performed with the antibody indicated for the respective experiment.

6.2.7. Tissue homogenization

Frozen brain tissue was cut on dry ice, weighed and homogenized in a 10-fold excess (w/v) of ice-cold 10 mM Tris-HCl pH 7.4, 0.8 M NaCl, 1 mM EDTA, 10% sucrose, 0.25 U/µl benzonase and

complete protease inhibitor cocktail with a dounce homogenizer. The homogenate was incubated for 1 h at 4 °C on a rotating wheel and centrifuged for 20 min at 2,700 x g (4 °C) to remove cell debris. Drosophila heads were processed comparably using 10 µl of ice-cold 10 mM Tris-HCl pH 7.4, 0.8 M NaCl, 1 mM EDTA, 10% sucrose and a complete protease inhibitor cocktail per fly head. Homogenates were centrifuged for 10 min at 8,000 rpm (4 °C). After centrifugation, supernatants were transferred to a new tube and total protein concentration was determined with a Pierce™ BCA assay using BSA as a standard. For FRASE analysis, 0.8-5 µg total protein per replicate were applied.

6.2.8. Immunodepletion of HTTex1 aggregates from mouse brain extracts

Protein G-coupled magnetic beads (Life Technologies) were incubated with 4 µg MW8 (Developmental Studies Hybridoma Bank, DSHB) or IgG isotype control (Invitrogen) antibody, respectively, for 10 min at RT to allow antibody binding. Free binding sites were saturated with Pierce protein-free blocking solution according to manufacturer recommendations. 500 µg brain homogenate in brain lysis buffer were incubated with antibody coupled beads for 3 h at 4 °C under constant overhead rotation. Subsequently, aliquots from the supernatants were taken and analyzed with the FRASE assay.

6.2.9. FRASE assay and quantification of mutant HTT seeding activity (HSA)

Purified GST-Ex1Q48-CyPet and GST-Ex1Q48-YPet (or GST-Ex1Q23-CyPet and GST-Ex1Q23-YPet or GST-Ex1Q35-CyPet and GST-Ex1Q35-YPet) were diluted in aggregation buffer at an equimolar ratio to a final concentration of 1.2 µM (0.6 µM each) with 14 U PSP per nmol sensor proteins if not stated otherwise. The solution was then mixed with preformed aggregates of Ex1Q48 (seeds) at varying concentrations with or without prior sonication and transferred to a black 384-well plate (with a final reaction volume of 30 µl per well and a sensor protein concentration of 1.2 µM). For quantification of seeding-competent HTT species in tissue samples, the sensor-protein mixture was supplemented with up to 10% (v/v) tissue homogenate. Fluorescence signals were measured every 20 min following a 5 s pulse of vertical shaking with a Tecan M200 fluorescence plate reader at 25 °C for up to 80 h. CyPet donor fluorescence was measured at excitation (Ex): 435 nm/emission (Em): 475 nm; YPet acceptor fluorescence at Ex: 500 nm/Em: 530 nm; the FRET channel (DA) was recorded at Ex: 435 nm/Em: 530 nm. Raw signals were processed by subtracting the background fluorescence of unlabeled Ex1Q48 in all channels. Signals in the FRET channel were corrected for donor bleed-through (cD) and acceptor cross excitation (cA) using donor- and acceptor-only samples to obtain sensitized emission. Finally, sensitized emission was normalized to the acceptor signals[331]. In brief, the FRET efficiency E (in %) was calculated as follows:

E = (DA-cDxDD-cAxAA)/AA with DD = donor channel signal and AA = acceptor channel signal. Seeding effects (Δt_{50} [h]) were quantified by subtracting the t_{50} values (time at half-maximal FRET efficiency) of the respective sample from the negative control. To obtain the t_{50} values, the aggregation kinetics were curve fitted by Richard's five-parameter dose-response curve using GraphPad Prism.

$$y = y_0 + (\frac{y_\infty - y_0}{1 + 10^{((Logxb - x) \times HillSlope)^S}})$$

6.3. Cell biology

6.3.1. Cell maintenance and seeding

CHO AA8 cells expressing HttEx1Q68-CFP and –YFP in a Tet-Off system were provided by A. Holloschi (Institute of Molecular and Cell Biology, University Mannheim)[261]. Cells were grown and maintained in Ham's F12-medium containing 10 % FBS, 100 units/ml penicillin G sodium, 100 µg/ml streptomycin sulphate, 0.2 mg/ml Hygromycine B, 0.1 mg/ml Geneticin and 10 ng/ml Doxycycline at 37 °C in a humidified atmosphere containing 5 % CO_2.

For the cell seeding assay, CHO cells were plated in 96-well plates (2 x 10^4 cells per well, 4 wells per condition) in Doxycycline free medium in order to induce the expression of HTTEx1Q68-CyPet/YPet for 72 hours. During that time cells were exposed to different concentrations of Ex1Q48 seeds of Ex1Q23 protein or aggregation buffer as control.

6.3.2. Preparation of cell lysates for FRA analysis

For the detection of SDS-stable intracellular aggregates, cell medium was discarded, cells were washed twice with 100 µl PBS and subsequently lysed in 65 µl Tris lysis buffer for 1 hour at 4 °C (tumbling). Lysates of two wells of one quadruplicate were combined and used for a FRA.

6.3.3. Fixation and staining

Cells were fixed with 65 µl 2 % PFA in PBS at RT for 20-30 min. After discarding the PFA solution, fixed cells were washed twice with 100 µl PBS and stored in PBS at 4 °C. To visualize nuclear DNA, fixed cells were stained with 40 µl DRAQ5™ (1:1000) per well for 30 min and analyzed with Cellomics high content fluorescence microscope.

6.4. Microscopy

6.4.1. High content fluorescence microscopy

Images of nine fields per well were recorded with a 20 x objective. Cells were identified by DRAQ5™ nuclear staining using Cy5 channel and cell shape was estimated by the software. Aggregates per cell were counted in the CFP-channel. A threshold was set to select only small aggregates.

6.4.2. Atomic force microscopy (AFM)

Aliquots of 15 µl aggregation reactions (24 h) were spotted onto freshly cleaved mica glued to a microscope slide. After incubation for 30 min to allow adsorption, samples were rinsed 4 times with 40 µl distilled water and dried over night at RT. Samples were imaged with a digital multimode Nanowizard II (JPK, Germany) atomic force microscope operating in intermittent-contact mode.

6.4.3. Electron microscopy (EM)

(EM analysis was performed by Severine Kunz (EM core facility, MDC, Berlin) and will be briefly described for the sake of completeness.)

Total brain homogenate was centrifuged at 18,000 x g at 4 °C for 20 min; the resulting supernatant was pelleted by ultra-centrifugation at 190,000 x g for 40 min and resuspended in 10 mM Tris-HCl (pH 7.4). Immunolabeling was performed with minor modifications as described (Laue, 2010). Briefly, samples were incubated on formvar-coated copper grids (Plano) for 10 min before immunolabeling. Grids were blocked and washed in PBS supplemented with 1% BSA and 0.1% glycine. Labeling was performed with the anti-HTT aggregate antibody AGG and an appropriate 12 nm colloidal gold-labeled secondary antibody (Jackson ImmunoResearch). Samples were stained with 2% uranyl acetate and imaged with a Zeiss EM 910 transmission electron microscope at 80 kV. Acquisition was performed with a CDD camera (Quemesa, Olympus Viewing System).

6.5. Animal models

6.5.1. *Caenorhabditis* elegans

(C.elegans work was performed by Janine Kirstein (FMP, Berlin) and will be briefly described for the sake of completeness)

C. elegans strains and maintenance

C. elegans Q35 AM140 (rmIs132 (unc-54p::Q35::YFP)) were grown on NGM plates seeded with the E. coli OP50 strain at 20 °C. Nematodes were transferred to fresh wells or plates every day in the course of the experiment to separate them from their progeny.

RNA interference

For synchronization, gravid adults from one 10 cm NGM plate were collected in a canonical tube and treated with 20% alkaline hypochlorite solution under vigorous agitation for 4 min. The eggs were then washed three times with cold 0.1 M NaCl solution. The eggs were allowed to hatch in M9 medium at 20 °C for 22 h. Animals were then placed as L1 larvae onto RNAi plates that were seeded with E. coli expressing dsRNAi against hsp-1 or the empty vector L4440 (control).

Motility assay

Nematodes were transferred from liquid culture onto a blank (unseeded) NGM plate and allowed to acclimate for 15 min. The movement of the animals was digitally recorded at 20 °C using a Leica M165FC microscope with a DFC3000G digital camera and the Leica LASX Software. Movies of 10 s were captured at 10 frames/s. Animals that crossed each other or those that escaped from the field of view were excluded from analysis. 20 animals were analyzed for each condition. Captured frames were merged into *.avi format, imported into Fiji[332] and analyzed using the wrMTrck plugin (http://www.phage.dk/plugins). The average speed of each animal was calculated by dividing its body length by the duration of each track (body length per second).

6.5.2. *Drosophila melanogaster*

Generation and maintenance of Drosophila strains

ElavGS-GAL4 and Elav-GAL4 lines were obtained from the Bloomington Drosophila Stock Center. w1118 line was provided by R.P. Zinzen (MDC, Berlin). HTTex1Q17 and HTTex1Q97 flies were generated by F. Schindler in the course of her PhD Thesis (MDC, Berlin). New transgenic flies were generated through cloning of cDNAs encoding HTTex1Q17-V5, HTTex1Q75-V5, HTTex1M1-V5, HTTex1M2-V5, HTTex1M3-V5, HTTex1M4-V5, HTTex1M5-V5 and HTTex1M6-V5 into pUAST-attB-rfA (provided by Prof. S. Sigrist, Freie Universität, Berlin) and subsequent site-directed insertion on the third chromosome (68E) using the PhiC31 integrase Rainbow Transgenic Flies Inc. (Camarillo, CA, USA). Transgenic lines were crossed with the balancer strain (CyO/Sp;TM6,Tb/MKRS,Sb) to produce a stable fly line. All Drosophila strains were cultured on standard medium at 25°C and 65% humidity with a 12 h light-dark cycle. In the elavGS-GAL4

system, transgene expression was induced by culturing flies on standard medium containing 400 µM RU486 (Mifepristone).

Genotyping of Drosophila strains

Genomic DNA was extracted using the DNeasy® Blood & Tissue Kit (Qiagen). Genomic DNA was PCR amplified with the genotyping primers 5`-CGTTAACAGATCTGCGGCC-3' and 5'-GGTTCCTTCACAAAGATCCTC -3' using the PWO DNA polymerase kit (Roche). PCR products were analyzed by agarose gel electrophoresis and DNA sequencing.

Viability analysis of adult Drosophila melanogaster

Viability assays were performed through quantification of lethality of female transgenic flies. Flies were aged at 25°C and 65% humidity with a 12 h light-dark cycle, with 10 flies per vial. Flies were transferred onto new media every 3-4 days. Dead flies were recorded every 2-3 days. The number of flies per biological replicate are specified in the figure legend of the respective experiment. Median lifespan (age at which half of the tested population has died) was calculated by fitting survival curves to the log(inhibitor) vs. normalized response (variable slope) equation using GraphPad Prism.

Analysis of motor performance (climbing assay)

Ten female flies were placed in a closed empty vial and gently tapped to the bottom of the vial. The percentage of flies that climbed 8 cm within 15 sec was recorded. Flies were aged at 25°C and 65% humidity with a 12 h light-dark cycle (10 flies per vial) and were monitored and transferred twice a week. The number of flies per biological replicate are specified in the figure legend of the respective experiment.

Analysis of circadian rhythm and activity

Locomotor activity was monitored using the Drosophila Activity Monitoring (DAM) System as previously described[291]. Male flies were placed individually into glass locomotor-monitoring tubes (65 mm x 5 mm) containing standard medium. The glass tubes were sealed using cotton buds. The tubes were inserted into the sensor system and aged at 25°C and 65% humidity with a 12 h light-dark cycle. Within the sensor system three infrared beams are directed through each glass tube. Activity of transgenic flies was assessed by recording the number of beam breaks within a 5 min interval. The number of flies per biological replicate are specified in the figure legend of the respective experiment.

Preparation of Drosophila head lysates for WB, FRA and FRASE analysis

Drosophila head lysates were produced by homogenizing fly heads in Tris-HCl pH 7.4, 0.8 M NaCl, 1 mM EDTA, 10% sucrose, 0.25 U/µl benzonase and complete protease inhibitor cocktail using a micro pestle. Lysates were centrifuged for 10 min at 8,000 rpm (4°C). The supernatant was transferred to a new tube and total protein concentration was determined with a Pierce™ BCA assay using BSA as a standard.

6.6. *In silico* analysis of secondary protein structure

Propensity of amyloid formation was predicted using the web-based tool Waltz using a low specificity threshold of 63 and assuming neutral pH (pH 7) (http://waltz.switchlab.org/[279,280]).
The algorithms Coils (https://embnet.vital-it.ch/software/COILS_form.html[278]) was used for the prediction of coiled-coil (CC) domain formation. CC probability is displayed as 1 minus the P-score assigned to each amino acid using a window size of 14, 21 and 28 residues.

6.7. Statistical analysis

Statistical parameters including the exact value of n, the definition of center, dispersion and precision measures (mean ± SEM or mean ± SD) as well as the statistical analysis chosen and statistical significance are reported in the figures and figure legends. Data is judged to be statistically significant when $p < 0.05$ by the indicated statistical test. In figures, asterisks denote statistical significance as calculated by Student's t test (*, $p < 0.05$; **, $p < 0.01$; ***, $p < 0.001$). Statistical analysis was performed in GraphPad PRISM 7.

7. Supplementary information

7.1. Supplementary data

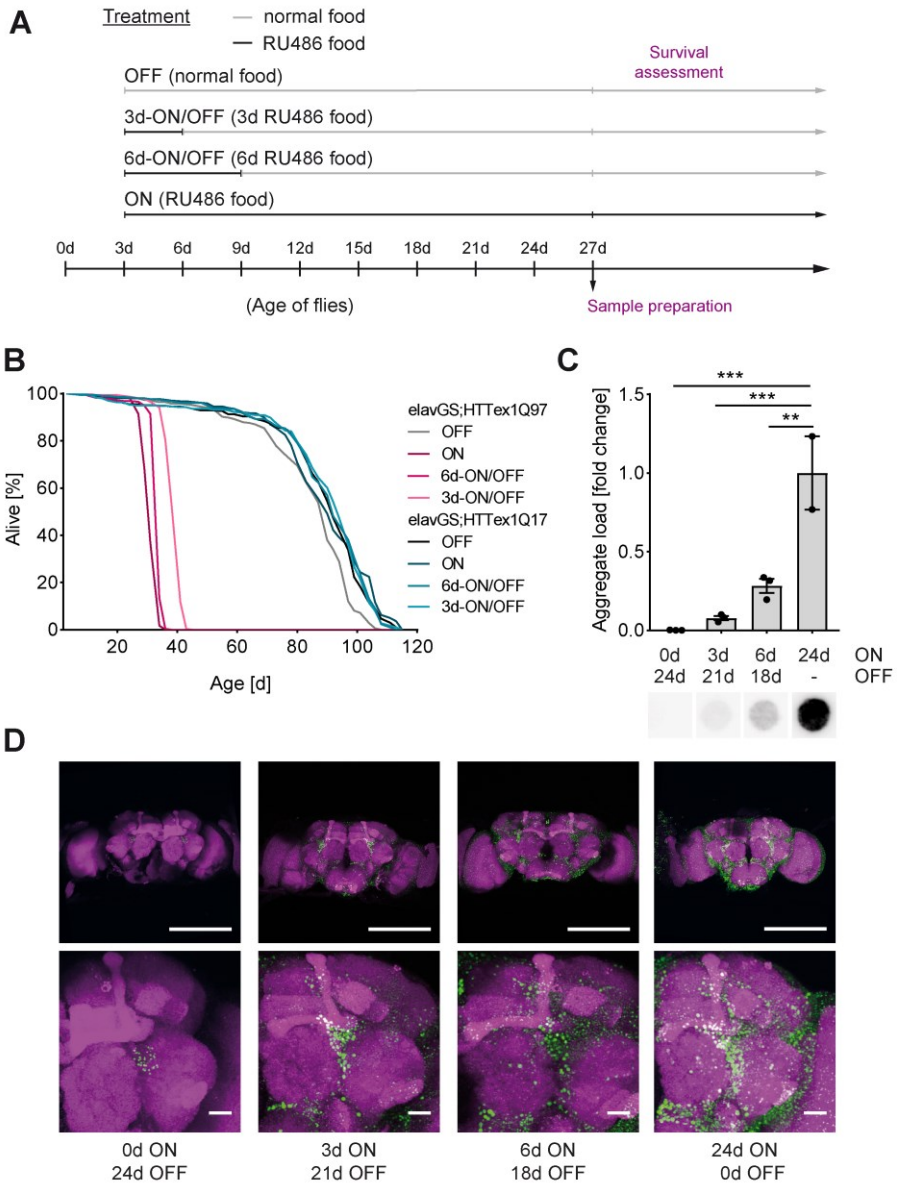

Suppl. Figure 1 (related to Figure 28): Phenotypic and biochemical characterization of a inducible HD fly model

(This figure is reproduced with modifications from the PhD thesis of F. Schindler[262,268])
(A) *Scheme of temporary hormone treatment. The black lines indicate time periods of hormone treatment (RU486 food); the grey lines indicate time periods without hormone treatment (normal food). Treatment started at day 3 post-eclosion.* ***(B)*** *Life span analysis of elavGS;HTTex1Q97 and elavGS;HTTex1Q17 flies expressing the respective transgene for 0d (OFF; $n^{elavGS;HTTex1Q97}$ = 99, 96, 107; $n^{elavGS;HTTex1Q17}$ = 107, 102, 100), 3d (3d-ON/OFF; $n^{elavGS;HTTex1Q97}$ = 107, 108, 107; $n^{elavGS;HTTex1Q17}$ = 109, 96, 97), 6d (6d-ON/OFF; $n^{elavGS;HTTex1Q97}$ = 108, 105, 94; $n^{elavGS;HTTex1Q17}$ = 110, 97, 100) or permanently (ON; $n^{GS;HTTex1Q97}$ = 102, 98, 106; $n^{GS;HTTex1Q17}$ = 100, 109, 101). Life span is plotted as the percentage of surviving flies of 3 biological replicates.*

Suppl. Figure 1 (continued)

(C) *Quantification of HTT aggregate load in fly heads by FRAs immunodetected with the MW8 antibody. Representative images for each condition are shown below the bar graph. Data are displayed as mean ± SEM; Individual measurements are presented as black dots (●); One-way ANOVA Dunnett's post hoc test.* ***(D)*** *Representative confocal images of elavGS;HTTex1Q97 whole fly brains (hormone treatment as in* ***A****. The RBP staining is shown in magenta and the MAB5492 staining in green (Scale bars: 200 µm). Magnifications are shown below (Scale bars: 20 µm).*

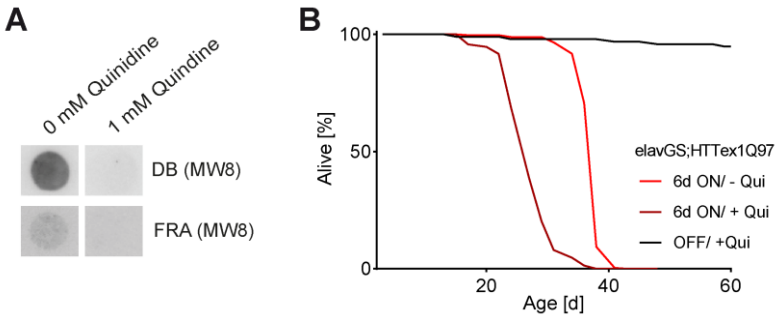

Suppl. Figure 2 (related to Figure 30): Quinidine treatment of transgenic HD flies reduces aggregate load but exacerbates mHTT induced survival defect

(This figure is reproduced with modifications from the PhD thesis of F. Schindler[262])

(A) *Assessment of aggregate load in head lysates of elavGS;HTTex1Q97 and elavGS;HTTex1Q17 flies expressing the respective transgene for 6d in the absence or presence of 1 mM Quinidine (+/- Qui). using DB and FRA. Aggregates were detected with the MW8 antibody.* ***(B)*** *Life span analysis of elavGS;HTTex1Q97 and elavGS;HTTex1Q17 flies treated as described above. Life span is plotted as the percentage of surviving flies (6dON/-Qui n = 86, 96, 82; 6dON/+Qui n = 90, 102, 89; OFF/+Qui n = 95).*

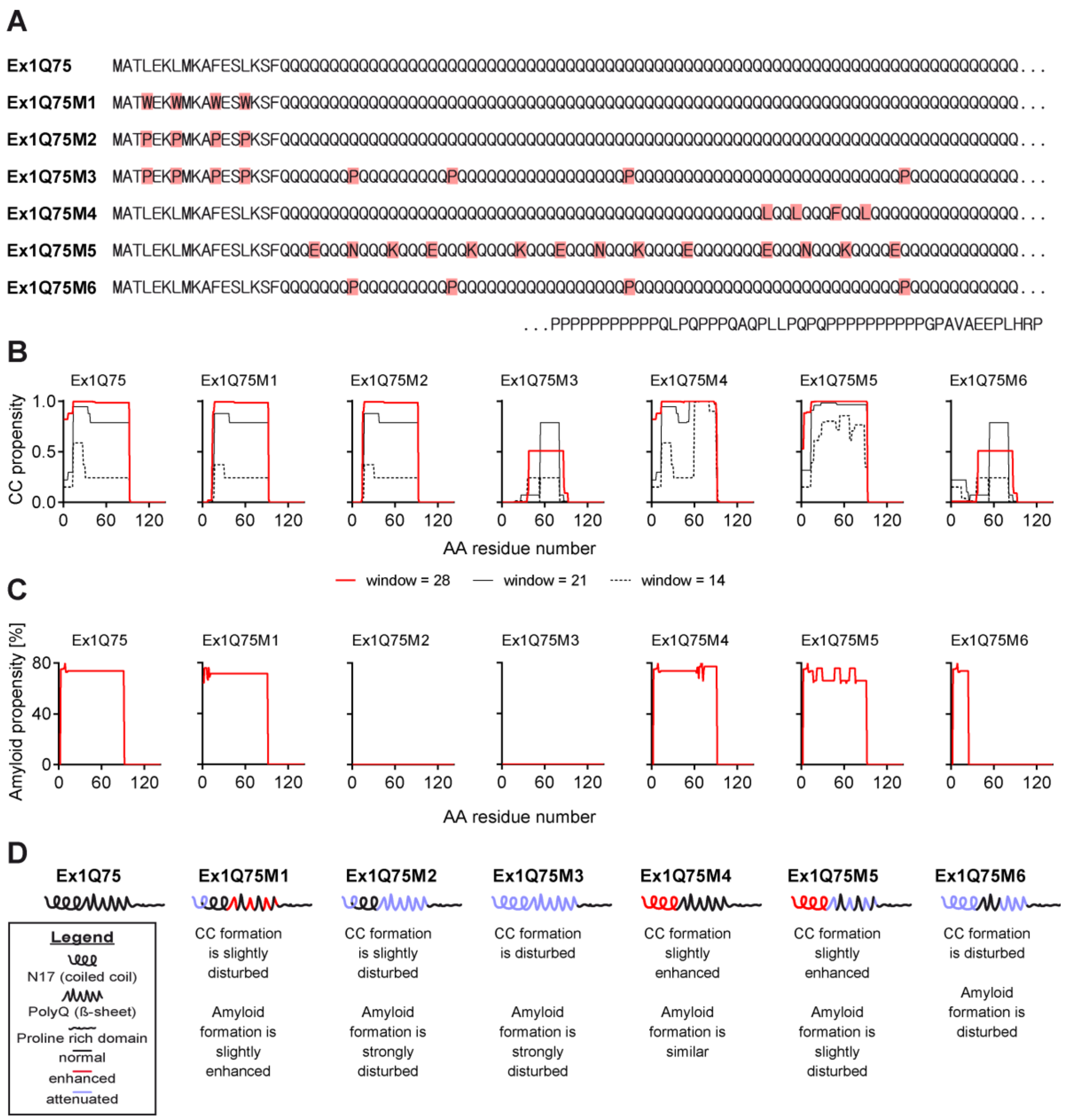

Suppl. Figure 3 (related to Figure 32): Protein variants of mutant Ex1Q75

__(A)__ Amino acid (AA) sequence of Ex1Q75 (top) and its protein variants. AA exchanges introduced in the sequence are highlighted in red. __(B)__ In silico analysis of protein variants using the COILS algorithm[278] predicted differences in coiled-coil domain formation. CC probability is displayed as 1 minus the P-score assigned to each amino acid using a window size of 14 (dashed black line), 21 (black line) and 28 (red line) residues. __(C)__ Protein variants were predicted to have different propensities to form amyloid structures using the Waltz algorithm[279,280] (low specificity threshold of 63 and neutral pH 7). __(D)__ Simplified model of Ex1Q75 and its protein variants illustrating predicted structural changes in amyloid and coiled-coil domain formation.

7.2. Contributions

- Initial establishment of the FRET-based aggregation assay was performed by Konrad Klockmeier during his Master Thesis (HU Berlin, 2013) supervised by Dr. Alexander Buntru.
- Figure 8B: SDS-PAGE and Coomassie staining were performed by Simon Berberich during his Master Thesis (TU Nürnberg, 2016) under my supervision.
- Figure 8D: AFM analysis of Ex1Q48-CyPet and Ex1Q48-YPet were performed by Konrad Klockmeier during his Master Thesis (HU Berlin, 2013).
- Figure 11B-D: AFM, FRA and FRASE analysis were performed by Isabelle Jansen during her Master Thesis (Heinrich-Heine-Universität Düsseldorf, 2015) under my supervision.
- Figure 17A: BN-PAGE analysis was performed by Regine Hasenkopf during her Master Thesis (HU Berlin, 2016).
- Figure 18B: Tau40, Aβ, IAPP and αSyn aggregates and the corresponding AFM images were prepared by Gerlinde Grelle.
- Figure 20: Immunoprecipitation and subsequent WB and FRASE analysis was performed by Regine Hasenkopf during her Master Thesis (HU Berlin, 2016).
- Figure 21C: FRASE analysis was performed by Regine Hasenkopf during her Master Thesis (HU Berlin, 2016).
- Figure 26D: EM analysis was performed by Severine Kunz, member of the EM core facility at the Max-Delbrück-Center for Molecular Medicine (MDC).
- Figure 27B: Fluorescence microscopy images were taken by Isabelle Jansen during her Master Thesis (Heinrich-Heine-Universität Düsseldorf, 2015) under my supervision.
- Figure 28: All related fly work was performed by Franziska Schindler during her PhD Thesis.
- Figure 29A: *C.elegans* work and mobility assay was performed by Janine Kirstein (FMP, Berlin).
- Figure 33B-D: SDS-PAGE and WB analysis were performed by Simon Berberich during his Master Thesis (TU Nürnberg, 2016) under my supervision.
- Figure 34E: Fractionation experiments were performed by Simon Berberich during his Master Thesis (TU Nürnberg, 2016) under my supervision.
- Suppl. Figure 1 and Suppl. Figure 2: Data were produced by Franziska Schindler during her PhD Thesis[262].

7.3. Relevant papers

Ast, A. et al. mHTT Seeding Activity: A Marker of Disease Progression and Neurotoxicity in Models of Huntington's Disease. Mol Cell 71, 675-688 e676, doi:10.1016/j.molcel.2018.07.032 (2018).

7.4. List of Figures

7.5. List of Tables

8. References

1 Drachman, D. A. Do we have brain to spare? *Neurology* **64**, 2004 (2005).

2 Azevedo, F. A. C. *et al.* Equal numbers of neuronal and nonneuronal cells make the human brain an isometrically scaled-up primate brain. *Journal of Comparative Neurology* **513**, 532-541, doi:doi:10.1002/cne.21974 (2009).

3 von Bartheld, C. S., Bahney, J. & Herculano-Houzel, S. The Search for True Numbers of Neurons and Glial Cells in the Human Brain: A Review of 150 Years of Cell Counting. *The Journal of comparative neurology* **524**, 3865-3895, doi:10.1002/cne.24040 (2016).

4 Bossy-Wetzel, E., Schwarzenbacher, R. & Lipton, S. A. Molecular pathways to neurodegeneration. *Nature Medicine* **10**, S2, doi:10.1038/nm1067 (2004).

5 Health, N. I. o. *Degenerative Nerve Diseases* <https://medlineplus.gov/degenerativenervediseases.html#cat_42> (2018).

6 The Challenge of Neurodegenerative Diseases in an Aging Population. *TRENDS IN THE SCIENCES* **22**, 6_92-96_93, doi:10.5363/tits.22.6_92 (2017).

7 Cuny, G. D. Neurodegenerative diseases: challenges and opportunities. *Future Medicinal Chemistry* **4**, 1647-1649, doi:10.4155/fmc.12.123 (2012).

8 Jones, C. *et al.* The societal cost of Huntington's disease: are we underestimating the burden? *European journal of neurology* **23**, 1588-1590, doi:10.1111/ene.13107 (2016).

9 Wynford-Thomas, R. & Robertson, N. P. The economic burden of chronic neurological disease. *Journal of neurology* **264**, 2345-2347, doi:10.1007/s00415-017-8632-7 (2017).

10 Yu, M., Tan, K., Koloms, K. & Bega, D. Assessment of Caregiver Burden in Huntington's Disease. *J Huntingtons Dis*, doi:10.3233/jhd-180326 (2018).

11 Zuccato, C., Valenza, M. & Cattaneo, E. Molecular mechanisms and potential therapeutical targets in Huntington's disease. *Physiol Rev* **90**, 905-981, doi:10.1152/physrev.00041.2009 (2010).

12 Vale, T. C. & Cardoso, F. Chorea: A Journey through History. *Tremor and other hyperkinetic movements (New York, N.Y.)* **5**, tre-5-296, doi:10.7916/D8WM1C98 (2015).

13 George Huntington, M. D. On Chorea. *The Medical and Surgical Reporter: A Weekly Journal* **26**, 317–321 (1872).

14 Bhattacharyya, K. B. The story of George Huntington and his disease. *Annals of Indian Academy of Neurology* **19**, 25-28, doi:10.4103/0972-2327.175425 (2016).

15 Wexler, A., Wild, E. J. & Tabrizi, S. J. George Huntington: a legacy of inquiry, empathy and hope. *Brain* **139**, 2326-2333, doi:10.1093/brain/aww165 (2016).

16 Group, T. H. s. D. C. R. A novel gene containing a trinucleotide repeat that is expanded and unstable on Huntington's disease chromosomes. The Huntington's Disease Collaborative Research Group. *Cell* **72**, 971-983 (1993).

17 Rubinsztein, D. C. *et al.* Phenotypic characterization of individuals with 30-40 CAG repeats in the Huntington disease (HD) gene reveals HD cases with 36 repeats and apparently normal elderly individuals with 36-39 repeats. *American journal of human genetics* **59**, 16-22 (1996).

18 Wheeler, V. C. *et al.* Factors associated with HD CAG repeat instability in Huntington disease. *Journal of Medical Genetics* **44**, 695-701, doi:10.1136/jmg.2007.050930 (2007).

19 Telenius, H. *et al.* Somatic and gonadal mosaicism of the Huntington disease gene CAG repeat in brain and sperm. *Nat Genet* **6**, 409-414, doi:10.1038/ng0494-409 (1994).

20 Myers, R. H., Madden, J. J., Teague, J. L. & Falek, A. Factors related to onset age of Huntington disease. *American journal of human genetics* **34**, 481-488 (1982).

21 Andrew, S. E. *et al.* The relationship between trinucleotide (CAG) repeat length and clinical features of Huntington's disease. *Nat Genet* **4**, 398-403, doi:10.1038/ng0893-398 (1993).

22 Rosenblatt, A. *et al.* Age, CAG repeat length, and clinical progression in Huntington's disease. *Movement disorders : official journal of the Movement Disorder Society* **27**, 272-276, doi:10.1002/mds.24024 (2012).

23 Foroud, T., Gray, J., Ivashina, J. & Conneally, P. M. Differences in duration of Huntington's disease based on age at onset. *Journal of neurology, neurosurgery, and psychiatry* **66**, 52-56 (1999).

24 Lee, J. M. *et al.* CAG repeat expansion in Huntington disease determines age at onset in a fully dominant fashion. *Neurology* **78**, 690-695, doi:10.1212/WNL.0b013e318249f683 (2012).

25 McColgan, P. & Tabrizi, S. J. Huntington's disease: a clinical review. *Eur J Neurol* **25**, 24-34, doi:10.1111/ene.13413 (2018).

26 Rosenblatt, A. *et al.* Familial influence on age of onset among siblings with Huntington disease. *American journal of medical genetics* **105**, 399-403 (2001).

27 Gusella, J. F., MacDonald, M. E. & Lee, J. M. Genetic modifiers of Huntington's disease. *Movement disorders : official journal of the Movement Disorder Society* **29**, 1359-1365, doi:10.1002/mds.26001 (2014).

28 Gusella, J. F. & Macdonald, M. Genetic criteria for Huntington's disease pathogenesis. *Brain Res Bull* **72**, 78-82, doi:10.1016/j.brainresbull.2006.10.014 (2007).

References

29 Georgiou, N. *et al.* Differential clinical and motor control function in a pair of monozygotic twins with Huntington's disease. *Movement disorders : official journal of the Movement Disorder Society* **14**, 320-325 (1999).

30 Consortium, G. M. o. H. s. D. G.-H. Identification of Genetic Factors that Modify Clinical Onset of Huntington's Disease. *Cell* **162**, 516-526, doi:10.1016/j.cell.2015.07.003 (2015).

31 Gusella, J. F. & MacDonald, M. E. Huntington's disease: the case for genetic modifiers. *Genome medicine* **1**, 80, doi:10.1186/gm80 (2009).

32 Fisher, E. R. & Hayden, M. R. Multisource ascertainment of Huntington disease in Canada: prevalence and population at risk. *Movement disorders : official journal of the Movement Disorder Society* **29**, 105-114, doi:10.1002/mds.25717 (2014).

33 Hayden, M. R., MacGregor, J. M. & Beighton, P. H. The prevalence of Huntington's chorea in South Africa. *South African medical journal = Suid-Afrikaanse tydskrif vir geneeskunde* **58**, 193-196 (1980).

34 Pringsheim, T. *et al.* The incidence and prevalence of Huntington's disease: a systematic review and meta-analysis. *Movement disorders : official journal of the Movement Disorder Society* **27**, 1083-1091, doi:10.1002/mds.25075 (2012).

35 Bates, G. P. *et al.* in *Nature reviews. Disease primers* Vol. 1 15005 (2015).

36 Paulsen, J. S. *et al.* Detection of Huntington's disease decades before diagnosis: the Predict-HD study. *Journal of neurology, neurosurgery, and psychiatry* **79**, 874-880, doi:10.1136/jnnp.2007.128728 (2008).

37 Siesling, S., van Vugt, J. P., Zwinderman, K. A., Kieburtz, K. & Roos, R. A. Unified Huntington's disease rating scale: a follow up. *Movement disorders : official journal of the Movement Disorder Society* **13**, 915-919, doi:10.1002/mds.870130609 (1998).

38 Unified Huntington's Disease Rating Scale: reliability and consistency. Huntington Study Group. *Movement disorders : official journal of the Movement Disorder Society* **11**, 136-142, doi:10.1002/mds.870110204 (1996).

39 Dorsey, E. R. *et al.* Natural history of Huntington disease. *JAMA neurology* **70**, 1520-1530, doi:10.1001/jamaneurol.2013.4408 (2013).

40 Rosenblatt, A. *et al.* The association of CAG repeat length with clinical progression in Huntington disease. *Neurology* **66**, 1016-1020, doi:10.1212/01.wnl.0000204230.16619.d9 (2006).

41 Paulsen, J. S. Cognitive impairment in Huntington disease: diagnosis and treatment. *Current neurology and neuroscience reports* **11**, 474-483, doi:10.1007/s11910-011-0215-x (2011).

42 Peavy, G. M. *et al.* Cognitive and functional decline in Huntington's disease: dementia criteria revisited. *Movement disorders : official journal of the Movement Disorder Society* **25**, 1163-1169, doi:10.1002/mds.22953 (2010).

43 Rosenblatt, A. Neuropsychiatry of Huntington's disease. *Dialogues in clinical neuroscience* **9**, 191-197 (2007).

44 Paoli, R. A. *et al.* Neuropsychiatric Burden in Huntington's Disease. *Brain sciences* **7**, 67, doi:10.3390/brainsci7060067 (2017).

45 Paulsen, J. S., Ready, R. E., Hamilton, J. M., Mega, M. S. & Cummings, J. L. Neuropsychiatric aspects of Huntington's disease. *Journal of neurology, neurosurgery, and psychiatry* **71**, 310-314, doi:10.1136/jnnp.71.3.310 (2001).

46 Tabrizi, S. J. *et al.* Predictors of phenotypic progression and disease onset in premanifest and early-stage Huntington's disease in the TRACK-HD study: analysis of 36-month observational data. *The Lancet. Neurology* **12**, 637-649, doi:10.1016/s1474-4422(13)70088-7 (2013).

47 van der Burg, J. M., Bjorkqvist, M. & Brundin, P. Beyond the brain: widespread pathology in Huntington's disease. *The Lancet. Neurology* **8**, 765-774, doi:10.1016/s1474-4422(09)70178-4 (2009).

48 Sassone, J., Colciago, C., Cislaghi, G., Silani, V. & Ciammola, A. Huntington's disease: the current state of research with peripheral tissues. *Experimental neurology* **219**, 385-397, doi:10.1016/j.expneurol.2009.05.012 (2009).

49 Zielonka, D., Piotrowska, I., Marcinkowski, J. T. & Mielcarek, M. Skeletal muscle pathology in Huntington's disease. *Frontiers in physiology* **5**, 380, doi:10.3389/fphys.2014.00380 (2014).

50 Heemskerk, A.-W. & Roos, R. A. C. Aspiration pneumonia and death in Huntington's disease. *PLoS currents* **4**, RRN1293-RRN1293, doi:10.1371/currents.RRN1293 (2012).

51 Abildtrup, M. & Shattock, M. Cardiac Dysautonomia in Huntington's Disease. *J Huntingtons Dis* **2**, 251-261, doi:10.3233/jhd-130054 (2013).

52 Mielcarek, M. Huntington's disease is a multi-system disorder. *Rare diseases (Austin, Tex.)* **3**, e1058464-e1058464, doi:10.1080/21675511.2015.1058464 (2015).

53 Gonzalez-Alegre, P. & Afifi, A. K. Clinical characteristics of childhood-onset (juvenile) Huntington disease: report of 12 patients and review of the literature. *Journal of child neurology* **21**, 223-229, doi:10.2310/7010.2006.00055 (2006).

54 Quarrell, O. W. J. *et al.* Managing juvenile Huntington's disease. *Neurodegenerative disease management* **3**, 10.2217/nmt.2213.2218, doi:10.2217/nmt.13.18 (2013).

55 Letort, D. & Gonzalez-Alegre, P. Huntington's disease in children. *Handbook of clinical neurology* **113**, 1913-1917, doi:10.1016/b978-0-444-59565-2.00061-7 (2013).

56 Nance, M. A. & Myers, R. H. Juvenile onset Huntington's disease--clinical and research perspectives. *Mental retardation and developmental disabilities research reviews* **7**, 153-157, doi:10.1002/mrdd.1022 (2001).

57 Jason, G. W. *et al.* Cognitive manifestations of Huntington disease in relation to genetic structure and clinical onset. *Archives of neurology* **54**, 1081-1088 (1997).

58 Health, N. I. o. *Huntington disease*, <https://ghr.nlm.nih.gov/condition/huntington-disease> (

59 Heinsen, H. *et al.* Cortical and striatal neurone number in Huntington's disease. *Acta Neuropathol* **88**, 320-333 (1994).

60 Kravitz, A. V. & Kreitzer, A. C. Striatal mechanisms underlying movement, reinforcement, and punishment. *Physiology (Bethesda, Md.)* **27**, 167-177, doi:10.1152/physiol.00004.2012 (2012).

61 Macpherson, T., Morita, M. & Hikida, T. Striatal direct and indirect pathways control decision-making behavior. *Frontiers in psychology* **5**, 1301-1301, doi:10.3389/fpsyg.2014.01301 (2014).

62 Rub, U., Vonsattel, J. P., Heinsen, H. & Korf, H. W. The Neuropathology of Huntington s disease: classical findings, recent developments and correlation to functional neuroanatomy. *Advances in anatomy, embryology, and cell biology* **217**, 1-146 (2015).

63 Lange, H. & Aulich, A. 25-41 (1986).

64 Rub, U. *et al.* Degeneration of the cerebellum in Huntington's disease (HD): possible relevance for the clinical picture and potential gateway to pathological mechanisms of the disease process. *Brain pathology (Zurich, Switzerland)* **23**, 165-177, doi:10.1111/j.1750-3639.2012.00629.x (2013).

65 Vonsattel, J. P. Huntington disease models and human neuropathology: similarities and differences. *Acta Neuropathol* **115**, 55-69, doi:10.1007/s00401-007-0306-6 (2008).

66 Rub, U. *et al.* Huntington's disease (HD): the neuropathology of a multisystem neurodegenerative disorder of the human brain. *Brain pathology (Zurich, Switzerland)* **26**, 726-740, doi:10.1111/bpa.12426 (2016).

67 Marques Sousa, C. & Humbert, S. Huntingtin: here, there, everywhere! *J Huntingtons Dis* **2**, 395-403, doi:10.3233/jhd-130082 (2013).

68 Saudou, F. & Humbert, S. The Biology of Huntingtin. *Neuron* **89**, 910-926, doi:10.1016/j.neuron.2016.02.003 (2016).

69 Lin, B. *et al.* Differential 3' polyadenylation of the Huntington disease gene results in two mRNA species with variable tissue expression. *Human Molecular Genetics* **2**, 1541-1545, doi:10.1093/hmg/2.10.1541 (1993).

70 Hughes, A. C. *et al.* Identification of novel alternative splicing events in the huntingtin gene and assessment of the functional consequences using structural protein homology modelling. *J Mol Biol* **426**, 1428-1438, doi:10.1016/j.jmb.2013.12.028 (2014).

71 Ruzo, A. *et al.* Discovery of novel isoforms of huntingtin reveals a new hominid-specific exon. *PLoS One* **10**, e0127687, doi:10.1371/journal.pone.0127687 (2015).

72 Gipson, T. A., Neueder, A., Wexler, N. S., Bates, G. P. & Housman, D. Aberrantly spliced HTT, a new player in Huntington's disease pathogenesis. *RNA biology* **10**, 1647-1652, doi:10.4161/rna.26706 (2013).

73 Sathasivam, K. *et al.* Aberrant splicing of HTT generates the pathogenic exon 1 protein in Huntington disease. *Proc Natl Acad Sci U S A* **110**, 2366-2370, doi:10.1073/pnas.1221891110 (2013).

74 Neueder, A. *et al.* The pathogenic exon 1 HTT protein is produced by incomplete splicing in Huntington's disease patients. *Scientific Reports* **7**, 1307, doi:10.1038/s41598-017-01510-z (2017).

75 Takano, H. & Gusella, J. F. The predominantly HEAT-like motif structure of huntingtin and its association and coincident nuclear entry with dorsal, an NF-kB/Rel/dorsal family transcription factor. *BMC neuroscience* **3**, 15 (2002).

76 Palidwor, G. A. *et al.* Detection of alpha-rod protein repeats using a neural network and application to huntingtin. *PLoS computational biology* **5**, e1000304-e1000304, doi:10.1371/journal.pcbi.1000304 (2009).

77 Liu, J. P. & Zeitlin, S. O. Is Huntingtin Dispensable in the Adult Brain? *J Huntingtons Dis* **6**, 1-17, doi:10.3233/JHD-170235 (2017).

78 Tartari, M. *et al.* Phylogenetic Comparison of Huntingtin Homologues Reveals the Appearance of a Primitive polyQ in Sea Urchin. *Molecular Biology and Evolution* **25**, 330-338, doi:10.1093/molbev/msm258 (2008).

79 Atwal, R. S. *et al.* Huntingtin has a membrane association signal that can modulate huntingtin aggregation, nuclear entry and toxicity. *Human Molecular Genetics* **16**, 2600-2615, doi:10.1093/hmg/ddm217 (2007).

80 Maiuri, T., Woloshansky, T., Xia, J. & Truant, R. The huntingtin N17 domain is a multifunctional CRM1 and Ran-dependent nuclear and cilial export signal. *Human Molecular Genetics* **22**, 1383-1394, doi:10.1093/hmg/dds554 (2013).

81 Miller, J., Rutenber, E. & Muchowski, P. J. Polyglutamine dances the conformational cha-cha-cha. *Structure (London, England : 1993)* **17**, 1151-1153, doi:10.1016/j.str.2009.08.004 (2009).

82 Giorgini, F. A flexible polyglutamine hinge opens new doors for understanding huntingtin function. *Proc Natl Acad Sci U S A* **110**, 14516-14517, doi:10.1073/pnas.1313668110 (2013).

83 Darnell, G., Orgel, J. P., Pahl, R. & Meredith, S. C. Flanking polyproline sequences inhibit beta-sheet structure in polyglutamine segments by inducing PPII-like helix structure. *J Mol Biol* **374**, 688-704, doi:10.1016/j.jmb.2007.09.023 (2007).

84 Darnell, G. D., Derryberry, J., Kurutz, J. W. & Meredith, S. C. Mechanism of cis-inhibition of polyQ fibrillation by polyP: PPII oligomers and the hydrophobic effect. *Biophysical journal* **97**, 2295-2305, doi:10.1016/j.bpj.2009.07.062 (2009).

85 Vijayvargia, R. *et al.* Huntingtin's spherical solenoid structure enables polyglutamine tract-dependent modulation of its structure and function. *eLife* **5**, e11184, doi:10.7554/eLife.11184 (2016).

References

86 Guo, Q. *et al.* The cryo-electron microscopy structure of huntingtin. *Nature* **555**, 117, doi:10.1038/nature25502 https://www.nature.com/articles/nature25502#supplementary-information (2018).

87 Wellington, C. L. *et al.* Caspase cleavage of mutant huntingtin precedes neurodegeneration in Huntington's disease. *J Neurosci* **22**, 7862-7872 (2002).

88 Ratovitski, T. *et al.* N-terminal proteolysis of full-length mutant huntingtin in an inducible PC12 cell model of Huntington's disease. *Cell cycle (Georgetown, Tex.)* **6**, 2970-2981, doi:10.4161/cc.6.23.4992 (2007).

89 Gafni, J. *et al.* Inhibition of calpain cleavage of huntingtin reduces toxicity: accumulation of calpain/caspase fragments in the nucleus. *J Biol Chem* **279**, 20211-20220, doi:10.1074/jbc.M401267200 (2004).

90 Ratovitski, T., Chighladze, E., Waldron, E., Hirschhorn, R. R. & Ross, C. A. Cysteine proteases bleomycin hydrolase and cathepsin Z mediate N-terminal proteolysis and toxicity of mutant huntingtin. *J Biol Chem* **286**, 12578-12589, doi:10.1074/jbc.M110.185348 (2011).

91 Miller, J. P. *et al.* Matrix metalloproteinases are modifiers of huntingtin proteolysis and toxicity in Huntington's disease. *Neuron* **67**, 199-212, doi:10.1016/j.neuron.2010.06.021 (2010).

92 Goldberg, Y. P. *et al.* Cleavage of huntingtin by apopain, a proapoptotic cysteine protease, is modulated by the polyglutamine tract. *Nat Genet* **13**, 442-449, doi:10.1038/ng0896-442 (1996).

93 El-Daher, M. T. *et al.* Huntingtin proteolysis releases non-polyQ fragments that cause toxicity through dynamin 1 dysregulation. *The EMBO journal* **34**, 2255-2271, doi:10.15252/embj.201490808 (2015).

94 Zhou, H. *et al.* Huntingtin forms toxic NH2-terminal fragment complexes that are promoted by the age-dependent decrease in proteasome activity. *The Journal of cell biology* **163**, 109-118, doi:10.1083/jcb.200306038 (2003).

95 Li, H., Li, S. H., Johnston, H., Shelbourne, P. F. & Li, X. J. Amino-terminal fragments of mutant huntingtin show selective accumulation in striatal neurons and synaptic toxicity. *Nat Genet* **25**, 385-389, doi:10.1038/78054 (2000).

96 Ratovitski, T. *et al.* Post-Translational Modifications (PTMs), Identified on Endogenous Huntingtin, Cluster within Proteolytic Domains between HEAT Repeats. *Journal of proteome research* **16**, 2692-2708, doi:10.1021/acs.jproteome.6b00991 (2017).

97 Ehrnhoefer, D. E., Sutton, L. & Hayden, M. R. Small changes, big impact: posttranslational modifications and function of huntingtin in Huntington disease. *The Neuroscientist : a review journal bringing neurobiology, neurology and psychiatry* **17**, 475-492, doi:10.1177/1073858410390378 (2011).

98 Caterino, M. *et al.* Huntingtin protein: A new option for fixing the Huntington's disease countdown clock. *Neuropharmacology* **135**, 126-138, doi:10.1016/j.neuropharm.2018.03.009 (2018).

99 Engelender, S. *et al.* Huntingtin-associated Protein 1 (HAP1) Interacts with the p150Glued Bubunit of Dynactin. *Human Molecular Genetics* **6**, 2205-2212, doi:10.1093/hmg/6.13.2205 (1997).

100 Caviston, J. P., Ross, J. L., Antony, S. M., Tokito, M. & Holzbaur, E. L. F. Huntingtin facilitates dynein/dynactin-mediated vesicle transport. *Proceedings of the National Academy of Sciences* **104**, 10045-10050, doi:10.1073/pnas.0610628104 (2007).

101 Zala, D., Hinckelmann, M. V. & Saudou, F. Huntingtin's function in axonal transport is conserved in Drosophila melanogaster. *PLoS One* **8**, e60162, doi:10.1371/journal.pone.0060162 (2013).

102 Wong, Y. C. & Holzbaur, E. L. F. The Regulation of Autophagosome Dynamics by Huntingtin and HAP1 Is Disrupted by Expression of Mutant Huntingtin, Leading to Defective Cargo Degradation. *The Journal of Neuroscience* **34**, 1293-1305, doi:10.1523/jneurosci.1870-13.2014 (2014).

103 Gauthier, L. R. *et al.* Huntingtin Controls Neurotrophic Support and Survival of Neurons by Enhancing BDNF Vesicular Transport along Microtubules. *Cell* **118**, 127-138, doi:https://doi.org/10.1016/j.cell.2004.06.018 (2004).

104 Caviston, J. P., Zajac, A. L., Tokito, M. & Holzbaur, E. L. Huntingtin coordinates the dynein-mediated dynamic positioning of endosomes and lysosomes. *Mol Biol Cell* **22**, 478-492, doi:10.1091/mbc.E10-03-0233 (2011).

105 Zala, D. *et al.* Vesicular Glycolysis Provides On-Board Energy for Fast Axonal Transport. *Cell* **152**, 479-491, doi:https://doi.org/10.1016/j.cell.2012.12.029 (2013).

106 Colin, E. *et al.* Huntingtin phosphorylation acts as a molecular switch for anterograde/retrograde transport in neurons. *The EMBO journal* **27**, 2124-2134, doi:10.1038/emboj.2008.133 (2008).

107 Waelter, S. *et al.* The huntingtin interacting protein HIP1 is a clathrin and α-adaptin-binding protein involved in receptor-mediated endocytosis. *Human Molecular Genetics* **10**, 1807-1817, doi:10.1093/hmg/10.17.1807 (2001).

108 Engqvist-Goldstein, A. E. Y. *et al.* The actin-binding protein Hip1R associates with clathrin during early stages of endocytosis and promotes clathrin assembly in vitro. *Journal of Cell Biology* **154**, 1209-1223, doi:10.1083/jcb.200106089 (2001).

109 Legendre-Guillemin, V. *et al.* HIP1 and HIP12 display differential binding to F-actin, AP2, and clathrin. Identification of a novel interaction with clathrin light chain. *J Biol Chem* **277**, 19897-19904, doi:10.1074/jbc.M112310200 (2002).

110 Modregger, J., Schmidt, A. A., Ritter, B., Huttner, W. B. & Plomann, M. Characterization of Endophilin B1b, a brain-specific membrane-associated lysophosphatidic acid acyl transferase with properties distinct from endophilin A1. *J Biol Chem* **278**, 4160-4167, doi:10.1074/jbc.M208568200 (2003).

111 Sittler, A. *et al.* SH3GL3 Associates with the Huntingtin Exon 1 Protein and Promotes the Formation of Polygln-Containing Protein Aggregates. *Molecular Cell* **2**, 427-436, doi:https://doi.org/10.1016/S1097-2765(00)80142-2 (1998).

112 Ochaba, J. *et al.* Potential function for the Huntingtin protein as a scaffold for selective autophagy. *Proceedings of the National Academy of Sciences* **111**, 16889-16894, doi:10.1073/pnas.1420103111 (2014).

113 Rui, Y.-N. *et al.* Huntingtin functions as a scaffold for selective macroautophagy. *Nature Cell Biology* **17**, 262, doi:10.1038/ncb3101
https://www.nature.com/articles/ncb3101#supplementary-information (2015).

114 Seong, I. S. *et al.* Huntingtin facilitates polycomb repressive complex 2. *Human Molecular Genetics* **19**, 573-583, doi:10.1093/hmg/ddp524 (2010).

115 Steffan, J. S. *et al.* The Huntington's disease protein interacts with p53 and CREB-binding protein and represses transcription. *Proceedings of the National Academy of Sciences* **97**, 6763-6768, doi:10.1073/pnas.100110097 (2000).

116 Dunah, A. W. *et al.* Sp1 and TAFII130 Transcriptional Activity Disrupted in Early Huntington's Disease. *Science* **296**, 2238-2243, doi:10.1126/science.1072613 (2002).

117 Zuccato, C. *et al.* Huntingtin interacts with REST/NRSF to modulate the transcription of NRSE-controlled neuronal genes. *Nature Genetics* **35**, 76, doi:10.1038/ng1219
https://www.nature.com/articles/ng1219#supplementary-information (2003).

118 Savas, J. N. *et al.* Huntington's disease protein contributes to RNA-mediated gene silencing through association with Argonaute and P bodies. *Proceedings of the National Academy of Sciences* **105**, 10820-10825, doi:10.1073/pnas.0800658105 (2008).

119 DiGiovanni, L. F., Mocle, A. J., Xia, J. & Truant, R. Huntingtin N17 domain is a reactive oxygen species sensor regulating huntingtin phosphorylation and localization. *Human molecular genetics* **25**, 3937-3945, doi:10.1093/hmg/ddw234 (2016).

120 Maiuri, T. *et al.* Huntingtin is a scaffolding protein in the ATM oxidative DNA damage response complex. *Hum Mol Genet* **26**, 395-406, doi:10.1093/hmg/ddw395 (2017).

121 Rigamonti, D. *et al.* Wild-type huntingtin protects from apoptosis upstream of caspase-3. *J Neurosci* **20**, 3705-3713 (2000).

122 Rigamonti, D. *et al.* Huntingtin's neuroprotective activity occurs via inhibition of procaspase-9 processing. *J Biol Chem* **276**, 14545-14548, doi:10.1074/jbc.C100044200 (2001).

123 Cheng, C. M., Huang, S. P., Chang, Y. F., Chung, W. Y. & Yuo, C. Y. The viral death protein Apoptin interacts with Hippi, the protein interactor of Huntingtin-interacting protein 1. *Biochemical and biophysical research communications* **305**, 359-364 (2003).

124 Gervais, F. G. *et al.* Recruitment and activation of caspase-8 by the Huntingtin-interacting protein Hip-1 and a novel partner Hippi. *Nat Cell Biol* **4**, 95-105, doi:10.1038/ncb735 (2002).

125 Nucifora, L. G. *et al.* Identification of novel potentially toxic oligomers formed in vitro from mammalian-derived expanded huntingtin exon-1 protein. *J Biol Chem* **287**, 16017-16028, doi:10.1074/jbc.M111.252577 (2012).

126 Landles, C. *et al.* Proteolysis of mutant huntingtin produces an exon 1 fragment that accumulates as an aggregated protein in neuronal nuclei in Huntington disease. *J Biol Chem* **285**, 8808-8823, doi:10.1074/jbc.M109.075028 (2010).

127 Davies, S. W. *et al.* Formation of neuronal intranuclear inclusions underlies the neurological dysfunction in mice transgenic for the HD mutation. *Cell* **90**, 537-548 (1997).

128 DiFiglia, M. *et al.* Aggregation of huntingtin in neuronal intranuclear inclusions and dystrophic neurites in brain. *Science* **277**, 1990-1993 (1997).

129 Scherzinger, E. *et al.* Huntingtin-encoded polyglutamine expansions form amyloid-like protein aggregates in vitro and in vivo. *Cell* **90**, 549-558 (1997).

130 Scherzinger, E. *et al.* Self-assembly of polyglutamine-containing huntingtin fragments into amyloid-like fibrils: Implications for Huntington's disease pathology. *Proceedings of the National Academy of Sciences* **96**, 4604 (1999).

131 Hoffner, G., Island, M. L. & Djian, P. Purification of neuronal inclusions of patients with Huntington's disease reveals a broad range of N-terminal fragments of expanded huntingtin and insoluble polymers. *Journal of neurochemistry* **95**, 125-136, doi:10.1111/j.1471-4159.2005.03348.x (2005).

132 Perutz, M. F., Johnson, T., Suzuki, M. & Finch, J. T. Glutamine repeats as polar zippers: their possible role in inherited neurodegenerative diseases. *Proceedings of the National Academy of Sciences* **91**, 5355-5358, doi:10.1073/pnas.91.12.5355 (1994).

133 Arrasate, M. & Finkbeiner, S. Protein aggregates in Huntington's disease. *Experimental neurology* **238**, 1-11, doi:10.1016/j.expneurol.2011.12.013 (2012).

134 Juenemann, K. *et al.* Dynamic recruitment of ubiquitin to mutant huntingtin inclusion bodies. *Scientific Reports* **8**, 1405, doi:10.1038/s41598-018-19538-0 (2018).

135 Xi Wen-Hui , W. G.-H. Amyloid- β peptide aggregation and the influence of carbon nanoparticles *Physics B* **25** (2016).

References

136 Eisenberg, D. & Jucker, M. The amyloid state of proteins in human diseases. *Cell* **148**, 1188-1203, doi:10.1016/j.cell.2012.02.022 (2012).

137 Chiti, F. & Dobson, C. M. Protein Misfolding, Amyloid Formation, and Human Disease: A Summary of Progress Over the Last Decade. *Annu Rev Biochem* **86**, 27-68, doi:10.1146/annurev-biochem-061516-045115 (2017).

138 van der Wel, P. C. A. Insights into protein misfolding and aggregation enabled by solid-state NMR spectroscopy. *Solid state nuclear magnetic resonance* **88**, 1-14, doi:10.1016/j.ssnmr.2017.10.001 (2017).

139 Hoop, C. L. *et al.* Huntingtin exon 1 fibrils feature an interdigitated beta-hairpin-based polyglutamine core. *Proc Natl Acad Sci U S A* **113**, 1546-1551, doi:10.1073/pnas.1521933113 (2016).

140 Hoop, C. L. *et al.* Polyglutamine amyloid core boundaries and flanking domain dynamics in huntingtin fragment fibrils determined by solid-state nuclear magnetic resonance. *Biochemistry* **53**, 6653-6666, doi:10.1021/bi501010q (2014).

141 Lin, H. K. *et al.* Fibril polymorphism affects immobilized non-amyloid flanking domains of huntingtin exon1 rather than its polyglutamine core. *Nat Commun* **8**, 15462, doi:10.1038/ncomms15462 (2017).

142 Baias, M. *et al.* Structure and Dynamics of the Huntingtin Exon-1 N-Terminus: A Solution NMR Perspective. *Journal of the American Chemical Society* **139**, 1168-1176, doi:10.1021/jacs.6b10893 (2017).

143 Kim, M. W., Chelliah, Y., Kim, S. W., Otwinowski, Z. & Bezprozvanny, I. Secondary structure of Huntingtin amino-terminal region. *Structure (London, England : 1993)* **17**, 1205-1212, doi:10.1016/j.str.2009.08.002 (2009).

144 Meisl, G. *et al.* Molecular mechanisms of protein aggregation from global fitting of kinetic models. *Nature protocols* **11**, 252-272, doi:10.1038/nprot.2016.010 (2016).

145 Chen, M. & Wolynes, P. G. Aggregation landscapes of Huntingtin exon 1 protein fragments and the critical repeat length for the onset of Huntington's disease. *Proc Natl Acad Sci U S A* **114**, 4406-4411, doi:10.1073/pnas.1702237114 (2017).

146 Kar, K., Jayaraman, M., Sahoo, B., Kodali, R. & Wetzel, R. Critical nucleus size for disease-related polyglutamine aggregation is repeat-length dependent. *Nature Structural &Amp; Molecular Biology* **18**, 328, doi:10.1038/nsmb.1992
https://www.nature.com/articles/nsmb.1992#supplementary-information (2011).

147 Li, S.-H. & Li, X.-J. Aggregation of N-Terminal Huntingtin is Dependent on the Length of Its Glutamine Repeats. *Human Molecular Genetics* **7**, 777-782, doi:10.1093/hmg/7.5.777 (1998).

148 Crick, S. L., Ruff, K. M., Garai, K., Frieden, C. & Pappu, R. V. Unmasking the roles of N- and C-terminal flanking sequences from exon 1 of huntingtin as modulators of polyglutamine aggregation. *Proceedings of the National Academy of Sciences* **110**, 20075-20080, doi:10.1073/pnas.1320626110 (2013).

149 Mishra, R. *et al.* Inhibiting the Nucleation of Amyloid Structure in a Huntingtin Fragment by Targeting α-Helix-Rich Oligomeric Intermediates. *Journal of Molecular Biology* **415**, 900-917, doi:https://doi.org/10.1016/j.jmb.2011.12.011 (2012).

150 Bhattacharyya, A. *et al.* Oligoproline Effects on Polyglutamine Conformation and Aggregation. *Journal of Molecular Biology* **355**, 524-535, doi:https://doi.org/10.1016/j.jmb.2005.10.053 (2006).

151 Thakur, A. K. *et al.* Polyglutamine disruption of the huntingtin exon 1 N terminus triggers a complex aggregation mechanism. *Nature Structural &Amp; Molecular Biology* **16**, 380, doi:10.1038/nsmb.1570 (2009).

152 Jayaraman, M. *et al.* Slow Amyloid Nucleation via α-Helix-Rich Oligomeric Intermediates in Short Polyglutamine-Containing Huntingtin Fragments. *Journal of Molecular Biology* **415**, 881-899, doi:https://doi.org/10.1016/j.jmb.2011.12.010 (2012).

153 Zhang, L. *et al.* Molecular Mechanism of Stabilizing the Helical Structure of Huntingtin N17 in a Micellar Environment. *The journal of physical chemistry. B* **121**, 4713-4721, doi:10.1021/acs.jpcb.7b01476 (2017).

154 Wetzel, R. Physical chemistry of polyglutamine: intriguing tales of a monotonous sequence. *J Mol Biol* **421**, 466-490, doi:10.1016/j.jmb.2012.01.030 (2012).

155 Kang, H. *et al.* Emerging β-Sheet Rich Conformations in Supercompact Huntingtin Exon-1 Mutant Structures. *Journal of the American Chemical Society* **139**, 8820-8827, doi:10.1021/jacs.7b00838 (2017).

156 Pandey, N. K. *et al.* The 17-residue-long N terminus in huntingtin controls stepwise aggregation in solution and on membranes via different mechanisms. *J Biol Chem* **293**, 2597-2605, doi:10.1074/jbc.M117.813667 (2018).

157 Kokona, B., Rosenthal, Z. P. & Fairman, R. Role of the Coiled-Coil Structural Motif in Polyglutamine Aggregation. *Biochemistry* **53**, 6738-6746, doi:10.1021/bi500449a (2014).

158 Wetzel, R. Kinetics and thermodynamics of amyloid fibril assembly. *Accounts of chemical research* **39**, 671-679, doi:10.1021/ar050069h (2006).

159 Wagner, A. S. *et al.* Self-assembly of Mutant Huntingtin Exon-1 Fragments into Large Complex Fibrillar Structures Involves Nucleated Branching. *J Mol Biol* **430**, 1725-1744, doi:10.1016/j.jmb.2018.03.017 (2018).

160 Sivanandam, V. N. *et al.* The aggregation-enhancing huntingtin N-terminus is helical in amyloid fibrils. *Journal of the American Chemical Society* **133**, 4558-4566, doi:10.1021/ja110715f (2011).

161 Requena, J. R. & Wille, H. The Structure of the Infectious Prion Protein and Its Propagation. *Progress in molecular biology and translational science* **150**, 341-359, doi:10.1016/bs.pmbts.2017.06.009 (2017).

162 Moreno-Gonzalez, I. & Soto, C. Misfolded protein aggregates: mechanisms, structures and potential for disease transmission. *Semin Cell Dev Biol* **22**, 482-487, doi:10.1016/j.semcdb.2011.04.002 (2011).

163 Prusiner, S. B. Novel proteinaceous infectious particles cause scrapie. *Science* **216**, 136-144 (1982).

164 Vilette, D. *et al.* Cellular mechanisms responsible for cell-to-cell spreading of prions. *Cell Mol Life Sci*, doi:10.1007/s00018-018-2823-y (2018).

165 Shearin, H. & Bessen, R. A. Axonal and transynaptic spread of prions. *Journal of virology* **88**, 8640-8655, doi:10.1128/JVI.00378-14 (2014).

166 Alais, S. *et al.* Mouse neuroblastoma cells release prion infectivity associated with exosomal vesicles. *Biology of the cell* **100**, 603-615, doi:10.1042/bc20080025 (2008).

167 Zhu, S., Victoria, G. S., Marzo, L., Ghosh, R. & Zurzolo, C. Prion aggregates transfer through tunneling nanotubes in endocytic vesicles. *Prion* **9**, 125-135, doi:10.1080/19336896.2015.1025189 (2015).

168 Mabbott, N. A. How do PrP(Sc) Prions Spread between Host Species, and within Hosts? *Pathogens (Basel, Switzerland)* **6**, 60, doi:10.3390/pathogens6040060 (2017).

169 Lee, J., Kim, S. Y., Hwang, K. J., Ju, Y. R. & Woo, H. J. Prion diseases as transmissible zoonotic diseases. *Osong public health and research perspectives* **4**, 57-66, doi:10.1016/j.phrp.2012.12.008 (2013).

170 Brundin, P., Melki, R. & Kopito, R. Prion-like transmission of protein aggregates in neurodegenerative diseases. *Nat Rev Mol Cell Biol* **11**, 301-307, doi:10.1038/nrm2873 (2010).

171 Jucker, M. & Walker, L. C. Self-propagation of pathogenic protein aggregates in neurodegenerative diseases. *Nature* **501**, 45-51, doi:10.1038/nature12481 (2013).

172 Jucker, M. & Walker, L. C. Pathogenic protein seeding in Alzheimer disease and other neurodegenerative disorders. *Ann Neurol* **70**, 532-540, doi:10.1002/ana.22615 (2011).

173 Gupta, S., Jie, S. & Colby, D. W. Protein misfolding detected early in pathogenesis of transgenic mouse model of Huntington disease using amyloid seeding assay. *J Biol Chem* **287**, 9982-9989, doi:10.1074/jbc.M111.305417 (2012).

174 Holmes, B. B. *et al.* Heparan sulfate proteoglycans mediate internalization and propagation of specific proteopathic seeds. *Proc Natl Acad Sci U S A* **110**, E3138-3147, doi:10.1073/pnas.1301440110 (2013).

175 Ren, P. H. *et al.* Cytoplasmic penetration and persistent infection of mammalian cells by polyglutamine aggregates. *Nat Cell Biol* **11**, 219-225, doi:10.1038/ncb1830 (2009).

176 Trevino, R. S. *et al.* Fibrillar structure and charge determine the interaction of polyglutamine protein aggregates with the cell surface. *J Biol Chem* **287**, 29722-29728, doi:10.1074/jbc.M112.372474 (2012).

177 Tan, Z. *et al.* Huntington's disease cerebrospinal fluid seeds aggregation of mutant huntingtin. *Mol Psychiatry* **20**, 1286-1293, doi:10.1038/mp.2015.81 (2015).

178 Costanzo, M. *et al.* Transfer of polyglutamine aggregates in neuronal cells occurs in tunneling nanotubes. *Journal of cell science* **126**, 3678-3685, doi:10.1242/jcs.126086 (2013).

179 Pecho-Vrieseling, E. *et al.* Transneuronal propagation of mutant huntingtin contributes to non-cell autonomous pathology in neurons. *Nat Neurosci* **17**, 1064-1072, doi:10.1038/nn.3761 (2014).

180 Babcock, D. T. & Ganetzky, B. Transcellular spreading of huntingtin aggregates in the Drosophila brain. *Proc Natl Acad Sci U S A* **112**, E5427-5433, doi:10.1073/pnas.1516217112 (2015).

181 Masnata, M. & Cicchetti, F. The Evidence for the Spread and Seeding Capacities of the Mutant Huntingtin Protein in in Vitro Systems and Their Therapeutic Implications. *Front Neurosci* **11**, 647, doi:10.3389/fnins.2017.00647 (2017).

182 Jeon, I. *et al.* Human-to-mouse prion-like propagation of mutant huntingtin protein. *Acta Neuropathol* **132**, 577-592, doi:10.1007/s00401-016-1582-9 (2016).

183 Yang, W., Dunlap, J. R., Andrews, R. B. & Wetzel, R. Aggregated polyglutamine peptides delivered to nuclei are toxic to mammalian cells. *Hum Mol Genet* **11**, 2905-2917 (2002).

184 Michalik, A. & Van Broeckhoven, C. Pathogenesis of polyglutamine disorders: aggregation revisited. *Hum Mol Genet* **12 Spec No 2**, R173-186, doi:10.1093/hmg/ddg295 (2003).

185 Adegbuyiro, A., Sedighi, F., Pilkington, A. W. t., Groover, S. & Legleiter, J. Proteins Containing Expanded Polyglutamine Tracts and Neurodegenerative Disease. *Biochemistry* **56**, 1199-1217, doi:10.1021/acs.biochem.6b00936 (2017).

186 Dragatsis, I., Levine, M. S. & Zeitlin, S. Inactivation of Hdh in the brain and testis results in progressive neurodegeneration and sterility in mice. *Nat Genet* **26**, 300-306, doi:10.1038/81593 (2000).

187 Tan, H., Xu, Z. & Jin, P. Role of noncoding RNAs in trinucleotide repeat neurodegenerative disorders. *Experimental neurology* **235**, 469-475, doi:10.1016/j.expneurol.2012.01.019 (2012).

188 Iwahashi, C. K. *et al.* Protein composition of the intranuclear inclusions of FXTAS. *Brain* **129**, 256-271, doi:10.1093/brain/awh650 (2006).

189 Nalavade, R., Griesche, N., Ryan, D. P., Hildebrand, S. & Krauß, S. Mechanisms of RNA-induced toxicity in CAG repeat disorders. *Cell Death &Amp; Disease* **4**, e752, doi:10.1038/cddis.2013.276 (2013).

190 de Mezer, M., Wojciechowska, M., Napierala, M., Sobczak, K. & Krzyzosiak, W. J. Mutant CAG repeats of Huntingtin transcript fold into hairpins, form nuclear foci and are targets for RNA interference. *Nucleic acids research* **39**, 3852-3863, doi:10.1093/nar/gkq1323 (2011).

191 Griesche, N. *et al.* Regulation of mRNA Translation by MID1: A Common Mechanism of Expanded CAG Repeat RNAs. *Frontiers in cellular neuroscience* **10**, 226, doi:10.3389/fncel.2016.00226 (2016).

192 Boutell, J. M. *et al.* Aberrant Interactions of Transcriptional Repressor Proteins with the Huntington's Disease Gene Product, Huntingtin. *Human Molecular Genetics* **8**, 1647-1655, doi:10.1093/hmg/8.9.1647 (1999).

References

193 Koyuncu, S., Fatima, A., Gutierrez-Garcia, R. & Vilchez, D. Proteostasis of Huntingtin in Health and Disease. *International journal of molecular sciences* **18**, doi:10.3390/ijms18071568 (2017).

194 Brehme, M. *et al.* A chaperome subnetwork safeguards proteostasis in aging and neurodegenerative disease. *Cell Rep* **9**, 1135-1150, doi:10.1016/j.celrep.2014.09.042 (2014).

195 Kim, Y. E. *et al.* Soluble Oligomers of PolyQ-Expanded Huntingtin Target a Multiplicity of Key Cellular Factors. *Mol Cell* **63**, 951-964, doi:10.1016/j.molcel.2016.07.022 (2016).

196 Mitsui, K., Doi, H. & Nukina, N. Proteomics of polyglutamine aggregates. *Methods in enzymology* **412**, 63-76, doi:10.1016/s0076-6879(06)12005-4 (2006).

197 Nucifora, F. C., Jr. *et al.* Interference by huntingtin and atrophin-1 with cbp-mediated transcription leading to cellular toxicity. *Science* **291**, 2423-2428, doi:10.1126/science.1056784 (2001).

198 Hipp, M. S., Park, S.-H. & Hartl, F. U. Proteostasis impairment in protein-misfolding and -aggregation diseases. *Trends in Cell Biology* **24**, 506-514, doi:10.1016/j.tcb.2014.05.003 (2014).

199 Toyama, B. H. & Hetzer, M. W. Protein homeostasis: live long, won't prosper. *Nature reviews. Molecular cell biology* **14**, 55-61, doi:10.1038/nrm3496 (2013).

200 Ross, C. A. & Tabrizi, S. J. Huntington's disease: from molecular pathogenesis to clinical treatment. *The Lancet. Neurology* **10**, 83-98, doi:10.1016/s1474-4422(10)70245-3 (2011).

201 Sahl, S. J., Weiss, L. E., Duim, W. C., Frydman, J. & Moerner, W. E. Cellular inclusion bodies of mutant huntingtin exon 1 obscure small fibrillar aggregate species. *Sci Rep* **2**, 895, doi:10.1038/srep00895 (2012).

202 Arrasate, M., Mitra, S., Schweitzer, E. S., Segal, M. R. & Finkbeiner, S. Inclusion body formation reduces levels of mutant huntingtin and the risk of neuronal death. *Nature* **431**, 805-810, doi:10.1038/nature02998 (2004).

203 Banez-Coronel, M. *et al.* RAN Translation in Huntington Disease. *Neuron* **88**, 667-677, doi:10.1016/j.neuron.2015.10.038 (2015).

204 Fiszer, A. & Krzyzosiak, W. J. Oligonucleotide-based strategies to combat polyglutamine diseases. *Nucleic acids research* **42**, 6787-6810, doi:10.1093/nar/gku385 (2014).

205 Illarioshkin, S. N., Klyushnikov, S. A., Vigont, V. A., Seliverstov, Y. A. & Kaznacheyeva, E. V. Molecular Pathogenesis in Huntington's Disease. *Biochemistry. Biokhimiia* **83**, 1030-1039, doi:10.1134/s0006297918090043 (2018).

206 Jimenez-Sanchez, M., Licitra, F., Underwood, B. R. & Rubinsztein, D. C. Huntington's Disease: Mechanisms of Pathogenesis and Therapeutic Strategies. *Cold Spring Harb Perspect Med* **7**, doi:10.1101/cshperspect.a024240 (2017).

207 Ross, C. A. *et al.* Huntington disease: natural history, biomarkers and prospects for therapeutics. *Nature reviews. Neurology* **10**, 204-216, doi:10.1038/nrneurol.2014.24 (2014).

208 Dickey, A. S. & La Spada, A. R. Therapy development in Huntington disease: From current strategies to emerging opportunities. *Am J Med Genet A* **176**, 842-861, doi:10.1002/ajmg.a.38494 (2018).

209 Huntington Study, G. Tetrabenazine as antichorea therapy in Huntington disease: a randomized controlled trial. *Neurology* **66**, 366-372, doi:10.1212/01.wnl.0000198586.85250.13 (2006).

210 van Duijn, E. Treatment of Irritability in Huntington's Disease. *Current treatment options in neurology* **12**, 424-433, doi:10.1007/s11940-010-0088-3 (2010).

211 Holl, A. K., Wilkinson, L., Painold, A., Holl, E. M. & Bonelli, R. M. Combating depression in Huntington's disease: effective antidepressive treatment with venlafaxine XR. *International clinical psychopharmacology* **25**, 46-50, doi:10.1097/YIC.0b013e3283348018 (2010).

212 Venuto, C. S., McGarry, A., Ma, Q. & Kieburtz, K. Pharmacologic approaches to the treatment of Huntington's disease. *Movement Disorders* **27**, 31-41, doi:doi:10.1002/mds.23953 (2012).

213 Ghosh, R. & Tabrizi, S. J. Clinical Features of Huntington's Disease. *Advances in experimental medicine and biology* **1049**, 1-28, doi:10.1007/978-3-319-71779-1_1 (2018).

214 Heiser, V. *et al.* Inhibition of huntingtin fibrillogenesis by specific antibodies and small molecules: Implications for Huntington's disease therapy. *Proceedings of the National Academy of Sciences* **97**, 6739-6744, doi:10.1073/pnas.110138997 (2000).

215 Chen, M. *et al.* Minocycline inhibits caspase-1 and caspase-3 expression and delays mortality in a transgenic mouse model of Huntington disease. *Nat Med* **6**, 797-801, doi:10.1038/77528 (2000).

216 Hochfeld, W. E., Lee, S. & Rubinsztein, D. C. Therapeutic induction of autophagy to modulate neurodegenerative disease progression. *Acta pharmacologica Sinica* **34**, 600-604, doi:10.1038/aps.2012.189 (2013).

217 Rose, C. *et al.* Rilmenidine attenuates toxicity of polyglutamine expansions in a mouse model of Huntington's disease. *Hum Mol Genet* **19**, 2144-2153, doi:10.1093/hmg/ddq093 (2010).

218 Tsunemi, T. *et al.* PGC-1alpha rescues Huntington's disease proteotoxicity by preventing oxidative stress and promoting TFEB function. *Sci Transl Med* **4**, 142ra197, doi:10.1126/scitranslmed.3003799 (2012).

219 Menalled, L. B. *et al.* Comprehensive Behavioral Testing in the R6/2 Mouse Model of Huntington's Disease Shows No Benefit from CoQ10 or Minocycline. *PLOS ONE* **5**, e9793, doi:10.1371/journal.pone.0009793 (2010).

220 Ferrante, R. J. *et al.* Therapeutic effects of coenzyme Q10 and remacemide in transgenic mouse models of Huntington's disease. *J Neurosci* **22**, 1592-1599 (2002).

221 Huntington Study, G. A randomized, placebo-controlled trial of coenzyme Q10 and remacemide in Huntington's disease. *Neurology* **57**, 397-404 (2001).

222 Cisbani, G. & Cicchetti, F. The fate of cell grafts for the treatment of Huntington's disease: the post-mortem evidence. *Neuropathology and applied neurobiology* **40**, 71-90, doi:10.1111/nan.12104 (2014).

223 Drouet, V. *et al.* Sustained effects of nonallele-specific Huntingtin silencing. *Ann Neurol* **65**, 276-285, doi:10.1002/ana.21569 (2009).

224 Kordasiewicz, H. B. *et al.* Sustained therapeutic reversal of Huntington's disease by transient repression of huntingtin synthesis. *Neuron* **74**, 1031-1044, doi:10.1016/j.neuron.2012.05.009 (2012).

225 Foundation, C. *PTC Therapeutics and CHDI Foundation Announce a Collaboration on a Small-Molecule Therapeutic for Huntington's Disease*, <https://chdifoundation.org/ptc-therapeutics-and-chdi-foundation-announce-a-collaboration-on-a-small-molecule-therapeutic-for-huntingtons-disease/> (2018).

226 Wild, E. J. & Tabrizi, S. J. Therapies targeting DNA and RNA in Huntington's disease. *The Lancet. Neurology* **16**, 837-847, doi:10.1016/S1474-4422(17)30280-6 (2017).

227 Yang, S. *et al.* CRISPR/Cas9-mediated gene editing ameliorates neurotoxicity in mouse model of Huntington's disease. *The Journal of clinical investigation* **127**, 2719-2724, doi:10.1172/jci92087 (2017).

228 Stout, J. C. *et al.* Evaluation of longitudinal 12 and 24 month cognitive outcomes in premanifest and early Huntington's disease. *Journal of neurology, neurosurgery, and psychiatry* **83**, 687-694, doi:10.1136/jnnp-2011-301940 (2012).

229 Rosas, H. D. *et al.* PRECREST: a phase II prevention and biomarker trial of creatine in at-risk Huntington disease. *Neurology* **82**, 850-857, doi:10.1212/wnl.0000000000000187 (2014).

230 Byrne, L. M. *et al.* Neurofilament light protein in blood as a potential biomarker of neurodegeneration in Huntington's disease: a retrospective cohort analysis. *The Lancet. Neurology* **16**, 601-609, doi:10.1016/s1474-4422(17)30124-2 (2017).

231 Johnson, E. B. *et al.* Neurofilament light protein in blood predicts regional atrophy in Huntington disease. *Neurology* **90**, e717-e723, doi:10.1212/wnl.0000000000005005 (2018).

232 Wild, E. J. *et al.* Quantification of mutant huntingtin protein in cerebrospinal fluid from Huntington's disease patients. *The Journal of clinical investigation* **125**, 1979-1986, doi:10.1172/jci80743 (2015).

233 Atarashi, R. *et al.* Ultrasensitive detection of scrapie prion protein using seeded conversion of recombinant prion protein. *Nat Methods* **4**, 645-650, doi:10.1038/nmeth1066 (2007).

234 Holmes, B. B. *et al.* Proteopathic tau seeding predicts tauopathy in vivo. *Proc Natl Acad Sci U S A* **111**, E4376-4385, doi:10.1073/pnas.1411649111 (2014).

235 Du, D. *et al.* A kinetic aggregation assay allowing selective and sensitive amyloid-beta quantification in cells and tissues. *Biochemistry* **50**, 1607-1617, doi:10.1021/bi1013744 (2011).

236 Herva, M. E. *et al.* Anti-amyloid compounds inhibit alpha-synuclein aggregation induced by protein misfolding cyclic amplification (PMCA). *J Biol Chem* **289**, 11897-11905, doi:10.1074/jbc.M113.542340 (2014).

237 Biancalana, M. & Koide, S. Molecular mechanism of Thioflavin-T binding to amyloid fibrils. *Biochim Biophys Acta* **1804**, 1405-1412, doi:10.1016/j.bbapap.2010.04.001 (2010).

238 Wanker, E. E. *et al.* Membrane filter assay for detection of amyloid-like polyglutamine-containing protein aggregates. *Methods in enzymology* **309**, 375-386 (1999).

239 Kayed, R. *et al.* Common structure of soluble amyloid oligomers implies common mechanism of pathogenesis. *Science* **300**, 486-489, doi:10.1126/science.1079469 (2003).

240 Zhang, J. H., Chung, T. D. Y. & Oldenburg, K. R. A simple statistical parameter for use in evaluation and validation of high throughput screening assays. *J Biomol Screen* **4**, 67-73, doi:Doi 10.1177/108705719900400206 (1999).

241 Carter, R. J. *et al.* Characterization of Progressive Motor Deficits in Mice Transgenic for the Human Huntington's Disease Mutation. *The Journal of Neuroscience* **19**, 3248 (1999).

242 Li, H. *et al.* Ultrastructural localization and progressive formation of neuropil aggregates in Huntington's disease transgenic mice. *Hum Mol Genet* **8**, 1227-1236 (1999).

243 Ko, J., Ou, S. & Patterson, P. H. New anti-huntingtin monoclonal antibodies: implications for huntingtin conformation and its binding proteins. *Brain Res Bull* **56**, 319-329 (2001).

244 Li, J. Y., Popovic, N. & Brundin, P. The use of the R6 transgenic mouse models of Huntington's disease in attempts to develop novel therapeutic strategies. *NeuroRx : the journal of the American Society for Experimental NeuroTherapeutics* **2**, 447-464, doi:10.1602/neurorx.2.3.447 (2005).

245 Bates, G. P., Mangiarini, L. & Davies, S. W. Transgenic mice in the study of polyglutamine repeat expansion diseases. *Brain pathology (Zurich, Switzerland)* **8**, 699-714 (1998).

246 Bates, G. P. & Davies, S. W. Transgenic mouse models of neurodegenerative disease caused by CAG/polyglutamine expansions. *Molecular medicine today* **3**, 508-515, doi:10.1016/s1357-4310(97)01142-8 (1997).

247 Larson, E., Fyfe, I., Morton, A. J. & Monckton, D. G. Age-, tissue- and length-dependent bidirectional somatic CAG*CTG repeat instability in an allelic series of R6/2 Huntington disease mice. *Neurobiology of disease* **76**, 98-111, doi:10.1016/j.nbd.2015.01.004 (2015).

248 Langbehn, D. R., Hayden, M., Paulsen, J. S. & the, P.-H. D. I. o. t. H. S. G. CAG-Repeat Length and the Age of Onset in Huntington Disease (HD): A Review and Validation Study of Statistical Approaches. *American journal of medical genetics. Part B, Neuropsychiatric genetics : the official publication of the International Society of Psychiatric Genetics* **153B**, 397-408, doi:10.1002/ajmg.b.30992 (2010).

References

249 Schilling, G. *et al.* Intranuclear inclusions and neuritic aggregates in transgenic mice expressing a mutant N-terminal fragment of huntingtin. *Hum Mol Genet* **8**, 397-407 (1999).

250 Aggarwal, M. *et al.* Spatiotemporal mapping of brain atrophy in mouse models of Huntington's disease using longitudinal in vivo magnetic resonance imaging. *NeuroImage* **60**, 2086-2095, doi:10.1016/j.neuroimage.2012.01.141 (2012).

251 Hult, S. *et al.* Mutant huntingtin causes metabolic imbalance by disruption of hypothalamic neurocircuits. *Cell Metab* **13**, 428-439, doi:10.1016/j.cmet.2011.02.013 (2011).

252 Lin, C. H. *et al.* Neurological abnormalities in a knock-in mouse model of Huntington's disease. *Hum Mol Genet* **10**, 137-144 (2001).

253 Ciamei, A., Detloff, P. J. & Morton, A. J. Progression of behavioural despair in R6/2 and Hdh knock-in mouse models recapitulates depression in Huntington's disease. *Behavioural brain research* **291**, 140-146, doi:10.1016/j.bbr.2015.05.010 (2015).

254 Woodman, B. *et al.* The Hdh(Q150/Q150) knock-in mouse model of HD and the R6/2 exon 1 model develop comparable and widespread molecular phenotypes. *Brain Res Bull* **72**, 83-97, doi:10.1016/j.brainresbull.2006.11.004 (2007).

255 Radde, R. *et al.* Abeta42-driven cerebral amyloidosis in transgenic mice reveals early and robust pathology. *EMBO reports* **7**, 940-946, doi:10.1038/sj.embor.7400784 (2006).

256 Serneels, L. *et al.* gamma-Secretase heterogeneity in the Aph1 subunit: relevance for Alzheimer's disease. *Science* **324**, 639-642, doi:10.1126/science.1171176 (2009).

257 Boy, J. *et al.* Reversibility of symptoms in a conditional mouse model of spinocerebellar ataxia type 3. *Hum Mol Genet* **18**, 4282-4295, doi:10.1093/hmg/ddp381 (2009).

258 Odeh, F. *et al.* Atlas of transgenic Tet-Off Ca2+/calmodulin-dependent protein kinase II and prion protein promoter activity in the mouse brain. *NeuroImage* **54**, 2603-2611, doi:10.1016/j.neuroimage.2010.11.032 (2011).

259 Vonsattel, J. P. *et al.* Neuropathological classification of Huntington's disease. *Journal of neuropathology and experimental neurology* **44**, 559-577 (1985).

260 Rosenblatt, A. *et al.* Predictors of neuropathological severity in 100 patients with Huntington's disease. *Ann Neurol* **54**, 488-493, doi:10.1002/ana.10691 (2003).

261 Holloschi, A., Ritz, S., Schäfer, I. & Kioschis, P. *Analysis of huntingtin aggregation by fluorescence and FRET microscopy*. (2014).

262 Schindler, F. *Analysis of mutant huntingtin aggregation and toxicity in Drosophila models of Huntington's disease*, Freie Universität Berlin, (2016).

263 Bischof, J., Maeda, R. K., Hediger, M., Karch, F. & Basler, K. An optimized transgenesis system for Drosophila using germ-line-specific phiC31 integrases. *Proc Natl Acad Sci U S A* **104**, 3312-3317, doi:10.1073/pnas.0611511104 (2007).

264 Osterwalder, T., Yoon, K. S., White, B. H. & Keshishian, H. A conditional tissue-specific transgene expression system using inducible GAL4. *P Natl Acad Sci USA* **98**, 12596-12601, doi:DOI 10.1073/pnas.221303298 (2001).

265 Latouche, M. *et al.* A conditional pan-neuronal Drosophila model of spinocerebellar ataxia 7 with a reversible adult phenotype suitable for identifying modifier genes. *J Neurosci* **27**, 2483-2492, doi:10.1523/JNEUROSCI.5453-06.2007 (2007).

266 Sofola, O. *et al.* Inhibition of GSK-3 ameliorates Abeta pathology in an adult-onset Drosophila model of Alzheimer's disease. *PLoS Genet* **6**, e1001087, doi:10.1371/journal.pgen.1001087 (2010).

267 Rogers, I. *et al.* Ageing increases vulnerability to aβ42 toxicity in Drosophila. *PloS one* **7**, e40569-e40569, doi:10.1371/journal.pone.0040569 (2012).

268 Ast, A. *et al.* mHTT Seeding Activity: A Marker of Disease Progression and Neurotoxicity in Models of Huntington's Disease. *Mol Cell* **71**, 675-688 e676, doi:10.1016/j.molcel.2018.07.032 (2018).

269 Nollen, E. A. *et al.* Genome-wide RNA interference screen identifies previously undescribed regulators of polyglutamine aggregation. *Proc Natl Acad Sci U S A* **101**, 6403-6408, doi:10.1073/pnas.0307697101 (2004).

270 Moffitt, H., McPhail, G. D., Woodman, B., Hobbs, C. & Bates, G. P. Formation of Polyglutamine Inclusions in a Wide Range of Non-CNS Tissues in the HdhQ150 Knock-In Mouse Model of Huntington's Disease. *PLOS ONE* **4**, e8025, doi:10.1371/journal.pone.0008025 (2009).

271 Sathasivam, K. *et al.* Formation of polyglutamine inclusions in non-CNS tissue. *Hum Mol Genet* **8**, 813-822 (1999).

272 Kosinski, C. M. *et al.* Myopathy as a first symptom of Huntington's disease in a Marathon runner. *Movement disorders : official journal of the Movement Disorder Society* **22**, 1637-1640, doi:10.1002/mds.21550 (2007).

273 Carlyle, B. C., Trombetta, B. A. & Arnold, S. E. Proteomic Approaches for the Discovery of Biofluid Biomarkers of Neurodegenerative Dementias. *Proteomes* **6**, 32, doi:10.3390/proteomes6030032 (2018).

274 T Dos Santos, M. C. *et al.* Evaluation of cerebrospinal fluid proteins as potential biomarkers for early stage Parkinson's disease diagnosis. *PloS one* **13**, e0206536-e0206536, doi:10.1371/journal.pone.0206536 (2018).

275 Fiumara, F., Fioriti, L., Kandel, E. R. & Hendrickson, W. A. Essential Role of Coiled Coils for Aggregation and Activity of Q/N-Rich Prions and PolyQ Proteins. *Cell* **143**, 1121-1135, doi:https://doi.org/10.1016/j.cell.2010.11.042 (2010).

276 Mason, J. M. & Arndt, K. M. Coiled coil domains: stability, specificity, and biological implications. *Chembiochem : a European journal of chemical biology* **5**, 170-176, doi:10.1002/cbic.200300781 (2004).

277 Sodek, J., Hodges, R. S., Smillie, L. B. & Jurasek, L. Amino-acid sequence of rabbit skeletal tropomyosin and its coiled-coil structure. *Proc Natl Acad Sci U S A* **69**, 3800-3804 (1972).

278 Lupas, A., Van Dyke, M. & Stock, J. Predicting coiled coils from protein sequences. *Science* **252**, 1162-1164, doi:10.1126/science.252.5009.1162 (1991).

279 Oliveberg, M. Waltz, an exciting new move in amyloid prediction. *Nat Methods* **7**, 187-188, doi:10.1038/nmeth0310-187 (2010).

280 Maurer-Stroh, S. *et al.* Exploring the sequence determinants of amyloid structure using position-specific scoring matrices. *Nature Methods* **7**, 237, doi:10.1038/nmeth.1432 https://www.nature.com/articles/nmeth.1432#supplementary-information (2010).

281 Kwok, S. C. & Hodges, R. S. Stabilizing and destabilizing clusters in the hydrophobic core of long two-stranded alpha-helical coiled-coils. *J Biol Chem* **279**, 21576-21588, doi:10.1074/jbc.M401074200 (2004).

282 Pawar, A. P. *et al.* Prediction of "aggregation-prone" and "aggregation-susceptible" regions in proteins associated with neurodegenerative diseases. *J Mol Biol* **350**, 379-392, doi:10.1016/j.jmb.2005.04.016 (2005).

283 Colloc'h, N. & Cohen, F. E. Beta-breakers: an aperiodic secondary structure. *J Mol Biol* **221**, 603-613 (1991).

284 Guo, M., Gorman, P. M., Rico, M., Chakrabartty, A. & Laurents, D. V. Charge substitution shows that repulsive electrostatic interactions impede the oligomerization of Alzheimer amyloid peptides. *FEBS Letters* **579**, 3574-3578, doi:https://doi.org/10.1016/j.febslet.2005.05.036 (2005).

285 Preisinger, E., Jordan, B. M., Kazantsev, A. & Housman, D. Evidence for a recruitment and sequestration mechanism in Huntington's disease. *Philosophical transactions of the Royal Society of London. Series B, Biological sciences* **354**, 1029-1034, doi:10.1098/rstb.1999.0455 (1999).

286 del Valle Rodriguez, A., Didiano, D. & Desplan, C. Power tools for gene expression and clonal analysis in Drosophila. *Nat Methods* **9**, 47-55, doi:10.1038/nmeth.1800 (2011).

287 Duffy, J. B. GAL4 system in Drosophila: a fly geneticist's Swiss army knife. *Genesis (New York, N.Y. : 2000)* **34**, 1-15, doi:10.1002/gene.10150 (2002).

288 Robinow, S. & White, K. The locus elav of Drosophila melanogaster is expressed in neurons at all developmental stages. *Developmental biology* **126**, 294-303 (1988).

289 Ali, Y. O., Escala, W., Ruan, K. & Zhai, R. G. Assaying locomotor, learning, and memory deficits in Drosophila models of neurodegeneration. *J Vis Exp*, doi:10.3791/2504 (2011).

290 Cook-Wiens, E. & Grotewiel, M. S. Dissociation between functional senescence and oxidative stress resistance in Drosophila. *Experimental gerontology* **37**, 1347-1357 (2002).

291 Pfeiffenberger, C., Lear, B. C., Keegan, K. P. & Allada, R. Locomotor activity level monitoring using the Drosophila Activity Monitoring (DAM) System. *Cold Spring Harbor protocols* **2010**, pdb.prot5518, doi:10.1101/pdb.prot5518 (2010).

292 Salvadores, N., Shahnawaz, M., Scarpini, E., Tagliavini, F. & Soto, C. Detection of misfolded Abeta oligomers for sensitive biochemical diagnosis of Alzheimer's disease. *Cell Rep* **7**, 261-268, doi:10.1016/j.celrep.2014.02.031 (2014).

293 LeVine, H. Thioflavine T interaction with synthetic Alzheimer's disease beta-amyloid peptides: detection of amyloid aggregation in solution. *Protein Science : A Publication of the Protein Society* **2**, 404-410 (1993).

294 Lualdi, M. *et al.* Natural fluorescence spectroscopy of human blood plasma in the diagnosis of colorectal cancer: feasibility study and preliminary results. *Tumori* **93**, 567-571 (2007).

295 Hasenkopf, R. *Detection of seeding competent Htt aggregates in HD mouse models and patient brains with a novel FRET-based assay*, Humbolt-Universität zu Berlin, (2016).

296 Pearce, M. M., Spartz, E. J., Hong, W., Luo, L. & Kopito, R. R. Prion-like transmission of neuronal huntingtin aggregates to phagocytic glia in the Drosophila brain. *Nat Commun* **6**, 6768, doi:10.1038/ncomms7768 (2015).

297 Narasimhan, S. *et al.* Pathological Tau Strains from Human Brains Recapitulate the Diversity of Tauopathies in Nontransgenic Mouse Brain. *J Neurosci* **37**, 11406-11423, doi:10.1523/jneurosci.1230-17.2017 (2017).

298 Cohen, M., Appleby, B. & Safar, J. G. Distinct prion-like strains of amyloid beta implicated in phenotypic diversity of Alzheimer's disease. *Prion* **10**, 9-17, doi:10.1080/19336896.2015.1123371 (2016).

299 Solforosi, L., Milani, M., Mancini, N., Clementi, M. & Burioni, R. A closer look at prion strains: characterization and important implications. *Prion* **7**, 99-108, doi:10.4161/pri.23490 (2013).

300 Nekooki-Machida, Y. *et al.* Distinct conformations of in vitro and in vivo amyloids of huntingtin-exon1 show different cytotoxicity. *Proceedings of the National Academy of Sciences* **106**, 9679-9684, doi:10.1073/pnas.0812083106 (2009).

301 Silveira, J. R. *et al.* The most infectious prion protein particles. *Nature* **437**, 257-261, doi:10.1038/nature03989 (2005).

302 Leitman, J., Ulrich Hartl, F. & Lederkremer, G. Z. Soluble forms of polyQ-expanded huntingtin rather than large aggregates cause endoplasmic reticulum stress. *Nat Commun* **4**, 2753, doi:10.1038/ncomms3753 (2013).

303 Muchowski, P. J., Ning, K., D'Souza-Schorey, C. & Fields, S. Requirement of an intact microtubule cytoskeleton for aggregation and inclusion body formation by a mutant huntingtin fragment. *P Natl Acad Sci USA* **99**, 727-732, doi:10.1073/pnas.022628699 (2002).

References

304 Baldwin, A. J. *et al.* Metastability of Native Proteins and the Phenomenon of Amyloid Formation. *Journal of the American Chemical Society* **133**, 14160-14163, doi:10.1021/ja2017703 (2011).

305 Walther, Dirk M. *et al.* Widespread Proteome Remodeling and Aggregation in Aging C. elegans. *Cell* **161**, 919-932, doi:https://doi.org/10.1016/j.cell.2015.03.032 (2015).

306 Kundra, R., Ciryam, P., Morimoto, R. I., Dobson, C. M. & Vendruscolo, M. Protein homeostasis of a metastable subproteome associated with Alzheimer's disease. *Proceedings of the National Academy of Sciences* **114**, E5703-E5711, doi:10.1073/pnas.1618417114 (2017).

307 Bauerlein, F. J. B. *et al.* In Situ Architecture and Cellular Interactions of PolyQ Inclusions. *Cell* **171**, 179-187.e110, doi:10.1016/j.cell.2017.08.009 (2017).

308 Busch, A. *et al.* Mutant huntingtin promotes the fibrillogenesis of wild-type huntingtin: a potential mechanism for loss of huntingtin function in Huntington's disease. *J Biol Chem* **278**, 41452-41461, doi:10.1074/jbc.M303354200 (2003).

309 Ruiz-Arlandis, G., Pieri, L., Bousset, L. & Melki, R. Binding, internalization and fate of Huntingtin Exon1 fibrillar assemblies in mitotic and nonmitotic neuroblastoma cells. *Neuropathology and applied neurobiology* **42**, 137-152, doi:10.1111/nan.12258 (2016).

310 Caron, N. S., Dorsey, E. R. & Hayden, M. R. Therapeutic approaches to Huntington disease: from the bench to the clinic. *Nature reviews. Drug discovery* **17**, 729-750, doi:10.1038/nrd.2018.133 (2018).

311 Figueiredo, M. *IONIS-HTTRx Shows Promising Results in Phase 1/2 Clinical Trial*, <https://huntingtonsdiseasenews.com/2018/03/08/ionis-httrx-shows-promising-results-in-huntingtons-disease-clinical-trial/> (2018).

312 Kuemmerle, S. *et al.* Huntington aggregates may not predict neuronal death in Huntington's disease. *Ann Neurol* **46**, 842-849 (1999).

313 Slow, E. J. *et al.* Absence of behavioral abnormalities and neurodegeneration in vivo despite widespread neuronal huntingtin inclusions. *Proc Natl Acad Sci U S A* **102**, 11402-11407, doi:10.1073/pnas.0503634102 (2005).

314 Jacob, J., Duclohier, H. & Cafiso, D. S. The Role of Proline and Glycine in Determining the Backbone Flexibility of a Channel-Forming Peptide. *Biophysical Journal* **76**, 1367-1376, doi:https://doi.org/10.1016/S0006-3495(99)77298-X (1999).

315 Nichols, M. R. *et al.* Growth of β-Amyloid(1−40) Protofibrils by Monomer Elongation and Lateral Association. Characterization of Distinct Products by Light Scattering and Atomic Force Microscopy. *Biochemistry* **41**, 6115-6127, doi:10.1021/bi015985r (2002).

316 Benzinger, T. L. *et al.* Propagating structure of Alzheimer's beta-amyloid(10-35) is parallel beta-sheet with residues in exact register. *P Natl Acad Sci USA* **95**, 13407-13412 (1998).

317 Wu, H. & Fuxreiter, M. The Structure and Dynamics of Higher-Order Assemblies: Amyloids, Signalosomes, and Granules. *Cell* **165**, 1055-1066, doi:10.1016/j.cell.2016.05.004 (2016).

318 Portillo, A. *et al.* Role of monomer arrangement in the amyloid self-assembly. *Biochim Biophys Acta* **1854**, 218-228, doi:10.1016/j.bbapap.2014.12.009 (2015).

319 Sun, C.-S. *et al.* Conformational switch of polyglutamine-expanded huntingtin into benign aggregates leads to neuroprotective effect. *Scientific Reports* **5**, 14992, doi:10.1038/srep14992 https://www.nature.com/articles/srep14992#supplementary-information (2015).

320 Girstmair, H. *et al.* Depletion of Cognate Charged Transfer RNA Causes Translational Frameshifting within the Expanded CAG Stretch in Huntingtin. *Cell Reports* **3**, 148-159, doi:https://doi.org/10.1016/j.celrep.2012.12.019 (2013).

321 Sahoo, B., Singer, D., Kodali, R., Zuchner, T. & Wetzel, R. Aggregation behavior of chemically synthesized, full-length huntingtin exon1. *Biochemistry* **53**, 3897-3907, doi:10.1021/bi500300c (2014).

322 Zheng, Z., Li, A., Holmes, B. B., Marasa, J. C. & Diamond, M. I. An N-terminal nuclear export signal regulates trafficking and aggregation of Huntingtin (Htt) protein exon 1. *The Journal of biological chemistry* **288**, 6063-6071, doi:10.1074/jbc.M112.413575 (2013).

323 Petrakis, S., Schaefer, M. H., Wanker, E. E. & Andrade-Navarro, M. A. Aggregation of polyQ-extended proteins is promoted by interaction with their natural coiled-coil partners. *BioEssays : news and reviews in molecular, cellular and developmental biology* **35**, 503-507, doi:10.1002/bies.201300001 (2013).

324 Mangiarini, L. *et al.* Exon 1 of the HD gene with an expanded CAG repeat is sufficient to cause a progressive neurological phenotype in transgenic mice. *Cell* **87**, 493-506, doi:Doi 10.1016/S0092-8674(00)81369-0 (1996).

325 Baldo, B., Soylu, R. & Petersen, A. Maintenance of basal levels of autophagy in Huntington's disease mouse models displaying metabolic dysfunction. *PLoS One* **8**, e83050, doi:10.1371/journal.pone.0083050 (2013).

326 Lin, D. M. & Goodman, C. S. Ectopic and increased expression of Fasciclin II alters motoneuron growth cone guidance. *Neuron* **13**, 507-523 (1994).

327 Hazelrigg, T., Levis, R. & Rubin, G. M. Transformation of white locus DNA in drosophila: dosage compensation, zeste interaction, and position effects. *Cell* **36**, 469-481 (1984).

328 Nguyen, A. W. & Daugherty, P. S. Evolutionary optimization of fluorescent proteins for intracellular FRET. *Nat Biotechnol* **23**, 355-360, doi:10.1038/nbt1066 (2005).

329 Theillet, F. X. *et al.* Structural disorder of monomeric alpha-synuclein persists in mammalian cells. *Nature* **530**, 45-50, doi:10.1038/nature16531 (2016).

330 Gao, M. *et al.* Modulation of human IAPP fibrillation: cosolutes, crowders and chaperones. *Phys Chem Chem Phys* **17**, 8338-8348, doi:10.1039/c4cp04682j (2015).

331 Jiang, X. & Sorkin, A. Coordinated traffic of Grb2 and Ras during epidermal growth factor receptor endocytosis visualized in living cells. *Mol Biol Cell* **13**, 1522-1535, doi:10.1091/mbc.01-11-0552 (2002).

332 Schindelin, J. *et al.* Fiji: an open-source platform for biological-image analysis. *Nat Methods* **9**, 676-682, doi:10.1038/nmeth.2019 (2012).

9. Acknowledgment

Looking back on the last five years, there are so many people who I would like to thank.

First of all, I would like to thank **Prof. Erich Wanker**, for giving me the opportunity to work in his lab and for providing me with a fascinating topic. His guidance, encouragement and critical appraisal paved my way to become an independent and confident scientist. I highly appreciated his trust in my scientific skills and the freedom to develop and pursue my own ideas. His enthusiasm and ingenuity has always been an inspiration to me.

I would also like to express my gratitude to **Prof. Oliver Daumke** who took an interest in my project and kindly agreed to supervise my these.

Furthermore, I am deeply grateful to our collaboration partners within this project. In particular, I would like to thank **Prof. Gill Bates** for generously sharing valuable biosamples.

I always appreciated the amicable spirit in the lab and would like to thank **my dear colleagues** for creating a work environment of mutual support, encouragement and creative exchange. In particular, I would like to thank **Philipp** and **Simona** for inspiring discussions. Thank you **Alex**, for supervising the initial stages of my PhD. It has been the smoothest and most educative start into PhD life that anyone could have wished for. Thank you **Gerlinde**, for your guidance and advice at the atomic force microscope. Thank you **Franzi**, for patiently introducing me to the world of flies. And thank you so much **Lydia**, for your untiring support. Without your commitment and flexibility, the flies would have probably eaten me alive.

In addition I would like to thank all **„Wanker's and associates"** for the amazing time outside the lab. I really enjoyed the barbeque dinners, table tennis competitions and all the great evenings with PALÉ ALÈ.

Die letzten Zeilen dieser Arbeit möchte ich den Menschen widmen, die schon immer für mich da waren. Meiner ganzen **Familie** möchte ich für ihren Humor, ihre Fürsorge und ihren Optimismus danken, mit denen sie mich begleiten. Ich danke euch **Mama** und **Papa**, für die kilometerlangen Abkürzungen und die Gurkenfrösche, die meine Welt geprägt haben. Und meinem **Flo** danke ich für die Neugier und die Ausdauer meinen Laborkram zu verstehen. Danke, dass du dich mit mir auch noch über die tausenste FRET-Kurve freust. Vor allem aber, danke ich dir für die Schneekugel voller Geborgenheit.